Effect of Phase-Equilibrium Uncertainties on the Process Design of Selected C_2 and C_3 Alcohol Separation Systems: A Monte Carlo Approach

by

Leon Burger

Thesis presented in partial fulfilment

of the requirements for the Degree

of

MASTER OF ENGINEERING

(CHEMICAL ENGINEERING)

in the Faculty of Engineering

at Stellenbosch University

Supervisor

Prof. Cara Schwarz

March 2017

Declaration

By submitting this thesis electronically, I declare that the entirety of the work contained therein is my own, original work, that I am the sole author thereof (save to the extent explicitly otherwise stated), that reproduction and publication thereof by Stellenbosch University will not infringe any third party rights and that I have not previously in its entirety or in part submitted it for obtaining any qualification.

Leon Burger — March 2017

…… …….

Signature — Date

Abstract

Process design uncertainties can significantly influence the safety and reliability of separation processes. It is broadly accepted that the process engineer must not only specify the best available thermodynamic model to obtain reasonable results, but also quantify the effects of uncertainties in thermodynamic models and data on the final process design.

Phase equilibrium correlations are reported as the most significant source of property uncertainties. **Thus, how can one best account for the thermodynamic model parametric input uncertainty and the propagation of said uncertainty through the process simulation model?** In this work, the effect of phase equilibrium uncertainties on the process design of the dehydration of C_2 and C_3 alcohols using extractive and azeotropic distillation was investigated. The extractive distillation of diisopropyl ether (DIPE) and isopropanol (IPA) with 2-methoxyethanol as the solvent, as well as the heterogeneous azeotropic distillation of ethanol and water using DIPE as entrainer, were considered.

Firstly, a systematic evaluation of thermodynamic models was performed. The objective was to identify the model that offered the closest prediction of experimental data of the underlying system (*What is the best model?*). The performance of the NRTL activity coefficient model in predicting the phase equilibria of the ***DIPE / IPA / 2-methoxyethanol*** extractive distillation system was of a high degree of accuracy. The prediction of the azeotrope temperature and composition were improved, although marginally, with the Hayden O'Connell and Nothnagel equations of state. However, this benefit was not extended to the binary vapour-liquid equilibrium (VLE) correlation ability of the model, thus the NRTL model was used. For the ***DIPE / ethanol / water*** azeotropic distillation system, the evaluation process revealed that the NRTL activity coefficient model offered largely excellent results, with a high degree of accuracy apparent in the azeotrope and phase envelope predictions. The inclusion of liquid-liquid equilibrium (LLE) data provided a meaningful improvement of the model's ability to predict experimentally measured equilibrium data, confirming the usefulness of the NRTL model for this system.

Secondly, a combined computer-based approach of stochastic models and process simulation was used to assess the effect of phase equilibrium uncertainties on the sizing of key process equipment. The Monte Carlo simulation technique generated a set of random input variables that represent the range of parametric uncertainty. For each system a process model was

developed and the simulation solved for each unique set of input parameters with Aspen Plus® v8.8. The results were subsequently combined to develop cumulative distribution functions (CDF) for each design output of interest e.g. reboiler duty, heat exchanger surface area or column diameter and thus used to estimate the confidence level of the design.

For the ***DIPE / IPA / 2-methoxyethanol*** system, it was observed that the extraction column uncertainty was predominantly in the bottom section of the column and was mainly related to the reboil rate. The design confidence could be improved to an acceptable level through a marginal increase of the reboil rate. The investigation further determined that the recovery column uncertainty was also limited to the bottom section of the column and only reboil ratio was of concern. The recovery column condenser and reboiler design confidence were 45% and 82%, but a small increase in duty restored the design confidence to the required levels. It was therefore concluded that the design of the extractive distillation process for the separation of the diisopropyl ether + isopropanol azeotrope with 2-methoxyethanol is acceptable and the identified risk areas can easily be resolved.

For the ***DIPE / ethanol / water*** system, it was observed that the azeotropic distillation column geometry was not significantly impacted by the phase equilibria uncertainty, but that reboil ratio, bottoms flow rate and condenser surface area were. It was further noted that the dilute component uncertainties were high in the decanter, but did not appear to effect the overall performance of the decanter as the ratio of organic to aqueous liquid phase was high. Lastly, in the top section of the recovery column the key design output variables sensitive to phase equilibrium uncertainty were those related to condenser thermal requirements and that the effect of the phase equilibria uncertainty on the column geometry was negligible.

In this work, it was thus shown that a systematic uncertainty quantification process based on a Monte Carlo approach reveals the effect of phase equilibrium uncertainty on the process design of C_2 and C_3 low molecular weight alcohol separation systems. The approach presented can be used to facilitate decision making in fields related to safety factor selection.

Opsomming

Proses ontwerp onsekerhede kan die veiligheid en betroubaarheid van skeidingsprosesse aansienlik beïnvloed. Dit word algemeen aanvaar dat die proses ingenieur die beste beskikbare termodinamiese model moet spesifiseer om redelike resultate te verkry. Verder word daar ook van hom 'n kwantitatiewe maatstaf vereis om die onsekerhede in termodinamiese modelle en data op die finale proses ontwerp te verreken.

Die korrelasies van fase-ewewig word beskou as die belangrikste bron van toestand onsekerhede. **Die vraag is dus hoe om die termodinamiese model parametriese insette onsekerheid en die voortsetting van hierdie onsekerheid deur die proses simulasiemodel die beste te verreken.** In hierdie tesis word die effek van fase-ewewig onsekerhede in die proses ontwerp van skeiding stelsels met lae molekulêre gewig alkohol beskou. Die twee sleutel azeotropiese skeidings tegnieke wat uit die literatuur geïdentifiseer is, is ekstraktiewe en azeotropiese distillasie. Die effek van fase-ewewigte onsekerhede oor hierdie stelsels is nog nie deeglik bestudeer nie.

Eerstens is daar 'n sistematiese evaluering van termodinamiese modelle uitgevoer. Die doel was om 'n model te identifiseer wat die akkuraatste voorspelling gee van die eksperimentele data wat aangebied word by die oorweging van die fase-ewewigte van die lae molekulêre gewig alkohol stelsels van belang vir hierdie tesis (Wat is die beste model?). Die NRTL aktiwiteitskoëffisiënt model was baie akkuraat in die voorspelling van die fase-ewewigte van die di-isopropiel eter / iso-propanol / 2-metoksie-etanol ekstraktiewe distillasie stelsel. Die voorspelling van die azeotropiese temperatuur en samestelling is effens verbeter met die Hayden O'Connell en Nothnagel toestandsvergelykings. Maar hierdie voordeel is nie uitgebrei word na die binêre VLE korrelasie vermoë van die model nie. Wat die ***DIPE / etanol / water*** azeotropiese distillasie stelsels betref, het die evalueringsproses aangetoon dat die voorgestelde NRTL aktiwiteitskoëffisiënt model grootliks uitstekende resultate lewer, met 'n hoë graad van akkuraatheid, soos wat duidelik blyk uit die azeotropiese en fase koevert voorspellings. Die insluiting van VVE data lewer 'n betekenisvolle verbetering van die vermoë van die model om eksperimentele ewewig data te voorspel. Die resultate bevestig die nut van die NRTL model vir lae molekulêre gewig alkohol azeotropiese stelsel modellering.

'n Gekombineerde rekenaargebaseerde benadering deur stogastiese modelle en proses simulasie is gebruik om die effek van fase-ewewig onsekerhede op die grootte bepaling van die

belangrikste proses toerusting te evalueer. Die Monte Carlo simulasie tegniek het 'n stel ewekansige inset veranderlikes gegenereer wat die variasie in die parametriese onsekerheid verteenwoordig. Dit is gevolg deur 'n proses simulasie vir elke unieke stel insette parameters met Aspen Plus® v8.8 te voltooi. Die resultate is daarna gekombineer om kumulatiewe verdelingsfunksies (KVF) te ontwikkel vir elke ontwerp uitset van belang bv. opkoker las, hitteruiler oppervlakte of kolom diameter. Die KVF is gebruik is om die betroubaarheidsvlak van die ontwerp te voorspel.

By die di-isopropiel eter / isopropanol / 2-metoksie-etanol stelsel is dit opgemerk dat die ekstraksiekolom onsekerheid oorwegend in die onderste gedeelte van die kolom was en hoofsaaklik verband hou met die opkooktempo. Die ontwerp vertroue kan verbeter word tot 'n aanvaarbare vlak deur 'n marginale hoër opkooktempo. Die ondersoek het verder bepaal dat die herwinningskolom onsekerheid ook beperk was tot die onderste deel van die kolom en net die opkook verhouding was ’n probleem. Die herwinningskolom kondenseerder en opkoker ontwerp vertroue het gewissel van 45% tot 82%, maar 'n klein toename in termiese werksverrigting herstel die ontwerp vertroue tot die vereiste vlakke. Daar is dus tot die gevolgtrekking gekom dat die ontwerp van die ekstraksie distillasie proses aanvaarbaar en die geïdentifiseerde risiko areas maklik opgelos kan word vir die skeiding van die di-isopropiel eter + isopropanol azeotrope met 2-methoksie-etanol.

By die DIPE / etanol / waterstelsel is dit opgemerk dat die azeotropiese distillasiekolom uitleg nie beduidend beïnvloed is deur die fase-ewewigte onsekerheid nie, maar wel deur die opkook verhouding, bodem vloeitempo en kondenseerder oppervlakte. Dit is verder opgemerk dat die verdunde komponent onsekerhede hoog was in die skeidingsdrom, maar blykbaar nie die algehele prestasie van die skeidingsdrom affekteer het nie, aangesien die verhouding van organiese tot waterfase onsekerheid laag was. Laastens, in die boonste deel van die herwinningskolom was die sleutel ontwerp uitsetveranderlikes sensitief vir fase ewewig onsekerheid wat verband hou met kondenseerder termiese vereistes. Die effek van fase-ewewig onsekerhede op die kolom uitleg was gering. **In hierdie tesis is dit dus aangetoon dat 'n sistematiese onsekerheids kwantifiseringsproses wat gebaseer is op 'n Monte Carlo benadering, die effek van fase-ewewig onsekerheid op die proses ontwerp van C2 and C3 lae molekulêre gewig alcohol skeidings stelsels toon.** Die benadering wat aangebied is, kan gebruik word om besluitneming te vergemaklik om ontwerpstoelating in die ontwerp van toerusting te kies.

"*And here I have come to the weak point in the study of the equation of state. I still wonder whether there is a better way. In fact this question continually obsesses me, I can never free myself from it, it is with me even in my dreams*."

J. D. van der Waals, Nobel Lecture

12 December 1910

Acknowledgements

This research has been financially supported by Sasol Oil (Pty) Ltd. Opinions expressed and conclusions arrived at are those of the author and are not necessarily attributed to the sponsor. The author acknowledges Aspen Plus®, a registered trademark of Aspen Technology Inc.

The author wishes to personally thank the following persons for their guidance, support and contributions to the completion of this work:

- Prof. Cara Schwarz for accepting me as a masters of engineering student, for the freedom she allowed me for my research and the constructive feedback on my ideas.
- Adri Visser of Fluor SA (Pty) Ltd for his willingness to listen and the interesting discussions about my work and chemical engineering in general. Our discussions always sharpened my ideas and I owe him a great deal of gratitude.
- Dr. Paul Mathias of Fluor Corporation for sharing his knowledge in the field of uncertainty quantification and the inspiration he provided.
- Arno and Sibylie Marais for their assistance in translating my abstract.
- The management team and my colleagues at work for supporting my academic pursuits.
- My deepest appreciation goes to my family, in particular my wife Hanli for her love, support and understanding that enabled me to pursue this goal.

To my Lord, Jesus Christ, for enduring mercy and favour. Thank you.

Glossary

A

Accuracy: Ability to indicate values that closely approximate the true value of the measured variable.

Activity: a measure of the effective concentration of a species in a real solution.

Azeotropes: a mixture of two or more components in such a ratio that when it is boiled, the vapour and liquid phases have the same composition.

B

Bias: Any influence on a result that produces an incorrect approximation of the true value of the variable being measured. Bias is the result of a predictable systematic error.

bubble-point temperature: the temperature at which bubbles first appear when a liquid mixture is heated.

C

Confidence interval: The range or interval within which the true value is expected to lie with a stated degree of confidence.

Confidence level: The degree of confidence that may be placed on an estimated range of uncertainty.

Chemical potential: the potential a substance has to produce a change in a system.

D

Deterministic models: the output of the model is fully determined by the parameter values and the initial conditions initial conditions

Distillation boundary: a residue curve that cannot be crossed via distillation alone.

E

Entrainer: an additive that forms an azeotrope with one or more components of a liquid mixture to aid in otherwise difficult separations by distillation, such as azeotropic distillation.

Error: The difference between true and observed values.

F

Fischer-Tropsch process:	a set of chemical reactions that convert a mixture of carbon monoxide and hydrogen to liquid hydrocarbons the synthesis of hydrocarbons and, to a lesser extent, of aliphatic oxygenated compounds by the catalytic hydrogenation of carbon monoxide.
Fouling:	refers to the accumulation of unwanted material on solid surfaces.
Fugacity:	the effective pressure of a real gas that replaces the true mechanical pressure inaccurate chemical equilibrium calculations.

G

Gibbs-Duhem equation:	describes the relationship between changes in chemical potential for components in a thermodynamic system.

H

Heterogeneous mixture:	a mixture that lacks uniformity in character and/or composition.
Homogeneous:	a mixture that is uniform in composition or character.
Hydrophilic substance:	a substance that is attracted to, and tends to be dissolved by water.
Hydrophobic substance:	a substance that is repelled by water.

L

Lipophilic:	refers to the ability of a compound to dissolve in fats and oils.

O

Oxygenates:	refers to compounds containing oxygen.

P

Phase envelope:	the region enclosed by the bubble point curve and dew point curve or the region on a ternary phase diagram enclosed by the LLE curve.
Plait point:	composition conditions at which the three coexisting phases of partially soluble components of a three-phase liquid system, approach each other in composition.
Precision:	The degree to which data within a set cluster together.

R

Raffinate: a liquid stream that is left after the extraction with the immiscible liquid to remove solutes from the original liquid.

Random error: An error that varies in an unpredictable manner when a large number of measurements of the same variable are made under effectively identical conditions.

Retentate: the substance unable to permeate through the membrane

S

Solvent: a substance in which another substance is dissolved.

Spurious error: A gross error in the procedure (for example, human errors or machine malfunctions).

Stochastic models: possess some inherent randomness. The same set of parameter values and initial conditions will lead to an ensemble of different outputs.

Systematic error: An error that, in the course of a number of measurements made under the same conditions on a material having the same true value of a variable, either remains constant in absolute value and sign or varies in a predictable manner. Systematic errors result in a bias.

T

Thermodynamic consistency: whether a set of data conforms to the constraints posed by the Gibbs-Duhem equation.

Tie-lines: a line on a phase diagram joining the two points which represent the composition of the phases in equilibrium.

V

Variance: The measure of the dispersion or scatter of the values of the random variable about the mean.

Nomenclature

Symbol/Abbreviation Description

A	Helmholtz energy
a	activity
AAD	average absolute deviation
ARD	% average absolute relative deviation percentage
B_i	bottoms of column *i*
B_{ij}	pure component Viral coefficient
C_2-alcohol	ethanol
C_3-alcohols	n-propanol and isopropanol
D	deviation in the McDermott-Ellis consistency test
Di	distillate of column *i*
DIPE	diisopropyl ether
D_{max}	maximum allowable deviation in the McDermott-Ellis consistency test
DNPE	di-n-propyl ether
DRS	data regression system
EtOH	ethanol
f	fugacity
F_i	feed to column *i*
G	Gibbs energy
Δh	change in heat of vaporization
H	enthalpy
H_2O	water
IPA	isopropanol
KF	Karl Fischer

k_{OT}, c_{OT}	Othmer-Tobias constants
LLE	liquid-liquid equilibrium
MSDS	material safety data sheet
n	number of moles
P_i	pressure at state *i* or of component *i*
R	ideal gas constant
ΔS	change in vapourisation entropy
S	entropy
SG	specific gravity
Temp	equilibrium temperature
T_i	temperature at state *i* or of component *i*
U	internal energy
UNIFAC LLE	UNIFAC with calculations based on LLE
UNIFAC VLE	UNIFAC with calculations based on VLE
V	Total volume
V_i^L	liquid molar volume of component *i*
VLE	vapour-liquid equilibrium
VLLE	vapour-liquid-liquid equilibrium

Symbol/Abbreviation Description

wt %	weight percentage
x_i	liquid phase composition of component i
y_i	vapour phase composition of component i
μ_i	chemical potential
ϕ	fugacity coefficient
γ	activity coefficient

Φ	ratio of fugacity coefficients with the Poynting correction factor
δ	term relating second Viral coefficient
τ_{ij}	parameter in NRTL and UNIQUAC models
Φ_i	UNIQUAC segment fraction
θ	UNIQUAC area fraction
Γ_k	UNIFAC residual activity coefficient
Ψ	UNIFAC group interaction parameter
σ	Standard deviation
μ	Mean

Table of Contents

Chapter 1
Introduction

A widely used and essential process technology in the petroleum and chemical industry is the separation of azeotropic mixtures using distillation. It involves the separation of highly non-ideal mixtures through the addition of a solvent or entrainer. A process of particular interest is the recovery of valuable low molecular weight alcohols (C_2 and C_3) from dilute solutions, for example, fermentation broths and Fischer-Tropsch waste water streams.

Worldwide there is a growing need for the production of dehydrated low molecular weight alcohols (Batista *et al.*, 2012; Bankar *et al.*, 2013). Ethanol and propanol isomers are widely used in chemical industry as a powerful solvent and as raw material or intermediate in chemical synthesis of aerosols, cosmetics, detergents, esters, medicine, organic and cyclic compound chains, paints, perfumes and food, among others (Lin and Wang, 2004; Riemenschneider and Bolt 2005). Anhydrous ethanol, for example, is regarded as a renewable energy source and is used as a gasoline blend component (Adair and Wilson, 2009).

Optimised and reliable design of distillation equipment is of vital importance as it is often the largest capital investment component of a C_2 and C_3 alcohol manufacturing facility (Tavan and Hosseini, 2013). Moreover, the operational expenses associated with distillation columns are also quite high. For the more than 40 000 distillation columns in the United States the operational energy requirements are approximately 7% of the total US energy consumption (Gmehling *et al.*, 1994; Kiss, 2013). Although non-distillation processes such as membrane separation and molecular sieve adsorption have increased in competiveness, the separation of azeotropic mixtures using distillation remains the dominant choice for manufacturing large quantities of high-purity low molecular weight alcohols (Vane *et al.*, 2009; Frolkova and Raeva, 2010).

As these processes operate in vapour and/or liquid phase, the modelling of the phase equilibrium is a significant factor in the process design (Hajipour *et al.*, 2014). Furthermore, the strong non-ideality of the C_2 and C_3 alcohol product mixtures formed during the manufacturing processes lead to the formation of azeotropes and accurate experimental phase equilibrium data is essential.

1.1 The research problem

Process simulation and design depends on thermodynamic models for estimating the basic properties and for sizing separation equipment (Mathias, 2014). Thermodynamic model parameters are subject to parametric uncertainties in experimental data and this influences the design and sizing of the equipment (Bjørner *et al.*, 2016). The size of the equipment directly effects the capital investment and operating expense of the chemical plant.

The mixture phase equilibria are reported as the most significant source of property uncertainties and may have a major impact on the simulation (Reed and Whiting, 1993; Diky *et al.*, 2012). The effect of property uncertainty was reported by Fair (1980) and is presented in Table 1.1.

Table 1.1. Effect of input errors on process equipment sizing. Redrawn from Fair (1980).

Property		% Error in Property	% Change in	
			Equipment Size	Equipment Cost
Thermal Conductivity		20%	13%	13%
Specific Heat		20%	6%	6%
Heat of Vaporisation		15%	15%	15%
Relative Volatility	50	10%	3%	3%
	1.5		20%	13%
	1.2		50%	31%
	1.1		100%	100%
Diffusivity		20%	6%	4%
		100%	40%	23%
Viscosity		50%	10%	10%
Density		20%	16%	16%
Interfacial Tension		20%	9%	9%

It is evident from Table 1.1 that distillation systems with close boiling components are especially prone to uncertainty and can lead to undersized equipment. The problem is that most chemical processes designs are performed under a determinist setting with fixed specifications. Therefore, it is important to examine the effects of the property uncertainties and determine the impact on the process model and final equipment design.

Process design is to a certain extent an inexact art. Uncertainties arise in the available design data and in the approximations necessary in design calculations (Towler and Sinnott, 2014). The traditional approach to handling potential uncertainties during the design phase, is to include a degree of over-design know as a *design factor*, or *design margin* or *safety factor* (Zhu

et al., 2010*)*. Thus, it is endeavoured to ensure that the design that is built meets product specifications and operates safely. In order to provide process operation flexibility, a typical design factor applied to process stream average flow rates is 10% (Rangaiah, 2016). Therefore, this factor will determine the maximum flows for equipment, instrumentation and piping design. These overdesign factors are often based on the design engineer's experience or an engineering contractors design guidelines and are therefore not at all times quantitatively derived (Zhu *et al.*, 2010; Rangaiah, 2016). Thus, this approach may result in conservative design decisions or infeasible designs. Kister (2002) observed, more than a decade ago, that primary design problems due to poor reality checking of simulations were rapidly increasing. Yet, Mathias (2014) recently reported that although experts in the field widely insist that property uncertainties be incorporated into process design, it is hardly used in practice.

Extensive literature publications on chemical process design uncertainty quantification are available. Whiting and co-worker (1993 – 2010) investigated the effect of uncertainties and developed methods to quantify their impact on the process using a Monte Carlo approach. Recently, Hajipour (2013) reported a similar approach that further incorporates the NIST Thermo Data Engine as a source of reliable property uncertainties. Furthermore, key thermodynamic journals (e.g. *Fluid Phase Equilibria, Journal of Chemical Thermodynamics, Journal of Chemical and Engineering Data*) mandated reporting of combined uncertainties with experimental data tables. These journals collectively represent approximately 80% of all thermophysical property data publishers (Diky *et al.*, 2009). The reporting of experimental data uncertainty is therefore likely to improve, but the question remains on whether the uncertainty information will be used. In addition and perhaps more importantly is how the data should be used.

The effect of mixture phase equilibria uncertainty on C_2 and C_3 alcohol separation systems has not been widely assessed. Thus, of interest here is whether the recent advances in uncertainty quantification and the improved availability of experimental data uncertainty information can assist in providing quantitative design factors in lieu of the effect of phase equilibria uncertainty.

1.2 Purpose of the study

In this study, the focus is on determining if advances in the uncertainty quantification methodology space applied to the design and simulation of azeotropic separation systems can aid the low molecular weight alcohol processing industry by improving the confidence in

process flow scheme development and equipment sizing. This work investigates the effect of phase equilibrium uncertainty on the process design of C_2 and C_3 alcohol separation systems.

1.3 Significance of this research

In broad terms, the expected outcomes of the research are to provide a contribution by way of supplementing existing literature and developing industry guidance for use by the C_2 and C_3 alcohol processing industry and associated engineering design community. Improving the robustness of process modelling through uncertainty analysis will provide a quantitative basis for design safety factors and a reference framework when conducting process optimisation and lean production initiatives. Optimising the design of azeotrope separation systems has the potential to not only significantly impact the capital investment, but also the future economic performance.

The final result expected is an increase in the understanding of how these uncertainties propagate through widely used C_2 and C_3 alcohol separation process calculations, how they affect the estimated performance and, most importantly, assist designers in defining equipment overdesign consistently thus optimising the process design.

1.4 The objectives of the study

The aim of this thesis is to determine the effect of phase equilibrium uncertainty on the process design of C_2 and C_3 low molecular weight alcohol separation systems. As such, the research shall be performed while targeting the following specific *objectives*.

(i.) Systematically evaluate the performance of selected thermodynamic models, by comparing phase equilibrium correlation to experimental data and identify the best model for the system of interest. (*What is the best model?*).

(ii.) Estimate the phase equilibrium uncertainty by propagating experimental data parametric uncertainty through the thermodynamic model.

(iii.) Quantify the effect of the phase equilibrium uncertainty on the key design variables of the unit operations in the process models. (*How reliable is the best model?*).

Although the focus of the project is primarily on assessing phase equilibrium uncertainty propagation, it is noted that the study strives for a holistic view by placing uncertainty quantification in the wider context of designing azeotrope separation processes.

1.5 Research Questions

To meet these objectives, this thesis answers the following *key research questions*:

- *What thermodynamic modelling approach provides the most accurate correlation with experimental data for the phase equilibria of low molecular weight alcohol separation systems? (**What is the best model?**)*

The following sub-questions need to be answered in order to answer the above.

a. *Does the inclusion of LLE experimental data provide a meaningful improvement in the model's predictive ability?*
b. *Is the assumption that the vapour phase is ideal appropriate for these systems?*

Having identified the fact that a need exists to quantify the effect of phase equilibrium uncertainty on the process design of low molecular weight alcohol separation systems, the extent to which, and how, this can be achieved is to be evaluated.

- *How can one best account for the thermodynamic model parametric input uncertainty and the propagation of said uncertainty through the process simulation model? (**How reliable is the best model?**)*

The following sub-questions are posed to answer this question (what is the confidence level of the model results?)

a. *What tools are available for assessing uncertainty related to model input parameters and quantifying the propagation of these uncertainties?*
b. *What is the extent of the uncertainty with respect to the modelled phase equilibria and the final process design?*
c. *How can the design uncertainty be treated, managed or reduced?*
d. *What are the required flow scheme parameters considering the consequence of uncertainty propagation?*

As it is known that minor deviations in thermodynamic model results from experimental data, or critical property values can have a significant impact on the accuracy of process flow scheme reliability (Reed and Whiting, 1993; Mathias, 2014), an evaluation needs to be performed with the aid of appropriate assessment techniques.

1.6 Scope and Limitations

A central tenet of this thesis is to support the advancement of uncertainty analysis in the chemical process industry. With this underlying principle in mind, ease of practical implementation of methods and procedures are considered a key qualifier for consideration. Therefore, it is necessary to define boundaries within which the investigation is conducted and several limitations are placed on the project scope. These limitations are listed below.

1.6.1 Thermodynamic models considered

The thermodynamic models applied in this research are limited to those available in Aspen Plus® version 8.8 as the thermodynamic model outputs are to be used for process modelling and equipment design.

1.6.2 Thermodynamic model constraints

The thermodynamic model parameter regression will be limited to phase equilibria experimental data. The regression of model parameters based on other properties e.g. vapour pressure or liquid molar volume is excluded.

1.6.3 Sources of uncertainty considered

Modelling uncertainty stems from errors, assumptions and approximations made when selecting a model and can be broken down into model form uncertainty and parametric uncertainty (Kennedy and O'Hagan, 2001). The first is related to the models ability to accurately represent the behaviour of the system and the second is often as a result of errors in experimental data or estimations of physical properties. In this work, the source of uncertainty is limited to parametric uncertainty related to experimental phase equilibria data. Pure compound properties (e.g. liquid density, heat capacity, etc.) are excluded as the pure compound properties from Aspen Plus® are from the DIPPR database and are expected to be sufficiently accurate (Mathias, 2016).

Furthermore, external uncertainties mainly affected by market conditions during the operation of the facility are also not considered. For example, the pricing changes in utilities can significantly affect the economic performance of the process. These external uncertainties are however normally accounted for during the early conceptual design phase of a project using mixed integer nonlinear programming (MINLP) techniques and are considered contractually fixed during the detailed design phase (Kallrath, 2005).

1.6.4 Design factors (Design margins)

Design factors typically applied to chemical process equipment are reported in literature. Generally these are: 10% for pumps and heat exchangers, 20% for control valves and separators and 15% for electrical drivers on pumps and compressors (Rangaiah, 2016). For distillation columns the vapour velocity is generally limited to 80% of flooding velocity (Ludwig, 1997; Towler and Sinnott, 2014). In this thesis it is assumed that a 10% over-design factor is representative of the current practise in the chemical process industries. Therefore, process uncertainties that exceed this value are considered significant as operational changes alone may not absorb the variability.

1.7 Thesis overview

The thesis is organised into three parts: Part I (Chapters 2-5) comprises theoretical aspects of phase equilibria, azeotrope separation technologies, thermodynamic modelling and uncertainty quantification methods. Part II (Chapters 6) provides details on the experimental procedures and uncertainty quantification method verification. Part III (Chapters 7-9) presents the results, discussions, conclusions and recommendations. The thesis layout is illustrated in Figure 1.1.

Part I Literature Review

Chapter 2 is focused on the fundamentals of azeotropes, how it relates to phase equilibria and the low molecular weight alcohol systems of interest are identified. The chapter concludes with the selection of extractive distillation and heterogeneous azeotropic distillation as the separation technologies of choice for this work.

Chapter 3 covers the theoretical aspects of thermodynamic modelling and establishes guidelines for selecting an appropriate thermodynamic model. The choice of a particular thermodynamic model is deferred until specific screening study is performed in Chapter 7.

Chapter 4 describes the types and sources of uncertainty, followed by a state-of-the-art summary of quantitative uncertainty evaluation methods. Probabilistic uncertainty quantification techniques relevant to process design are then discussed and a method is selected.

Chapter 5 concludes the literature review section, provides a summary of the salient findings from the literature and consolidates the conclusions on thermodynamic model selection and the most appropriate uncertainty analysis technique to apply.

Part II Experimental Procedures

Chapter 6 details the research design and methodology employed to meet the investigational objectives of the work. Verification of the uncertainty quantification method is provided.

Part III Results

Chapter 7 evaluates the ability of the candidate thermodynamic models (identified in Chapter 3) to successfully correlate the experimental phase equilibria behaviour in order to select the best model. The parametric uncertainty of the experimental data is then propagated through the selected model to the phase equilibria calculations using a Monte Carlo simulation approach.

Chapter 8 evaluates the effect of the phase equilibrium uncertainties on the process simulation results in order to determine the confidence level in the design and identify areas of over or under design.

Chapter 9 presents a summary of the conclusions from this work and recommendations.

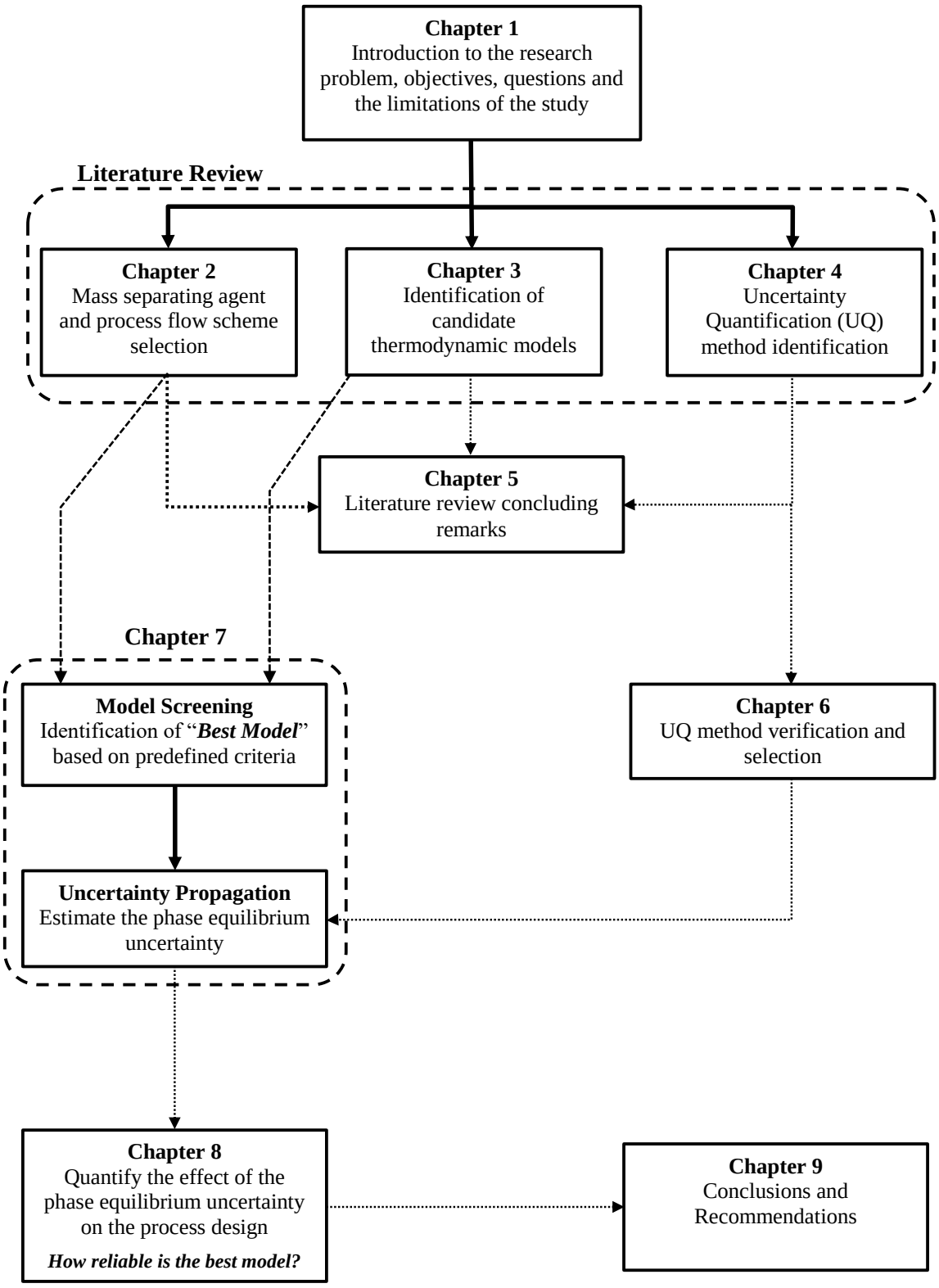

Figure 1.1: Illustration of thesis layout.

I LITERATURE REVIEW

Chapter 2
Separation of Azeotropic Alcohol Mixtures

The production of C_2 and C_3 alcohols depends on the separation of azeotropic alcohol mixtures to produce high purity products. The final separation strategy and process design is dictated by how the azeotropic mixtures are processed. Distillation is a thermal separation process widely applied as the separation technology of choice, despite its high energy demands.

The phase behaviour of a system is a determining factor in the design of a thermal separation process. The aims of this chapter are to review the phase behaviour of C_2 and C_3 alcohol systems and identify the preferred process separation technologies, with focus on entrainer-addition methods. The systems of interest are identified and mass separating agents are then selected for the thermodynamic modelling and process design to be conducted.

2.1 Low-pressure vapour-liquid equilibrium in non-ideal mixtures

Liquid-phase ideality occurs when the activity coefficients (γ_1) are equal to unity; this is only when the components are very similar. For example, in a mixture of benzene/toluene the activity coefficients for both components are close to unity. However, if the mixture components are appreciably different then non-ideal behaviour is observed (Kiss, 2013). Non-ideality in the vapour and liquid phases are quantified as:

$$x_i \gamma_i f_i^0 = y_i \varphi_i^V P \tag{2.1}$$

with

x_i the molar fraction of component *i* in the liquid solution.

γ_i the activity coefficient of component *i* in the liquid solution (*gamma*).

f_i^0 the standard fugacity, usually the fugacity of the pure liquid at system temperature and pressure.

y_i the molar fraction of component *i* in the vapour phase.

φ_i^V the vapour phase fugacity coefficient of component *i* in the solution (*phi*).

P the system pressure.

At low to moderate pressures and temperatures the vapour-liquid equilibrium is expressed as:

$$x_i \gamma_i P_i^{vap} = y_i P \tag{2.2}$$

Where, P_i^{vap} = *saturated vapour pressure of component i*.

Furthermore, at ideal conditions the activity coefficient is equal to unity and Equation 2.2 simplifies to *Raoult's law*:

$$y_i P = x_i P_i^{vap} \tag{2.3}$$

In many distillation systems, the behaviour is non-ideal and this complicates the vapour-liquid equilibrium calculations. A non-ideal system exhibits deviations from Raoult's law as a result of the non-linear composition dependence of the species activity coefficients (Sandler, 2006). When chemically different molecules are mixed (with emphasis on the liquid phase), it results in repulsion and attraction forces. Thus, Raoult's law serves as a convenient reference for describing non-ideal behaviour in vapour-liquid equilibrium.

The experimental data available in the literature for non-ideal solutions reveal that if the species in the mixture repel each other, a higher partial pressure is exerted, relative to if they were ideal (Sandler, 2006). If

$$P > \sum x_i P_i^{vap} \tag{2.4}$$

then the activity coefficient for at least one of the species in the mixture is greater than unity and a *positive deviation from Raoult's law* is observed. Similarly, if the species in the mixture attract each other,

$$P < \sum x_i P_i^{vap} \tag{2.5}$$

a lower partial pressure is exerted and a *negative deviation from Raoult's law* is observed. In this case, the activity coefficients for one or more species are less than unity. These deviations from Raoult's law are often evident in the formation of an azeotrope or an azeotropic mixture and occur in a number of industrial processes of interest (Horsley, 1973; Gmehling *et al.*, 1994), in particular in low molecular weight (C_2 and C_3) alcohol systems (Luyben, 2010).

Quasi-chemical forces are responsible for these deviations and lead to complex phenomena such as association and solvation; inherently attributed to non-ideal behaviour (Koretsky, 2010). Hydrogen bonding and charge transfer complexes (generally called Lewis acid-Lewis base) are two prominent quasi-chemical interactions of practical importance (Kontogeorgis and

Folas, 2010). In general, one can differentiate between two broad categories of hydrogen bonding related phenomena namely association and solvation.

Association or *self-association* is when different molecules of the same type form molecular clusters due to hydrogen bonding, for example between two like molecules of alcohol or water, thus leading to a positive deviation from Raoult's law.

Cross-association or *solvation* occurs between different types of molecules, for example between water-ethanol or chloroform-acetone (Prausnitz *et al.*, 1999), thus leading to a negative deviation from Raoult's law.

The mixtures of interest to this study (C_2 and C_3 alcohol azeotropes) display strong self-association and cross-association and this leads to the formation molecular clusters (dimers and tetramers) that are different from the monomeric molecules (Koretsky, 2010). This affects the physical properties of the mixture and directly affects the phase-behaviour of the system (i.e. azeotrope formation), thus the separation boundaries.

2.1.1 Phase equilibrium non-ideality and azeotropes

In practise, phase equilibrium calculations are often performed using the distribution coefficient, equilibrium ratio or also often called the K-value; this describes the ratio of the molar fraction in the vapour phase and the liquid phase for each component in the solution (de Hemptinne, 2012). The distribution coefficient is described by Equation (2.6) and is a convenient measure of the tendency of a given chemical substance to partition itself preferentially between the liquid and vapour phases i.e. favour the vapour phase (Smith *et al.*,2005):

$$K_i \equiv \frac{y_i}{x_i} \tag{2.6}$$

If K_i is less than unity, then species *i* exhibits a higher concentration in the liquid phase, when more, a higher concentration in the vapour phase.

The component K-values can be used to describe the relative volatility of a mixture. The relative volatility (α_{ij}) of a mixture generally changes with composition, temperature and pressure and serves as an indicator on how easy a mixture can be separated. For example, if the relative volatility significantly deviates from unity, the mixture is generally easy to separate.

$$\alpha_{ij} = \frac{K_i}{K_j} = \frac{y_i/x_i}{y_j/x_j} = \frac{\gamma_i P_i^{sat}}{\gamma_j P_j^{sat}} \tag{2.7}$$

Azeotropic mixtures are vapour-liquid mixtures of two or more species where the equilibrium vapour and liquid compositions are identical at a specific temperature and pressure. Thus, all K-values are at unity and no separation can take place (Sandler, 2006; Seader and Henley, 2006). Therefore, azeotropes represent a distillation boundary, as there is no further change in the vapour and liquid compositions from tray to tray in a distillation column (Kiss, 2013).

Azeotropes, particularly in the context of binary mixtures, can be classified as either *minimum-boiling azeotropes* or *maximum-boiling azeotropes* as shown in Figure 2.1. If the liquid mixture is homogeneous at the equilibrium temperature, the azeotrope is referred to as a *homogeneous azeotrope*. Conversely, if the vapour coexists with two liquid phases, it is a *heterogeneous azeotrope*.

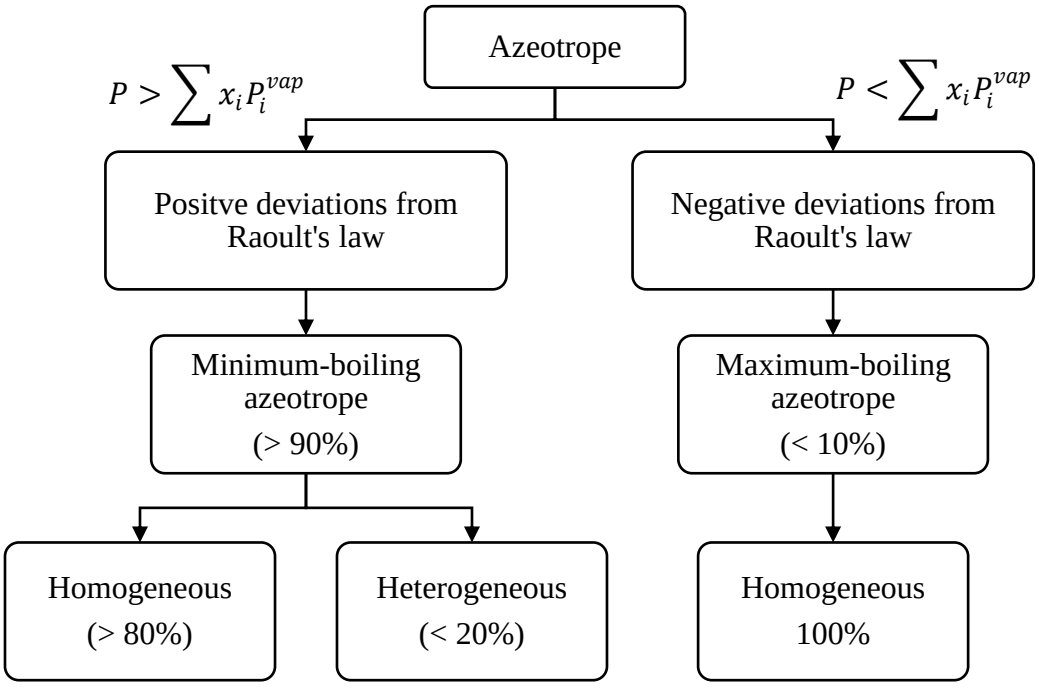

Figure 2.1: Classification of azeotropes based on deviation from ideal behaviour. The percentage values are from (Rousseau, 1987; Gmehling *et al.*, 1994; Gmehling *et al.*, 2004).

2.1.2 Minimum-boiling azeotropes

Minimum-boiling azeotropes occur in mixtures where the attraction between identical molecules is stronger than between different molecules(Hilmen, 2000). This results in an overall increase of the component vapour pressure and in a decrease in the mixtures boiling point below that of the pure component boiling points as illustrated in Figure 2.2.

Approximately 90% of all known azeotropes can be classified as minimum-boiling azeotropes (Rousseau, 1987; Gmehling *et al.*, 2004). Of these, more than 80% is classed as homogeneous azeotropes and less than 20% heterogeneous azeotropes (Gmehling *et al.*, 1994). Low molecular weight alcohols (methanol, ethanol, isopropanol or n-propanol) and water azeotropic systems are examples of minimum-boiling homogeneous azeotropes. Heavier alcohols (e.g. n-butanol) and water forms minimum-boiling heterogeneous azeotropes.

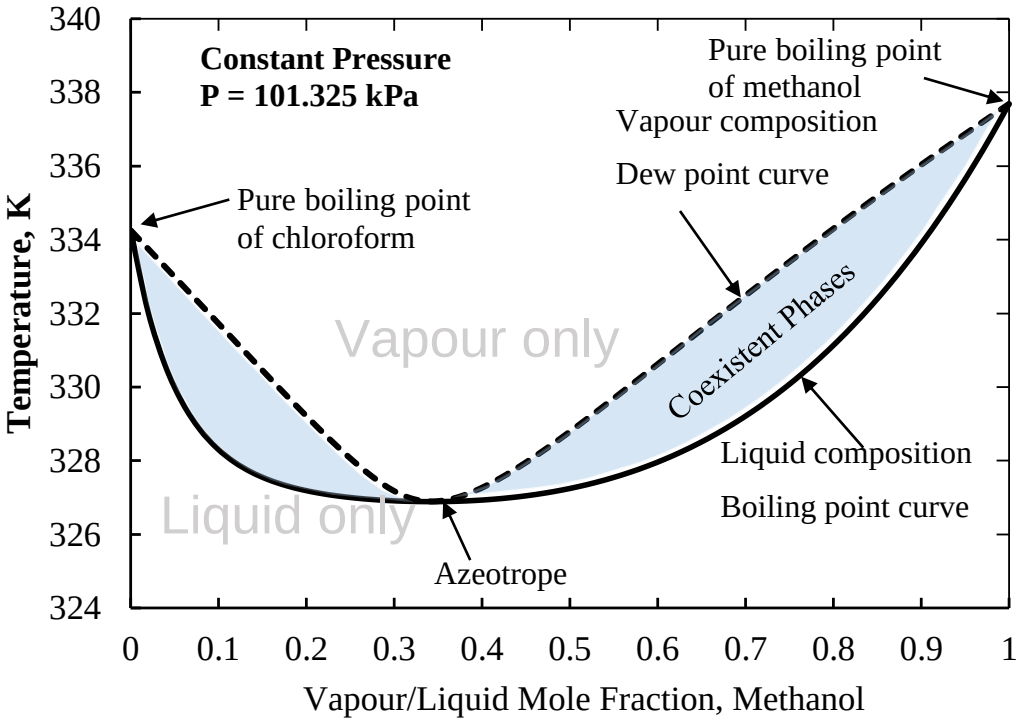

Figure 2.2: Typical homogeneous mixtures with minimum boiling azeotrope methanol and chloroform, a positive deviation from Raoult's law.

The ethanol/water azeotrope is presented in Figure 2.3 and illustrates a positive deviation from Raoult's law. The NRTL physical property method was used to generate the plots at 101.3 kPa.

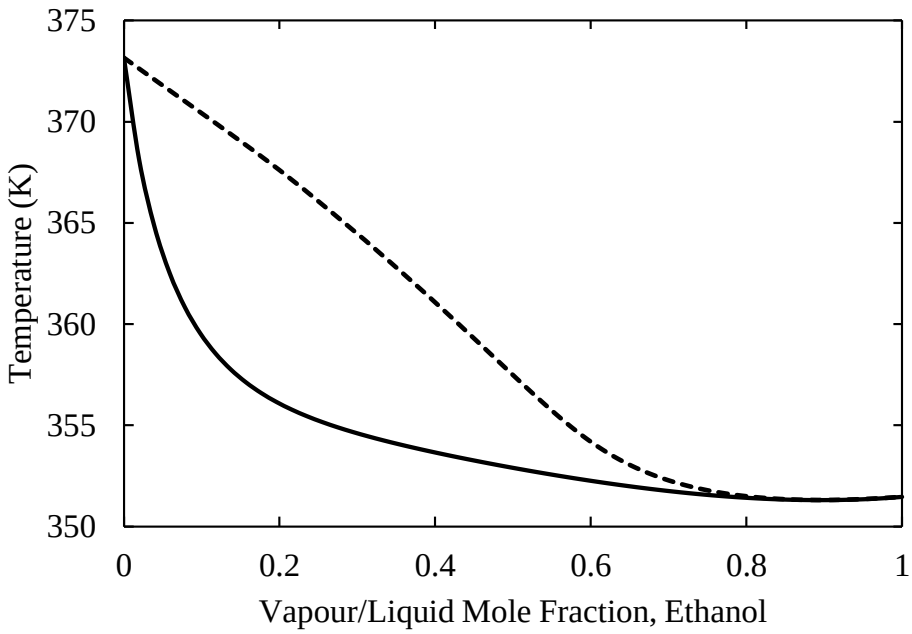

Figure 2.3: An example of a low molecular weight alcohol minimum boiling azeotrope for ethanol and water, a positive deviation from Raoult's law.

2.1.3 Maximum-boiling azeotropes

Maximum-boiling azeotropes occur in mixtures where the attraction between different molecules is stronger than between identical molecules (Hilmen, 2000). This results in an overall decrease of the component vapour pressure and in an increase in the mixtures boiling point above that of the pure component boiling points. Examples of binary mixtures that display this type of behaviour are acetone/water, acetone/chloroform and nitric acid/water (Luyben, 2010; Brits, 2015).

The composition of azeotropic mixtures as a function of temperature and pressure has to be known for the design of thermal separation processes. A large body of research on azeotropic compositions is available in the literature (Rousseau, 1987; Gmehling and Bölts, 1996; Shulgin *et al.*, 2001; Gmehling *et al.*, 2004; Abbas and Gmehling, 2008) and on licensed databases, for example, the Dortmund Data Bank (DDB-AZD).

2.2 Low molecular weight alcohols

The low molecular weight alcohols of interest to this study are ethanol and the isomers of propanol. The synthesis and purification requirements are reviewed to assist in the selection of a suitable separation process.

2.2.1 Ethanol

Ethanol or ethyl alcohol (CH_3CH_2OH) is a low molecular weight alcohol of industrial significance. High purity ethanol, also referred to as absolute alcohol, has a purity of greater than 99% and is used extensively in pharmaceutical preparations, as a solvent and preservative, antiseptic and in perfume (Riemenschneider and Bolt, 2005). Ethanol is widely used as the primary functional component of alcoholic beverages. Moreover, global biofuels legislation generates a significant demand for anhydrous ethanol as a fuel additive and has become the largest single user. Ethanol has widely replaced methyl tert-butyl ether (MTBE) as an oxygenate due to MTBE's associated environmental risk (Henley *et al.*, 2014) and almost all US gasoline is blended with 10% anhydrous ethanol (Adair and Wilson, 2009).

The industrial manufacture of ethanol is via two primary routes, namely fermentation or synthetic. The fermentation of carbohydrates (starch, sugar and/or cellulose) accounts for approximately 70% of global ethanol production (Davenport *et al.*, 2002). Ethanol produced via the anaerobic fermentation route refers to the conversion of sugars (glucose, fructose and sucrose) to ethanol by yeast.

The synthetic route mainly uses the indirect or direct hydration of ethylene, although there has been a shift towards the direct route due to better yields, less by-products, and reduced quantities of pollutants (Riemenschneider and Bolt, 2005). In the primary chemical reaction for the direct hydration process, water vapour and ethylene are mixed at an elevated temperature and pressure and passed over a catalyst impregnated with phosphoric acid. The reaction produces a dilute crude alcohol. A minimum anhydrous ethanol purity of 99.3% is required for fuel grade applications. As water is present in both processing routes, further purification steps are required to produce anhydrous ethanol (Riemenschneider and Bolt, 2005).

2.2.2 Propanols

The propanols (C_3H_7OH) comprise two isomers, 1-propanol and 2-propanol of which the latter is industrially the more important (Riemenschneider and Bolt, 2005). The propanol isomers are mainly used as solvents for coatings, in antifreeze compositions, personal products, chemical intermediates for the production of esters and other organic derivatives. Isopropanol (2-propanol) is extensively used in various stages of the semiconductor manufacturing process for cleaning and washing (Lin and Wang, 2004). Moreover, it is widely used in tobacco production and synthetic chemistry and as an aerosol solvent in medical and veterinary products (Choi *et al.*, 2016). Isopropanol is commonly abbreviated as IPA.

The propanol isomers can be produced via fermentation, but industrial manufacture is mainly by the direct or indirect hydration of propene for IPA and by the hydrogenation of propanal for 1-propanol starting from ethylene. A detailed review of the synthesis routes is offered by Riemenschneider and Bolt (2005). Diisopropyl ether (DIPE) is a by-product of the two major commercial processes for the production of IPA and needs to be recovered from the reaction products in order to produce high purity isopropanol.

The separation of DIPE and IPA is a key downstream process that determines the economic feasibility of the entire process (Lladosa *et al.*, 2007; Luo *et al.*, 2014). However, IPA and DIPE cannot be separated by conventional distillation process because they form a binary minimum boiling homogeneous azeotrope (You, Rodriguez-Donis and Gerbaud, 2016). The minimum purity for IPA is typically 99.8% and the product needs to comply with ASTM D770, DIN 53245 or FED MIL Spec TT-I-735A (Riemenschneider and Bolt, 2005).

An industrial process of interest that produces the abovementioned alcohols in aqueous form is the Fischer-Tropsch process. A typical Fischer-Tropsch aqueous product stream composition (on a dry basis) is shown in Figure 2.4 and indicates an appreciable amount of low molecular weight alcohols may be recovered.

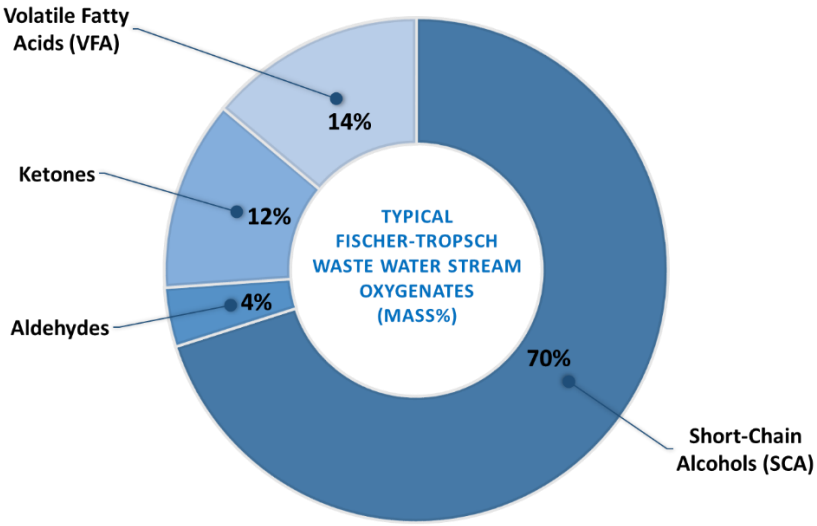

Figure 2.4. Typical Fischer-Tropsch aqueous product stream components. Data from Nel and de Klerk (2007) on a dry basis in mass percentage.

The process involves a series of chemical reactions that produce hydrocarbons of which the majority is alkanes such as diesel. Competing reactions lead to the formation of alcohols and other oxygenated hydrocarbons, for example, ketones that are condensed as an aqueous phase

commonly referred to as reaction water. Short-chain alcohols form approximately 70% (dry basis) of the waste water stream of which the majority are ethanol and propanol isomers, therefore an economic incentive often exists to recover these alcohols (Nel and de Klerk, 2007).

2.2.3 Systems of interest

The main industrial manufacturing processes for C_2 and C_3 low molecular weight alcohols all require reaction mixture separation and purification steps to meet the product marketing specifications, and all these synthesis routes result in an azeotropic mixture. **The primary azeotropic mixture of interest for *ethanol production* is ethanol/water and for *isopropanol production* is diisopropyl ether/isopropanol.**

Diisopropyl ether / isopropyl alcohol azeotropic mixture

The binary mixture of DIPE and IPA form a minimum boiling homogeneous azeotrope with a composition of 78.2 mole% DIPE and 21.8 mole% IPA with a boiling point of 66.16 °C at 101.3 kPa (Lladosa *et al.*, 2007). The azeotrope composition was previously studied by Yorizane *et al.*, (1967) and Verhoeye (1970).

Ethanol / water azeotropic mixture

Ethanol and water forms an azeotrope with a composition of 89.5 mole% ethanol and 10.5 mole% water at 78.12 °C at 101.3 kPa (Gmehling *et al.*, 1994).

Now as the systems of interest are azeotropic in nature, attention is shifted to the selection of appropriate separation technologies.

2.3 Alcohol azeotrope processing options

The separation technologies which can be used to recover C_2 and C_3 alcohols can be considered in two groupings: (i) technologies applicable to the recovery of alcohols from dilute solutions and (ii) those that are used for the dehydration and azeotropic separation of relatively concentrated alcohol streams close to the alcohol solutions azeotrope. The first group includes adsorption, ordinary distillation, liquid-liquid extraction, pervaporation, gas stripping and steam stripping. A detailed review is provided by Vane *et al.*, (2009). The focus of this project is on the dehydration and azeotropic separation of C_2 and C_3 alcohols and thus the literature review is limited to the second group.

As noted in Section 2.1.1 the vapour and liquid compositions of an azeotropic mixture are identical and this results in a distillation boundary. Therefore, for the separation of azeotropic mixtures, advanced distillation techniques are required as a process in which the minor

component in the mixture is selectively removed. These technologies have been classified into four major categories: adsorption, membrane processes, process intensification and enhanced distillation, as shown in Figure 2.5.

Enhanced distillation includes azeotropic, reactive, pressure swing and extractive distillation and have in common that the process modifies the phase behaviour of the azeotropic system, thus resolving the azeotrope. Process intensification, membrane processes and adsorption are typically used in conjunction with distillation, thus forming a hybrid distillation system (Doherty and Knapp, 2000). These processes are grouped together as *alternative separation technologies* and are discussed in the next section.

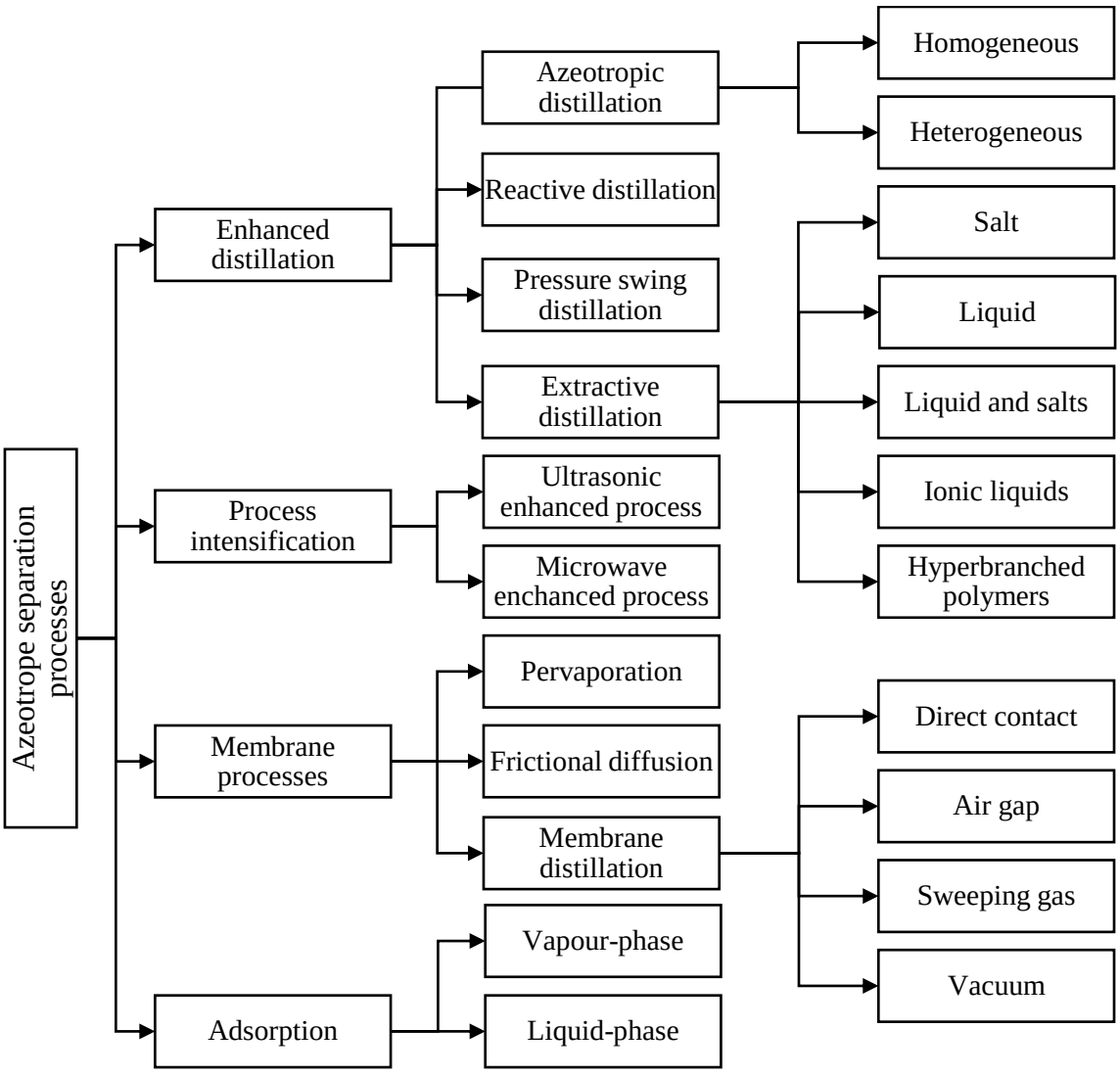

Figure 2.5: Overview of various processing techniques for the separation of azeotropic mixtures. Redrawn and adapted from Vane *et al*., (2009), Frolkova and Raeva (2010) and You (2015).

2.3.1 Alternative separation technologies

Adsorption and adsorption-distillation hybrids

Adsorption (dehydration) processes work on the principle that water is preferentially transferred from the feed to a solid adsorbent material and takes advantage of the difference of molecular size of ethanol and water molecules. Adsorption operates on a cyclic basis of adsorption and desorption as the adsorbed species (e.g. water) must be recovered from the extractant material as it becomes saturated. For the separation of water/ethanol mixtures two adsorption techniques are available, namely, vapour-phase and liquid-phase, but vapour-phase adsorption is usually practiced (Vane *et al.*, 2009). The first relies on inorganic adsorbents such as zeolite molecular sieve (e.g. 3A and 4A), silica gel or lithium chloride (Frolkova and Raeva, 2010). Similarly, for liquid-phase adsorption, type A zeolites or cellulosed-based material are widely used (Vane *et al.*, 2009). In either case, the solid adsorbent is required to exhibit a certain sorption selectively toward the water relative to the ethanol. The same applies to IPA/water azeotropic mixtures.

Although vapour-phase adsorption processes are included in most current corn-to-ethanol production facilities it is not a standalone technology and needs to be combined with a distillation column (Vane *et al.*, 2009). Thus, a molecular sieve system removes water from the ethanol/water vapour mixture leaving the rectification column. Furthermore, Frolkova and Raeva (2010) reported that, compared to membrane-based processes, water adsorption is attracting much less attention from industry and research is limited to mostly process modelling and capacity determination of various adsorbents. Finally, the design specifics of molecular sieve dehydration systems are typically protected by intellectual property rights and internal details are not often disclosed (Vane *et al.*, 2009).

Membrane Processes

Membrane processes include pervaporation, frictional diffusion and membrane-distillation hybrids. Membrane processes work on the principle that one component preferentially moves through a permeable membrane. For alcohol dehydration, the membrane is hydrophilic and selectively transports water. In contrast to molecular sieves, membrane processes can be operated continuously (Frolkova and Raeva, 2009). A further advantage of membrane separation process is that it is not limited by the relative volatility of the mixture (You, 2015). To date, however, this emerging technology has not made significant penetration into the ethanol dehydration market (Vane *et al.*, 2009). Pervaporation accounts for only ca. 4% of all membrane applications in the chemical and pharmaceutical industries (Knauf *et al.*, (1998).

According to Szitkai *et al.*, (2002), the higher capital cost and lower capacities are major disadvantages and does not offset the lower operating costs compared to azeotropic columns.

Process intensification

Process intensification, in terms of separation processes, is a process design approach to increase the functionality of a distillation column. The application of microwave-intensification to distillation systems are limited to a few application, for example extraction, desorption and drying (Mahdi *et al.*, 2014). Gao *et al.*, (2015) investigated the effect of microwaves on the ethanol/benzene binary mixture and concluded that the azeotrope is sensitive to microwave energy. The effect of ultrasonic waves on the VLE of ethers and alcohols were studies by Ripin *et al.*, (2009) and observed that the relative volatility of the mixture could be favourably changed to break the azeotrope. Thus, it appears that these technologies may move or resolve the azeotrope of a mixture by selecting suitable operating conditions. However, these technologies are still in early development phase and further research is required (Mahdi *et al.*, 2014).

2.3.2 Enhanced distillation

Enhanced distillation includes azeotropic, reactive, pressure swing and extractive distillation and have in common that the process modifies the phase behaviour of the azeotropic system, thus resolving the azeotrope (Doherty and Knapp, 2000; Mahdi *et al.*, 2014).

- **Heterogeneous Azeotropic distillation**, uses a mass separating agent known as an entrainer to introduce simultaneously a new azeotrope to the mixture and generates two liquid phases that allows for the separation of the mixture.
- **Reactive distillation**, wherein a separating agent is added to an azeotropic mixture and chemically reacts with a specific component in the original mixture, thus modifying the composition of the mixture.
- **Pressure swing distillation**, where pressure-sensitive azeotropic mixtures can be separated by using two or more columns operated at different pressures.
- **Extractive distillation** is based on the addition of a solvent that shows affinity with one of the components of the original azeotropic mixture and alters its relative volatility. Thus, enhancing the separation of the original mixture.

The dehydration of low molecular weight alcohols through reactive distillation is not widely reported in literature. Dirk-Faitakis and Chuang (2004) performed simulation studies on the water removal from ethanol mixtures using reactive distillation. The water was reacted with

isobutylene to form *tert*-butyl alcohol (TBA) ethyl *tert*-butyl ether (ETBE). The water removal efficiency was ca. 90% and the final reaction product was a mixture of ethanol, TBA and ETBE. The disadvantage was that the TBA and ETBE reactions were reversible and equilibrium limited, thus preventing the production of a high purity ethanol product. An *et al.*, (2014) proposed an improved reactive distillation process to remove the water from the near-azeotropic ethanol/water mixture by reacting the water with ethylene oxide. The benefit is that the reaction is irreversible and not equilibrium limited. However, the authors noted that further research was required. Nonetheless, although an area of active research, no large scale commercial reactive distillation processes to produce anhydrous C_2 and C_3 alcohols have been reported.

For pressure-swing distillation, azeotropic mixtures that completely disappear at a specific pressure may be of interest. However, the ethanol/water azeotropic mixture is not considered as an acceptable candidate for pressure-swing distillation due to its pressure insensitive nature (Hilmen, 2000). For the IPA/DIPE azeotrope, Lladosa *et al.*, (2007) determined that the binary azeotrope is very sensitive to pressure and that pressure-swing distillation could be a useful technique. Luo *et al.*, (2014) investigated the separation of IPA/DIPE with 2-methoxyethanol and compared pressure-swing distillation and extractive distillation. The results showed that the pressure-swing distillation offered a ca. 6.0% reduction on total annual cost and a possible ca. 8.0% energy saving if the system is completely heat-integrated. However, thermal integration can affect the ability to adequately control the distillation columns. Thus, a compromise between plant control and the potential economic advantages offered by pressure-swing distillation is required (Doherty and Knapp, 2000).

Azeotropic and extractive distillation are widely reported as the dominant processes for the production of high-purity C_2 and C_3 alcohols (Riemenschneider and Bolt, 2005; Kiss and Ignat, 2012; Kiss *et al.*, 2012; Ramos *et al.*, 2014). These enhanced distillation technologies based on entrainer-addition methods are reviewed in more detail in the following section.

2.4 Enhanced distillation: Entrainer-addition methods

2.4.1 Azeotropic distillation

In azeotropic distillation, an entrainer forming a new azeotrope with the components of the original azeotropic mixture is added to effect the desired separation. If a single liquid phase is maintained after entrainer addition, the process is referred to as homogeneous azeotropic distillation. For the instance where two liquid phases are formed, the process is known as heterogeneous azeotropic distillation and requires a decanter to separate the organic and

aqueous liquid phases. Homogeneous azeotropic distillation is considered if the mixture formed after entrainer-addition is usable without further separation (Seader and Henley, 2006). The only currently known entrainer for the homogeneous azeotropic distillation of ethanol/water mixtures is ethylenediamine and is known to form a maximum boiling azeotrope (Frolkova and Raeva, 2010).

A typical separation sequence for heterogeneous azeotropic distillation is presented in Figure 2.6. In this process the distillation boundary is crossed by exploiting liquid-liquid immiscibility through the addition of an entrainer that results in liquid-liquid phase splitting. This technique is widely used in the C_2 and C_3 alcohol industries. For example, the United States and Brazil are considered the largest producers of bioethanol in the world and in Brazil ca. 60% of all ethanol dehydration plants are based on heterogeneous azeotropic distillation with cyclohexane as entrainer (Bastidas and Gil, 2010).

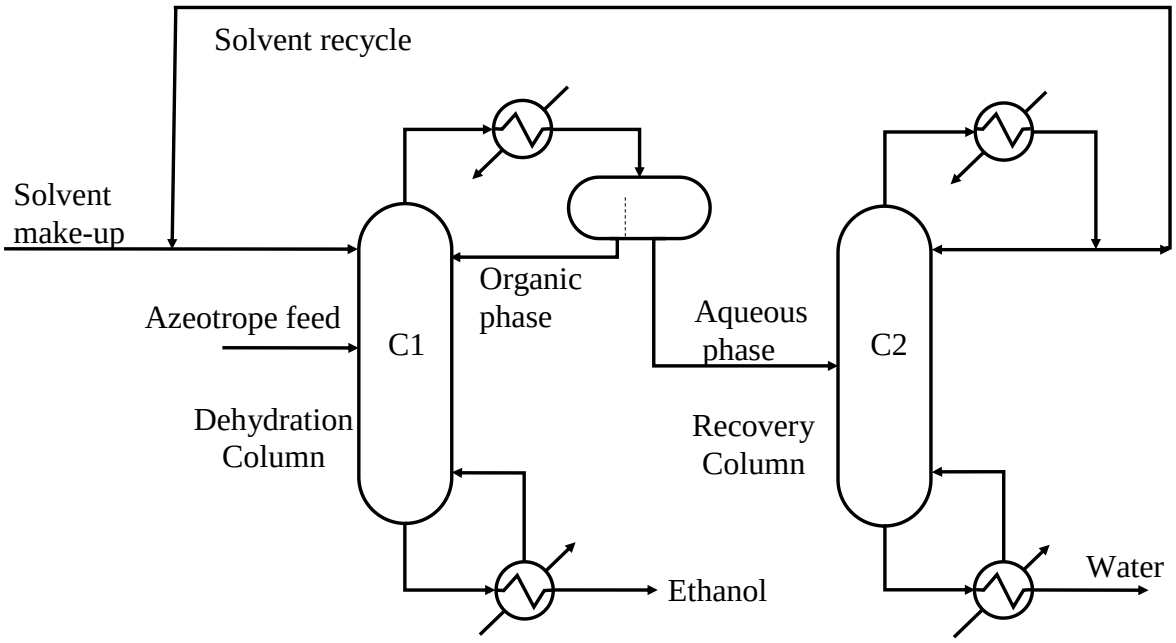

Figure 2.6: Typical separation sequence for azeotropic distillation of ethanol and water. Redrawn from Seader and Henley (2006).

Although heterogeneous azeotropic distillation is often industrially preferred over homogeneous azeotropic distillation at has several disadvantages. The operating range of the system under different feed disturbances is limited by multiple steady states, non-linear behaviour and long transients (Mahdi *et al.*, 2014). Furthermore, it may be difficult to find a thermodynamic model that represents both the VLE and LLE data accurately (Kontogeorgis &

Folas, 2010). Moreover, the entrainer must be vaporised through the top of the azeotropic column, thus consuming large amounts of energy (Vane *et al.*, 2009).

2.4.2 Extractive distillation

Extractive distillation utilises an entrainer (solvent) with a boiling-point appreciably higher than the original azeotropic mixture. Furthermore, the solvent is required to have an affinity with one of the components of the azeotropic mixture in order to change the relative volatility. A typical separation sequence for extractive distillation is presented in Figure 2.7.

The process is normally performed in a two-column system, the solvent is introduced above the feed tray in the first column and is mostly removed as a bottom product. It is essential that the solvent does not form an azeotrope with any of the components in the feed (Seader and Henley, 2006). Solvent examples for ethanol dehydration included ethylene glycol, for IPA/water is DMSO and for IPA/DIPE is 2-methoxyethanol (Lladosa *et al.*, 2007; Frolkova and Raeva, 2010; Liang *et al.*, 2014; Yuan *et al.*, 2014).

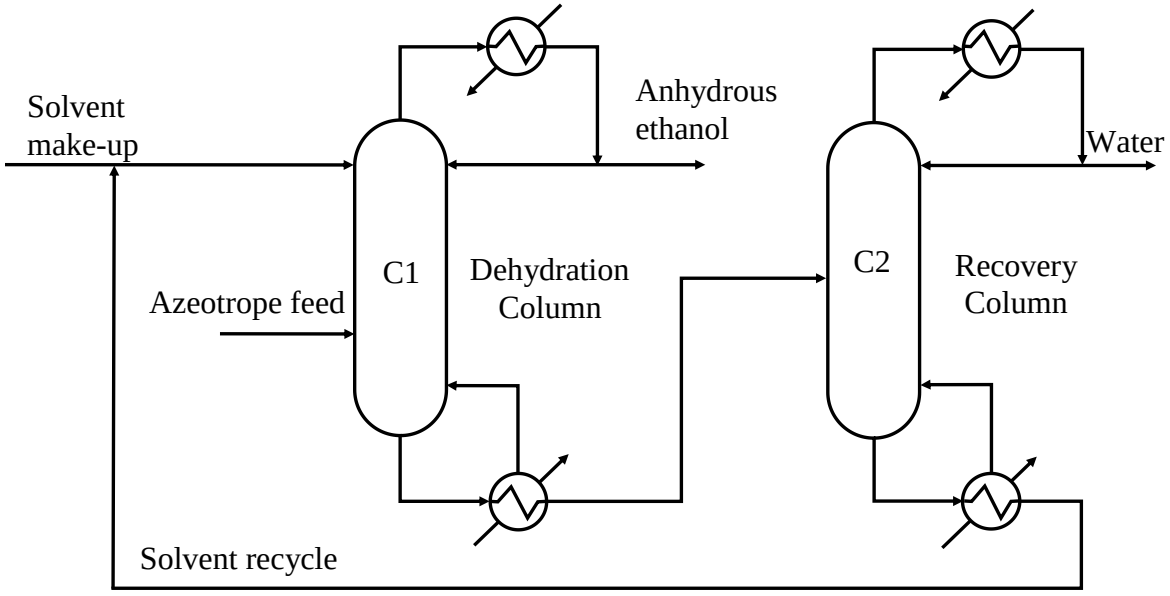

Figure 2.7: Typical separation sequence for extractive distillation of ethanol and water. Redrawn and simplified from (Gil, García, and Rodríguez, 2014).

Extractive distillation shows some advantages compared to heterogeneous azeotropic distillation. Extractive distillation is a partial vapourisation process, thus less energy intensive. Furthermore, the quantity of solvent is lower, which affects the diameter of the columns, thereby reducing the capital cost of the equipment (Bastidas and Gil, 2010). Extractive

distillation is a proven separation technique for non-ideal mixtures, including minimum boiling azeotropes present in the C_2 and C_3 manufacturing industry (Luyben and Chien, 2010).

2.5 Mass separating agent selection

2.5.1 Ethanol/water azeotropic mixture

A widely known example of a heterogeneous azeotropic distillation process is the dehydration of an ethanol/water mixture using benzene. However, despite the excellent entrainer properties of benzene, the fact that it is a cancer-causing agent prompted the consideration of alternative entrainers. Thus, for a number of years, hydrocarbons (e.g. hexane to octane and their isomers) have been proposed as alternative entrainers to benzene, the most popular being cyclohexane (Lladosa *et al.*, 2008). Additionally, common fuel additives such as DIPE and di-n-propyl ether (DNPE) have also been proposed.

These hydrocarbons and dipropyl ethers generally occur, or are favourable in fuels. Furthermore, they form heterogeneous azeotropes with alcohols and water. Thus, they are attractive entrainers, because alcohol purity constraints in the entrainer recovery system is reduced (Pla-Franco *et al.*, 2014). DIPE is a branched ether and is regarded as a less polluting and non-toxic alkyl ether. For several years, DIPE has been the subject of several studies in order to determine its potential as a fuel additive (Alonso *et al.*, 2004; Hwang *et al.*, 2008; Lladosa *et al.*, 2008). Furthermore, the low water solubility of DIPE (Hwang *et al.*, 2008) reduces concerns over groundwater contamination, a major shortcoming with the use of MTBE and ETBE (Vorenburg *et al.*, 2005).

The Separation Technology group of Stellenbosch University is actively involved in research to identify suitable mass separating agents (MSA) for ethanol/water azeotropic mixtures and several other industrial azeotropes. This is to improve process energy efficiency and to mitigate carbon footprints by providing sustainable entrainer options for the future (Pienaar, 2012; Brits, 2015). Furthermore, the phase equilibrium measurements as well as modelling with property methods of these systems are also of interest. In recent work published by Pienaar *et al.*, (2013) DIPE was confirmed as a suitable entrainer for the azeotropic distillation of the ethanol/water mixture. However, it was concluded that improved thermodynamic modelling work is required to develop a reliable process simulation. In support of continuing the research work, DIPE is selected in this thesis as the mass separating agent for the ethanol/water azeotropic mixture using heterogeneous azeotropic distillation. **Therefore, this project will consider the heterogeneous azeotropic distillation of ethanol and water using DIPE as entrainer.**

2.5.2 Diisopropyl ether/isopropyl alcohol azeotropic mixture

The two key azeotrope separation technologies identified from literature is extractive and azeotropic distillation. In the previous section, the ethanol/water/DIPE heterogeneous azeotropic distillation system was selected. Accordingly, for the case of the minimum boiling azeotrope of DIPE and IPA only extractive distillation is considered.

Lladosa *et al.* (2007) investigated this system and reported that 2-methoxyethanol (widely known by its trade name, methyl cellosolve™) is an excellent solvent to break the azeotrope based on the vapour-liquid equilibrium experimental data. Scheibel's criterion (Scheibel and Montross, 1948) and calculation of the separation factor were employed to support the selection. Luo *et al.*, (2014) further investigated the extractive distillation of DIPE/IPA with 2-methoxyethanol and confirmed the findings of Lladosa *et al.* (2007) by comparing the relative volatility of several possible entrainers, as shown in Table 2.1.

Table 2.1: Results of entrainer selection for extractive distillation system. Redrawn from (Luo *et al.*, 2014)

DIPE + IPA azeotrope system		
Entrainer (100 wt%)	Bubble point (K)	Relative volatility (average)
2-methoxyethanol	397.67	2.30
1-methoxy-2-propanol	393.24	1.77
3-methyl-1-butanol	404.16	1.41

A known heuristic is that the higher the relative volatility, the easier the separation. As such, 2-methoxyethanol shows a higher relative volatility and also does not create further azeotropes in the system. Luo *et al.*, (2014) regressed the binary interaction parameters for the NRTL activity coefficient model from the experimental data of Lladosa *et al.* (2007) and proposed a two column extractive distillation process. **As a second separation process this project thus consider the extractive distillation of DIPE and IPA with 2-methoxyethanol as the solvent.**

2.6 Chapter summary

The aims of this chapter were to review the phase behaviour of C_2 and C_3 alcohol systems and identify the preferred process separation technologies. A key outcome was that heterogeneous azeotropic and extractive distillation are the two separation technologies most widely used for the purification of C_2 and C_3 alcohols and were thus selected for the separation of the selected systems.

Furthermore, the phase behaviour of a system was identified as a determining factor in the design of azeotropic separation processes. The mixtures of interest to this study (DIPE/ethanol/water and DIPE/IPA/2-methoxyethanol) display strong self-association and cross-association. As such, the phase behaviour and thermodynamic properties of these mixtures are strongly affected as the actual molecular properties of the molecular clusters (dimers and tetramers) are different from the monomeric molecules. In order to obtain reliable thermodynamic modelling results in systems where hydrogen bonding is encountered, the molecular dynamics of association and solvation need to be accounted for by the selected thermodynamic model. Subsequently, the next section will review thermodynamic models applicable to these conditions.

Chapter 3
Thermodynamic Modelling Basis

This chapter performs a review of thermodynamic modelling approaches for strongly non-ideal systems, especially C_2 and C_3 alcohol azeotropic mixtures. The aim is to identify models from literature that are most likely to accurately correlate the fluid phase equilibria of low-pressure systems with polar compounds and multiple liquid phases. In order to gain an understanding of the thermodynamic basis, the foundation texts of Prausnitz *et al.* (1999), Smith *et al.* (2005), and Sandler (2006) were reviewed and are used throughout. Moreover, the recent works of Kontogeorgis and Folas (2010) and de Hemptinne (2012) provide supplemental insights in terms of the industrial application of thermodynamic models. The theoretical aspects such as fugacity and activity coefficients are presented first, followed by a model screening process based on literature guidelines for the nature of the mixtures in this work. The chapter is concluded by considering the identified models in further detail and shortlisting candidate models for further screening and selection in Chapter 7.

3.1 Important factors in thermodynamic model selection

An essential requirement for commercial process simulation software is the reliable estimation of a mixtures phase behaviour and its physical properties. All unit operation models need a property method, which is a collection of the property calculation routes inherent in the software. These property methods are generally classified as either thermodynamic or transport property methods. The thermodynamic property methods class typically includes calculation methods for the mixtures fugacity coefficient, K-value, enthalpy, Gibbs energy and volume. The transport property methods class includes for example viscosity, thermal conductivity, diffusion coefficient and surface tension (Sandler, 2015).

Multiple methods are available to calculate a given property of interest, for example, vapour-liquid equilibrium or if phase splitting occurs, and making an appropriate choice for a specific problem is important. A number of factors, listed in Table 3.1, determine which methods are more suitable than others for a particular case.

Table 3.1: Important factors in basic data method selection. Adapted from (Carlson, 1996).

Factors	Example
Available/preferred simulation software	Aspen Plus, PRO/II, HYSYS, ChemCAD, Prosim, VMGSim, STFlash,
Type of system	Pure component, binary mixture or multicomponent mixture
Kind of physical property	Thermodynamic, transport, surface
Nature of substance(s)	Non-polar, polar, associating fluids, electrolytes, polymers, solids
Conditions of the system or process	Sub- or supercritical temperature Low or high pressure Dilute or concentrated mixture Expected phase behaviour
Required accuracy	Screening or design purpose Importance of missing parameters
Availability of experimental data	Fit or estimate missing parameters
Computational speed	Simple or complex model(s)

In this study, the focus is on determining how phase equilibrium uncertainty effects the final process design. The thermodynamic property methods and its description of phase equilibria are therefore reviewed next.

3.2 Generalised thermodynamic modelling approaches

An important assumption in thermodynamic and process simulation calculations is that the vapour and liquid phases, and sometimes a second liquid, are in thermodynamic equilibrium. The criterion for phase equilibrium, for a mixture of components, is the equality of fugacities (f) for each component in each phase (Sandler, 2006):

$$f_i^L(T,P,x) = f_i^V(T,P,y) \tag{3.1}$$

The fugacity (f) of a component within a given phase can, in concept, be thought of as the tendency of that component to move from one phase to another (Kontogeorgis and Folas, 2010). To provide a tangible connotation to the fugacity of a species, it can be thought of as the pressure

of an ideal gas displaying properties equivalent to the real fluid at the reference temperature and composition (Sandler, 2006).

In reality though, fugacity is not itself a fundamental fluid property, but rather derived from the chemical potential of the species. So, the actual thermal equilibrium conditions from which Equation 3.1 was derived are the equality of temperature, pressure and chemical potential of each species (i) in each phase (θ,λ):

$$T^{\theta} = T^{\lambda} \tag{3.2}$$

$$P^{\theta} = P^{\lambda} \tag{3.3}$$

$$\mu_i^{\theta} = \mu_i^{\lambda} \tag{3.4}$$

Furthermore, at these conditions the Gibbs energy is at its lowest (de Hemptinne, 2012). In order to calculate the fugacity a reference state is required, which is either an ideal gas or an ideal liquid solution.

3.2.1 The vapour phase fugacity

Using the ideal gas as the reference state the vapour phase fugacity is expressed using the residual approach (Smith *et al.*, 2005):

$$f_i^V = y_i \varphi_i^V P \tag{3.5}$$

with

f_i^V the vapour phase fugacity of component *i* in the solution.

y_i the molar fraction of component *i* in the vapour phase.

φ_i^V the vapour phase fugacity coefficient of component *i* in the solution (*phi*).

P the system pressure.

With the residual approach, the vapour phase fugacity coefficient (φ_i^V) is calculated with an equation of state and is in reference to the residual Gibbs energy:

$$ln\varphi_i = \left[\frac{\partial\left(\frac{nG^R}{RT}\right)}{\partial n_i}\right]_{P,T,n_j} \tag{3.6}$$

with

n_i the mol of component *i* in the solution.

G^R the residual molar Gibbs energy, determine by and EoS.

φ_i the fugacity coefficient of component *i* in the solution (*phi*).

At a system pressure below 10 bar and if the temperature is not very low, the ideal gas approximation can be used, which states (de Hemptinne, 2012): $\varphi_i^V = 1$.

3.2.2 The liquid phase fugacity

Similarly, using the ideal gas as the reference state the liquid phase fugacity can also be expressed using the residual approach (Smith *et al.*, 2005):

$$f_i^L = x_i \varphi_i^L P \tag{3.7}$$

with

f_i^L the liquid phase fugacity of component *i* in the solution.

x_i the molar fraction of component *i* in the liquid phase.

φ_i^L the liquid phase fugacity coefficient of component *i* in the solution (*phi*).

Here, again, the liquid phase fugacity coefficient (φ_i^L) is calculated with an equation of state and Equation 3.6 applies.

Alternatively, an ideal solution can be selected as the reference state, then:

$$f_i^L = x_i \gamma_i f_i^0 \tag{3.8}$$

with

f_i^L the liquid phase fugacity of component *i* in the liquid solution.

γ_i the activity coefficient of component *i* in the liquid solution (*gamma*).

x_i the molar fraction of component *i* in the liquid solution.

f_i^0 the standard fugacity, usually the fugacity of the pure liquid at system temperature and pressure.

When using the definition of the activity coefficient to calculate the liquid fugacity, it is known as the excess approach and is in reference to the excess Gibbs energy:

$$ln\gamma_i = \left[\frac{\partial\left(\frac{nG^E}{RT}\right)}{\partial n_i}\right]_{P,T,n_j} \tag{3.9}$$

with

n_i the mol of component *i* in the solution.

G^E the excess Gibbs energy, determined by an activity coefficient model.

The most general expression for the liquid phase fugacity is then given by (Sandler, 2006):

$$f_i^L = P_i^{Sat} \varphi_i^{Sat} \wp_i \gamma_i x_i \tag{3.10}$$

with

f_i^L the liquid phase fugacity of component *i* in the liquid solution.

P_i^{Sat} the saturation pressure of pure component *i*, here the liquid vapour pressure.

φ_i^{Sat} the liquid phase fugacity coefficient of pure component *i* at saturation using the vapour phase.

γ_i the activity coefficient of component *i* in the liquid solution (*gamma*).

x_i the molar fraction of component *i* in the liquid solution.

$\wp_i = exp\left(\frac{1}{RT}\int_{P_i^{Sat}}^{p} v_i^L dP\right)$ and is the Poynting correlation.

3.2.3 Excess approach with asymmetric convention

The expression of Equation 3.8 in the excess approach assumes that properties of component *i* can be calculated at the temperature and pressure of the mixture (i.e. exists as a pure component). For species at infinite dilution, for example in an azeotropic separation system decanter, this may be a strong restriction (de Hemptinne, 2012). By selecting a generalised reference state for the activity coefficient Equation 3.8 is redefined:

$$f_i^L = x_i \gamma_i^{ref} f_i^{L,ref} \tag{3.11}$$

with

f_i^L the liquid phase fugacity of component *i* in the liquid solution.

$f_i^{L,ref}$ the liquid phase fugacity of component *i* at the reference state.

γ_i^{ref} the activity coefficient of component *i* in the liquid solution at a reference state.

The reference state can be the pure component or user-defined and is most often at infinite dilution (de Hemptinne, 2012).

Alternatively, Henry's constant may be used to calculate the fugacity and is defined as:

$$H_{i,s}^{Sat}(T) = \lim_{\substack{x_i \to 0 \\ P \to P_s^{Sat}}} \left[\frac{f_i^L(T,P)}{x_i}\right] \tag{3.12}$$

with

$H_{i,s}^{Sat}$ the Henry's constant defined at the solvent's vapour pressure P_s^{Sat} (i.e. infinite dilution).

As Henry's constant is not a function of pressure the Poynting correction is used to account for pressure; the liquid fugacity for the solute is then calculated as (de Hemptinne, 2012):

$$f_i^L = H_{i,s}^{Sat} \wp_i^{\infty} \gamma_i^H x_i \tag{3.13}$$

with

$\wp_i^{\infty}$ the dilute Poynting correction:

$$\wp_i^{\infty}(T,P) = exp\frac{v_i^{-\infty}(P - P_S^{Sat})}{RT} \tag{3.14}$$

$v_i^{-\infty}$ the infinite dilution partial molar volume of component *i* in the solution.

$\gamma_i^H(T,x)$ the asymmetric activity coefficient

Similar types of models are used to calculate both the asymmetric and symmetric activity coefficients. It is shown in Equation (3.15) that the asymmetric activity coefficient becomes one at infinite dilution:

$$\gamma_i^H(T,x) = \frac{\gamma_i(T,x)}{\gamma_i^{\infty}(T,x_i = 0)} \tag{3.15}$$

with

$\gamma_i^{\infty}(T,x_i = 0)$ the activity coefficient of the solute at infinite dilution of component *i* in the solute given by the symmetric activity coefficient.

According to de Hemptinne (2012), Equation 3.13 is only used for the solutes and Equation 3.10 remains valid for the solvents. As such, it is referred to as the asymmetric approach in a solvent + solute mixture. This approach can be extended to all cases where the solutes are in low concentration in a phase. For example, gases dissolved in a liquid (Hou, Maitland, and Trusler, 2013), all solutes in an aqueous phase (Faramarzi et al., 2009) and ions in an aqueous phase (de Hemptinne, 2012).

3.2.4 Section highlights

Thermodynamic terminology often refers to two common approaches for vapour-liquid equilibria calculations; the homogeneous (*phi-phi*) approach or the heterogeneous (*gamma-phi*) approach (Kontogeorgis and Folas, 2010) and is summarised in Table 3.2.

Starting from the iso-fugacity condition, the two different approaches can be applied (Schmid and Gmehling, 2010):

$$\textit{Homogeneous approach}: \quad x_i\varphi_i^L = y_i\varphi_i^V \tag{3.16}$$

$$\textit{Heterogeneous approach}: \quad x_i\gamma_i f_i^0 = y_i\varphi_i^V P \tag{2.1}$$

Table 3.2: Nomenclature of thermodynamic approaches. Redrawn from (de Hemptinne, 2012).

Approach	**Vapour fugacity calculation**	**Liquid fugacity calculation**
Homogeneous approach (*φ- φ)*	Residual approach	Residual approach
Heterogeneous approach *(γ-φ)*		Excess approach, symmetric convention
Heterogeneous approach *(γ-φ)*		Excess approach, asymmetric convention.

The *Homogeneous approach* (*phi-phi)* uses fugacity coefficients (φ_i) to account for the real behavior in both the liquid and the vapour phase. For this approach an equation of state (EoS) with dependable mixing rules is required to describe the pressure–volume–temperature behaviour as a function of composition of the liquid and the vapour phase (Schmid and Gmehling, 2010).

The *Heterogeneous approach* (*gamma-phi)* uses the ideal gas as the reference state for the vapour and the ideal solution for the liquid phase. This approach is used for excess Gibbs energy (g^E)- or group contribution models, such as UNIFAC (Fredenslund *et al.*, 1975) or modified UNIFAC (Gmehling and Weidlich, 1986).

Kontogeorgis and Folas (2010) explain that the distinction between the *gamma-phi* (*γ-φ*) and *phi-phi* (*φ-φ*) approaches is not fundamental in nature, but rather a legacy approach. The classical cubic equations of state initially used in combination with the van der Waals one-fluid mixing rules were mostly suitable for simple systems containing mixtures of hydrocarbons and gasses. As this was a limitation, numerous activity coefficient models were subsequently developed to describe systems that are more complex. Chen and Mathias (2002) provides a concise overview on the historic development of thermodynamic models.

Deiters and de Reuck (1999) estimates the total count of published models if variants are considered, in excess of 2000 (as of 1999). These models have varying theoretical backgrounds and mathematical complexity. The next section reviews the typical classification of thermodynamic models and identifies the most suitable candidate models for the systems in this study.

3.3 Thermodynamic evaluation and model selection

In general, thermodynamic models can be classified as shown in Figure 3.1. The list does not cover all available thermodynamic models, but indicates the most representative methods from each of the various classes. The classical models include the Equations of State (EoS), activity coefficient models and the excess Gibbs energy mixing rules for EoS. An additional class of thermodynamic models, typically referred to as advanced models, cover methods based on association theories for example SAFT (Statistical Association Fluid Theory) and CPA (Cubic-Plus-Association).

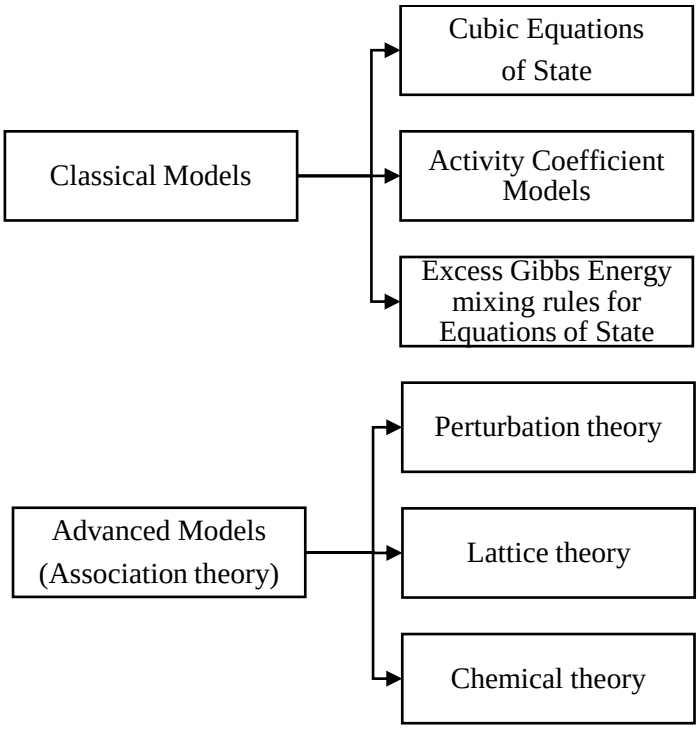

Figures 3.1: Typical classification of thermodynamic models.

The selection of a thermodynamic model that will accurately describe the phase equilibrium of the C_2 and C_3 low molecular weight alcohol systems is extremely important. To this end, Figures 3.2 and 3.3 provide model selection guidelines based on the behaviour of the system. The thermodynamic model names presented here are given as in the Aspen Plus® process simulator.

A summary of the model selection guidelines with important limitations is shown in Table 3.3 and it is noted that for low pressure systems with polar compounds and multiple liquid phases the local composition activity coefficient models are recommended. In the case of vapour phase association, the Hayden O'Connell EoS coupled with an activity coefficient model is an option

or an advance model such as the cubic plus association EoS. The PSRK and SR-POLAR models may be reliable options if no experimental data is available.

In terms of local composition activity coefficient models, **only NRTL and UNIQUAC** are considered suitable, as the Wilson model is intended for a single liquid phase only.

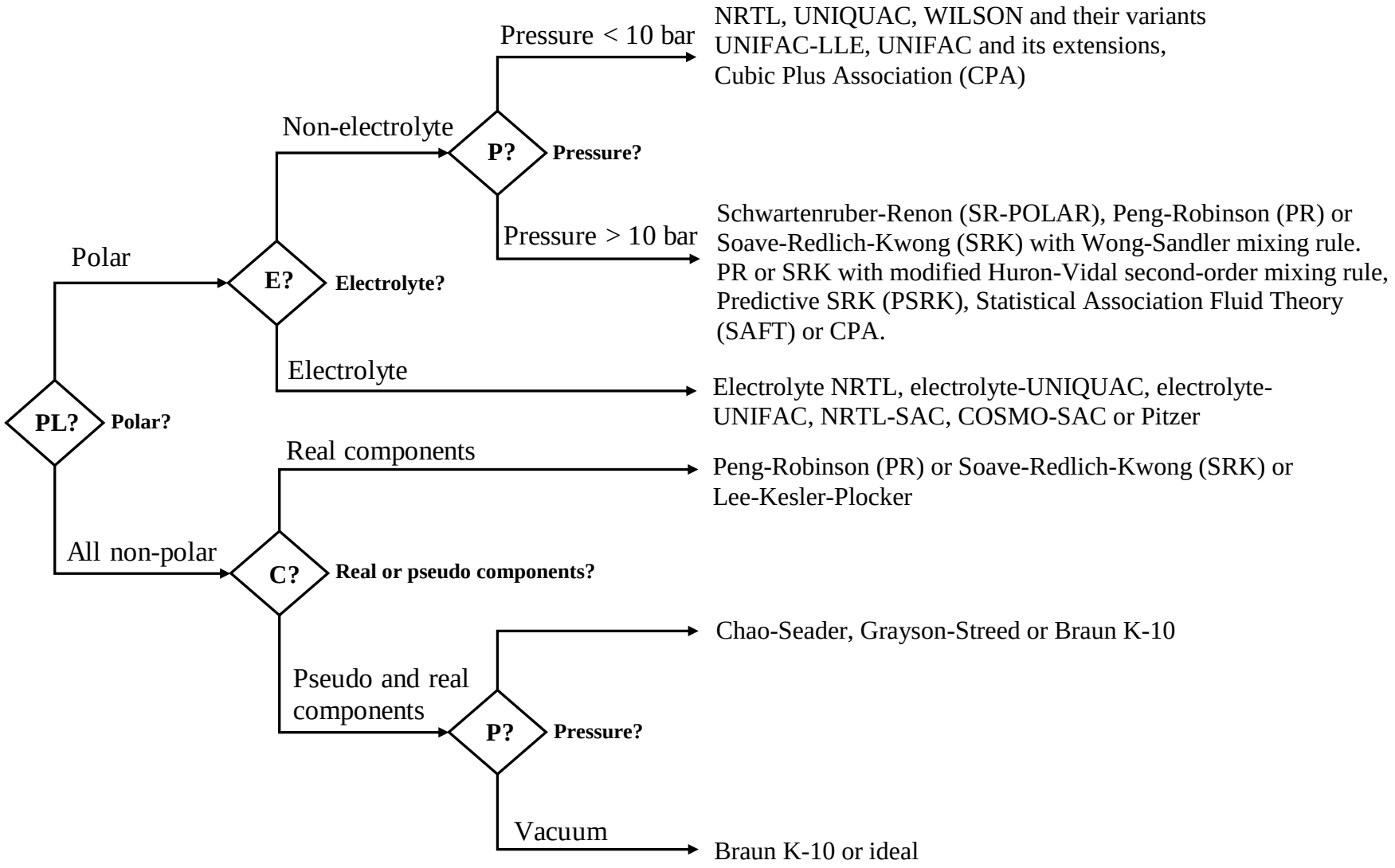

Figure 3.2: Thermodynamic models and an example selection tree. Adapted from Kontogeorgis and Folas (2010) and (de Hemptinne, 2012).

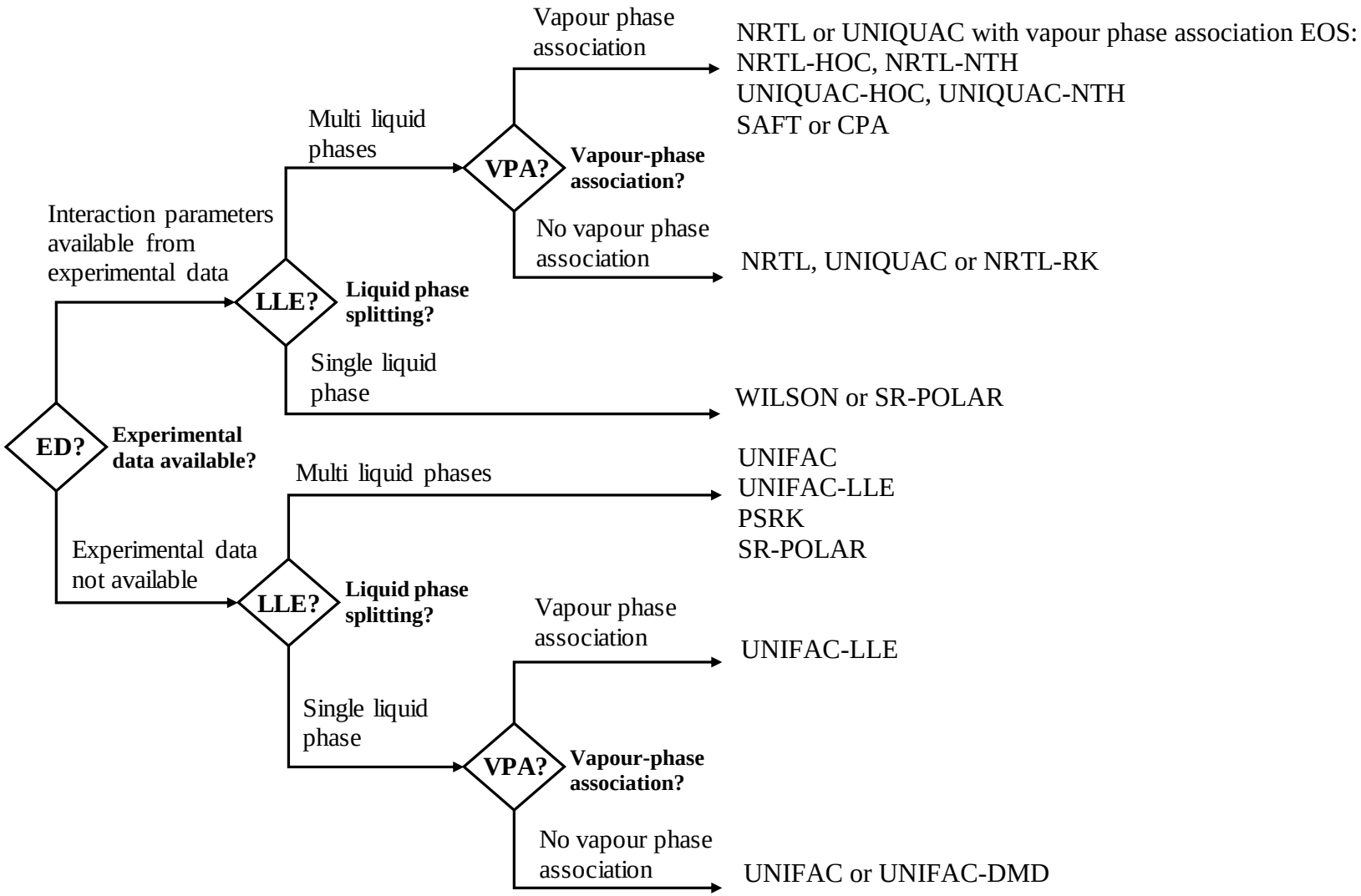

Figure 3.3: Available thermodynamic models in commercial process simulators and an example of a selection tree. Adapted from Carlson (1996).

Table 3.3. Summary of model selection guidelines with limitations. Redrawn and adapted from Kontogeorgis and Folas (2010).

Types of mixtures	**Low pressure - recommended models**	**High pressure - recommended models**	**Limitations**
Hydrocarbons	Ideal solution, Simple activity coefficient models, Cubic EoS	Cubic EoS	Infinite dilution conditions High-molecular-weight compounds
Hydrocarbons/gases (CO_2, N_2, C_1, C_2, H_2S)	Cubic EoS	Cubic EoS with k_{ij}	Need of k_{ij} databases/correlations for solid-gas systems
Polar compounds *General*	Activity coefficient model (Margules, Van Laar) Local Composition e.g. Wilson, NRTL, UNIQUAC	EoS/G^E models, e.g. MHV2, LCVM, PSRK and WS SAFT, CPA, SR-POLAR	Systems with complex chemical, water-hydrogen bonding compounds, solids, liquid, polymers, electrolytes Multiphase equilibria, multi-component
Gas/polar compounds	-	EoS/G^E models, e.g. MHV2, LCVM, PSRK SR-POLAR	Systems and gases for which parameters are not available
Polar compounds with S*ize/asymmetric systems*	Activity coefficient models, modified UNIFAC	LCVM	Systems and gases for which parameters are not available
Complex and associating systems	UNIQUAC	EoS/G^E using UNIQUAC PC-SAFT CPA	Water systems, LLE
Predictions	UNIFAC	EoS/GE using UNIFAC SR-POLAR	Often good only for preliminary design

MHV2: modified Huron-Vidal second order mixing rule; ***LCVM***: a linear combination of the Vidal and Michelsen mixing rules coupled with the original UNIFAC; ***PSRK***: predictive Soave-Redlich-Kwong; ***WS***: Wong-Sandler mixing rule; ***CPA***: cubic-plus-association equation of state; ***LLE***: liquid-liquid equilibrium.

Therefore, it is clear the activity coefficient models (NRTL and UNIQUAC) or EoS/G^E models are most likely to accurately correlate the fluid phase equilibria of low-pressure systems with polar compounds and multiple liquid phases as encountered in C_2 and C_3 alcohol azeotropic systems. The SR-POLAR and CPA EoS are also of interest and will thus be considered as well.

3.4 Evaluating activity coefficients: Excess Gibbs energy models

The classification of activity coefficient models according to Kontogeorgis and Folas (2010) is presented in Figure 3.4. The NRTL and UNIQUAC models were identified as potential property methods for the modelling of the phase equilibrium of the systems in this work and are considered next.

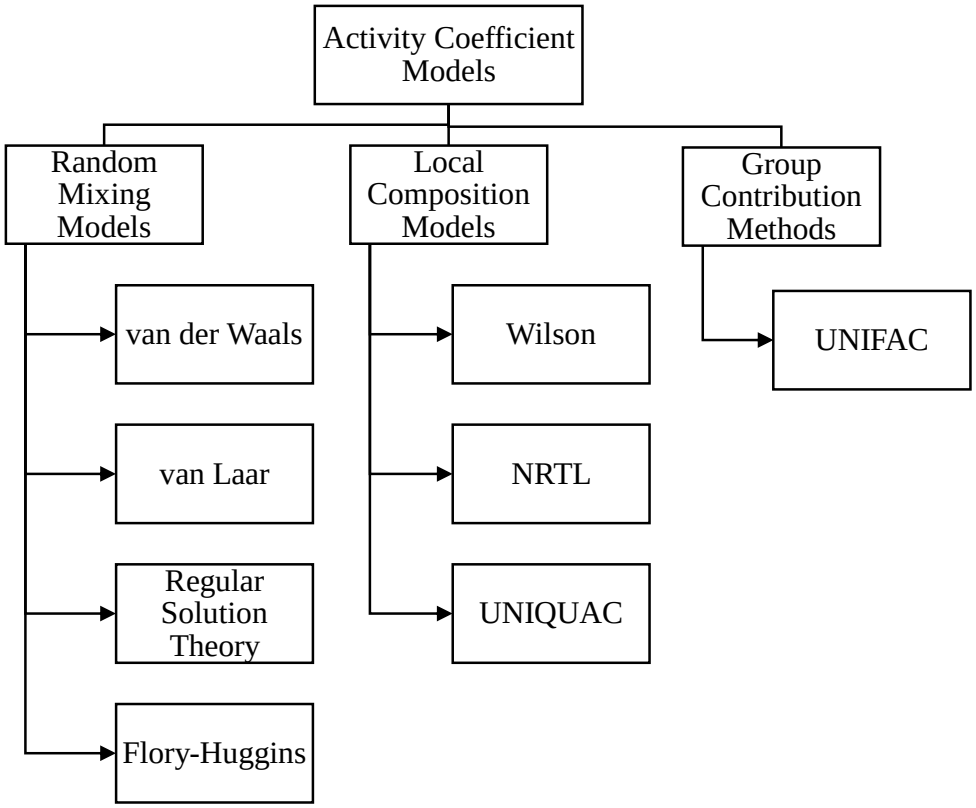

Figure 3.4: Classification of activity coefficient models according to Kontogeorgis and Folas (2010).

3.4.1 Non-random two-liquid (NRTL) model

The NRTL model was developed by Renon and Prausnitz (1968) and is a widely used activity coefficient models in fluid phase equilibria. The model is based on the local composition theory of Wilson and the two-liquid solution theory of Scott (Hildebrand and Scott, 1964). For a binary system, the NRTL model requires three adjustable parameters, which include two energy interaction parameters (a_{ij} and a_{ji}) and a non-randomness factor (α_{ij}).

The NRTL equation for multi-component mixtures:

$$\frac{G^E}{RT} = \sum_i x_i \frac{\sum_j x_i \tau_{ji} G_{ji}}{\sum_k x_k G_{ki}} \tag{3.17}$$

where

$$G_{ij} = exp\left(-a_{ij}\tau_{ij}\right) \tag{3.18}$$

$$\tau_{ij} = a_{ij} + \frac{b_{ij}}{T} + e_{ij}lnT + f_{ij}T \tag{3.19}$$

Here α_{ij} is the non-randomness factor in the mixture, G_{ij} is energy interaction between i and j component molecules, a_{ij} is energy interaction parameter, x_i is the mole fraction of component i, R is the universal gas constant and T is the mixture temperature. In general the non-randomness factor (α_{ij}) depends on the mixture properties and is temperature independent.

The NRTL activity coefficient expressions for any component i is given by:

$$ln\gamma_i = \frac{\sum_j x_j\tau_{ji}G_{ji}}{\sum_k x_k G_{ki}} + \sum_j \frac{x_j G_{ij}}{\sum_k x_k G_{kj}}\left(\tau_{ij} - \frac{\sum_m x_m\tau_{mj}G_{mj}}{\sum_k x_k G_{kj}}\right) \tag{3.20}$$

3.4.2 Universal Quasi-Chemical (UNIQUAC) model

The UNIQUAC model developed by Abrams and Prausnitz (1975) generalises the analysis by Guggenheim (Sandler, 2006) and extends it to asymmetric mixtures (molecules that significantly differ in shape and size). It combines concepts set forth from the Wilson and NRTL excess models in that it applies the local composition concept and the two-fluid theory to produce a two parameter expression.

However, UNIQUAC uses the local area fraction (θ_{ij}) as the most important concentration variable, as opposed to the local volume fractions (Bhownath, 2008). The local area fraction (θ_{ij}) is approximated by expressing a molecule through a set of bonded segments, where r is the relative number of segments per molecule (volume parameter) and q is the relative surface area of the molecule (surface parameter).

The UNIQUAC model for a multi-component mixture is:

$$\frac{G^E}{RT} = \left(\frac{G^E}{RT}\right)_{combinatorial} + \left(\frac{G^E}{RT}\right)_{resiual} \tag{3.21}$$

$$\left(\frac{G^E}{RT}\right)_{combinatorial} = \sum_i x_i \ln\frac{\Phi_i}{x_i} + \frac{z}{2}\sum_i q_i x_i \ln\frac{\theta_i}{\Phi_i} \tag{3.22}$$

$$\left(\frac{G^E}{RT}\right)_{residual} = -\sum_i q_i' x_i \ln\left[\sum_j \theta_j' \tau_{ji}\right] \tag{3.23}$$

The combinatorial term corrects for the effects due to asymmetric molecules and the residual term for differences in intermolecular forces, with segment fraction Φ_i and area fractions θ_i and θ_i' are given by

$$\Phi_i = \frac{x_i r_i}{\sum_j x_j r_j} \tag{3.24}$$

$$\theta_i = \frac{x_i q_i}{\sum_j x_j q_j} \tag{3.25}$$

$$\theta_i' = \frac{x_i q_i'}{\sum_j x_j q_j'} \tag{3.26}$$

Additionally,

$$\tau_{ij} = exp\left[a_{ij} + \frac{b_{ij}}{T} + c_{ij}\ln T + d_{ij}T + e_{ij}T^2\right] \tag{3.27}$$

The only adjustable parameters are the binary parameters a_{ij}, b_{ij}, c_{ij}, d_{ij}, *and* e_{ij}.

The activity coefficient expressions are a combination of the combinatorial and residual terms:

$$\ln\gamma_i = \ln\gamma_i^C + \ln\gamma_i^R \tag{3.28}$$

$$\ln\gamma_i^C = \ln\frac{\Phi_i}{x_i} + \frac{z}{2}q_i \ln\frac{\theta_i}{\Phi_i} + l_i - \frac{\Phi_i}{x_i}\sum_j x_j l_j \tag{3.29}$$

$$\ln \gamma_i^R = -q' \ln\left(\sum_j \theta_j' \tau_{ji}\right) + q_j' - q_i' \sum_j \frac{\theta_j' \tau_{ij}}{\sum_k \theta_k' \tau_{kj}} \tag{3.30}$$

where

$$\mathrm{l}_i = \frac{z}{2}(r_i - q_i) - (r_i - 1) \tag{3.31}$$

The UNIQUAC model, as is the case for the NRTL model, is readily extendable to handle multi-component mixtures and has limited explicit temperature dependence (Prausnitz *et al.*, 1980).

3.5 Vapour phase non-ideality

It is common for vapour-liquid equilibrium studies performed at atmospheric to moderate pressures (10 to 15 bar) to assume the vapour phase behaviour is ideal (Kontogeorgis & Folas, 2010). However, describing fluid-phase equilibria at moderate to high pressures or in mixtures of complex substances requires accurate vapour-phase properties. The low moleculare weight alcohols in this study may be considered complex mixtures due to association and solvation.

Frurip, Curtiss and Blander (1981) studied the hydrogen bonding of alcohol vapours (methanol, ethanol, IPA and t-butanol) as a function of temperature (330 - 420 K) and pressure (11 - 240 kPa) and concluded that in addition to the monomer species, dimer and tetramer clusters also exist in the vapour phase. Thus, the thermodynamic methods selected in this work may have to account for the non-ideal behaviour introduced by vapour phase association. Contemporary methods use cubic EoS with complex combining and mixing rules for their parameters to factor in vapour phase association.

However, if liquid-phase non-idealities are modelled by excess Gibbs energy expressions, vapour non-idealities can be adequately correlated by the virial equation, often truncated at the 2nd virial coefficient which is based on molecular theory. The model of Hayden and O'Connell (1975) is among the most-cited in literature consistent with this approach (Lilwanth, 2014). The interested reader is referred to the publication by Hayden and O'Connell (1975) and Appendix A of Prausnitz *et al*. (1980) to review the calculation procedure.

3.6 Combined EoS and excess Gibbs energy (G^E) mixing rules

The combination of EoS and excess Gibbs energy (G^E) models are made possible by the so-called EoS/ G^E models. This approach enables the incorporation of an activity coefficient model inside the mixing rules of EoS, thereby extending its application to polar compounds (Kontogeorgis & Folas, 2010).

3.6.1 Predictive Soave-Redlich-Kwong (PSRK)

The predictive Soave-Redlich-Kwong (PSRK) group contribution equation of state was published by Holderbaum and Gmehling (1991) and combines the Soave-Redlich-Kwong (SRK) EoS with the UNIFAC group contribution model. The PSRK model merges the advantages of the EoS, local composition concepts and the group contribution approach and is now widely implemented in commercial process simulation software (Horstmann *et al.*, 2005).

The PSRK model was selected to test the predictive capabilities as an alternative to UNIFAC model.

The SRK equation of state (Soave, 1972):

$$P = \frac{RT}{v-b} - \frac{a(T)}{v(v+b)} \tag{3.32}$$

used with the pure component parameters a_{ii} and b_i calculated from the critical data T_c and P_c of the pure components

$$a_{ii}(T) = 0.42748 \frac{R^2 T_{c,i}^2}{P_{c,i}} \alpha_i(T) \tag{3.33}$$

$$b_i = 0.08664 \frac{RT_{c,i}}{P_{c,i}} \tag{3.34}$$

allows for the correct representation of pure component vapour pressure with the assistance of the Mathias-Copeman parameters $c_{1,i}$, $c_{2,i}$ and $c_{3,i}$ fitted to vapour pressure experimental data (Mathias & Copeman, 1983):

$$\alpha_i(T) = \left[1 + c_{1,i}\left(1 - \sqrt{T_{r,i}}\right) + c_{2,i}\left(1 - \sqrt{T_{r,i}}\right)^2 + c_{3,i}\left(1 - \sqrt{T_{r,i}}\right)^3\right]^2 \tag{3.35}$$

or using the acentric factor ω in the generalised form (Soave, 1972):

$$c_{1,i} = 0.48 + 1.57\omega_i - 0.176\omega_i^2, \qquad c_{2,i} = 0, \qquad c_{3,i} = 0 \tag{3.36}$$

When applied to mixtures, the parameters *a(T)* and *b* from the SRK equation of state can be calculated if the pure component parameters $a_{ii}(T)$, b_i and the excess Gibbs energy at a reference state G_0^E is known (Horstmann *et al.*, 2005). At a liquid reference state of atmospheric pressure and if the optimized ratio of the inverse packing fraction $u = \frac{v}{b} = 1.1$ and $v^E = 0$ is assumed, the following equation (Fischer & Gmehling, 1996) results:

$$\frac{a(T)}{bRT} = \sum x_i \frac{a_{ii}(T)}{b_i RT} + \frac{\frac{G_0^E}{RT} + \sum x_i \ln \frac{b}{b_i}}{\ln \frac{u}{u+1}} \tag{3.37}$$

The classical linear mixing rule is used for the parameter *b*:

$$b = \sum x_i b_i \tag{3.38}$$

To improve the calculation of polar compound liquid densities the Péneloux volume translation (Péneloux *et al.*, 1982) can be used with cubic equations of state:

$$v = v_{SRK} - \sum x_i c_i \tag{3.39}$$

Here, the constant c_i can be estimated from the complete set of critical data for component *i*:

$$c_i = 0.40768 \frac{RT_{c,i}}{P_{c,i}} \left(0.29441 - \frac{P_{c,i} v_{c,i}}{RT_{c,i}} \right) \tag{3.40}$$

or from liquid density experimental data.

The UNIFAC parameters published in literature by Hansen *et al.* (1991) can be used with the PSRK method for systems that are temperature independent:

$$\Psi_{nm} = exp\left(-\frac{a_{nm}}{T}\right) \tag{3.41}$$

For systems where the phase equilibrium behaviour has strong temperature dependence or where a large temperature range is covered the PSRK model parameters recently published by

Horstmann *et al.* (2005) is recommended and the parameter Ψ_{nm} has the following temperature dependence relation :

$$\Psi_{nm} = exp\left(-\frac{a_{nm} + b_{nm}T + c_{nm}T^2}{T}\right) \tag{3.42}$$

3.6.2 SR-POLAR model

The SR-POLAR model is based on the SRK EoS combined with the Schwartzentruber-Renon mixing rule for the energy parameter (Schwartzentruber and Renon, 1991).

The equation for the model as implemented in Aspen Plus® (Aspen, 2006):

$$P = \frac{RT}{V_m + c - b} - \frac{a}{(V_m + c)(V_m + c + b)} \tag{3.43}$$

where

energy parameter $a = \sum_i \sum_j x_i\, x_j \left(a_i a_j\right)^{0.5} \left[1 - k_{a,ij} - l_{ij}\left(x_i - x_j\right)\right]$

size parameter $b = \sum_i \sum_j x_i\, x_j \frac{b_i + b_j}{2}\left(1 - k_{b,ij}\right)$

volume parameter $c = \sum_i x_i c_i$

The binary parameters $k_{a,ij}$, $k_{b,ij}$,and l_{ij} are temperature-dependent.

3.7 Discussion

Walas (1985) studied the regression of five activity coefficient models on the binary VLE equilibrium data in the DECHEMA collection. The database includes more than 3500 data sets of a diverse group of chemical species, for example, aqueous organics and alcohols. Table 3.4 is a summary of the frequency with which each model provided the best fit of the data for each respective class of chemical species.

The results indicate that the Wilson model provides the best fit of the total VLE data collection. Furthermore, the NRTL model is the best choice for aqueous-organic systems (Part 1 of the collection) and is ranked second for Part 2A containing the alcohol binary data. The limitation of the regression analysis is that the VLE data did not include partly-miscible systems. The Wilson model cannot be used for vapour-liquid-liquid systems, but the NRTL model is an acceptable option. Although the analysis by Walas (1985) is now dated, is serves a starting

point to assess the likely performance of the activity coefficient models for the systems of interest to this project. Moreover, it supports the model selection tree recommendation to consider the NRTL or UNIQUAC models as the best model choices.

Table 3.4: Frequencies of best fits for DECHEMA binary VLE data collection. Redrawn from Walas (1985).

Part of Collection		**Number of data**	**Margules**	**Van Laar**	**Wilson**	**NRTL**	**UNIQUAC**
1	Aqueous organics	504	0.143	0.071	0.240	0.403	0.143
2A	Alcohols	574	0.166	0.085	0.395	0.223	0.131
2B	Alcohols and phenols	480	0.213	0.119	0.342	0.225	0.102
3&4	Alcohols, ketones, esters	490	0.280	0.167	0.243	0.155	0.155
6A	$C_4 - C_6$ hydrocarbons	587	0.172	0.133	0.365	0.232	0.099
6B	$C_7 - C_{18}$ hydrocarbons	435	0.225	0.17	0.260	0.209	0.136
7	Aromatics	493	0.259	0.186	0.224	0.159	0.171
Total		3563	0.206	0.131	0.300	0.230	0.133

Even in more recent studies, the activity coefficient models still remain widely reported in literature as the models selected for entrainer/low molecular weight alcohols/water VLLE system predictions (Gomis *et al*., 2007; Lladosa *et al*., 2008; Lee & Shen 2003; Font *et al*., 2003; Gomis *et al.*, 2006; Gomis *et al*., 2005). The NRTL model and its derivatives have been widely used to correlate the phase behaviours of highly non-ideal systems with chemicals (Chen, 1993; Chen and Song, 2004). Prausnitz *et al.* (1999) confirm that the NRTL model provides a decent representation of experimental equilibrium data for strongly non-ideal mixtures and partially immiscible systems.

However, Lladosa *et al.* (2008) and Pienaar (2012) reported that the NRTL and UNIQUAC models did not yield accurate phase equilibrium predictions for the DIPE/ethanol/water system and recommended that further detailed thermodynamic modelling work is performed. In recent literature publications by Reddy, Benecke and Ramjugernath (2013) the VLE data for binary mixtures of DIPE and ethanol was correlated with the *gamma-phi (γ-φ)* approach using the NRTL and UNIQUAC G^E models combined with the Hayden and O'Connell correlation. It was found that the modelling approach provided reasonably good fits to the experimental data.

An investigation on the phase equilibrium of ethanol dehydration by azeotropic distillation was performed by Batista and Meirelles (2011). The NRTL model was selected for the liquid activity coefficient and the Hayden and O'Connell correlation for the vapour fugacity coefficients. Likewise, for the azeotropic distillation of ethanol and 1-propanol using propyl acetate as entrainer, a similar approach was successfully applied by Pla-Franco *et al.* (2014).

In terms of the PSRK model, Kontegeorgis and Folas (2010) reports that the model can have serious limitations in correlating VLE for size-asymmetric systems e.g. light hydrocarbons (ethane) mixed with heavy hydrocarbons (*n*-C_{44}). However, based on data published by Boukouvalas *et al.* (1994) the deviations between experimental and predicted data for the ethanol-water system bubble point pressures were only 1.6% and considered acceptable.

Furthermore, Kontegeorgis and Folas (2010) cautions that zero reference pressure EoS/G^E models, such as PSRK, are typically not better at low pressure than the activity coefficient model they are combined with. The EoS/G^E models do not perform well for highly immiscible mixtures and are not suitable for liquid-liquid equilibrium modelling. Yet, Reddy et al., (2013) found that in modelling VLE for binary mixtures of DIPE and low molecular weight alcohols (methanol and ethanol) the PSRK model performed the same or better than UNIFAC.

The SR-POLAR model can be used to model chemically non-ideal systems with an accuracy similar to activity coefficient property methods, such as the NRTL property method. This EoS is recommended for highly non-ideal systems at high temperatures and pressures (Aspen, 2006).

Therefore, given the review performed in this chapter the models identified as candidates are summarised in Table 3.5.

Table 3.5. Summary of potenial model's capable of modelling C_2 and C_3 alcohol systems.

DIPE + IPA + 2-methoxyethanol system	**DIPE + ethanol + water system**
NRTL, UNIQUAC	NRTL, UNIQUAC
NRTL-RK	NRTL-RK
NRTL-NTH and NRTL-HOC	NRTL-NTH and NRTL-HOC
SR-POLAR	SR-POLAR
CPA	CPA

3.8 Chapter summary

This chapter performed a review of thermodynamic modelling approaches for strongly non-ideal systems, especially C_2 and C_3 alcohol azeotropic mixtures. It was clear from literature that activity coefficient models, in particular the NRTL and UNIQUAC models are most likely to accurately correlate the fluid phase equilibria of low-pressure systems with polar compounds and multiple liquid phases. The C_2 and C_3 alcohol separation systems operate at low pressure, thus allowing for the ideal gas law to represent the vapour phase fugacities. Nonetheless, some literature showed that vapour phase association is possible for ethanol and IPA systems.

Furthermore, the EoS/G^E models were also identified as suitable candidates for the modelling of low molecular weight alcohol systems, although less widely reported in the literature. **Therefore, this project will consider the NRTL and UNIQUAC activity coefficient models using the ideal gas law, as well as, the Hayden and O'Connell and Nothnagel EoS as part of the model selection process. This project will also consider the CPA and SR-POLAR models as additional options.** The choice of a final thermodynamic model for the process design is deferred until specific selection study is performed in Chapter 7.

Chapter 4
Uncertainty Quantification in Process Design

In this chapter, general aspects of uncertainty analysis with respect to philosophy and approaches are described with pertinent emphasis on thermodynamic modelling and process simulation. The types and sources of uncertainty are reviewed, followed by a state-of-the-art summary of quantitative uncertainty evaluation methods. Probabilistic uncertainty quantification techniques relevant to process design are then discussed and a method is selected.

4.1 Uncertainty

The Scientific and Engineering literature contains different definitions of uncertainty. For example, Ascough *et al.*, (2008) refer to uncertainty as incomplete information about a particular subject; Sigel *et al.*, (2010) considers uncertainty a lack of confidence in knowledge related to a specific question and quoting Walker *et al.*, (2003) "*any deviation from the unachievable ideal of completely deterministic knowledge of the relevant system*".

Uncertainty effects almost all aspects of engineering modelling and design (Duong *et al.*, 2016). This is, in part, because no two physical experiments ever produce exactly the same output values and many relevant inputs may be unknown or unmeasurable (Vasquez and Whiting, 2005). Engineers have long dealt with measurement uncertainty, uncertain material properties, and unknown design demand profiles by including design safety factors and extensively testing designs (Clarke *et al.*, 2001; Mathias, 2014). An improved understanding of the sources (*identification*) and extent (*quantification*) of uncertainty, leads to improved decisions with known levels of confidence. Recognising this is the first step of uncertainty analysis.

"If a man will begin with certainties, he shall end in doubts; but if he will be content to begin with doubts he shall end in certainties".

- Sir Francis Bacon

(English author and philosopher, 1561 - 1626)

4.2 Types of uncertainty

Two distinctive philosophical types of uncertainty are commonly identified in the literature; aleatory uncertainty or epistemic uncertainty (Helton and Burmaster, 1996; Helton and Oberkampf, 2004; Sullivan, 2015).

4.2.1 Aleatoric

Aleatoric uncertainty is uncertainty that is irreducible in principle and may be considered inherent in a system. Aleatory uncertainty arises because of intrinsic randomness in the performance of the system under study. This type of uncertainty cannot be diminished by conducting extensive measurements or defining an improved model (Helton and Burmaster, 1996).

4.2.2 Epistemic

Epistemic uncertainty is uncertainty that results from a lack of knowledge about the behaviour of the system. Thus, epistemic uncertainty could conceptually be reduced by taking more measurements or implementing a better model (Helton and Burmaster, 1996). For example, the modelling parameters required for a particular design may not be known with certainty.

4.3 Common sources of uncertainty

Epistemic uncertainty can be present in system parameters, initial and boundary conditions of input parameters, computational techniques and the models themselves. These uncertainties can be grouped into the following categories: uncertain inputs, model form and parameter uncertainty, computational and numerical errors, and measurement error (van der Spek, Ramirez and Faaij, 2015).

4.3.1 Uncertain inputs

Any input to a system may be subject to uncertainty; examples include initial and boundary conditions (Wang, Qiu and Yang, 2016). Uncertain inputs may be theoretically constant or follow known relationships but have some inherent uncertainty. This is often the case with measured inputs, manufacturing tolerance, and material property variations (Knol *et al.*, 2009).

4.3.2 Modelling form and parametric uncertainty

Models are, at best, an approximation of reality. Modelling uncertainty stems from errors, assumptions and approximations made when selecting a model and can be broken down into model form uncertainty and parametric uncertainty. The first is related to the models ability to accurately represent the behaviour of the system and the second is often as a result of errors in experimental data or estimations of physical properties (Ferrari, Gutiérrez and Sin, 2016). For example, the binary interaction parameters for the NRTL model is regressed from experimental

data that may be subject to uncertainty, thus parametric uncertainty is inevitably included in the model parameters.

4.3.3 Computational and numerical uncertainty

In order to solve mathematical models and simulate systems, simplification of the underlying equations are required. This introduces truncation and convergence computational errors. Even for the same system and model, different numerical solvers depend on unique approximations and settings, leading to error variations (Sadeq, Duarte and Serth, 1997). Moreover, machine precision limitations and rounding errors inherent in digital computing systems introduce further numerical errors (van der Byl and Inggs, 2016).

4.3.4 Measurement error

Measurement error can be considered as either a random error or a systematic error.

A random error is a result of imperfect measuring equipment and observational techniques and includes instrument related errors and instrument user error. Repeating the measurements results in a mean value with a statistical variation about the mean. Random error is dependent on the number of measurements, equipment accuracy and instrument user skill (Regan *et al.*, 2008).

Measuring equipment or sampling procedure bias results in a systematic error. A more formal definition is the difference between the true value of the quantity of interest and the value to which the mean of the measurements converges as the sample sizes increase (Regan *et al.*, 2008). Contrary to random error, it is not obviously random and, therefore, a measurement with a systematic error does not demonstrate statistical variation around a mean value.

Systematic error can be as a result of a conscious decision of a data user to include (or exclude) data, or from an unintentional error in equipment calibration or consistent measurements with a constant offset (Regan *et al.*, 2008). For example, Whiting and Vasquez, (2005) showed that systematic errors present in experimental measurements can play a very significant role in uncertainty related to chemical and physical property estimates, thus affecting the process design. Liquid-liquid phase equilibrium in particular has been noted to include systematic errors (Vasquez and Whiting, 1999).

4.4 Uncertainty quantification

Uncertainty quantification is the end-to-end study of how reliable a scientific inference is; more specifically, it is the process of systematic quantification, characterization, tracing and managing of uncertainty in computational modelling of real world systems. The objective of uncertainty quantification is to incorporate the probabilistic behaviour of real world systems into engineering and systems analysis. Deterministic models and simulations can reveal a systems response to a single set of inputs. Uncertainty quantification expands upon this by using probabilistic methods to determine what is likely to happen when the system is subjected to a range of uncertain input variables (Sullivan, 2015).

Nearly all analysis of process technologies in all phases of research and engineering involve uncertainties (Frey *et al.*, 1994). The uncertainties inherent in the data used for process modelling help inform and improve understanding of the data's use. Furthermore, the effects of uncertainties in thermodynamic models and data are fundamentally important in predicting process performance, simulation, process design, and optimisation (Frey, 1992; Whiting and Reed, 1993; Whiting and Vasquez, 2004; Mathias, 2013).

Failure to account for uncertainties may result in misleading estimates that are subsequently used for decision making during technology screening, selection, and design. For example, Kister (2002) reported that approximately 20% of distillation operation malfunctions (flooding or weeping) were as a direct result of discrepancies between simulation and actual phase behaviour during the design phase. Currently, it is widely recognised by experts that the effect of property uncertainties should be incorporated into the modelling and design process (Mathias, 2014). The benefits of including property uncertainties, comprise predicting a systems response across a range of uncertain inputs and the ability to quantify a confidence in these predictions. It is however not presently a routine component of industrial practice, although several approaches have been proposed (Mathias, 2014).

4.5 Quantitative uncertainty evaluation methods

A multitude of approaches, methods and tools to evaluate model uncertainty is available, although not all conform to the definition of uncertainty quantification. A comprehensive summary of the prominent works in the field of uncertainty evaluation methods (adapted from van der Spek *et al.*, 2015) is presented in Table 4.1 and supplemented with **additional literature sources** marked in bold**.** The contributions from these methods range from data validation to scenario analysis, but the common idea is a characterization of specific model

output parameters by using a probabilistic approach. A few examples of these methods, as used in process modelling and design, will be discussed in this section.

Qualitative non-probabilistic approaches are also reported in the literature, but are considered as mostly complementary and non-competitive to the quantitative probabilistic approaches and is not considered in this thesis. A summary is provided in Appendix E. The methods used in process modelling and design will be discussed in this section.

4.5.1 Data validation

The validation of a model's calculation results against an independent experimental data set is one of the single most common uncertainty evaluation methods. A goodness of fit is established through visual inspection of a parameter of interest, for example, bubble and dew point curves for binary systems or ternary plots for multicomponent systems. Descriptive statistic techniques are also applied to quantify the average absolute deviation (AAD) as shown in Equation 4.1 and the average absolute relative deviation (ARD) as shown in Equation 4.2 (Lee and Shen, 2003):

$$AAD = \frac{1}{N_T}\sum_{i=1}^{N_T}|x_{calculated} - x_{measured}| \tag{4.1}$$

$$ARD = \frac{100}{N_T}\sum_{i=1}^{N_T}\left|\frac{x_{calculated} - x_{measured}}{x_{measured}}\right| \tag{4.2}$$

The benefit of Equations 4.1 and 4.2 is, in contrast to variance and standard deviation, that AAD does not square the distance from the mean and is, therefore, less sensitive to extreme observations. ARD is similar to AAD, but it also takes the relative size of each data point into account (Lee and Shen, 2003).

Table 4.1. General quantitative uncertainty evaluation methods. Redrawn from supplementary data in (van der Spek, Ramirez and Faaij, 2015) and adapted with additional references relevant to manufacturing and chemical process industries.

Method/tool	Short description	Reference
Data Validation	To determine how well input data correspond to real/measured values	(Van der Sluijs *et al.*, 2004)
Error Propagation	To quantify output uncertainty by propagating sources of uncertainty through the model	(Mathias, 2016) **(Mathias, 2014)** (Van der Sluijs *et al.*, 2004)
Model Comparison	To determine model uncertainty by comparing the structure, and equations of the different model.	**(Bjørner, Sin and Kontogeorgis, 2016)** (Van der Sluijs *et al.*, 2004)
Model Validation	To determine how well model outputs correspond to real/measured data	**(Pla-franco *et al.*, 2013)** **(Bayarri *et al.*, 2007)** **(Lladosa *et al.*, 2007)** (Van der Sluijs *et al.*, 2004)
Multiple Model Simulation	To evaluate model uncertainty or generate ensemble predictions via consideration of multiple plausible models	(Van der Sluijs *et al.*, 2004) (**Sadeq, Duarte and Serth, 1997)**
Scenario Analysis	To determine robustness of model outputs in different plausible input scenarios	**(Wechsung *et al.*, 2009)** (Van der Sluijs *et al.*, 2004)
Sensitivity Analysis	To determine which inputs are most significant, and how robust outputs are to changes in inputs	**(Nguyen-Tuan *et al.*, 2016)** (Van der Sluijs *et al.*, 2004) **(Seferlis and Hrymak, 1996)** **(Nelson, Olson and Sandler, 1983)**

Table continues on the next page.

Table 4.1 continued from the previous page. Quantitative uncertainty evaluation methods.

Method/tool	Short description	Reference
Bayesian Networks	To combine prior distributions of uncertainty with general knowledge and site-specific data to yield an updated (posterior) set of distributions	**(Mara *et al.*, 2016)** **Nannapaneni, Mahadevan, and Rachuri, 2016)** **(Mandur and Budman, 2014)** (Mattot *et al.*, 2009)
Interval Analysis	It is assumed that the uncertain parameters are taking value from a known interval. It is somewhat similar to the probabilistic modelling with a uniform PDF. This method finds the bounds of output variables.	**(Moore *et al.*, 2009)** **(Gau and Stadtherr, 2002)** **(Gruhn and Colditz, 1996)**
Monte Carlo Simulation - Sequential - Non-sequential - Pseudo-sequential	To quantify output uncertainty by propagating probability density functions of uncertainty through the model	**(Bjørner, Sin and Kontogeorgis, 2016)** **(Hajipour, Satyro and Foley, 2014)** **(Hajipour, 2013)** **(Hajipour and Satyro, 2011)** **(Vásquez, Whiting and Meerschaert, 2010)** (Van der Sluijs *et al.*, 2004) **(Reed and Whiting, 1993)**
Polynomial Chaos Expansion	To simultaneously quantify output uncertainty by propagating probability density functions of uncertainty through the model, and evaluate sensitivities of model uncertainties to input parameters.	**(Duong *et al.*, 2016)** **(Içten, Nagy, and Reklaitis, 2015)** **(Nagy and Braatz, 2007)** (Reagan *et al.*, 2005) **(Red-Horse and Benjamin, 2004)**

4.5.2 Sensitivity vs. uncertainty analysis

Uncertainty analysis aims at identifying the overall output uncertainty in a given system. On the other hand, sensitivity analysis aims to relate the input parameters and the output variable of a process model; more specifically, it investigates how the change in an output of interest is connected to a specific model input. Furthermore, it also identifies which input sources dominate the system response. A fundamental difference is that understanding the response of an output variable with respect to the input parameter, as is the case for sensitivity analysis, is not useful unless (1) it is normalised in a sensible way, and (2) and it is representative of the entire possible range of the output variable (Whiting, 1996).

Furthermore, it is possible that the identified output sensitivities do not translate to important uncertainties since the input parameter uncertainty is too small for the system of interest. In the thermodynamic modelling and process simulation space it is well-documented (Macchietto *et al.*, 1986) that key output variables, e.g. reflux ratio, respond in a non-linear fashion with respect to input parameters e.g. binary interaction parameters. Moreover, sensitivity analysis does not provide insight into the likelihood that a response will occur, thus limiting its useful application to uncertainty quantification.

Thus, the real question is not how sensitive the process design is to changes in the input data, but rather how sensitive the design is to the actual input data uncertainty (Whiting, 1996). As such, methods that provide insight into the uncertainty of key output variables are required to perform uncertainty quantification.

4.5.3 Error analysis and probabilistic uncertainty analysis

Error analysis and probabilistic uncertainty analysis focus on the quantitative representation of the respective error or uncertainty in the model inputs and converts that into compiled errors or probabilities of the output variables of interest in the form of error bars or probability distribution functions (van der Spek *et al.*, 2015). Error propagation or Monte Carlo simulation (MCS) is often used as tools to propagate the uncertainty through the deterministic model and is classified as non-intrusive uncertainty propagation techniques.

An alternative is to use intrusive uncertainty quantification methods; here the governing equations of the mathematical model describing the physical processes is reformulated. Although commercial process simulation software caters to some extent for creating user models or customising default property methods, this thesis will focus only on non-intrusive

uncertainty propagation techniques in support of the aim of making uncertainty quantification a routine industrial practise. In the next section, methods to propagate the uncertainty through a deterministic model are reviewed.

4.6 Propagation of Uncertainty

In the design of chemical processes, the importance of understanding parametric uncertainty is widely recognised. Propagation of uncertainty calculates the effects of the uncertainty in model inputs on the model outputs. This information is essential when quantifying confidence in a model's outputs and helps to determine whether model outputs will meet requirements given the anticipated variation in inputs. Once probability distributions are available for the input parameters, the objective is to determine the probability distribution function (PDF) or error range of the output variables of interest; the process is illustrated in Figure 4.1 (Vasquez and Whiting, 2005).

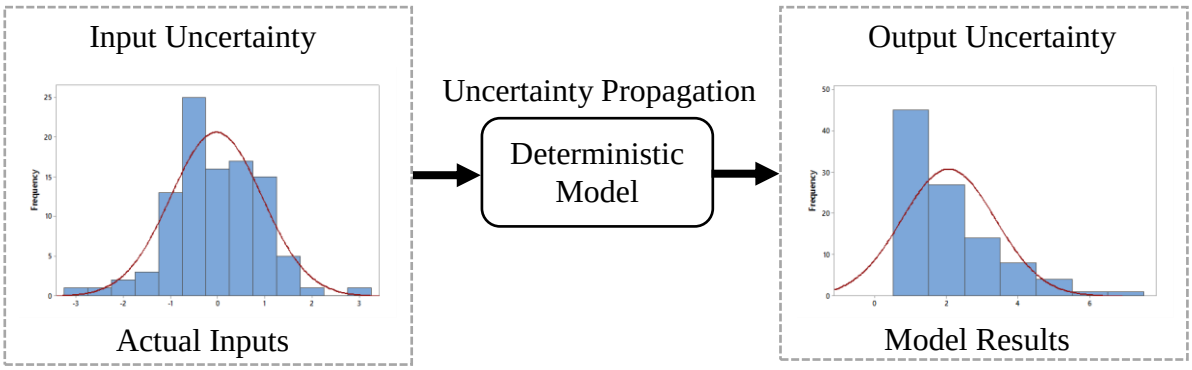

Figure 4.1: Propagation of uncertainty process flow through a process model.

Whiting and co-workers provided perhaps the most notable contribution to parametric uncertainty quantification of thermodynamic models. The authors performed extensive investigations to determine the impact of physical property uncertainty on process design and demonstrated uncertainty propagation techniques through the use of MCS (Reed and Whiting, 1993; Whiting, 1996; Vasquez and Whiting, 1998; Clarke *et al.*, 2001; Vásquez, Whiting and Meerschaert, 2010).

As an example, Whiting *et al.*, (1999) studied the effect of the experimental data source on the uncertainty of thermodynamic models by using different data sets for the regression of NRTL binary interaction parameters. The regressed information was used to perform MCS to generate 100 sets of binary interaction parameters to represent a statistical sampling of the most probable model parameters, assuming accurate and precise measurement of experimental data. The

statistical analysis concluded that a dependency existed between the values of the binary interaction parameters and the data source. Furthermore, combining different experimental data sources into a combined experimental data pool did not improve the uncertainty estimates. However, performing analysis on individual data sets yielded an improved quantification of uncertainty and risk (Whiting *et al.*, 1999). The study also observed that the uncertainties associated with different experimental data sources could not be correlated with the goodness of fit of the regressions. At the time, limited quantitative parametric uncertainty information was available and these earlier studies were performed using average uncertainties estimated for different physical properties, such as the evaluations performed by the Design Institute for Physical Properties (DIPPR).

Hajipour and Satyro (2011) expanded on these techniques through the development of an extensive database of critical parameters, acentric factors and binary interaction parameters and encoded it with parametric uncertainty information (Hajipour and Satyro, 2011; Hajipour, 2013; Hajipour *et al.*, 2014). A unique feature of their database is that it includes fundamental physical property data available through NIST Thermo Data Engine (TDE). This feature is a notable improvement on the approach of earlier studies as it is based on actual parametric uncertainty. The authors also used MCS to evaluate the effect of the propagated physical property uncertainties on process simulation results.

Bjørner, Sin and Kontogeorgis, (2016) recently applied uncertainty quantification as a tool to evaluate and compare the performance of the cubic plus association (CPA) thermodynamic model. The authors note that in an effort to improve the performance of models such as CPA and SAFT additional terms are often added, leading to an increase in adjustable parameters. The resultant high correlation between parameters makes it difficult to estimate pure compound parameters that are unique. The field of heavy hydrocarbon supercritical fluid extraction with CO_2 is particularly plagued by this problem due to the quadrupolar moment of the solvent. A MCS was used to propagate the effect of parametric uncertainty to various model properties and binary phase equilibrium calculations by using three and five adjustable parameter model variants. The study confirmed significant parameter uncertainties because of high parameter correlation.

Mathias (2014) proposed an error propagation scheme as an approach to perform parametric uncertainty quantification. In this approach, probabilistic methods (i.e. Monte Carlo) are not utilised, but instead, a semi-empirical method perturbs the activity coefficients in proportion to

the derived experimental data uncertainty. This is based on the simplifying assumption that the liquid mixture can be approximated by the Margules equation as a set of pseudo binaries. Mathias demonstrated the use of the method and how it relates uncertainties in K-values with variabilities in process design through several examples (Mathias, 2014; Mathias, 2016). The results were consistent with the rules of thumb published by Fair (1980). As this technique cannot provide a probabilistic view it is not considered for this work.

The majority of the literature related to chemical process design uncertainty quantification has used probabilistic methods to represent sources of uncertainty and then methods, such MCS, to propagate the sources through a deterministic model. MCS is considered the state of the art method (Villegas *et al.*, 2012). In the event that a probabilistic description of the required input parameter uncertainties is not available, an alternative non-sampling-based method is generalised polynomial chaos expansion (gPC). This method is described as a spectral representation of a random process by the orthonormal polynomials of a random variable (Duong *et al.*, 2016).

Although Ghanem and Spanos, (2003) reported that gPC is suitable for engineering purpose it has seen limited application in chemical process design. Villegas *et al.*, (2012) reported a study in which polynomial chaos expansion was used for uncertainty quantification in chemical reactors. In this case, it was coupled with computational fluid dynamic calculations for modelling and simulating reactive flows. Duong *et al.*,(2016) applied gPC for uncertainty quantification and sensitivity analysis of a complex chemical process. The gPC method was developed in a Matlab™ environment and connected to HYSYS™. The gPC method performed in agreement with the results from a Monte Carlo method. The gPC method is expected to mature in the future and appears to be promising, but will not be considered in this thesis. The details of the MCS approach is reviewed in the following section.

4.7 Monte Carlo simulation

A brief overview of MCS is provided in this section, including the types of MCS sampling techniques available and the required sample sizes. Rubinstein and Kroese (2016) published a state-of-the-art review of MCS that reflects the latest developments in the field and presents a fully updated and comprehensive account of the theory, methods and applications. The definition used in this thesis is aligned with this text.

4.7.1 Monte Carlo simulation procedure

MCS involves performing a relatively large number of repeated simulations (or realisations) by using a selection of values for a specific model input parameter. The different values are randomly obtained from the input variables probability density functions and uncertainty ranges. The process can be applied to every model input parameter or only those of interest. As a result, a set of probable values of the modelled output variables are obtained (Rojas *et al.*, 2016).

Consider the deterministic function $Y = g(X)$ (e.g. a computational model), where $Y \in \mathbb{R}, X \in \mathbb{R}^{Nvar}$ is a random vector of N_{var} marginal (input random variables describing uncertainties), X is a vector of random variables and $g(\cdot)$ can be computational expensive to assess (Vořechovský and Novák, 2009). The information on the random vector is limited to marginal probability distributions and the target correlation matrix $\boldsymbol{T}$ (user defined with entries $T_{i,j}$):

$$\boldsymbol{T} = \begin{matrix} X_1 \\ X_2 \\ \vdots \\ x_{N_{var}} \end{matrix} \begin{pmatrix} 1 & T_{1,2} & \cdots & T_{1,N_{var}} \\ \vdots & 1 & \cdots & \vdots \\ \vdots & \vdots & \ddots & \vdots \\ sym. & \cdots & \cdots & 1 \end{pmatrix} \tag{4.3}$$

Here, N_{var} is the number of variables (marginal). The objective is to perform sensitivity, statistical and perhaps reliability analysis of Y. If the analytical solution (e.g. Taylor series expansion) of the transformation of input variables to Y is not possible, then the most common technique for solving the task is the stochastic method know as MCS (Iman and Conover, 1982; Vasquez and Whiting, 2005). The MCS procedure is to draw N_{sim} (number of simulations) realizations of X and calculate an equivalent number of output realizations of Y using model $g(\cdot)$. For certain cases the model can be computational intensive and it is worthwhile to use a more advance sampling scheme.

4.7.2 Random sampling techniques

Sampling is the process by which values are randomly drawn from the input probability distributions. If samples are drawn from a probability distribution, they become distributed in a manner that approximates the known input probability distribution. The statistics of the sampled distribution (mean and standard deviation) approximate the true statistics input for the distribution (Shapiro, 2003).

Several techniques for drawing random samples are reported in the literature, for example *standard Monte Carlo sampling* (Knuth, 1974), *Latin Hypercube sampling* (Reed and Whiting, 1993; Whiting, 1996; Bjørner, Sin and Kontogeorgis, 2016), *Shifted Hammersley sampling* (Diwekar and Kalagnanam, 1997) and *Equal probability sampling* (Whiting, Vasquez and Meerschaert, 1999). A detailed review of the theory related to MCS techniques is offered by Shapiro, (2003).

As noted in Section 4.4, Whiting and co-workers developed notable contributions to the field of chemical process uncertainty quantification, specifically related to the application of Monte Carlo simulation based analysis (Whiting *et al.*, 1993; Whiting, 1996). The authors recommend using a stratified sampling technique for choosing the values for each run of the Monte Carlo simulation when performing uncertainty quantification on thermodynamic models and process simulations. One such technique is Latin Hypercube Sampling (LHS) and was successfully applied by Frey (1992).

Latin Hypercube Sampling (LHS) is a stratified sampling technique and works by controlling the way that random samples are generated for a probability distribution by distributing samples equally over the sample space (McKay *et al.*, 1979). This ensures sampling from the entire range of probable data distribution in a proportional manner. Moreover, an acceptable level of accuracy is obtained with a small number of samples (Vořechovský and Novák, 2009). The cumulative distribution for each input variable is divided into N equal probability intervals. A value is selected randomly from each i^{th} interval and the sampled cumulative probability can be written as (Wyss and Jorgensen, 1998):

$$p_i = \frac{1}{N} r_u + (i-1)N \tag{4.4}$$

Where

p_i is the sampled cumulative probability

N is number of equal probability intervals

r_u is a uniformly distributed random number ranging from 0 to 1.

i is the sample interval

The LHS technique is however not without limitations. Whiting *et al.*, (1999) reported obtaining extreme binodal curves with the LHS technique sampling binary interaction parameter for ternary systems. The result was a large set of infeasible simulation results. If the sampling technique takes samples evenly (in a probability sense) across the sample space, large numbers

of samples with a low probability is included. A large number of samples may be required to prevent the model outputs from varying widely and to account for the effect of the extreme parameter values.

4.7.3 Types of probability distributions

The purpose of a probability density function (PDF) is to graphically represent the relative probability (likelihood) or frequency at which a variable or value may be obtained. Furthermore, the PDF illustrates the symmetry or skewness of a particular probability distribution (Frey, 1992). The cumulative distribution function (CDF) is an alternative method to represent a probability distribution. The CDF show probability fractiles on the y-axis and the value of the distribution associated with each fractile on the x-axis. The CDF is able to characterise probability distributions if some details of the various fractiles are available, for example, the 5th, 50th and 95th percentile values.

Illustrations of two common types of probability distributions are shown in Figure 4.2 as both probability density functions (PDF) and the associated cumulative distribution function (CDF).

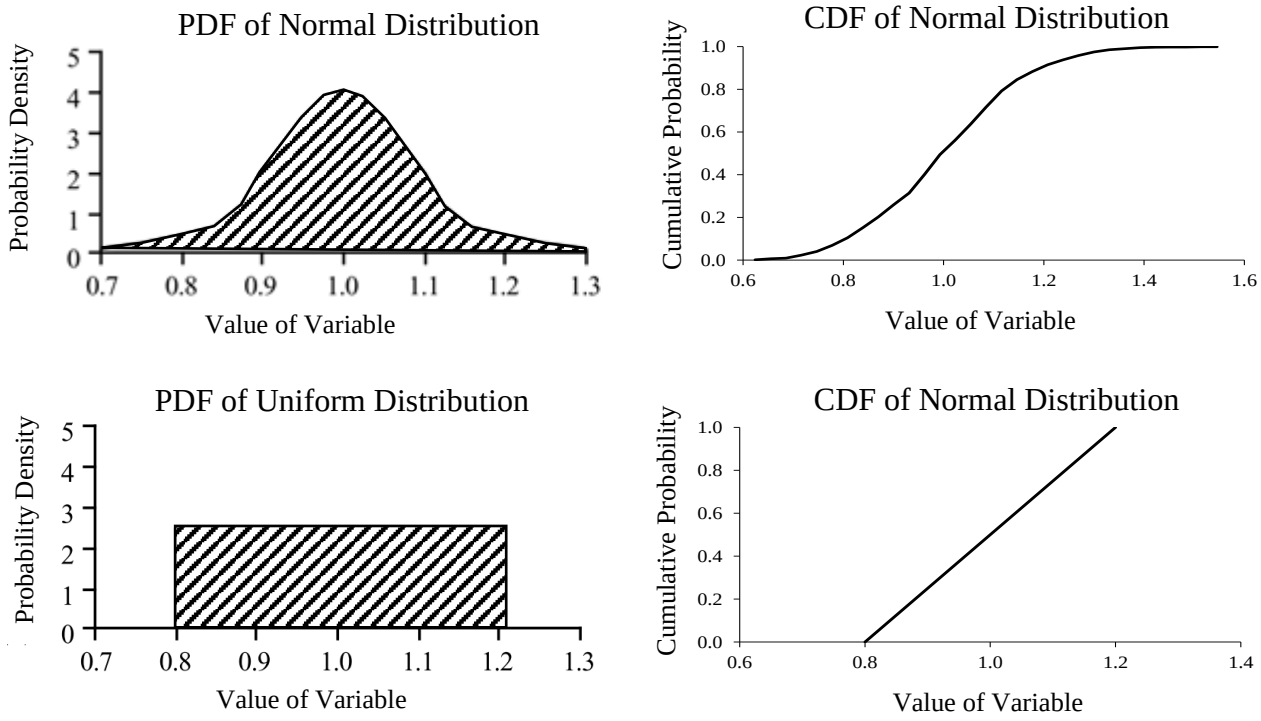

Figure 4.2: Two common types of probability distributions. Redrawn from Frey (1992).

4.7.4 Random Sampling Size

In order to perform uncertainty quantification on the design of a chemical process, the different values of the thermodynamic model input parameters are randomly drawn from the input probability distributions. A MCS requires a minimum number of random sample sets to generate credible results. As such, the number of simulations performed is determined by the desired confidence level. The literature provides several recommendations on the number of random samples required for the MCS. For approximately normal distributions the required number of simulations (n) is given by (Perry and Green, 1997)

$$n = \left(\frac{2z}{d}\right)^2 p(1-p) \tag{4.5}$$

Where z is the value of the standard normal variable associated with the confidence level desired and d is the width of the confidence interval centred on the fractile p.

In a study of Reed and Whiting (1993) uncertainty quantification of thermodynamic data and model parameters was performed. The authors selected 100 simulation runs and the probability distribution for each input variable was divided into 100 regions of 0.01 probability each. The results provided a 90% confidence level. Hajipour, (2013) performed a sensitivity analysis on the results of MCS using 100, 1000 and 10 000 random samples. At a 95% confidence level, the observed differences in output variable mean and the standard deviation were of limited statistical significance. In a recent investigation reported by Bjørner *et al.*, (2016) the authors selected 500 random samples with the latin hypercube sampling technique.

The typical range reported is 100 to 10 000 random samples, although Equation 4.5 may be used to calculate the minimum samples required based on the required confidence level.

4.7.5 Limitations of Monte Carlo simulation based uncertainty analysis

As with any scientific and engineering technique, the MCS based uncertainty quantification approach has some common drawbacks. The probability density functions and uncertainty ranges of the input variables may not be known and then the generalised polynomial expansion based methods may be more suitable. However, Hajipour (2013) reported that the NIST Thermo Data Engine (TDE) requires uncertainty estimates for all experimental data and assumes a normal distribution with a 95% confidence level. Furthermore, the experimental phase equilibrium data for the azeotrope mixtures investigated in this thesis is provided with uncertainty estimates (Lladosa *et al.*, 2007; Pienaar *et al.*, 2013).

In the case of a large and multi-dimensional process model, the Monte Carlo simulation based approach to uncertainty propagation may be computationally expensive and time-consuming. However, considering that the process models reported in the literature for extractive and azeotropic distillation typically only contains two distillation columns and a decanter (in the case of azeotropic distillation) model complexity is not considered sufficient justification to not consider Monte Carlo simulation.

4.8 Chapter summary

In this chapter the general aspects of uncertainty analysis with respect to thermodynamic modelling and process simulation were reviewed. In particular, the probabilistic uncertainty quantification techniques relevant to process design were identified. The majority of the literature related to chemical process design uncertainty quantification has used probabilistic methods to represent sources of uncertainty and then used methods, such MCS, to propagate the sources through a deterministic model. **Therefore, this project will consider the Monte Carlo simulation approach using LHS as the method to propagate the parametric uncertainty of the experimental data to the process design of C_2 and C_3 alcohol separation systems.**

Chapter 5
Literature Review: Concluding Remarks

The main industrial manufacturing processes for C_2 and C_3 low molecular weight alcohols all require reaction mixture separation and purification steps to meet the product marketing specifications; this is because all the synthesis routes result in a minimum-boiling azeotropic mixture. It was established that heterogeneous azeotropic distillation and extractive distillation account for the majority of low molecular weight alcohol dehydration and separation processes. This project will consider the heterogeneous azeotropic distillation of ethanol and water using DIPE as entrainer and the extractive distillation of DIPE and IPA with 2-methoxyethanol as the solvent.

A review of thermodynamic modelling approaches revealed that the NRTL and UNIQUAC models remain among the most extensively used activity coefficient models for low-pressure systems with polar compounds and multiple phases. A major limitation, however, is that experimental data may be required to ensure the activity coefficient models provide reliable results. The SR-POLAR model was identified from the combined equation of state-excess Gibbs energy modelling approach. The cubic-plus-association (CPA) equation of state was also identified as a possible candidate. The choice of a particular thermodynamic model is deferred to Chapter 7 where a screening study is performed, however, the following models will be considered: NRTL and UNIQUAC activity coefficient models using the ideal gas law, as well as, the Hayden and O'Connell and Nothnagel EoS, as well as, the CPA and SR-POLAR models.

The effects of uncertainties in thermodynamic models and data are fundamentally important in predicting process performance, simulation, process design, and optimisation. It is, therefore, important to minimise the effect of thermodynamic model uncertainties. The correlations of phase equilibrium are reported as the most significant source of property uncertainties in process design. The majority of the literature related to chemical process design uncertainty quantification has used probabilistic methods to represent sources of uncertainty and then used methods, such as Monte Carlo simulation, to propagate the sources through a deterministic model. Monte Carlo simulation is considered the state-of-the-art method and was selected for this work. The Monte Carlo simulation based techniques proposed by Hajipour (2013) and Whiting *et al*., (1999) were chosen for verification and then final selection.

II EXPERIMENTAL PROCEDURES

Chapter 6
Research Design and Methodology

With the theoretical foundation for the work presented in this thesis covered in the previous Chapters, attention now shifts to the means by which the work was done and the results obtained. In the sections that follow, the research methods and modelling procedures employed to meet the investigational objectives of the work are presented.

6.1 Research design overview

The thesis content is two-fold, as the title indicates. Firstly, phase equilibrium modelling and regression analysis are performed to seek improved correlation between experimental and predicted data. This serves to answer the first research question of the study ***"What is the best model?"*** Secondly, the effect of the phase equilibrium uncertainty on the key design variables of unit operations in the process models are quantified through Monte Carlo simulations using Aspen Plus®; this part serves to answer the second research question "***How reliable is the best model?"*** The research design is illustrated in Figure 6.1.

Details of the application of these steps are explained in the following sections.

6.1.1 Recap on the research questions

What is the best model? "*What thermodynamic modelling approach provides accurate correlation with experimental data for the phase equilibria of low molecular weight alcohol separation systems?*" In the context of this thesis the definition is based on the model accuracy compared to experimental data. Descriptive statistics are used to determine the average absolute relative deviation (ARD) for the azeotrope and binary phase equilibrium.

How reliable is the best model? *"How can one best account for the thermodynamic model parametric input uncertainty and the propagation of said uncertainty through the process simulation model?"* In the context of this work, it is the confidence in the final design when using the best model. It is not model form uncertainty, but model output confidence given the parametric uncertainty.

6.1.2 Research design structure

The research design is based on three common fundamental evaluation aspects and is applied in a sequential manner; *scientific*, *statistic* and *probabilistic*. This philosophy is based on

recommendations of Derwent *et al.*, (2010). The literature study is considered as a *scientific* evaluation of the thermodynamic modelling approaches. It is a review of the equations, assumptions and identification of the range of use; this is to identify the candidate models for further screening and selection and is shown on the left of Figure 6.1.

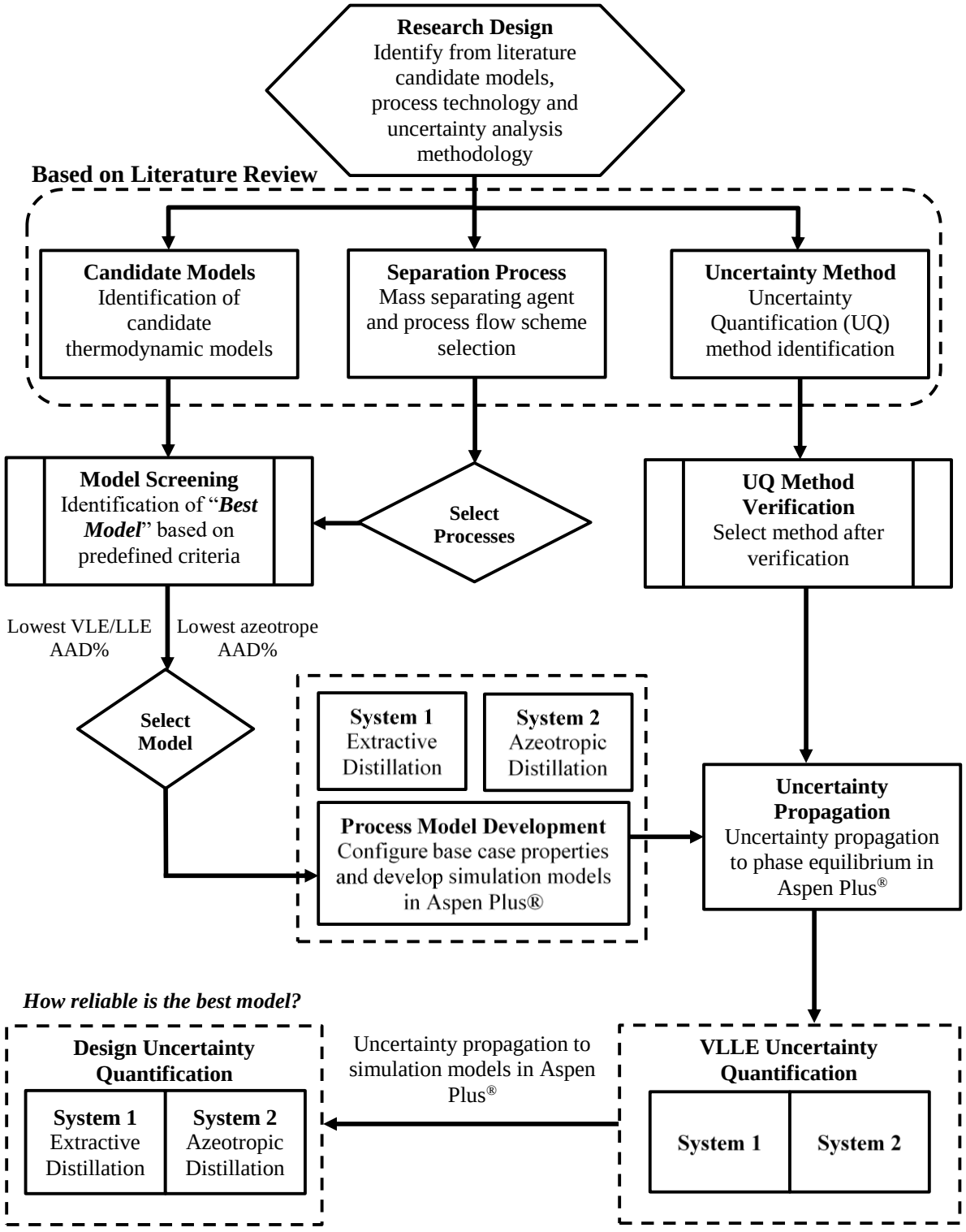

Figure 6.1. Framework of the overall research design.

Statistical evaluation mainly involves comparing model predictions with observations. It provides concise information on model performance and serves as a tool to support the first research question (*What is the best model?*). Lastly, *probabilistic* evaluation aims to identify the uncertainty in the process design introduced by the parametric variability of the inputs. The technique of uncertainty quantification is utilised to answer the second research question (*How reliable is the best model?*) and is shown on the right of Figure 6.1. The selection of the uncertainty quantification method is deferred to this chapter and is based on the outcome of a verification procedure. Reference is made in subsequent sections, as applicable.

6.2 Thermodynamic model screening and selection

Assessing the ability of a thermodynamic model to accurately predict experimental data is of key importance for the design of thermal separation processes. Comparison of model predictions to experimental data on phase equilibrium diagrams, for example, T-xy or ternary plots, is often used. Furthermore, descriptive statistics is also useful and widely reported in the literature (Lee, Shen 2003). In this work, both these methods are used.

The equations for average absolute deviation (AAD) and absolute relative deviation (ARD), as discussed previously in Chapter 4, are shown here for convenience:

$$AAD = \frac{1}{N_T}\sum_{i=1}^{N_T}|x_{calculated} - x_{measured}| \tag{4.1}$$

$$ARD = \frac{100}{N_T}\sum_{i=1}^{N_T}\left|\frac{x_{calculated} - x_{measured}}{x_{measured}}\right| \tag{4.2}$$

Thermodynamic model regression based on experimental data is to be completed to identify the most appropriate thermodynamic model for each system. The built-in Data Regression System (DRS) of the commercial process simulator Aspen Plus® version 8.8 is used. The method is based on the maximum likelihood method with the Britt-Luecke algorithm and is shown in Equation 6.1 (Aspen, 2006):

$$Q = \sum_{x=1}^{NDG} w_n \sum_{i=1}^{NP}\left[\left(\frac{T_{e,j}-T_{m,j}}{\sigma_{T,j}}\right)^2 + \left(\frac{P_{e,j}-P_{m,i}}{\sigma_{P,i}}\right)^2 + \sum_{j=1}^{NC-1}\left(\frac{x_{e,i,j}-x_{m,i,j}}{\sigma_{x,i,j}}\right)^2 + \sum_{j=1}^{NC-1}\left(\frac{y_{e,i,j}-y_{m,i,j}}{\sigma_{y,i,j}}\right)^2\right] \tag{6.1}$$

with

Q	Objective function to be minimised by regression of the data

NDG	Number of data groups in the regression case
w_n	Weight of data group
NP	Number of points in data group *n*
NC	Number of components present in the data group
T, P, x, y	Temperature, pressure, liquid and vapour mole fractions
e	Estimated data
m	Measured data
i	Data for point *i*
j	Fraction data for component *j*
σ	Standard deviation of the indicated data

The objective function (Q) is minimised by manipulating the physical property parameters identified in the regression case and adjusting the estimated value corresponding to each measurement. The phase equilibrium data sets can be assigned unique weights in the data regression process in order to improve the model fit, as this compensates for the characteristics of the mixture. Furthermore, the screening process is supplemented with binary interaction parameters from literature and the default Aspen Plus® model parameters as available.

A vital test for the thermodynamic models and parameters used for process simulation is how the azeotropic behaviour and the composition of azeotropic mixtures as a function of temperature and pressure are reproduced. Falsely predicted azeotropic behaviour may render simulation results that are mostly unrealistic. The accurate prediction of infinite dilution and azeotropic behaviour is in practice often favoured at the expense of less accurate VLE descriptions. In order to evaluate thermodynamic models, in particular activity coefficient models, a reliable source of experimental data is required (Kontogeorgis and Folas, 2010).

6.3 Sources of experimental data

There are a number of sources for thermophysical and equilibrium data. The most important collections are:

Pure component properties:

i). The NIST Chemistry WebBook (http://webbook.nist.gov/chemistry/)

ii). The Korea Thermophysical Properties Databank (https://www.cheric.org/research/kdb/)

iii). The Dortmund Databank (DDB) (http://www.ddbst.com/ddb.html)

iv). The DECHEMA Data collection (http://dechema.de/en/CDS.html)

v). The Detherm Databank (http://i-systems.dechema.de/detherm/mixture.php)

Equilibrium data:

i). The Dortmund Databank (http://www.ddbst.com/vle-databanks.html)
ii). The DECHEMA Data collection (http://dechema.de/en/CDS.html)
iii). The Detherm Databank (http://i-systems.dechema.de/detherm/mixture.php)

The NIST and Korea databanks are free and the data contained in them (especially the NIST databank) are of reliable quality. When equilibrium data are required, the DDB and Detherm are usually the first preference. Both these databanks include the majority of data that are published in the open literature, as well as data measured by the respective organisations. It is possible to search the contents of these databanks for free. The Detherm databank is searchable over the web, while an indexing program is available for the DDB (http://www.ddbst.com/software-package.html).

Aspen Plus® NIST ThermoData Engine (TDE):

The ThermoData Engine (TDE) is a thermodynamic data correlation, evaluation, and prediction tool implemented in Aspen Plus® and Aspen Properties through a long-standing partnership agreement with the National Institute of Standards and Technology (NIST). The purpose of the TDE software is to provide critically evaluated thermodynamic and transport property data founded on the principles of dynamic data evaluation (Diky *et al.*, 2009).

Hajipour and Satyro (2011) reported the benefit of incorporating the actual parametric uncertainty of phase equilibrium data directly from the NIST TDE in uncertainty quantification studies. In the TDE, uncertainty is assumed to be characterised by a normal (Gaussian) distribution. Thus, for a 95% confidence level, if the calculated value is set as the mean value (μ), the standard deviation (σ) is half of the evaluated uncertainty. Therefore, the range of probabilistic values that each property can assume in the 95% confidence interval would lie in the interval $\mu \pm 2\sigma$ (Hajipour, 2013). For this reason, the NIST ThermoData Engine was chosen as a reliable source of experimental data for this study.

6.4 Process model development

It is general industrial practice to process binary azeotropes using either homogeneous or heterogeneous liquid-phase entrainers. In the case of homogeneous entrainers, separation is made possible by removing the distillation boundary between the two components. For

heterogeneous entrainers, liquid-phase immiscibility's are exploited to cross distillation boundaries. In the context of this work the systems of interest were discussed in Section 2.7. Extractive distillation was chosen for the DIPE/IPA binary azeotrope and heterogeneous azeotropic distillation for the ethanol/water binary azeotrope.

It is evident from literature that various strategies have been explored for the sequencing of azeotropic separation processes of which notable contributions are by Ryan and Doherty (1989), Pham and Doherty (1990) and more recently Kiss (2013). The general consensus appears to be that the distinction between a three-column and two-column sequence is lost as the feed stream becomes richer in the primary component to be recovered e.g. ethanol. Furthermore, the aim of this project is to determine the effect of the phase equilibria uncertainty on the process design and as such the optimal sequencing of columns is beyond of the scope of this investigation.

Ample literature is available to assist in the selection of appropriate and representative flow schemes. Thus, a two-column sequence was chosen for the modelling and design of the DIPE/IPA extractive distillation process based on the flow scheme reported by Luo *et al.*, (2014). Similarly, for the ethanol/water azeotropic distillation process the two-column flow scheme reported by Pienaar *et al.*, (2013) was chosen. The details of the respective process flow schemes are provided in Chapter 8.

6.5 Uncertainty quantification methodology

Assessing effects of uncertainties in process design can be carried out in several ways depending on the nature of the problem and was reviewed in Chapter 4. In this work, a combined computer-based approach through stochastic models and process simulation was used to assess the effect of phase equilibrium uncertainties on the sizing of key process equipment. The MCS technique generated a set of random input variables that represent the range of parametric uncertainty. This was followed by completing a process simulation for each unique set of input parameters with Aspen Plus® v8.8. The results were subsequently combined to develop cumulative distribution functions (CDF) for each design output of interest e.g. reboiler duty, heat exchanger surface area or column diameter. The CDF's were used to estimate the confidence level of the design. The MCS output was coupled to the process simulation software by Aspen Simulation Workbook.

6.5.1 Aspen Simulation Workbook

Aspen Simulation Workbook (ASW) was used as a tool in this thesis to run parametric simulations with a chosen uncertainty propagation approach as illustrated in Figure 6.2. It is a tool that allows Aspen Plus® to link process models to an Excel workbook (Aspen, 2006).

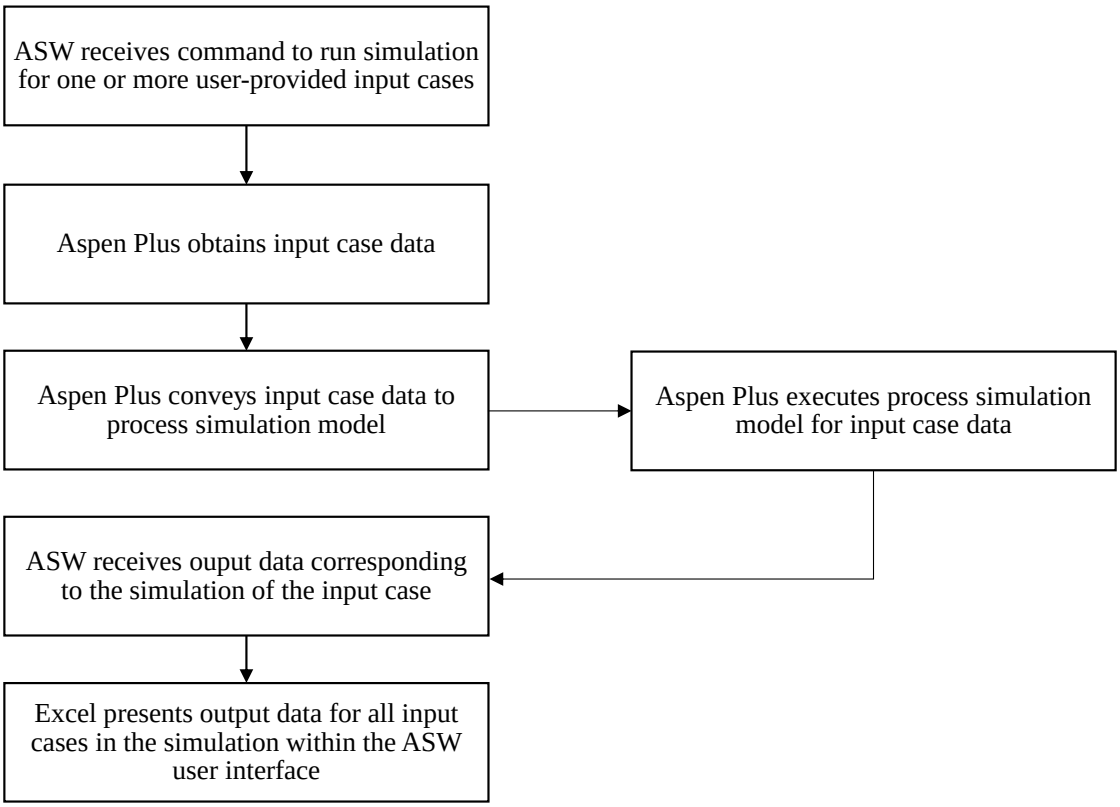

Figure 6.2. Aspen Simulation Workbook (ASW) operation concept.

ASW allows the user to set up a number of different scenario runs for a simulation in Excel. The process model input variables are determined by the user, and are conveniently entered into Excel. Then, Excel feeds these values to Aspen Plus® and runs the simulation for each of the scenarios. The user can define which output variables they want Aspen Plus® to feed to Excel. Thus, Excel becomes the controlling program as the simulation is run from Excel. This tool is very suitable when parametric studies have to be performed since the output format allows for easy data analysis.

The use of ASW provides a convenient means of performing MCS simulation based uncertainty propagation with commercial process simulation software like Aspen Plus®. The two primary factors in the MCS process, enabling a reliable estimate of the output variables, are the sampling technique and the number of samples (Frey, 1992).

6.5.2 Random sampling technique

The latin hypercube sampling (LHS) technique was reviewed in Section 4.5.1 and is widely recommended by workers in the field. Furthermore, it is also included as a standard feature in commercial risk analysis tools (Crystal Ball, @RISK) and statistical analysis software. In this study, the LHS technique was used as implemented in Statistica® 13.

6.5.3 Number of samples

For this work, a 95% confidence level (z = 1.96) was chosen for the ±0.05 confidence interval on the 0.95 fractile (95th percentile), which is similar to the approach of Hajipour and Satyro (2011). Therefore, a 95% confidence is ascribed to the calculated output variable that is actually at the 95th percentile to be somewhere between the 90^{th} and 99^{th} percentiles. Therefore, based on Equation 4.5, it was estimated that 100 Monte Carlo simulations per case provide the required 95% confidence level.

6.6 Uncertainty quantification methods considered

It was concluded from the literature review that the uncertainty quantification methods proposed by Hajipour and co-workers (Hajipour and Satyro, 2011; Hajipour, 2013; Hajipour, Satyro and Foley, 2014) and Whiting and co-workers (Reed and Whiting, 1993; Vasquez and Whiting, 1998; Vásquez, Whiting and Meerschaert, 2010) are the most widely investigated probabilistic based methods with a range of process design related examples.

The conceptual schemes of the respective approaches proposed by Hajipour and Whiting are reviewed next to understand the practical stepwise implementation. As a matter of convenience, the methods are referred to as Approach I (Hajipour and co-workers) and Approach II (Whiting and co-workers).

6.6.1 Approach I: Hajipour and co-workers method

One of the most recent, and simplest, uncertainty quantification approaches is the one developed by (Hajipour, 2013). In this approach, the experimental data involved in the study serves as the probabilistic input variables as shown in Figure 6.3.

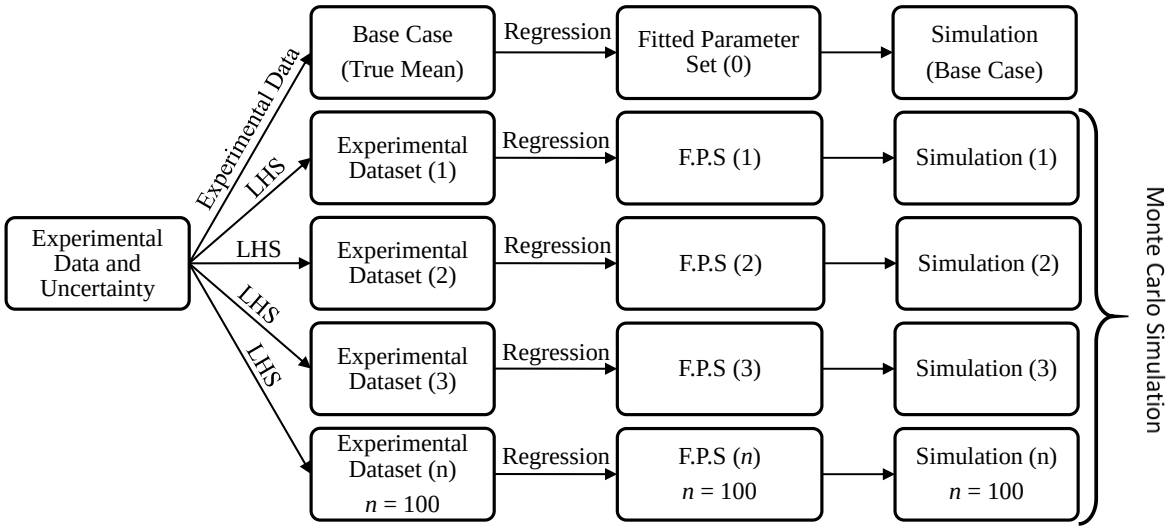

Figure 6.3. Conceptual scheme of Approach I as proposed by Hajipour. Redrawn and adapted from Hajipour (2013).

Firstly, the probability density functions for the phase equilibrium experimental data (e.g. *T*, *P*, *x* and *y*) is specified by assuming the reported value is the mean (μ) and at a 95% confidence level the parametric uncertainty is determined by the standard deviation (σ) according to μ±2σ assuming a normal (Gaussian) distribution.

Next, the Monte Carlo simulation sample sets (*n*) are generated for each input parameter with the help of the latin hypercube sampling (LHS) method. The generated experimental data sets (1,2,3…*n*) are entered as input case data into the process simulation software and regression is performed using the chosen thermodynamic model (e.g. NRTL) to calculate the binary interaction parameters (fitted parameter set in Figure 6.3) for each case. Once this is completed, the output parameters are calculated by passing each fitted parameter set (1,2,3…*n*) through the simulation model.

Note that the number of binary interaction parameters is dependent on the number of components and model parameters. For example, if the NRTL model is used and the regression is performed on a_{ij}, a_{ji}, b_{ij}, b_{ji} and α_{ij} for a three component system, then there are a total of 15 binary interaction parameters per set. So, if *n* is 100, a total of 100 fitted parameter sets are passed through the simulation model and 100 possible design values for each output value of interest is calculated. Statistical analysis of the results is then performed to evaluate the uncertainty of the model outputs.

6.6.2 Approach II: Whiting and co-workers method

The following approach was developed by Whiting *et al.*, (1993). It provides a methodology for the development of design uncertainty estimates arising from the model parameter uncertainty. In this approach, the binary interaction parameters serve as the probabilistic input variables as shown in Figure 6.4. A Monte Carlo simulation with Latin Hypercube Sampling (LHS) and Iman-Conover correlation control is employed to quantify the effect of binary interaction parameter uncertainty by propagating the uncertainties to the phase equilibrium calculations.

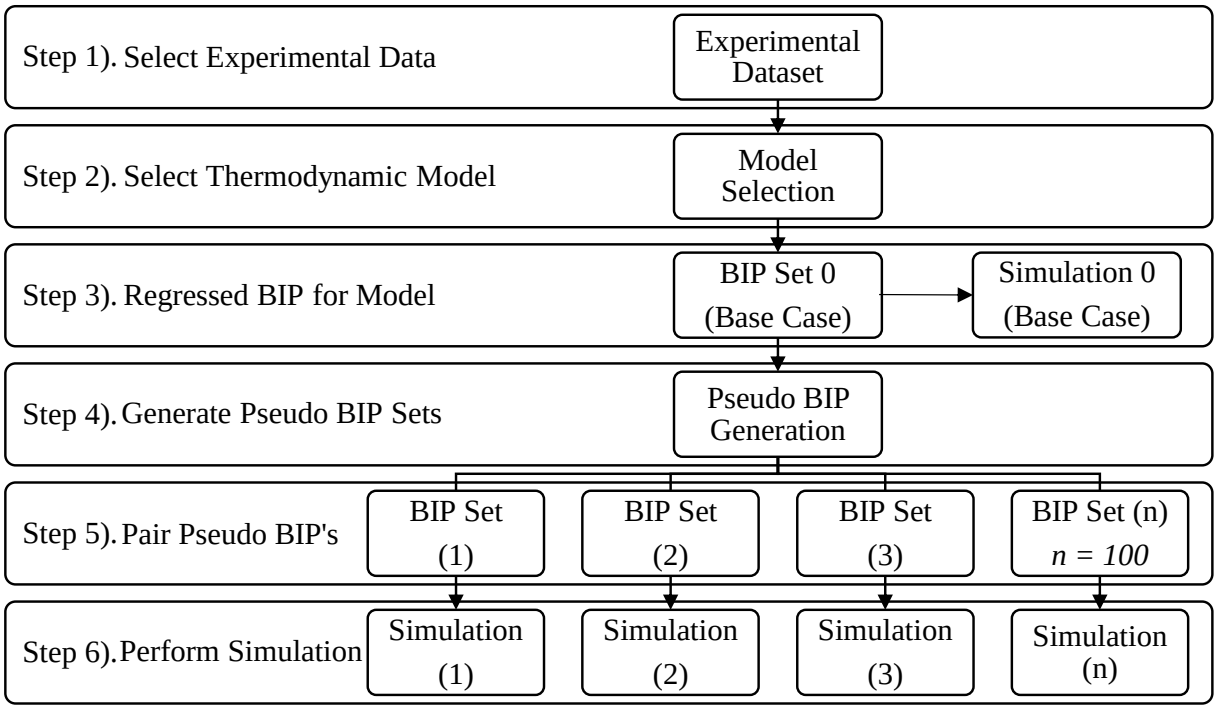

Figure 6.4. Conceptual scheme of Approach II as proposed by Whiting *et al.*, (1993)

In this approach, the first step is to identify suitable experimental data for the system of interest followed by selecting an appropriate thermodynamic model. Next, binary interaction parameters (BIP) are calculated through regression of the experimental data with the chosen thermodynamic model. The regressed BIP set serves as the base case for all further simulations. The probability density functions for the base case BIP set is specified by assuming the regressed value is the mean (μ) and at a 95% confidence level, the parametric uncertainty is determined by the standard deviation (σ) according to $\mu \pm 2\sigma$ assuming a normal (Gaussian) distribution. The standard deviation (σ) is obtained from the regression analysis report in Aspen Plus®.

Next, as shown by *Step 4* in Figure 6.4, Monte Carlo simulation with latin hypercube sampling is used to generate *n* (e.g. *n* = 100) binary interaction parameter sets. In order to correct for BIP correlation, the Iman-Conover input correlation control method is used. This method ensures the generated binary interaction parameters are correctly paired as shown in *Step 5*. To conclude the process, the design output parameters are calculated by passing each BIP set (1,2,3…*n*) through the simulation model.

In summary, Approach I applies the probabilistic method to the experimental data based on the reported accuracy of the data, whereas, Approach II applies the probabilistic method directly to the binary interaction parameters of the thermodynamic model based on the regression error. The next step was to select the uncertainty quantification approach.

6.7 Verification of uncertainty quantification methods

In this section, the procedures applied to verify the accurate implementation of the uncertainty analysis methods is provided. The general approach was to identify an example application from the literature and then implement the specific method with the intention to replicate the published results. The conceptual scheme of the respective uncertainty analysis methods is as per the previous section. As the approaches were in principle fairly similar a selection was then made based on which method was successfully verified.

6.7.1 Approach I

The approach proposed by Hajipour *et al.*, (2014) is illustrated by an example of a de-ethaniser used to stabilise liquefied petroleum gas (LPG). The column operates at 2758 kPa (400 PSI) with purity specifications on the distillate of 0.99 mole fraction and 0.98 mole fraction on the bottoms product. In the original publication (Hajipour *et al.*, 2014) the authors did not report details on the process model, but rather focused on the uncertainty propagation of the experimental data to the phase equilibrium curves (i.e. dew point and bubble point curves). As the probabilistic component in this approach starts with the experimental data it nonetheless served as a suitable verification example, since the subsequent process modelling is arbitrary.

Step 1: Selection of experimental data and associated uncertainty

The experimental vapour-liquid equilibrium data used by Hajipour *et al.*, (2014) was from Matschke and Thodos, (1962) for the system ethane + propane at 2758 kPa. The reported uncertainties on the experimental data were, on average, equal to 0.5 K for temperature, 0.0015

for liquid phase composition (x) and 0.0015 for vapour composition (y) and are presented in Table 6.1.

Table 6.1: Experimental VLE data for the system ethane + propane at 2758 kPa as reported by Hajipour *et al.*, (2014).

Data Point	Temperature (K) σ_{avg} = 0.25 K	Liquid (x) σ_{avg} = 0.00075	Vapour (y) σ_{avg} = 0.00075
1	337.5	0.0000	0.0000
2	336.6	0.0200	0.0286
3	334.4	0.0700	0.1000
4	331.1	0.1404	0.2000
5	327.5	0.2120	0.3000
6	323.5	0.2856	0.4000
7	319.0	0.3625	0.5000
8	314.0	0.4447	0.6000
9	310.5	0.5000	0.6623
10	308.2	0.5356	0.7000
11	301.2	0.6415	0.8000
12	292.3	0.7776	0.9000
13	279.6	0.9900	0.9968

Step 2: Verification of the experimental data thermodynamic consistency

Hajipour *et al.*, (2014) applied a range of tests to confirm the thermodynamic consistency of the VLE data used in their study in order to verify if it was within accepted error margins. The data for the 2758 kPa pressure case (amongst others) were considered to be acceptable for evaluation of binary interaction parameters.

Step 3: Generation of pseudo-experimental data sets

The latin hypercube sampling (LHS) method was employed to select random data points from the normal distribution defined for each input variable based on their uncertainty information. In this approach, the input variables are the experimental data namely temperature, liquid composition and vapour composition at isobaric conditions. A total of 100 Monte Carlo sample sets were generated using Statistica® 13 and a sample case is presented in Table 6.2.

Table 6.2: The latin hypercube sampling generated pseudo VLE data set for one (out of 100) sample sets for the system ethane + propane at 2758 kPa using Approach I as adapted from Hajipour *et al.*, (2014).

Data Point	Temperature (K)	Liquid (x)	Vapour (y)
1	337.0	0.0000	0.0000
2	336.3	0.0201	0.0287
3	334.8	0.0703	0.1016
4	331.7	0.1397	0.1998
5	327.2	0.2114	0.3012
6	323.9	0.2833	0.3991
7	319.0	0.3615	0.4999
8	314.4	0.4442	0.5996
9	310.6	0.4985	0.6622
10	307.4	0.5356	0.7001
11	301.0	0.6419	0.7994
12	292.3	0.7769	0.9000
13	279.5	0.9900	0.9967

The temperature-composition diagrams incorporating the phase equilibrium uncertainty propagation are shown in Figure 6.5 and Figure 6.6 respectively for the original results published by Hajipour *et al.*, (2014) and the results obtained in the verification procedure of this work. The graphical representation convention used by Hajipour and co-workers is to show every Monte Carlo simulation result as a single solid black line and the resulting thickness of the combined lines represent the uncertainty range. In this thesis, the Monte Carlo simulation results are grey lines, the mean of the Monte Carlo simulations a solid black line and the 5^{th} and 95^{th} confidence interval levels are dashed red lines.

The dew point and bubble point curve result from the verification procedure closely represent the original results of Hajipour *et al.*, (2014). Therefore, it is concluded that the method can be used with confidence as it produced comparable results.

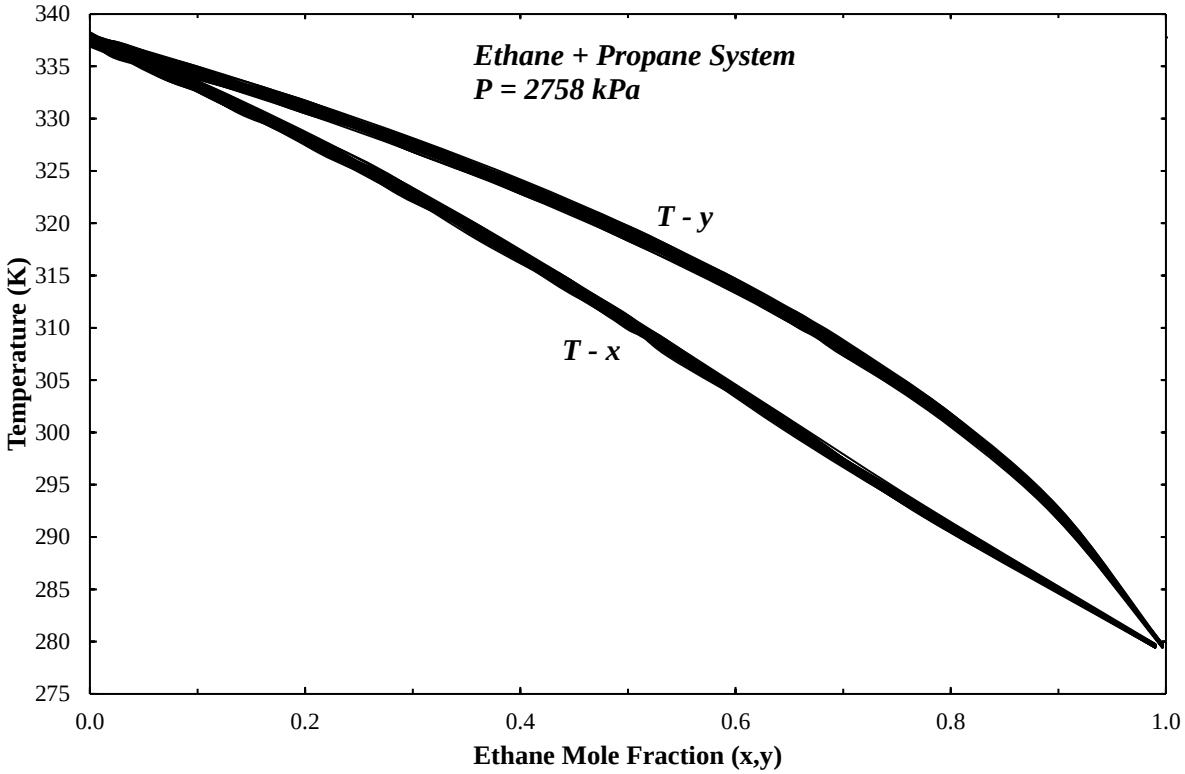

Figures 6.5: Temperature-composition diagram calculated taking into account the estimated uncertainties in composition for ethane + propane system at a pressure of 2758 kPa. Redrawn from Hajipour *et al.*, (2014).

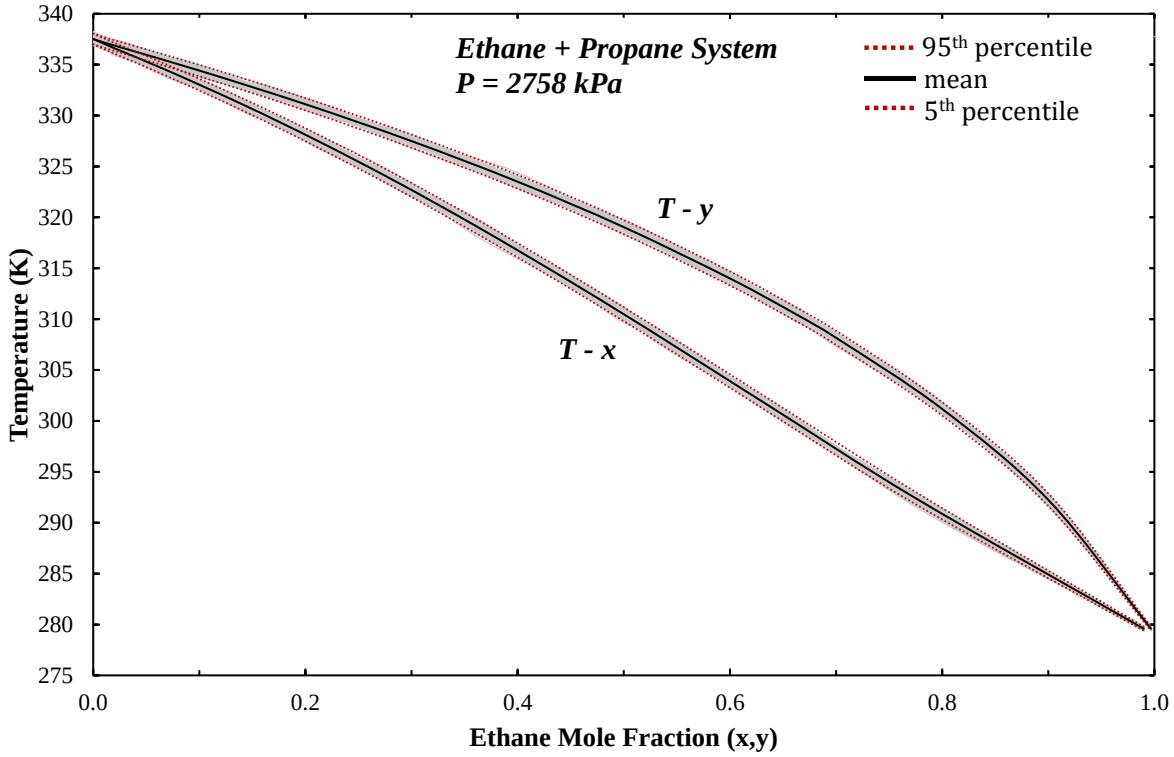

Figures 6.6: Approach I verification results for the temperature-composition diagram of ethane + propane system at a pressure of 2758 kPa. Grey lines are the individual Monte Carlo simulation results, the black line is the simulation mean and red lines represent the confidence intervals.

6.7.2 Approach II

For the verification of Approach II, an example of a liquid-liquid extraction operation reported by Whiting, Vasquez and Meerschaert (1999) was used. The operating conditions were originally reported by Smith (1963). Water is used to separate a mixture of chloroform and acetone in a counter current extraction column with two equilibrium stages. The column operates at 25 °C and 1 atmosphere. The feed consists of equal amounts (weight basis) of chloroform and acetone. A solvent to feed mass ratio of 1.565 is used. The percentage of acetone extracted was the output variable of interest as was previously by Whiting *et al.*, (1999).

The model configuration parameters are summarised in Table 6.4.

Table 6.4: Aspen Plus® Extract model configuration parameters.

Parameter	Value
Feed flow rate	100 kg/hr
Solvent flow rate	156.5 kg/hr
Feed composition	Mass fraction
Chloroform	0.5
Acetone	0.5
Solvent composition	Mass fraction
Water	1.0
Pressure	1 Atm
Temperature	25 °C

Step 1: Experimental data selection

Three sets of experimental data were used by Whiting *et al.*, (1999) and all data was taken from the DECHEMA liquid-liquid equilibrium data collection (DECHEMA and Arlt *et al.*,, 1979). The details of the experimental data were not reported but were also not required to perform the verification procedure.

Step 2: Thermodynamic model selection

The NRTL activity coefficient model was used for the liquid phase modelling of the extraction process. The NRTL model can describe VLE and LLE for combinations of polar and non-polar compounds, as well as strongly non-ideal solutions. The model requires binary interaction parameters; these parameters were reported by Whiting *et al.*, (1999).

Step 3: Regression of binary interaction parameters

The original regressions by Whiting *et al.*, (1999) were performed using Aspen Plus®. The binary interaction parameters obtained with some statistical indicators are shown in Table 6.3. The error estimate (ERR) is based on the weighted sum of squares (S) and the number of experimental data (n) and is calculated with Equation 6.2.

$$ERR = \sqrt{\frac{S}{n}} \tag{6.2}$$

Table 6.3: Binary parameters b_{ij} and b_{ji} regressed for the NRTL model ($\alpha = 0.2$) for the system chloroform (1) + acetone (2) + water (3) at 25 °C as regressed by Whiting *et al.*, (1999).

i	j	b_{ij}	Standard deviation	b_{ji}	Standard deviation
		Set 1	$(S/n)^{0.5} = 133.89$		
1	2	334.71	985.36	-623.27	519.65
1	3	518.27	214.56	1554.90	174.54
2	3	378.08	554.84	282.94	285.88
		Set 2	$(S/n)^{0.5} = 71.77$		
1	2	34.30	5.29	-681.75	3.24
1	3	1636.27	36.30	1744.10	2.03
2	3	80.26	1.62	392.63	0.87
		Set 3	$(S/n)^{0.5} = 128.25$		
1	2	-300.07	273.73	-227.84	278.75
1	3	1044.28	168.30	1499.60	74.07
2	3	-43.37	120.13	518.20	96.08

Step 4: Generation of pseudo-binary interaction parameters

In the work of Whiting *et al.*, (1999) the samples were chosen using latin hypercube sampling (LHS) and a normal distribution was assumed for the binary interaction parameters with the standard deviations as per Table 6.3. A total of $n = 100$ Monte Carlo input parameter samples were generated for the six binary interaction parameters using Statistica® 13 and the method is further illustrated only for Set 1. An example of the unpaired sets is provided in the next step as input matrix $\boldsymbol{X}$. For convenience, only the first 10 sample sets (out of the total of 100) are shown.

Step 5: Input parameter correlation control

Input parameter correlation was induced by applying the Iman-Conover correlation control method. The technique is discussed in detail by Iman and Conover (1982) and its application is illustrated next. The input matrix (***X***) was

$$\boldsymbol{X} = \begin{array}{c} \begin{matrix} b_{12} & b_{21} & b_{13} & b_{31} & b_{23} & b_{32} \end{matrix} \\ \begin{bmatrix} -1\,074.89 & -441.20 & 828.28 & 1\,606.12 & -231.25 & 496.87 \\ -972.08 & -1\,093.52 & 663.55 & 1\,585.44 & -187.39 & 460.04 \\ -720.04 & -1\,347.88 & 504.92 & 1\,354.96 & 553.73 & 377.56 \\ -274.01 & -1\,213.20 & 374.41 & 1\,216.36 & 727.71 & 200.62 \\ 363.54 & 783.33 & 515.30 & 1\,516.40 & -598.72 & 70.49 \\ 412.17 & -396.40 & 245.99 & 1\,974.60 & 356.48 & -150.04 \\ 471.57 & -494.05 & 71.17 & 1\,833.95 & 1\,058.94 & 280.46 \\ 557.98 & 15.72 & 709.62 & 1\,777.97 & 627.12 & 527.64 \\ 660.36 & -907.40 & 273.20 & 1\,551.13 & 209.03 & 402.44 \\ 661.00 & -1\,760.35 & 574.20 & 1\,581.56 & -389.59 & -469.50 \end{bmatrix} \end{array} \begin{matrix} n \\ 1 \\ 2 \\ 3 \\ 4 \\ 5 \\ 6 \\ 7 \\ 8 \\ 9 \\ 10 \end{matrix}$$

The NRTL equation correlation matrix (***S***) used for the system chloroform + acetone + water for Set 1 was reported in a separate publication (Vasquez and Whiting, 2000):

$$\boldsymbol{S} = \begin{bmatrix} \mathbf{1.000000} & -0.877468 & -0.461489 & 0.583567 & 0.890708 & -0.738413 \\ -0.877468 & \mathbf{1.000000} & 0.175802 & -0.397162 & -0.913656 & 0.809210 \\ -0.461489 & 0.175802 & \mathbf{1.000000} & -0.506065 & -0.606787 & 0.490189 \\ 0.583567 & -0.397162 & -0.506065 & \mathbf{1.000000} & 0.471075 & -0.376053 \\ 0.890708 & -0.813656 & -0.606787 & 0.471075 & \mathbf{1.000000} & -0.930917 \\ -0.738413 & 0.809210 & 0.490189 & -0.376053 & -0.930917 & \mathbf{1.000000} \end{bmatrix}$$

The Choleski decomposition of ***S*** was

$$\boldsymbol{C} = \begin{bmatrix} 1.0000 & -0.8775 & -0.4615 & 0.5836 & 0.890708 & -0.73841 \\ 0.0000 & 0.4796 & -0.4777 & 0.2396 & -0.0669 & 0.336249 \\ 0.0000 & 0.0000 & 0.7475 & -0.1636 & -0.3046 & 0.414779 \\ 0.0000 & 0.0000 & 0.0000 & 0.7585 & -0.1088 & 0.055606 \\ 0 & 0 & 0 & 0 & 0.312321 & -0.37884 \\ 0 & 0 & 0 & 0 & 0 & 0.151758 \end{bmatrix}$$

Created the intermediate matrix

$$\boldsymbol{M} = \begin{pmatrix} -1.92062 & -0.34878 & 1.008597 & 1.008597 & -1.50709 & 0.068745 \\ -1.50709 & -1.50709 & 1.507091 & -0.82015 & -1.0086 & 0.348785 \\ -1.22896 & 1.228964 & -0.82015 & -0.06875 & 0.820149 & 1.228964 \\ -1.0086 & -0.65151 & -0.20723 & 1.228964 & -0.49584 & -1.0086 \\ -0.82015 & -0.20723 & 0.348785 & 0.651508 & 1.228964 & 0.651508 \\ -0.65151 & -1.92062 & 0.820149 & -1.22896 & 0.495844 & 1.008597 \\ -0.49584 & 0.495844 & 0.651508 & -0.65151 & -1.92062 & 1.920616 \\ -0.34878 & -1.22896 & -0.06875 & -0.34878 & 1.920616 & -0.34878 \\ -0.20723 & 0.068745 & 0.207226 & -1.0086 & -0.34878 & -0.82015 \\ -0.06875 & 0.207226 & 0.495844 & 0.495844 & -0.06875 & -0.06875 \end{pmatrix}$$

Then, calculated the covariance matrix of $\boldsymbol{M}$

$$\boldsymbol{E} = \begin{pmatrix} \mathbf{1.0000} & 0.3705 & -0.5226 & 0.0717 & 0.1888 & -0.3182 \\ 0.3705 & \mathbf{1.0000} & -0.3781 & 0.3091 & -0.1069 & 0.1582 \\ -0.5226 & -0.3781 & \mathbf{1.0000} & -0.4904 & -0.0452 & 0.2341 \\ 0.0717 & 0.3091 & -0.4904 & \mathbf{1.0000} & 0.1031 & 0.0373 \\ 0.1888 & -0.1069 & -0.0452 & 0.1031 & \mathbf{1.0000} & -0.0416 \\ -0.3182 & 0.1582 & 0.2341 & 0.0373 & -0.0416 & \mathbf{1.0000} \end{pmatrix}$$

And $\boldsymbol{E}$ had Choleski decomposition

$$\boldsymbol{F} = \begin{pmatrix} 1.0000 & 0.3705 & -0.5226 & 0.0717 & 0.188817 & -0.31819 \\ 0.0000 & 0.9288 & -0.1986 & 0.3042 & -0.19041 & 0.297271 \\ 0.0000 & 0.0000 & 0.8291 & -0.4735 & 0.018929 & 0.152964 \\ 0.0000 & 0.0000 & 0.0000 & 0.8235 & 0.189978 & 0.051118 \\ 0 & 0 & 0 & 0 & 0.944268 & 0.066176 \\ 0 & 0 & 0 & 0 & 0 & 0.883174 \end{pmatrix}$$

Thus $\boldsymbol{T = MF^{-1}C}$ was given by

$$\boldsymbol{T} = \begin{pmatrix} -1.92062 & 1.872676 & 0.774035 & -0.05378 & -2.34565 & 2.08157 \\ -1.50709 & 0.832549 & 1.64928 & -1.3241 & -1.7494 & 1.409481 \\ -1.22896 & 1.948169 & -1.29303 & -1.13513 & -0.09834 & 0.287408 \\ -1.0086 & 0.741569 & -0.10724 & 0.361265 & -0.89635 & 0.344291 \\ -0.82015 & 0.769578 & 0.27543 & 0.151947 & -0.38544 & 0.192224 \\ -0.65151 & -0.29545 & 1.273191 & -1.35605 & -0.29634 & -0.03832 \\ -0.49584 & 0.786018 & 0.364019 & -0.70968 & -1.13962 & 1.751225 \\ -0.34878 & -0.26184 & 0.288343 & -0.61343 & 0.583545 & -1.15589 \\ -0.20723 & 0.256987 & 0.138019 & -0.99981 & -0.1348 & 0.076048 \\ -0.06875 & 0.180487 & 0.371533 & 0.578411 & -0.42089 & 0.462485 \end{pmatrix}$$

Performed check to confirm that $\boldsymbol{T}$ had a correlation matrix $\boldsymbol{S}$

$$\boldsymbol{S} = \begin{pmatrix} \mathbf{1.0000} & -0.8775 & -0.4615 & 0.5836 & 0.8907 & -0.7384 \\ -0.8775 & \mathbf{1.0000} & 0.1758 & -0.3972 & -0.8137 & 0.8092 \\ -0.4615 & 0.1758 & \mathbf{1.0000} & -0.5061 & -0.6068 & 0.4902 \\ 0.5836 & -0.3972 & -0.5061 & \mathbf{1.0000} & 0.4711 & -0.3761 \\ 0.8907 & -0.8137 & -0.6068 & 0.4711 & \mathbf{1.0000} & -0.9309 \\ -0.7384 & 0.8092 & 0.4902 & -0.3761 & -0.9309 & \mathbf{1.0000} \end{pmatrix}$$

The difference to the target correlation $\boldsymbol{S}$ was

$$\boldsymbol{\Delta S} \begin{pmatrix} \mathbf{0.0} & 0.0 & 0.0 & 0.0 & 0.0 & 0.0 \\ 0.0 & \mathbf{0.0} & 0.0 & 0.0 & 0.1 & 0.0 \\ 0.0 & 0.0 & \mathbf{0.0} & 0.0 & 0.0 & 0.0 \\ 0.0 & 0.0 & 0.0 & \mathbf{0.0} & 0.0 & 0.0 \\ 0.0 & 0.0 & 0.0 & 0.0 & \mathbf{0.0} & 0.0 \\ 0.0 & 0.0 & 0.0 & 0.0 & 0.0 & \mathbf{0.0} \end{pmatrix}$$

And the resulting re-ordering of $\boldsymbol{X}$ was

$$\boldsymbol{X} = \begin{array}{c} \begin{matrix} b_{12} & b_{21} & b_{13} & b_{31} & b_{23} & b_{32} \end{matrix} \\ \begin{pmatrix} 511.16 & -67.99 & 208.81 & 1\,569.13 & -435.03 & 239.00 \\ -1\,227.75 & -279.54 & 508.27 & 1\,578.39 & -185.22 & 564.00 \\ 623.43 & -848.40 & 197.76 & 1\,562.75 & -511.88 & -126.71 \\ 649.72 & 428.27 & 174.57 & 1\,461.14 & 1\,154.66 & 850.37 \\ 180.04 & -765.41 & 445.38 & 1\,520.53 & 533.90 & 106.18 \\ 857.01 & -737.63 & 157.52 & 1\,372.00 & 318.77 & -128.69 \\ 2\,232.96 & -141.08 & 378.68 & 1\,560.13 & 616.83 & 460.69 \\ -458.92 & -470.70 & 663.78 & 1\,587.98 & 142.25 & 338.69 \\ 903.06 & -822.80 & 358.94 & 1\,372.55 & 871.21 & 244.44 \\ 37.10 & -463.29 & 576.61 & 1\,523.25 & 391.83 & 73.13 \end{pmatrix} \end{array} \begin{matrix} n \\ 1 \\ 2 \\ 3 \\ 4 \\ 5 \\ 6 \\ 7 \\ 8 \\ 9 \\ 10 \end{matrix}$$

Although the overall correlation control appeared to be reasonable, it was observed that a marginal difference exists between the target correlation matrix and the final correlation matrix for one of the pairs.

Step 6: Perform process simulations with correlated input parameters

Whiting *et al.*, (1999) performed the process simulations using ChemCAD® (Chemstations™) and in this work, Aspen Plus® was used exclusively. In reference to work by Sadeq, Duarte and Serth (1997), Whiting *et al.*, (1996) reported differences in simulation outputs when using two or more simulation software packages. For that reason, it was foreseen that the results of Whiting *et al.*, (1999) may not be replicated exactly.

The Aspen Plus® *Extract model* was selected as it is a rigorous model for simulating liquid extraction with a solvent and is shown in Figure 6.7. The distribution coefficients were calculated using the NRTL activity coefficient model as noted in Step 2 of this procedure. Complete model configuration details were not provided by Whiting *et al.*, (1999). The adiabatic thermal option was selected and the pressure drop was assumed to be zero. The key component for the 1st liquid phase was chloroform and for the 2nd liquid phase was water. The *Broyden method* was specified for the outside loop convergence and the *Broyden-Wegstein* method for inside loop convergence.

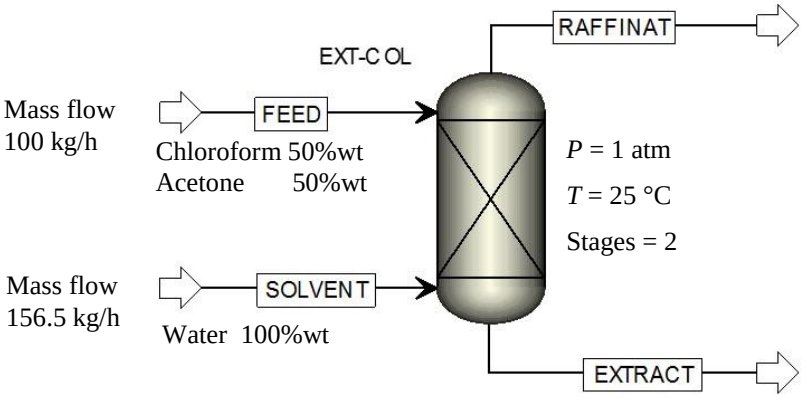

Figure 6.7. Aspen Plus® liquid-liquid extraction model for system chloroform (1) + acetone (2) + water (3) at 25 °C to verify methodology for Approach II.

The cumulative distribution function curves for Set 1, 2 and 3 are presented in Figure 6.8 and Figure 6.9 respectively for the original results published by Whiting *et al.*, (1999) and the results obtain in the verification procedure of this work.

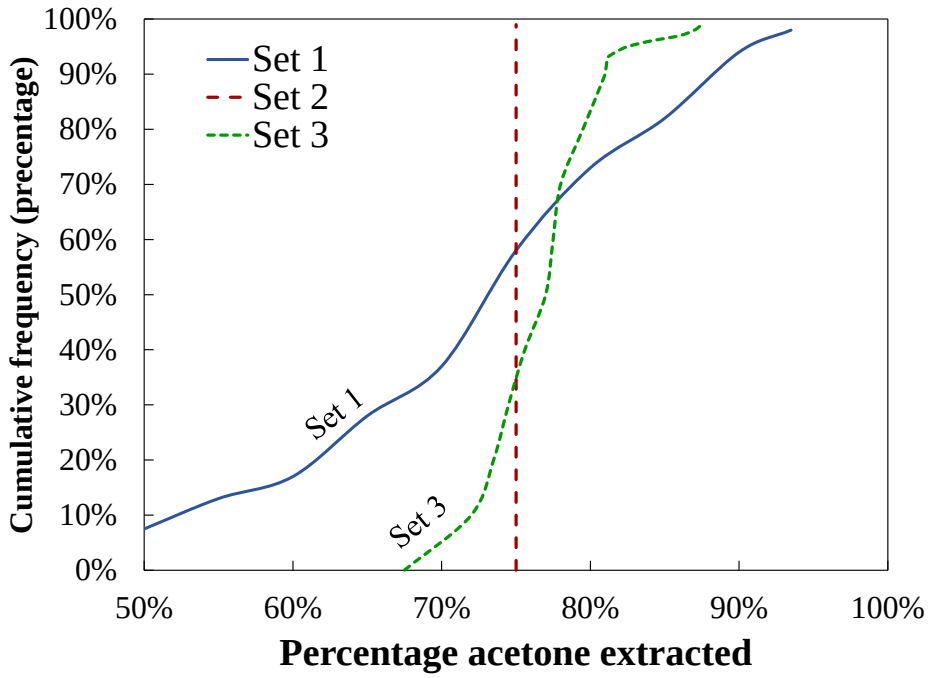

Figure 6.8. Comparison of verification results of Approach II for the uncertainty of percentage of acetone extracted in the liquid-liquid extractor. Redrawn from Whiting *et al.*, (1999).

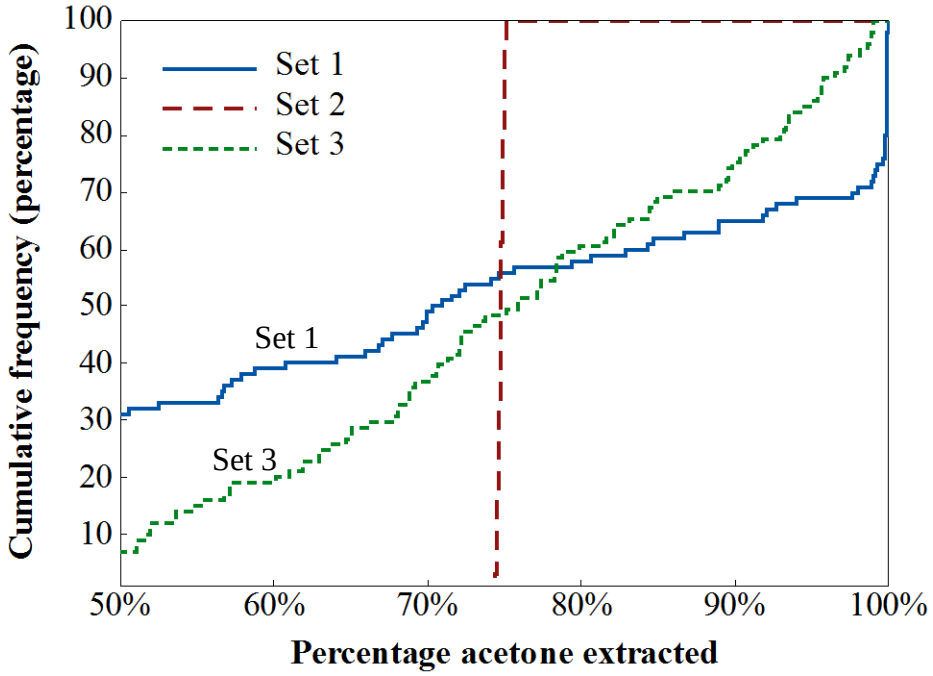

Figure 6.9. Comparison of verification results of Approach II for the uncertainty of percentage of acetone extracted in the liquid-liquid extractor for this work.

A comparative summary of the 50th and 90th percentile confidence levels are provided in Table 6.5. The verification procedure results for the 50th percentile confidence level compares favourably with the original work of Whiting *et al.*, (1999). However, the difference in slopes of the CDF's for Figure 6.8 vs. Figure 6.9. is evident in the results obtained for the 90th percentile confidence level.

Table 6.5. Results of the verification procedure. Comparison of extraction uncertainty with results published by Whiting *et al.*, (1999) and the verification procedure of this work.

Confidence level	BIP Set	Whiting *et al.*	This work
50th	Set 1	73%	71%
	Set 2	75%	75%
	Set 3	77%	77%
90th	Set 1	82%	97%
	Set 2	75%	75%
	Set 3	87%	100%

It is possible that the verification procedure results are different as a result of using different simulation software, extraction column convergence algorithms or the imperfect input parameter correlation control results obtain by the Iman-Conover method. In order to ensure that the verification procedure was correctly applied, a sensitivity analysis was performed on the model configuration within Aspen Plus®. The process was repeated with the *Wegstein*

method outside loop convergence, but no significant improvement was observed. Next, the theoretical tray efficiency was tested at 75%, 80% and 100% with no improvement. Lastly, the NRTL α-value was increased from 0.2 to 0.3 and also yielded no improvement.

The result of the tail-end of the CDF's is important in this work because the 95th percentile is chosen. Therefore, it is essential that reliable results are obtained in this area. Considering these findings a decision was made to select Approach I.

6.8 Chapter summary

In this chapter the research design and methodologies were presented. A two-column sequence was chosen for the modelling and design of the DIPE/IPA extractive distillation process based on the flow scheme reported by Luo *et al.*, (2014). Similarly, for the ethanol/water azeotropic distillation process the two-column flow scheme reported by Pienaar *et al.*, (2013) was chosen. The uncertainty quantification methods proposed by Hajipour and co-workers and Whiting and co-workers were reviewed in detail and a procedure performed to verify the accurate implementation of the methods. In the following section the results of this thesis are presented and the findings discussed.

III RESULTS & FINDINGS

Chapter 7
Phase Equilibrium Uncertainty Results

In this chapter, the aims are as follows. Firstly, a thermodynamic model screening and selection process is performed to evaluate the ability of the candidate thermodynamic models (identified in Chapter 3) to successfully correlate the experimental phase equilibria behaviour of the respective systems; thereby addressing project *Objective (i)* (***What is the best model?)*** Secondly, the effect of the experimental data parametric uncertainties on the phase-equilibrium calculations is evaluated using the selected thermodynamic model; thereby addressing project *Objective (ii).*

7.1 Model selection method

In modelling the measured phase equilibria data the first step is to determine the model parameters, specifically the binary interaction parameters of the components. The parameter regression may be based on only vapour-liquid equilibrium (VLE) data or a combination of VLE data with liquid-liquid equilibrium (LLE) data. The regression procedure was previously discussed in Section 6.2 and furthermore the NIST TDE was chosen as the source of experimental data. Only phase equilibrium data is considered for regression of model parameters and all other properties are excluded, for example, vapour pressure and liquid molar volume.

In general, three parameter options are considered namely, (1) those reported in the literature, (2) the Aspen Plus library parameters or (3) parameters regressed in this work. The first only serves as a reference and (2) and (3) further considers the effect of the type of equilibrium data i.e. VLE or VLE and LLE. Once the model parameters are obtained the ability of the respective models to correlate the experimental data is assessed based on the ARD for the azeotropic temperature, azeotropic composition, and binary system temperature-composition predictions.

The approach is common to both the extractive distillation system (*System 1*) and the heterogeneous azeotropic distillation system (*System 2*). Although, for *System 2*, the binary temperature-composition predictions is replaced by the ternary phase equilibrium correlation ability. The results of the extractive distillation system are presented first, followed by the results of the azeotropic distillation system.

7.2 System 1: Extractive distillation model selection

In this case, the extractive distillation of the minimum boiling azeotrope of diisopropyl ether (DIPE) and isopropyl alcohol (IPA) with heavy entrainer 2-methoxyethanol (2MET) is investigated.

7.2.1 Thermodynamic model screening results

Table 7.1 provides the absolute average relative deviation (ARD) results listed per model for the azeotrope and binary VLE and is ranked from highest to lowest on total ARD. It is noted that the models fitted with parameters regressed from individual VLE data sets produce the best results. In general, the Aspen Plus default parameters were comparable or within ca. 10% of the total ARD of the best performing models. A decrease in model accuracy is observed for model parameters regressed from a combined VLLE data set and produced the poorest predictions.

Table 7.1. Descriptive statistics results for various model phase equilibrium calculations.

Total ARD	**Azeotrope**	**DIPE+IPA VLE**	**DIPE+2MET VLE**	**IPA+2MET VLE**	**Sum**
NRTL-HOC (VLLE)	35.4%	46.4%	218.8%	13.4%	314%
NRTL (VLLE)	29.0%	47.0%	222.5%	13.7%	312%
NRTL-RK (VLLE)	31.8%	46.3%	218.9%	14.3%	311%
UNIQUAC (VLLE)	18.1%	47.5%	223.2%	19.4%	308%
NRTL-NTH (VLLE)	29.1%	46.5%	218.2%	13.4%	307%
CPA (VLE)	3.3%	46.9%	235.7%	19.9%	306%
NRTL (Luo *et al.*, 2014))	7.7%	45.6%	222.3%	19.1%	295%
UNIQUAC (Aspen)	6.8%	47.5%	223.2%	13.7%	291%
UNIQUAC (VLE)	6.6%	47.5%	222.5%	13.7%	290%
NRTL (VLE)	6.2%	47.0%	222.5%	13.7%	289%
NRTL (Aspen)	6.6%	47.5%	221.0%	14.1%	289%
NRTL-HOC (Aspen)	10.5%	46.4%	218.8%	13.4%	289%
NRTL-RK (Aspen)	8.0%	46.3%	218.9%	14.3%	288%
NRTL-RK (VLE)	7.6%	46.3%	218.9%	14.3%	287%
SR-POLAR (VLE)	2.5%	46.4%	222.3%	13.7%	285%
NRTL-NTH (Aspen)	6.0%	46.5%	218.2%	13.4%	284%
NRTL-NTH (VLE-NTH)	2.8%	46.5%	218.2%	13.4%	281%
NRTL-HOC (VLE-HOC)	1.8%	46.4%	218.8%	13.4%	281%

When analysing the ARD results, it is evident that the NRTL model, including its variants, appear to be overall the best performing model and produce the best fits of the experimental phase equilibrium data, although the SR-POLAR model performance is comparable, as shown in Figure 7.1. The CPA model accurately predicted the azeotrope composition and temperature,

but the VLE was the least accurate for the models with parameters regressed from the VLE data. The 2B association term was chosen and only the CPA K_{ij} binary parameter was considered as the other CPA parameters require fitting experimental vapour pressure and liquid molar volume data and this may be the reason the model was less accurate.

The model prediction for the azeotropic composition can be determined by finding the x-intercept of model prediction curve in a plot of (y-x) vs. x as presented in Figure 7.1. Here, the predicted azeotropic composition for the NRTL model with different parameter sets is illustrated and it is clear that the binary interaction parameters regressed as part of this work provide an accurate azeotrope composition.

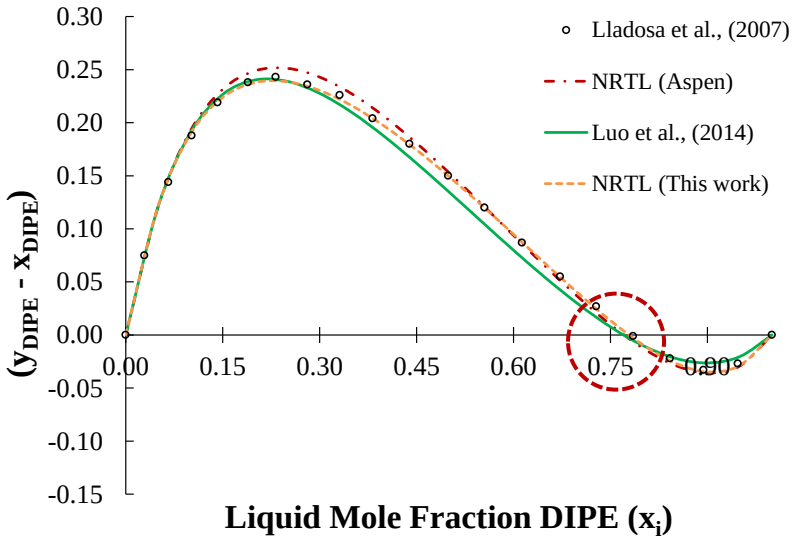

Figure 7.1a. Plot of (y-x) vs.x yielding azeotropic composition predicted by NRTL with different regression parameters. Red circle expaned in Figure 7.1b.

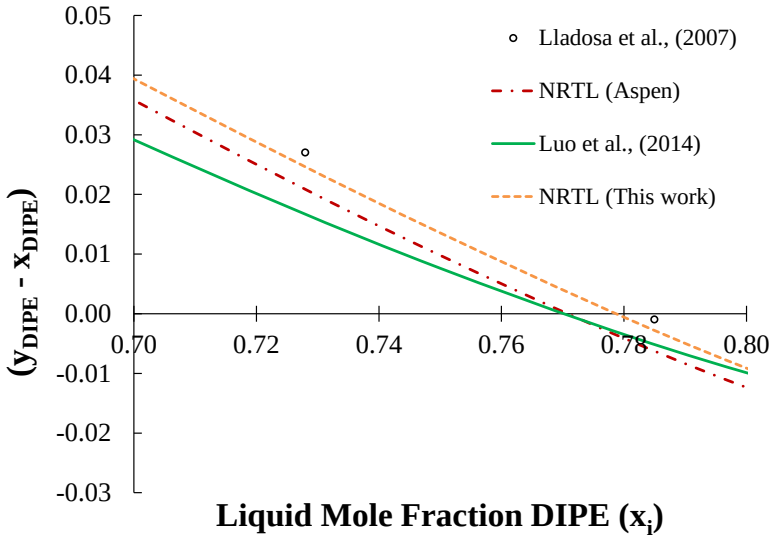

Figure 7.1b. Plot of (y-x) vs.x yielding azeotropic composition predicted by NRTL with different regression parameters.

Table 7.2 provides a summary of the azeotrope temperature and composition predictions for all the candidate models. It is apparent from Table 7.2 that models that calculate the vapour phase thermodynamic properties with an equation of state that considers gas phase interactions as opposed to the ideal gas law produce the best fits for the azeotrope predictions. For example, the NRTL-HOC model produced an improved azeotrope estimate over the NRTL model of ca. 5%, although no apparent benefit is observed on the binary VLE predictions. The observations are further illustrated in Figure 7.2 with a Pareto chart of the azeotrope ARD results and Figure 7.3 with a bar chart of the total model ARD results.

Table 7.2. Azeotrope results. Predicted azeotrope mixture temperature and composition for different thermodynamic models for System 1.

Azeotrope	Temp (C)	Type	No. Comp.	DIPE	IPA	2-MET
NRTL-HOC (Aspen)	66.00	Homogeneous	2	0.764	0.236	0
CPA (This work VLE)	66.07	Homogeneous	2	0.787	0.213	0
Experimental (Yorizane *et al.*, 1967)	66.10	Homogeneous	2	0.800	0.200	0
NRTL-RK (This work VLE)	66.13	Homogeneous	2	0.769	0.231	0
Experimental (Lladosa *et al.*, 2007)	**66.16**	**Homogeneous**	**2**	**0.782**	**0.218**	**0**
NRTL-RK (Aspen)	66.16	Homogeneous	2	0.768	0.232	0
NRTL-HOC (This work VLE)	66.19	Homogeneous	2	0.779	0.221	0
Experimental (Verhoeye, 1970)	66.20	Homogeneous	2	0.787	0.213	0
SR-POLAR (This work VLE)	66.24	Homogeneous	2	0.778	0.222	0
NRTL (This work VLE)	66.28	Homogeneous	2	0.772	0.229	0
NRTL-HOC (This work VLLE)	66.28	Homogeneous	2	0.722	0.278	0
NRTL (Aspen)	66.30	Homogeneous	2	0.771	0.229	0
NRTL-NTH (Aspen)	66.30	Homogeneous	2	0.772	0.228	0
UNIQUAC-HOC (VLE)	66.31	Homogeneous	2	0.774	0.226	0
UNIQUAC (Aspen)	66.34	Homogeneous	2	0.771	0.229	0
SR-POLAR (This work VLLE)	66.34	Homogeneous	2	0.757	0.243	0
UNIQUAC (This work VLE)	66.35	Homogeneous	2	0.771	0.229	0
NRTL-NTH (This work VLE)	66.48	Homogeneous	2	0.786	0.214	0
NRTL-RK (This work VLLE)	66.49	Homogeneous	2	0.728	0.272	0
NRTL (This work VLLE)	66.66	Homogeneous	2	0.734	0.266	0
NRTL-NTH (This work VLLE)	66.67	Homogeneous	2	0.733	0.267	0
UNIQUAC (This work VLLE)	66.76	Homogeneous	2	0.752	0.248	0
NRTL (Luo *et al.*, 2014))	66.82	Homogeneous	2	0.770	0.230	0
CPA (This work VLLE)	68.13	Homogeneous	2	0.987	0.013	0

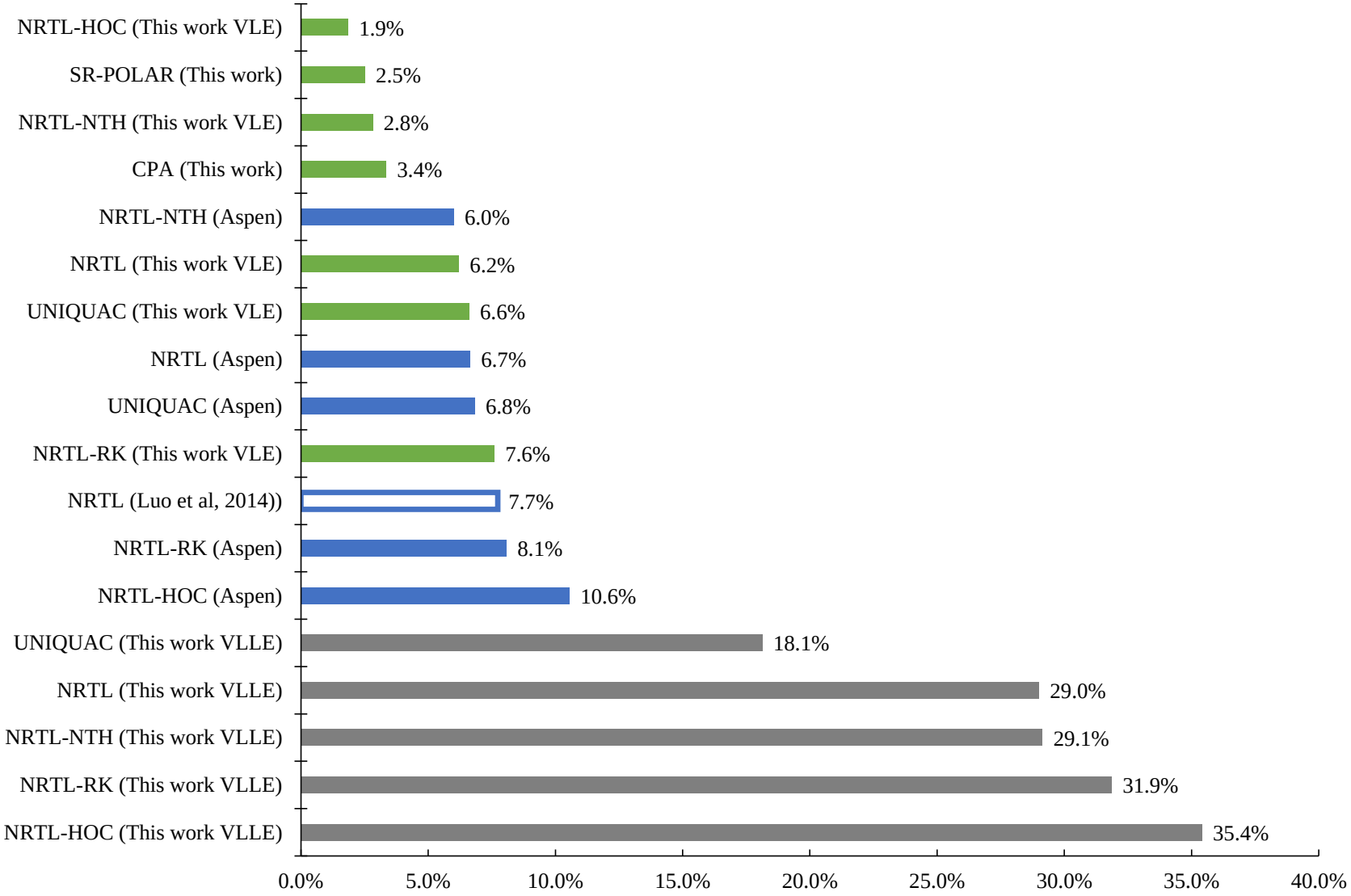

Figure 7.2. Pareto chart for azeotrope ARD for extractive distillation thermodynamic model screening.

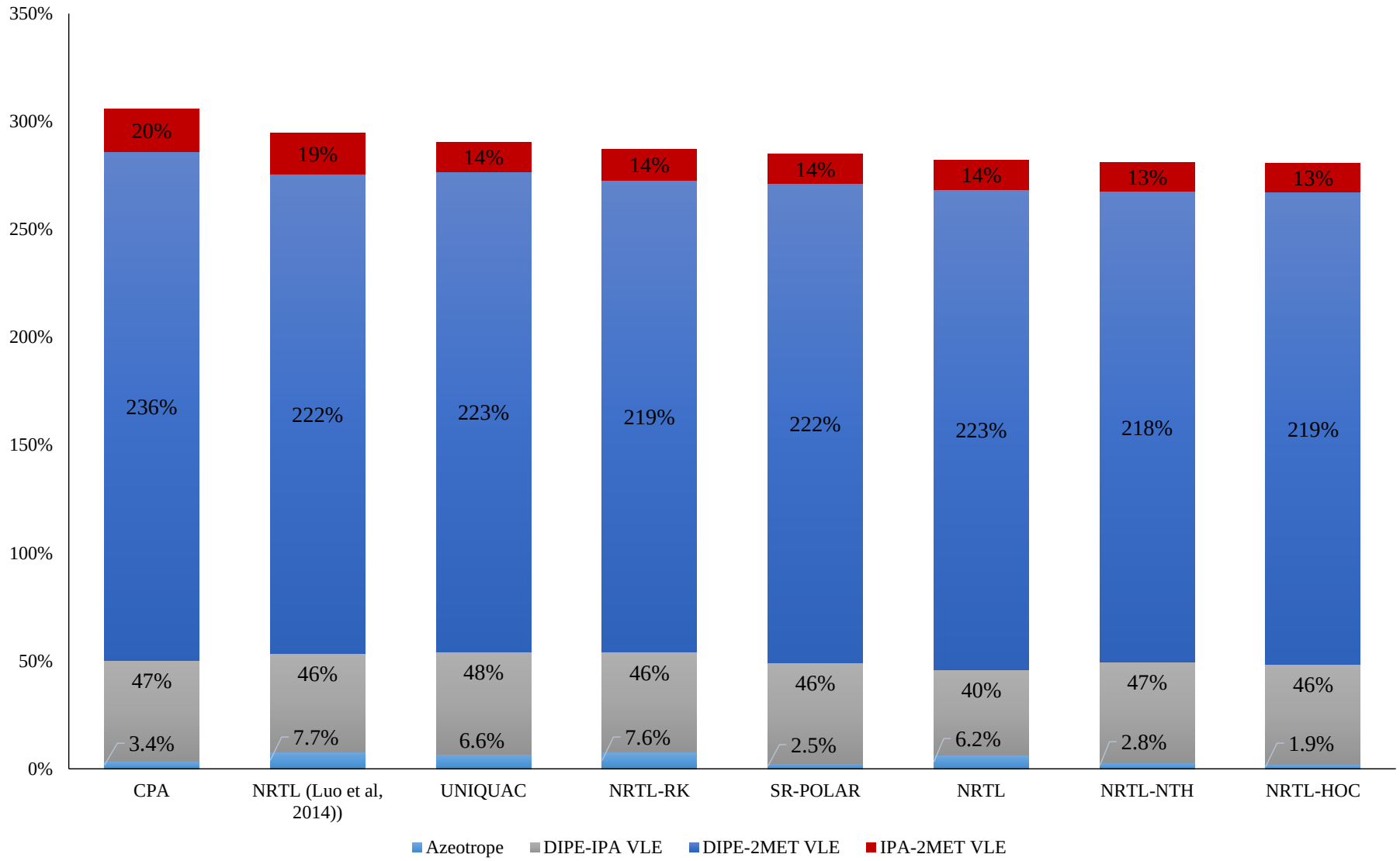

Figure 7.3. Bar chart for total model ARD for extractive distillation thermodynamic model screening.

7.2.2 Results of DIPE/IPA binary VLE predictions

With respect to the equilibria of the *DIPE/IPA* binary system, it is noted from Figure 7.4 that the NRTL model consistently predicts the boiling points of the components with great accuracy. The parameters regressed in this work and the Aspen Plus® default values predict the liquid phase accurately and provide improved results compared to those of Luo *et al.*, (2014). The vapour phase is under predicted and deviations are apparent in the dew curve, notably the lower concentration regions.

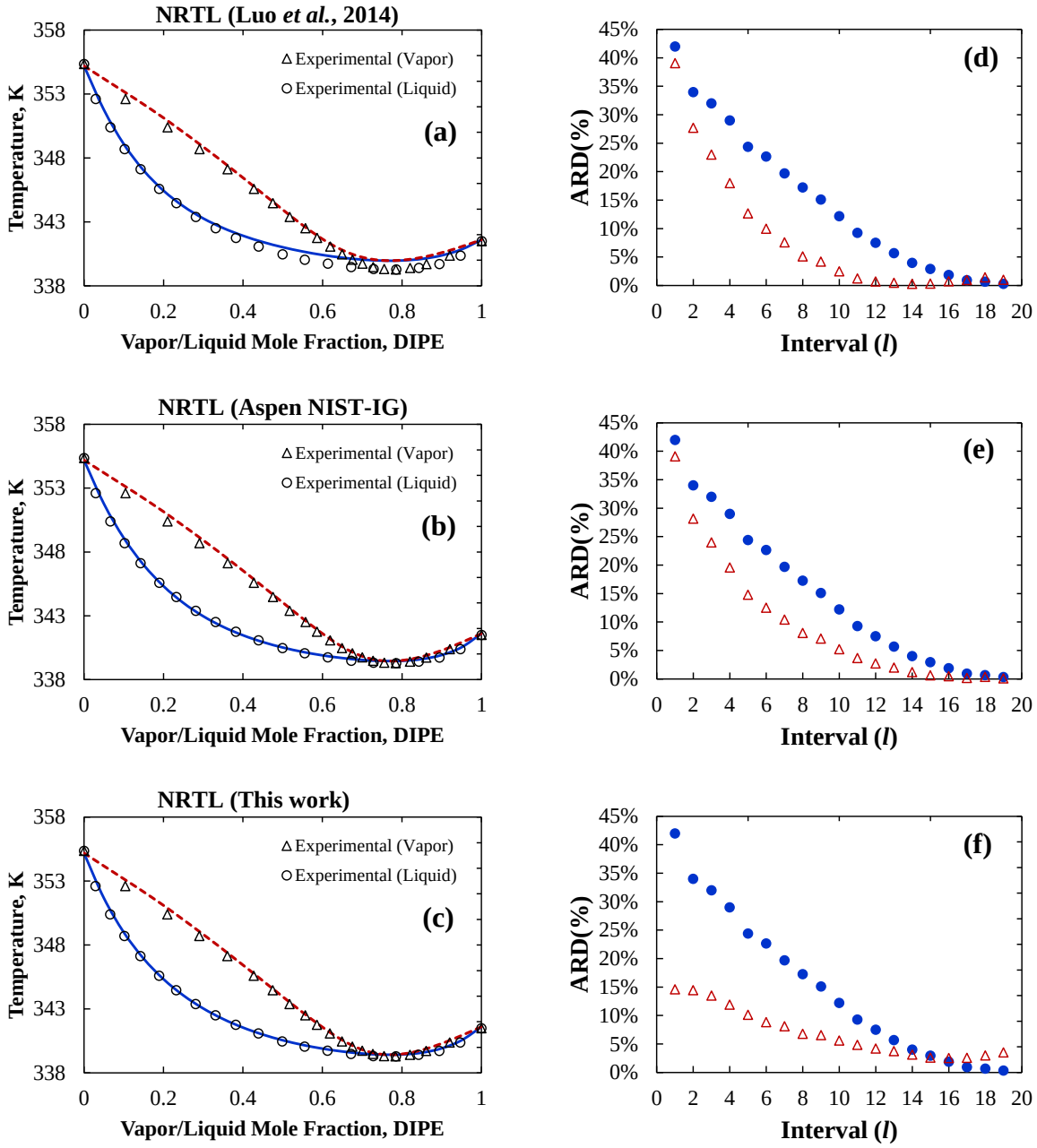

Figure 7.4. Binary system DIPE/IPA, (a-c) Temperature-composition diagrams for NRTL model with binary interaction parameters regressed by Luo *et al.*, (2014), Aspen default and this work (VLE), (d-f) Deviations in the individual Txy diagram points (ARD) for liquid phase (○) and vapour phase (△).

7.2.3 Results of DIPE/2-methoxyethanol binary VLE predictions

The *DIPE/2-methoxyethanol* binary system results for the NRTL model are presented in Figure 7.5. The parameters regressed in this work and the Aspen Plus® default values predict both the vapour and liquid phases with improved accuracy compared to those of Luo *et al.*, (2014). However, deviations are apparent in the dew curve and bubble curve, notably the lower concentration regions and upwards from ca. 80% mole percent DIPE.

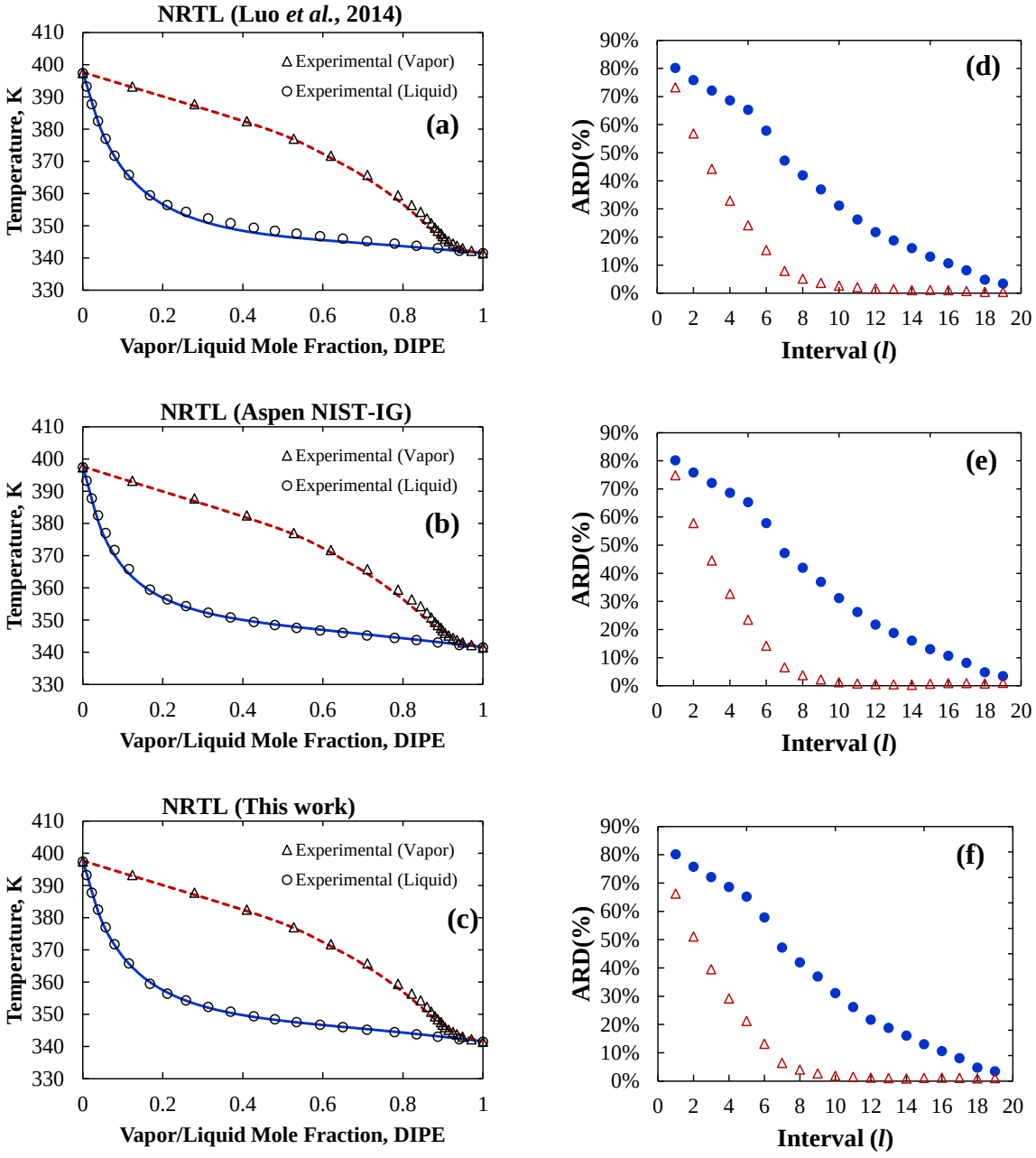

Figure 7.5. Binary system DIPE/2-Methoxyethanol, (a-c) Temperature-composition diagrams for NRTL model with binary interaction parameters regressed by Luo *et al.*, (2014), Aspen default and this work (VLE), (d-f) Deviations in the individual Txy diagram points (ARD) for liquid phase (○) and vapour phase (△).

7.2.4 Results of IPA/2-methoxyethanol binary VLE predictions

The *IPA/2-methoxyethanol* binary is the most accurately predicted of the three binary systems and the results are presented in Figure 7.6. As is the case with the previous binary systems, the parameters regressed in this work and the Aspen Plus® default values predict both the vapour and liquid phases with improved accuracy compared to those of Luo *et al.*, (2014) with ARD less than 7% for both phases. Further model results are presented in Appendix B.

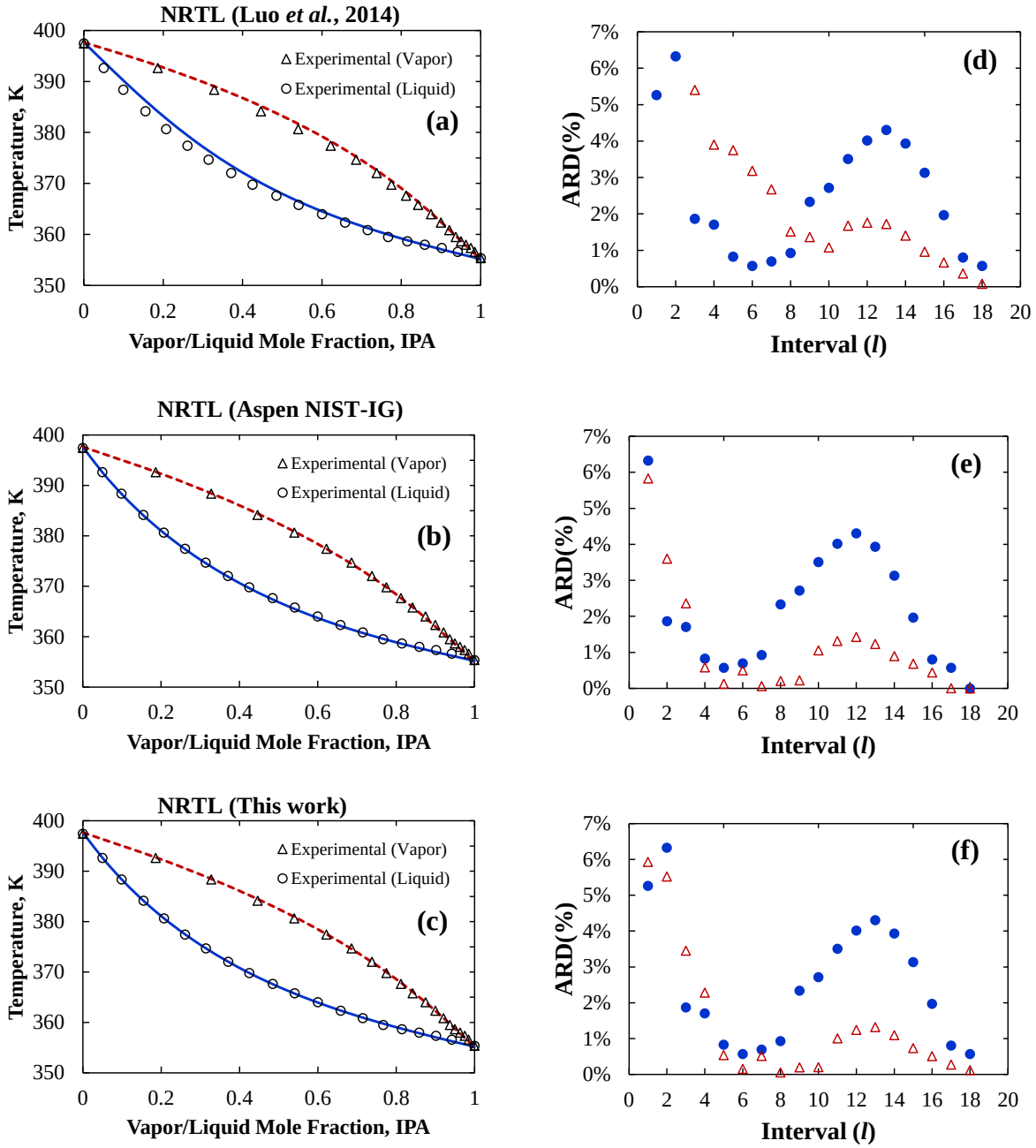

Figure 7.6. Binary system IPA/2-Methoxy-ethanol, (a-c) Temperature-composition diagrams for NRTL model with binary interaction parameters regressed by Luo *et al.*, (2014), Aspen default and this work (VLE), (d-f) Deviations in the individual Txy diagram points (ARD) for liquid phase (○) and vapour phase (△).

7.2.5 Thermodynamic model selection

The performance of the NRTL activity coefficient model in predicting the phase equilibria of the *DIPE/IPA/2-methoxyethanol* system is of a high degree of accuracy. The binary VLE results of the NRTL model with parameters regressed in this work are presented in Figures 7.7 to 7.9 as a qualitative reference for the following section.

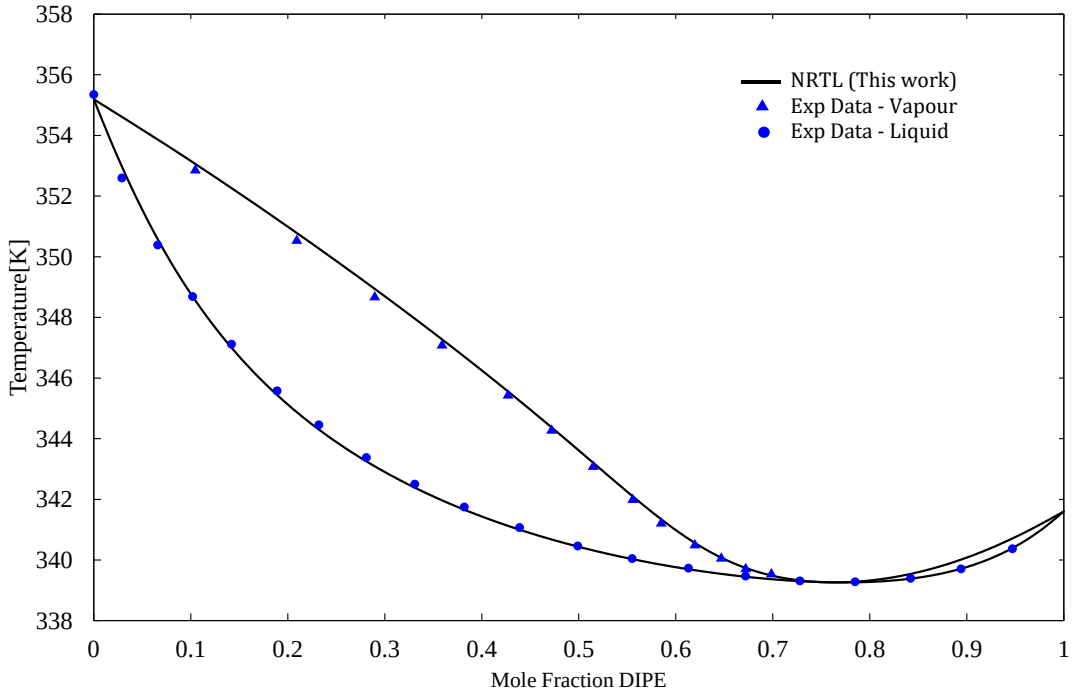

Figure 7.7. NRTL model predictions for isobaric VLE of the binary system DIPE/IPA at 101.3 kPa.

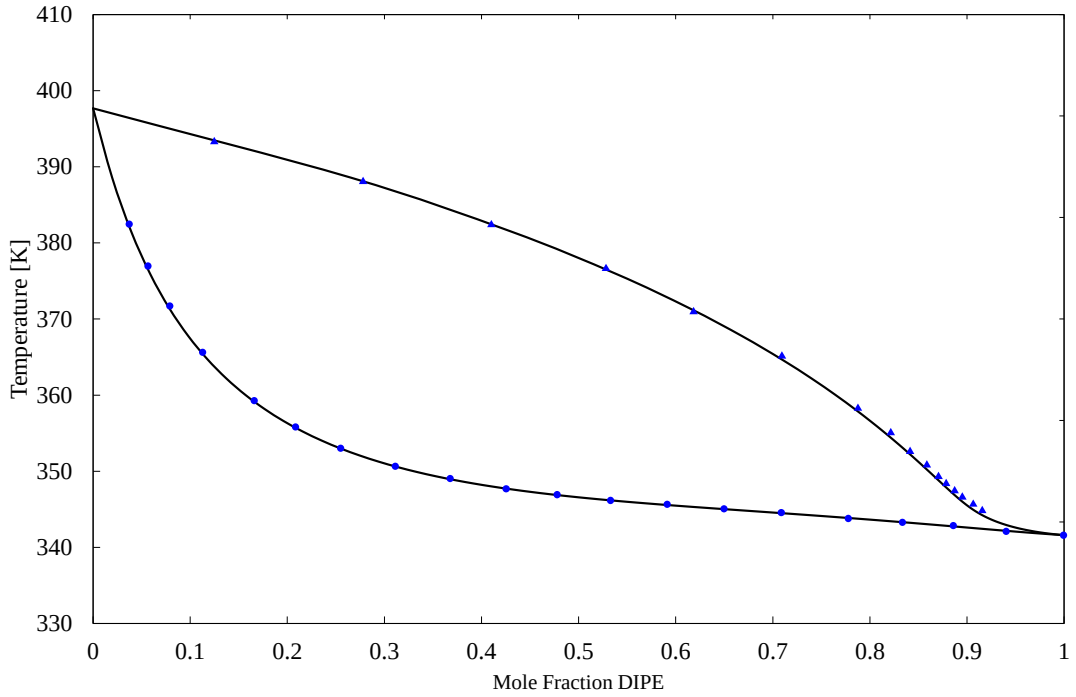

Figure 7.8. NRTL model predictions for isobaric VLE of the binary system DIPE/2-Methoxyethanol VLE at 101.3 kPa.

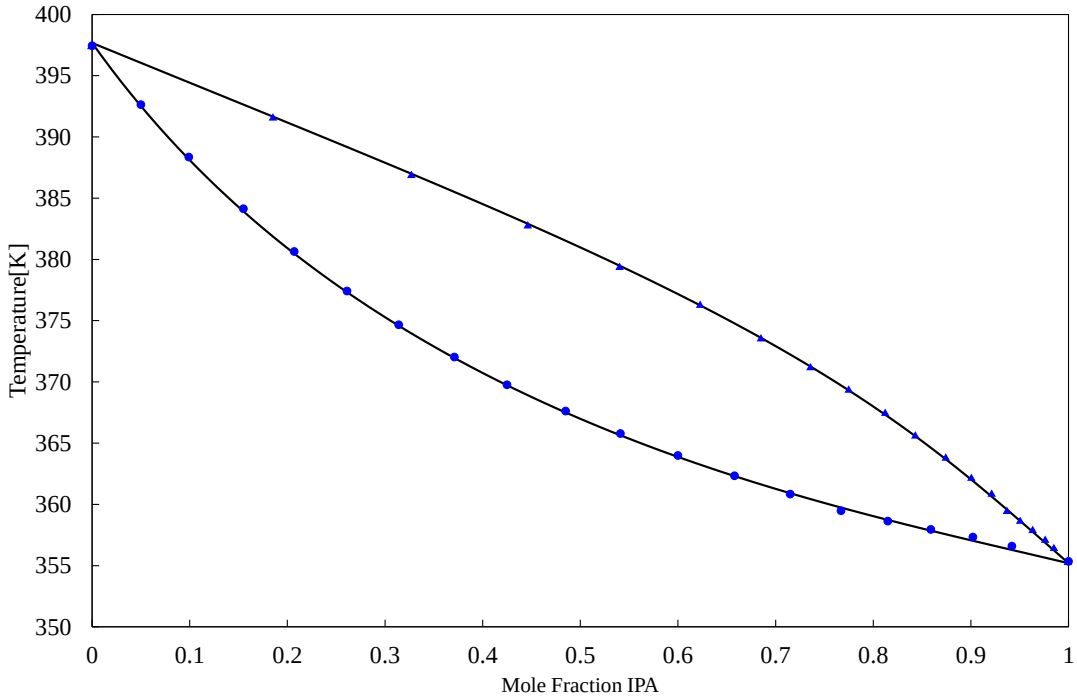

Figure 7.9. NRTL model predictions for isobaric VLE of the binary system IPA/2-Methoxyethanol at 101.3 kPa.

Therefore, the screening results support the selection of the NRTL activity coefficient model with fitted parameters using the ideal gas law for the design of the *DIPE/IPA/2-methoxyethanol* system. The prediction of the azeotrope temperature and composition is improved, although, marginally with the Hayden O'Connell and Nothnagel equations of state. It may be of interest to perform a sensitivity analysis in this regard. Now that the model selection is complete, the uncertainty propagation to the phase equilibria is considered.

7.3 System 1: Phase equilibrium uncertainty propagation

7.3.1 Experimental data parametric uncertainty

The accurate experimental vapour–liquid equilibrium data reported by Lladosa *et al.*, (2007) for DIPE (1) / IPA (2) / 2-methoxyethanol (3) was used for generating the input uncertainty probability distributions and is presented in Appendix D. The data was retrieved from NIST TDE using the Aspen Plus® user interface. The average standard deviations for each input parameter is shown in Tables 7.3 to 7.5 for the respective binary pairs.

Table 7.3. Binary phase equilibrium data parametric uncertainty DIPE (1) + IPA (2).

DIPE+IPA	Temperature (K)	Pressure (kPA)	x_1	x_2	y_1	y_2
Standard deviation	0.2300	1.153	0.001	0.001	0.001	0.012
% of mean	0.07%	1.14%	0.50%	0.34%	0.22%	3.20%

Table 7.4. Binary phase equilibrium data parametric uncertainty for DIPE (1) + 2MET (3).

DIPE+2MET	Temperature (K)	Pressure (kPA)	x_1	x_3	y_1	y_3
Standard deviation	0.23	1.175	0.001	0.001	0.0085	0.001
% of mean	0.06%	1.19%	0.70%	0.31%	1.39%	0.88%

Table 7.5. Binary phase equilibrium data parametric uncertainty for IPA (2) + 2MET (3).

IPA+2MET	Temperature (K)	Pressure (kPA)	x_2	x_3	y_2	y_3
Standard deviation	0.1235	0.625	0.001	0.001	0.0077	0.001
% of mean	0.033%	0.62%	0.36%	0.36%	1.43%	1.224%

7.3.2 Monte Carlo simulation and model regression

A total of 100 Monte Carlo simulation sets were generated using latin hypercube sampling for each experimental data set with the standard deviations as per the previous tables. The resultant 300 data sets were entered into Aspen Plus® as a unique instance of the experimental data. Regression analysis was performed on each set with the Data Regression System (DRS) using the maximum likelihood method (Equation 6.1) with the Britt-Luecke algorithm. The NRTL activity coefficient model was selected to perform the thermodynamic property calculations and the regression results are presented in Table 7.6. The probability distribution for the model parameters is provided in Appendix C.

Table 7.6. NRTL model binary interaction parameters and standard deviations. $\alpha_{ij} = 0.3$.

Component *i*	Component *j*	Parameter	Mean (μ)	Standard deviation (σ)
DIPE	IPA	a_{12}	-17.88	1.72
IPA	DIPE	a_{21}	13.57	0.00
DIPE	IPA	b_{12}	6386.83	576.02
IPA	DIPE	b_{21}	-4496.76	48.60
DIPE	2-MET	a_{13}	1.93	3.56
2-MET	DIPE	a_{31}	0.38	1.81
DIPE	2-MET	b_{13}	-321.18	1222.83
2-MET	DIPE	b_{31}	74.44	618.20
IPA	2-MET	a_{23}	5.40	4.36
2-MET	IPA	a_{32}	-1.71	1.51
IPA	2-MET	b_{23}	-1367.45	1574.29
2-MET	IPA	b_{32}	247.36	561.03

7.3.3 Error propagation to phase equilibrium predictions

Figures 7.10 to 7.12 show the results of the propagated input uncertainties on the phase equilibria for all the regressed binary interaction parameters.

In the case of the *DIPE/IPA* phase equilibria, presented in Figure 7.10, a similar pattern is observed between the vapour phase composition and the liquid phase composition. The uncertainty of the bubble point temperature is approximately the same order of magnitude as the dew point temperature. Furthermore, the highest uncertainty occurs at ca. 15% of either side of the equal-concentration region i.e. 0.35 to 0.65 mole fraction range. Both the bubble and dew curves are narrow near the boiling temperature for DIPE and IPA, although this is more likely as a result of the vapour pressure correlation and not the thermodynamic model.

The temperature uncertainty appears to be insignificant with a maximum of 1.1 K at any specific concentration for both the bubble and dew point curves. On the other hand, at a constant temperature the uncertainty of the component concentration may vary up to a maximum of ca. 8 mole percent. Nonetheless, the model could predict the experimental data within its 95% percentile.

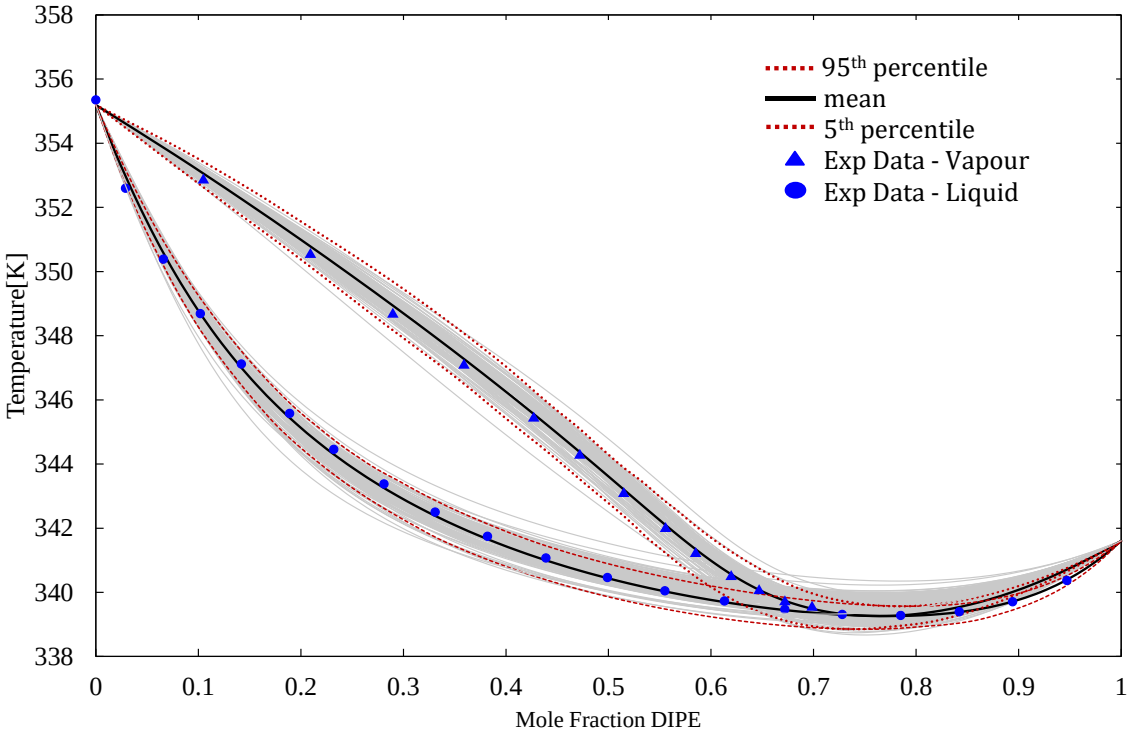

Figure 7.10. Propagated uncertainty in the NRTL model predictions for DIPE/IPA VLE at 101.3 kPa. Grey lines represent the Monte Carlo simulations, red dashed lines are the 5th and 95th percentile of the simulations and black full lines are the mean of the simulation.

The *DIPE/2-methoxyethanol* binary system results are as per Figure 7.11 and a notable difference in uncertainty is observed between the bubble point curve and dew point curve. For the dew point curve a temperature uncertainty of ca. 5 Kelvin is observed most notably at the

equal-concentration region. Conversely, the bubble point curve uncertainty appears to be low and no more than 2 Kelvin in the region of highest uncertainty, which is in the lower concentration region.

It is further encouraging to note that the model could predict the experimental data within its 95% percentile, although a small decline in accuracy is observed for the vapour phase in the higher concentration region.

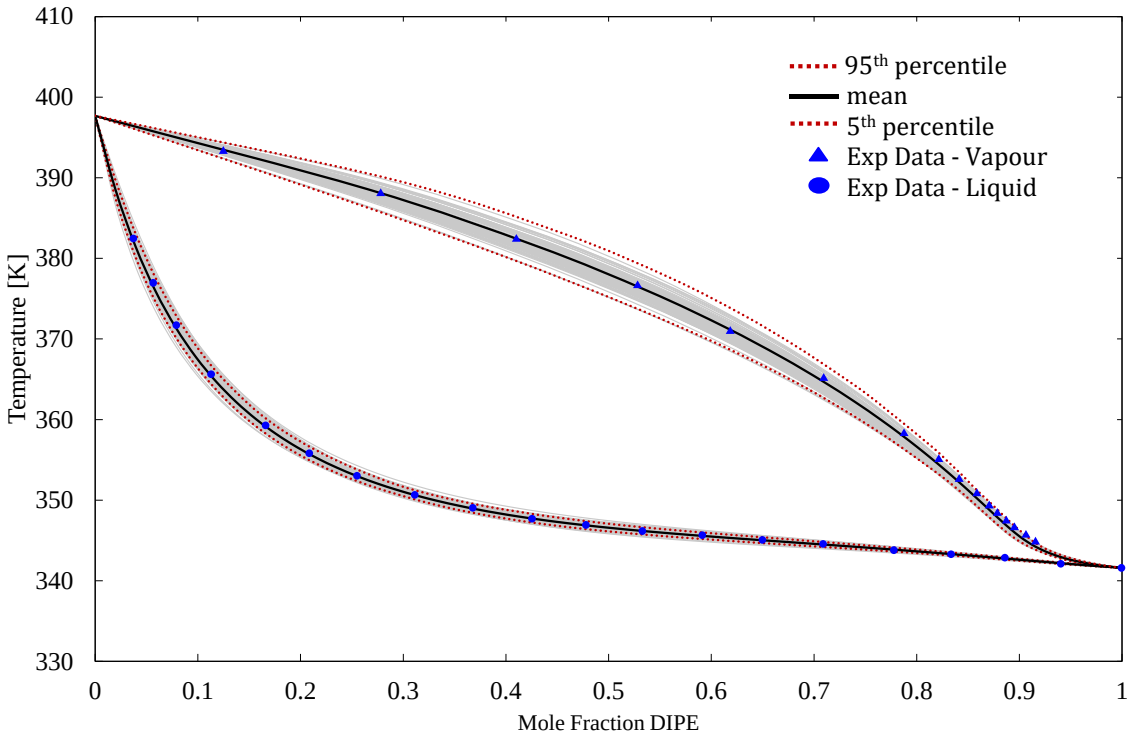

Figure 7.11. Grey lines represent the Monte Carlo simulations, red dashed lines are the 5th and 95th percentile of the simulations and black full lines are the mean of the simulation. DIPE/2-Methoxyethanol VLE at 101.3 kPa.

For the *IPA/2-methoxyethanol* binary system the vapour phase composition may be either over predicted or under predicted for ca. 70% of the concentration space, as can be seen in Figure 7.12. A similar, although smaller, pattern is observed in the liquid composition in the lower concentration region. Notwithstanding, for both the vapour and liquid compositions the temperature uncertainty is smaller than 5 K. The uncertainty is reduced in the higher concentration region for both the vapour phase and liquid phase.

The model could predict the experimental data within its 95% percentile as with the other component pairs. However, a minimal loss of performance can be seen in the liquid phase

prediction when exceeding ca. 0.9 mole fraction IPA and this is not accounted for by the uncertainty propagation. Nonetheless, it is considered acceptable as the overall uncertainty in the area appears to be small.

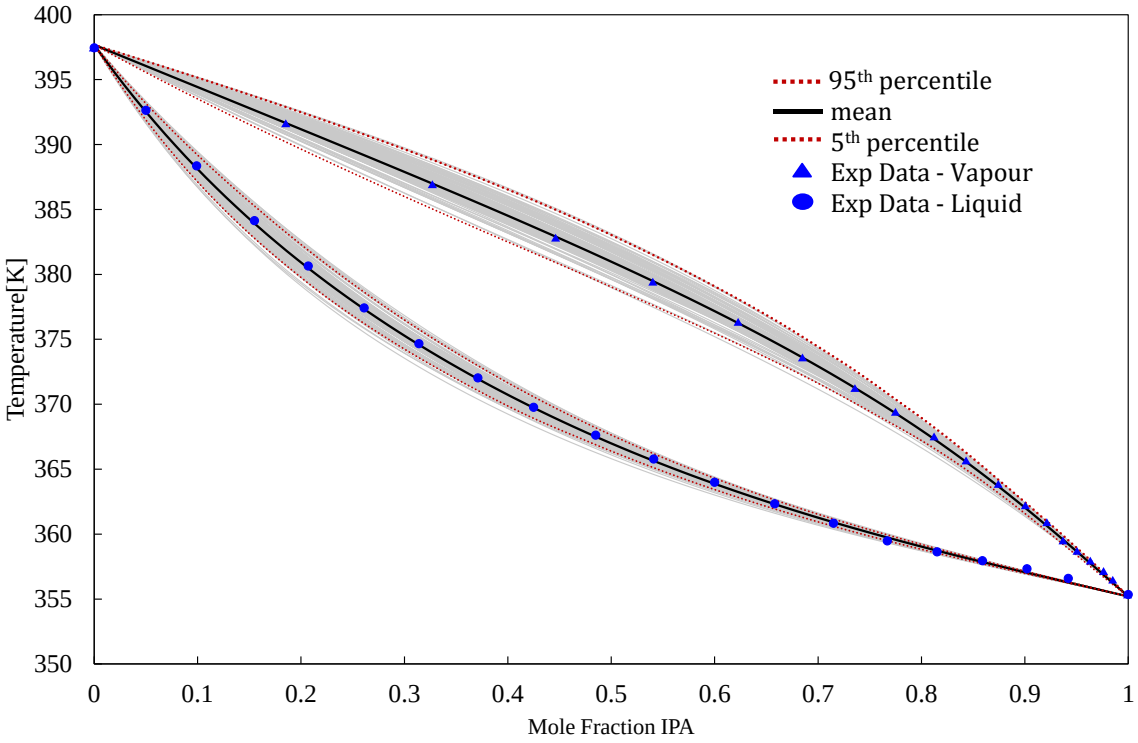

Figure 7.12. Grey lines represent the Monte Carlo simulations, red dashed lines are the 5th and 95th percentile of the simulations and black full lines are the mean of the simulation. IPA/2-Methoxyethanol VLE at 101.3 kPa.

7.3.4 Section Highlights

The performances of several thermodynamic models were evaluated. The objective was to identify a model that offered the closest prediction of experimental data when considering the phase equilibria of the *DIPE/IPA/2-methoxyethanol* system. The NRTL activity coefficient model offered largely excellent results, with a high degree of accuracy apparent in the azeotropic temperature and composition. Subsequently, the parametric uncertainty of the experimental data was propagated through the NRTL model to the phase equilibria estimates using a Monte Carlo simulation approach. In the following section, the model selection and uncertainty propagation process are applied to the heterogeneous azeotropic distillation case.

7.4 System 2: Heterogeneous azeotropic distillation

In this case, the heterogeneous azeotropic distillation of the minimum boiling azeotrope of water and ethanol with entrainer diisopropyl ether (DIPE) is investigated.

7.4.1 Thermodynamic model screening results

The Separation Technology Group of Stellenbosch University investigated this system and concluded that improved thermodynamic modelling work is required to develop a reliable process design (Pienaar *et al.*, 2013). As such, the previous modelling results of our Group is reported alongside this work as a reference. The thermodynamic model screening and selection process was detailed previously (Section 7.1). Here, as for System 1, a comparison was made between models and different parameters for those models.

First, consider the results in Table 7.5 and Figure 7.13. Table 7.5 provides the descriptive statistics (AAD and ARD) for the model screening process. The screening of the candidate models revealed that the NRTL and UNIQUAC activity coefficient models were the only two models that provided phase equilibria predictions worthwhile considering, specifically the liquid-liquid equilibrium. Although the SR-POLAR model provided a reasonable fit of the experimental azeotropes and equilibrium compositions (tie-lines), the phase envelope was over-predicted completely. This is likely to result in the model predicting a higher aqueous liquid phase in the decanter than actually possible, thus not suitable for process design. The ternary diagram for the SR-POLAR model is shown in Appendix F.

Furthermore, the CPA equation of state provided inaccurate estimates of the phase envelope and either over predicted or under predicted the heterogeneous region. As was observed for the extractive distillation case, this may be as a result of insufficient parameter regression with data other than phase equilibria and not necessarily a model deficiency. The inclusion of these parameters is likely to improve the results of these models, but a more in-depth investigation to increase the accuracy of the models is beyond the scope of this work.

Rather, the focus is limited to obtaining acceptable model results that closely correlate experimental data in order to answer the first research question, but within the constraints of this study. Therefore, only the NRTL and UNIQUAC models are discussed further. In terms of the NRTL and UNIQUAC models, it is apparent from Table 7.5 that the vapour-liquid equilibrium predictions are accurate regardless of the parameter source as there is no appreciable difference between the Aspen Plus® default parameters and those regressed in this

work. This is consistent with the findings previously reported by Pienaar *et al.*, (2013) and serves to validate this work. The predicted ethanol concentration in the VLE is the least accurate at ca. 15% ARD across all models and parameter sets. On the other hand, the DIPE and water concentrations are quite accurate with an average ARD of ca. 3% for all models and parameter combinations.

Regarding the phase envelope, in terms of the Aspen Plus® default parameters, it is noted that the parameters reported from version 7.1 are now improved in version 8.8. For example, the UNIQUAC model results with the parameters by Pienaar *et al.*, (2013) were reported to provide an improved prediction over the Aspen Plus version 7.1 default parameters and was identified as the best compared to NRTL and UNIFAC. Now, as observed in Figure 7.13, the Aspen Plus® version 8.8 default parameters (i.e. Aspen-LLE and Aspen-IG) demonstrate a qualitative improvement over the previous best of Pienaar *et al.*, (2013). Although this observation is not supported by the descriptive statistics in Table 7.7 and is therefore elaborated upon next.

The UNIQUAC model AAD with version 7.1 default parameters was 0.3282 and version 8.8 is now 0.3334; similarly, the ARD was 208.62 and is now 324.15. This clearly suggests a decrease in accuracy. However, when qualitatively evaluating the shapes of the phase envelopes on the ternary phase diagrams in Figure 7.13 the experimental data is more closely matched. The discrepancy contributes to the model's loss in fidelity for the DIPE concentration in the aqueous liquid phase at the cost of improving the overall performance. The average deviation is observed as “high” primarily due to the low concentration of DIPE in the water phase.

Although it appears the model is less accurate based on the descriptive statistics, it is actually not the case. It is thus concluded, the descriptive statistics do not necessarily provide a representative indication of the results if the ternary diagrams are also considered, and suggesting that ARD should not be used as the only evaluation criteria.

Lastly, in terms of the phase envelope, the NRTL model with parameters regressed in this work yields the most accurate results based on the total ARD. The UNIQUAC model with parameters regressed in this work offered comparable results, although with an ARD ca.7% higher, which indicates a slight decrease in the accuracy. This conclusion is supported by the results presented in Figures 7.14 to 7.18. Note that only the top five combinations are shown.

Table 7.7. AAD and ARD results for the VLLE of DIPE/ethanol/water by candidate thermodynamic models at 101.3 kPa.

	Organic liquid			Aqueous liquid			Vapour			Sum
	x_{DIPE}	$x_{Ethanol}$	x_{Water}	x_{DIPE}	$x_{Ethanol}$	x_{Water}	y_{DIPE}	$y_{Ethanol}$	y_{Water}	
				NRTL (This work)						
AAD	0.0800	0.0519	0.0575	0.0032	0.0261	0.0282	0.0206	0.0250	0.0057	0.2982
ARD	82.40%	28.66%	25.15%	52.73%	25.48%	3.34%	3.16%	16.79%	3.08%	240.79%
				UNIQUAC (This work)						
AAD	0.0620	0.0580	0.0674	0.0036	0.0190	0.0212	0.0180	0.018	0.0052	0.2732
ARD	78.54%	29.60%	25.93%	73.25%	19.13%	2.53%	2.81%	12.68%	2.81%	247.26%
				NRTL (Aspen-IG)						
AAD	0.0914	0.0600	0.0763	0.0200	0.04642	0.0730	0.0223	0.0223	0.0060	0.4182
ARD	20.70%	30.72%	21.94%	329.45%	33.43%	8.99%	3.49%	15.27%	3.19%	467.18%
				UNIQUAC (Aspen-IG)						
AAD	0.0125	0.0559	0.0776	0.0134	0.0559	0.0776	0.0148	0.0177	0.0077	0.3334
ARD	14.59%	25.67%	20.77%	195.96%	38.81%	9.58%	2.31%	12.38%	4.09%	324.15%
				NRTL (Pienaar, 2012)						
AAD	0.0502	0.0345	0.0376	0.0033	0.0248	0.0226	0.0136	0.0144	0.0124	0.2134
ARD	14.14%	15.97%	18.35%	145.93%	23.10%	2.71%	2.20%	12.23%	6.64%	241.27%
				UNIQUAC (Pienaar, 2012)						
AAD	0.0914	0.0601	0.046	0.0039	0.0357	0.0388	0.0238	0.0282	0.007	0.3349
ARD	27.11%	21.64%	25.96%	75.25%	24.54%	4.79%	3.85%	17.61%	3.63%	204.38%

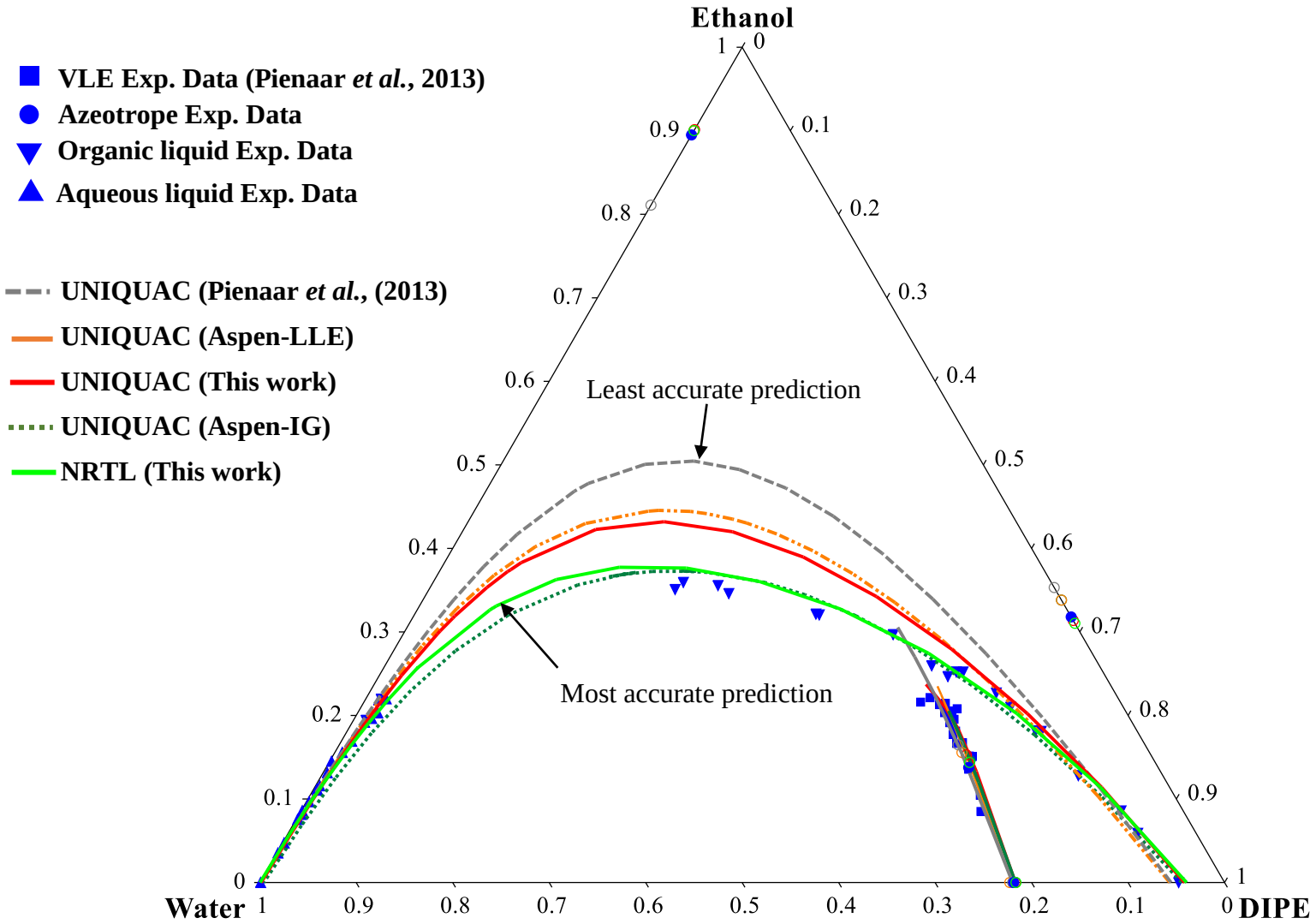

Figure 7.13. Ternary phase diagram of thermodynamic models as per the screening and selection process for System 2. Experimental data from Pienaar *et al.*, (2013).

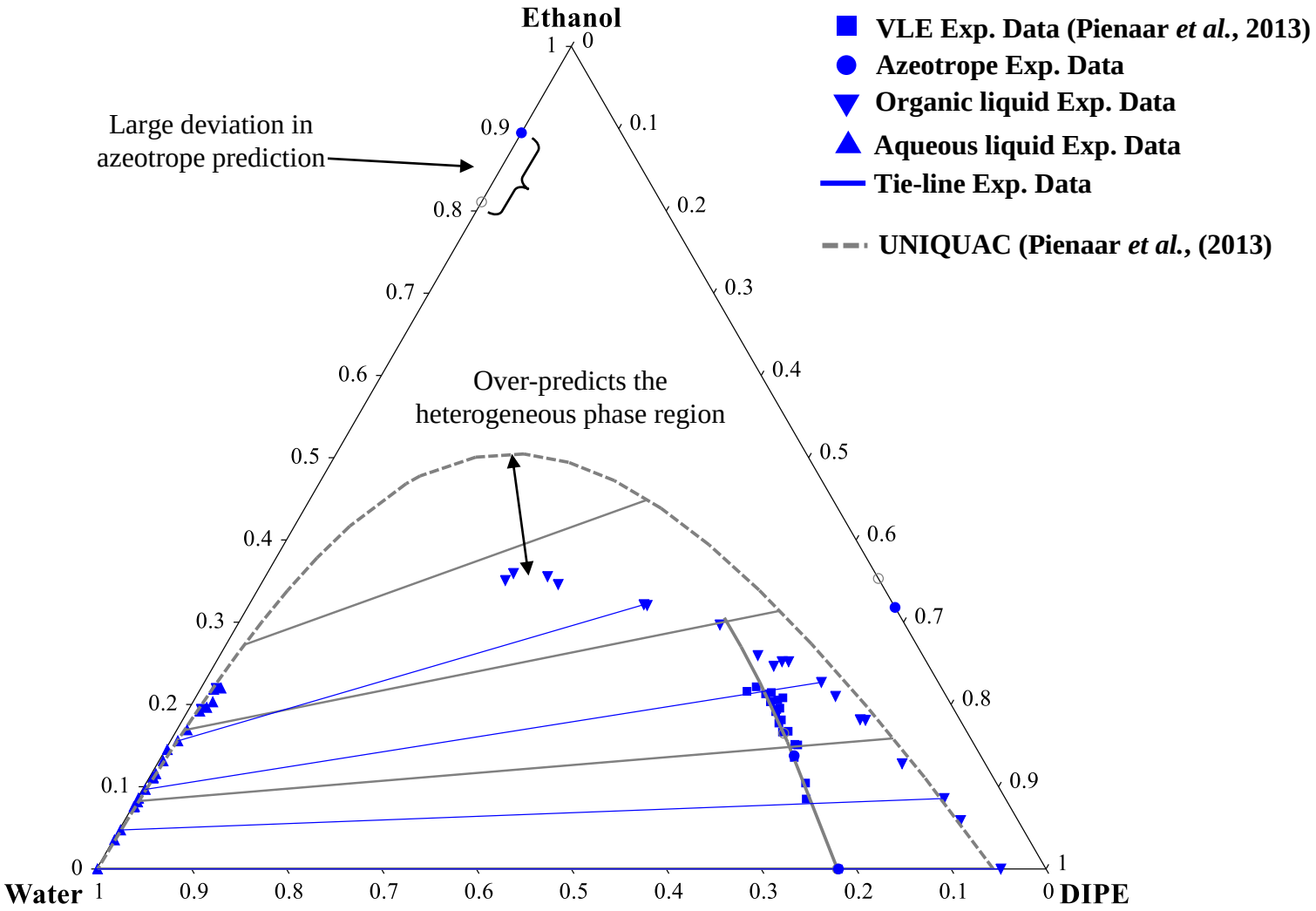

Figure 7.14. Ternary phase diagram of UNIQUAC model with parameters from Pienaar (2013) for System 2. Experimental data from Pienaar *et al.*, (2013).

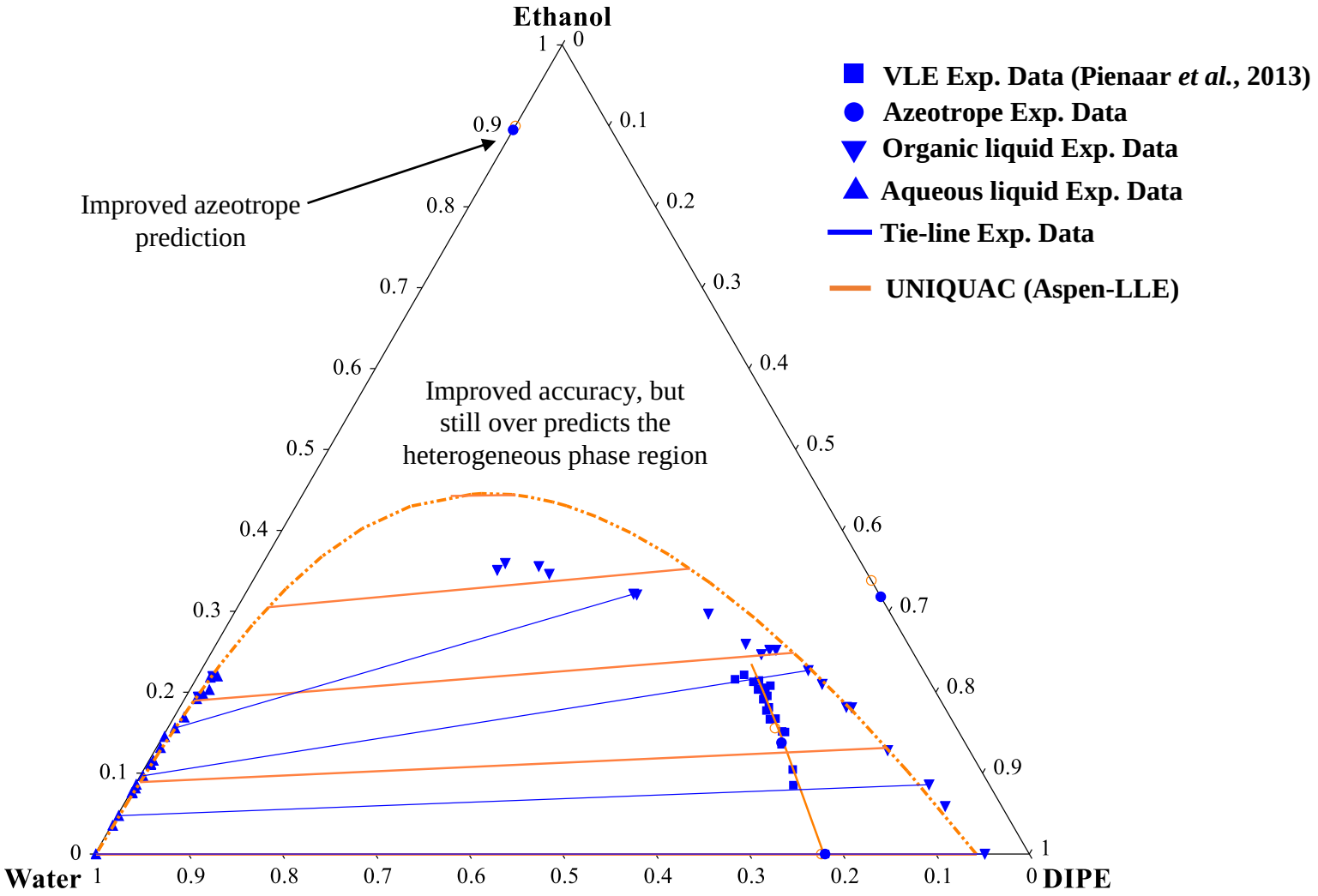

Figure 7.15. Ternary phase diagram of UNIQUAC model with ASPEN-LLE parameters for System 2. Experimental data from Pienaar *et al.*, (2013).

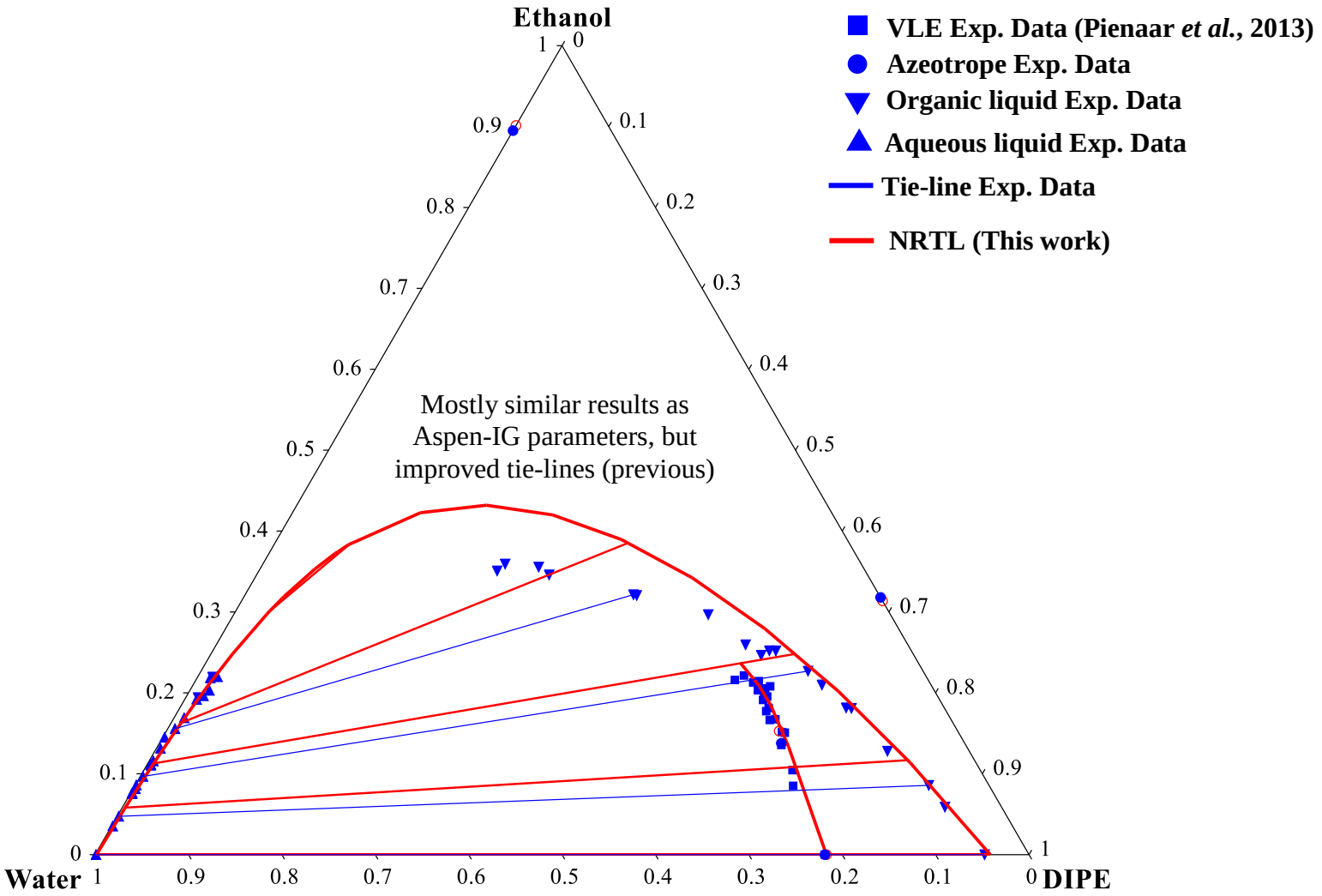

Figure 7.16. Ternary phase diagram for UNIQUAC model with parameters regressed from this work for System 2. Experimental data from Pienaar *et al.*, (2013).

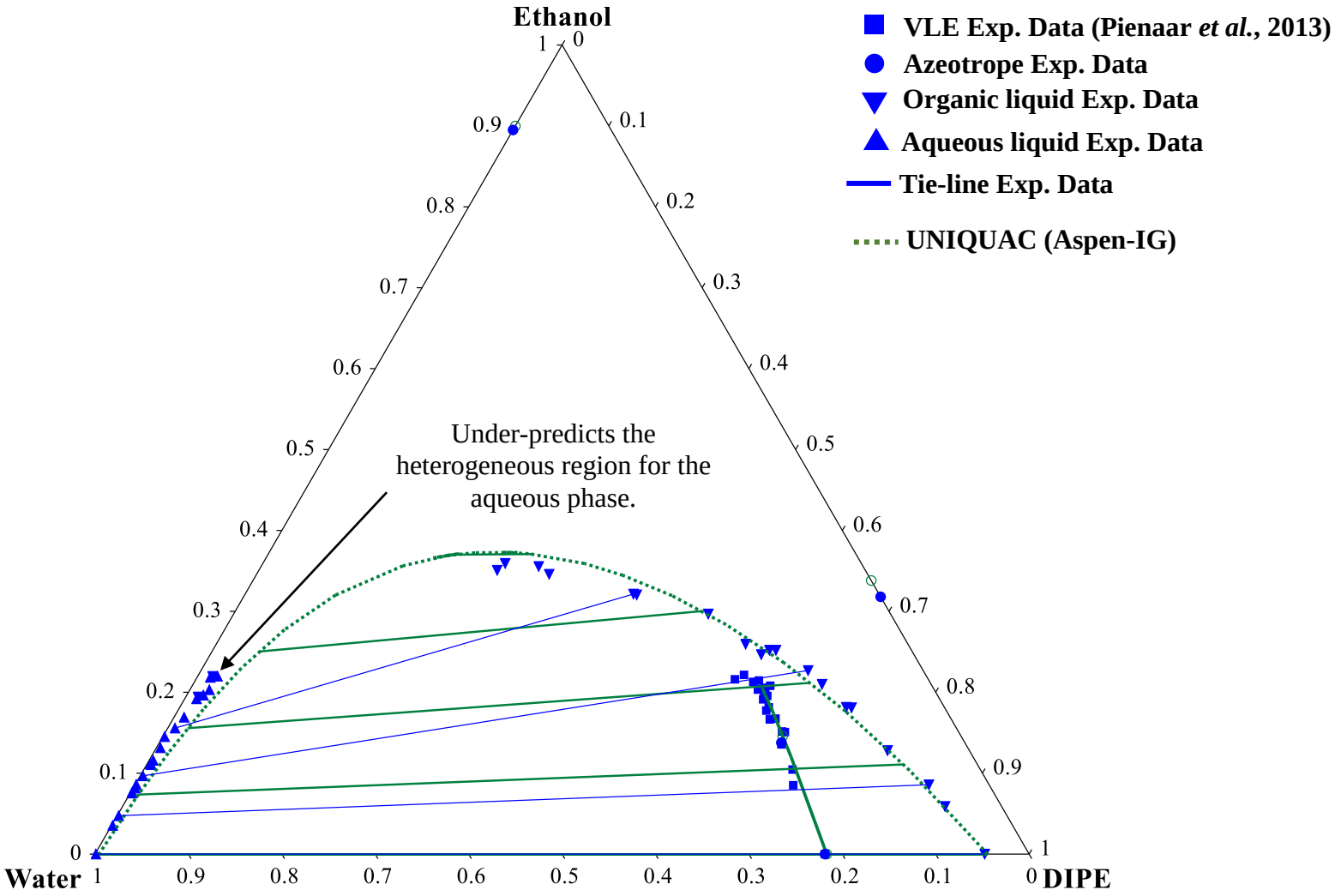

Figure 7.17. Ternary phase diagram of UNIQUAC model with ASPEN-IG parameters for System 2. Experimental data from Pienaar *et al.*, (2013).

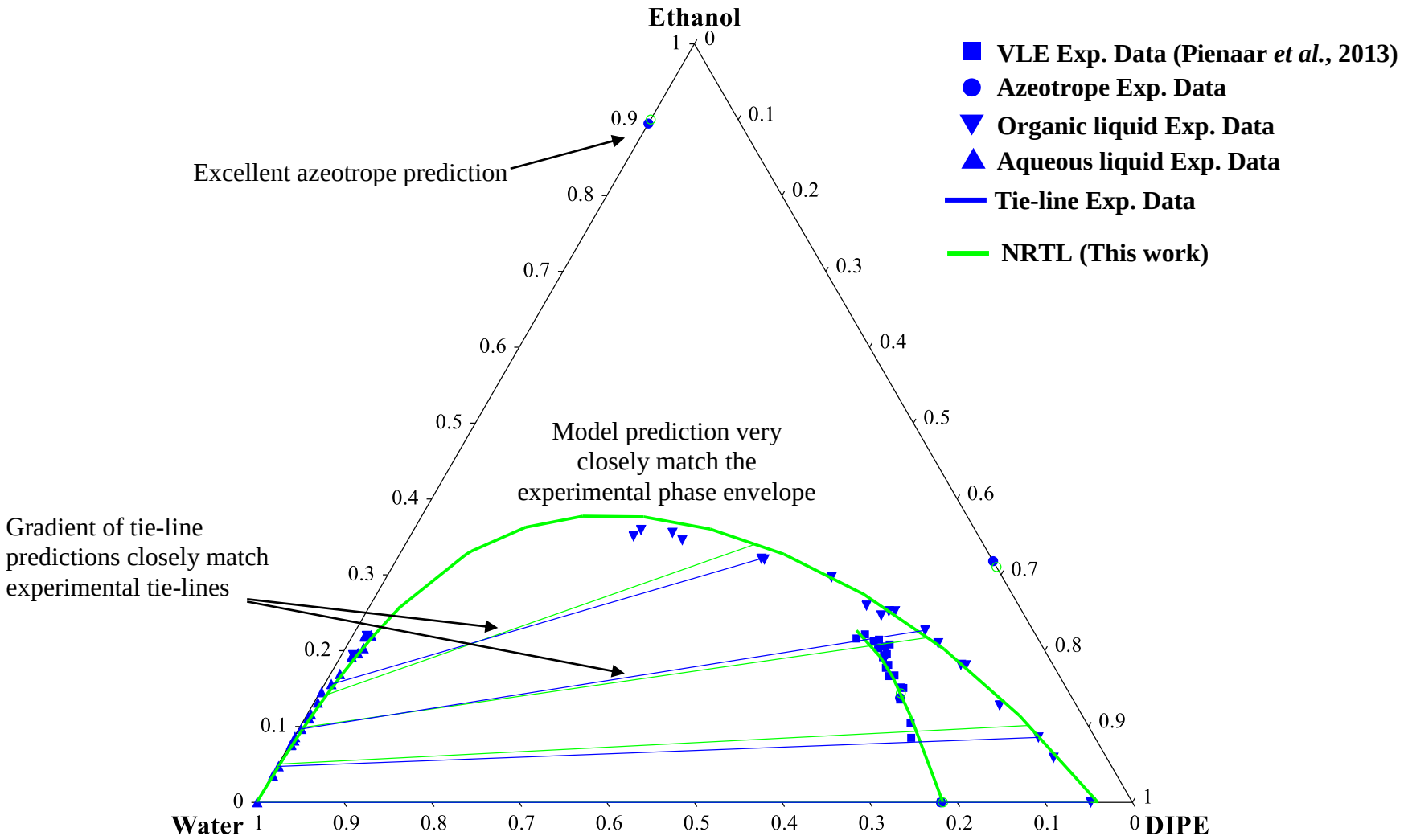

Figure 7.18. Ternary phase diagram for NRTL model with parameters regressed from this work for System 2. Experimental data from Pienaar *et al.*, (2013).

7.4.2 Thermodynamic model selection

The performance of the NRTL activity coefficient model in predicting the phase envelope, vapour-liquid equilibrium and azeotropes of the DIPE/ethanol/water ternary system is of a high degree of accuracy. Furthermore, the gradients of the tie-lines are also closely matched to the experimental tie-lines. Therefore, the screening results support the selection of the NRTL activity coefficient model with the fitted binary interaction parameters regressed in this work coupled with the ideal gas law for the design of the heterogeneous azeotropic distillation system. Thus, with the model selection complete, the uncertainty propagation to the phase equilibrium is considered next.

7.5 System 2: Phase equilibrium uncertainty propagation

7.5.1 Experimental data parametric uncertainty

Three sets of experimental data sources were used for generating the input uncertainty probability distributions. The DIPE (1)/water (3) liquid-liquid equilibrium data was reported by Stephenson (1992), the DIPE (1)/ethanol (2) vapour-liquid equilibrium by Ku and Tu (2006) and the ethanol (2)/water (3) vapour-liquid equilibrium by Lai *et al.*, (2014).

The data was retrieved from NIST TDE using the Aspen Plus® user interface. The average standard deviations for each input parameter is shown in Tables 7.8 to 7.10 for the respective binary pairs.

Table 7.8. Liquid-liquid equilibrium data parametric uncertainty DIPE (1)/water (3).

DIPE + ethanol	Temperature (K)	Pressure (kPA)	$x_{1(DIPE)}$	$x_{1(water)}$	$x_{2(DIPE)}$	$x_{2(water)}$
Standard deviation	0.1	0.1	-	-	-	-
% of mean	-	0.1%	0.1%	1.0%	1.0%	0.1%

Table 7.9. Vapour-liquid equilibrium data parametric uncertainty for DIPE (1)/ethanol (2).

DIPE + water	Temperature (K)	Pressure (kPA)	x_1	x_2	y_1	y_2
Standard deviation	0.1	0.46	-	-	-	-
% of mean	-	0.5%	0.1%	0.1%	1.5%	1.5%

Table 7.10. Vapour-liquid equilibrium data parametric uncertainty for ethanol (2)/water (3).

Ethanol + water	Temperature (K)	Pressure (kPA)	x_2	x_3	y_2	y_3
Standard deviation	0.16	0.41	-	-	-	-
% of mean	-	0.4%	0.1%	0.1%	1.0%	1.0%

7.5.2 Thermodynamic consistency test

The experimental data retrieved from the NIST TDE was evaluated to ensure thermodynamic consistency. The Aspen Plus® area test was used for the vapour-liquid equilibrium data sets, but no thermodynamic consistency test was performed on the liquid-liquid equilibrium and the results are presented in Table 7.11. A review of the theory of thermodynamic consistency tests is provided in Appendix A.

Table 7.11. Results of thermodynamic consistency tests for vapour-liquid equilibrium data.

Data set	Test method	Result	Value	Tolerance
VLE DIPE/ethanol	AREA	PASSED	-3.14	10%
VLE ethanol/water	AREA	PASSED	-7.74	10%

The data was confirmed to be thermodynamically consistent and suitable to use for further process design.

7.5.3 Monte Carlo simulation and model regression

A total of 100 Monte Carlo simulation sets were generated using LHS for each experimental data set with the standard deviations as per the previous tables. The resultant 300 data sets were entered into Aspen Plus® as a unique instance of the experimental data. Regression analysis was performed on each set with the Data Regression System (DRS) using the maximum likelihood method (Equation 6.1) with the Britt-Luecke algorithm. The regression results are presented in Table 7.12.

Table 7.12. NRTL model binary interaction parameters and standard deviations.

Component *i*	Component *j*	Parameter	Mean (μ)	Standard deviation (σ)
DIPE	ETHANOL	a_{12}	-28.49	0.057
ETHANOL	DIPE	a_{21}	22.97	0.046
DIPE	ETHANOL	b_{12}	9913.38	19.827
ETHANOL	DIPE	b_{21}	-7585.70	15.171
DIPE	WATER	a_{13}	1.47	0.003
WATER	DIPE	a_{31}	16.31	0.033
DIPE	WATER	b_{13}	347.49	0.695
WATER	DIISO-01	b_{31}	-3236.62	6.473
ETHANOL	WATER	a_{23}	-3.10	0.006
WATER	ETHANOL	a_{32}	2.44	0.005
ETHANOL	WATER	b_{23}	1111.46	2.223
WATER	ETHANOL	b_{32}	-245.90	0.492

The following parameters were kept fixed during the regression procedure:

- α_{12} = 0.3, the temperature-dependent parameter for DIPE/ethanol VLE.
- α_{13} = 0.27, the temperature-dependent parameter for DIPE/water LLE.
- α_{23} = 0.4, the temperature-dependent parameter for ethanol/water VLE.

7.5.4 Phase equilibrium uncertainty propagation

The results of the propagated input uncertainties on the phase equilibria are presented in Figures 7.19 to 7.25. When analysing the uncertainty propagation to the phase envelope in Figure 7.19, it is evident that the system appears to exhibit limited uncertainty in the aqueous phase region. The water mole fraction uncertainty is only noticeable as the phase envelope approaches the plait point and the phase transition is made to the organic phase.

The section of the phase envelope with the highest uncertainty is presented in Figure 7.20 and here the respective variability for DIPE and ethanol is estimated at ca. 0.02 and 0.025 mole fraction. Therefore, it is concluded that the maximum concentration uncertainty for DIPE is ca. 8.3%, ethanol is ca. 4.9% and water is ca. 5.2%. In terms of the organic phase, a similar trend is observed as with the aqueous phase, whereas the phase envelope uncertainty is initially small in the high DIPE concentration area and gradually increases towards the plait point in the higher alcohol concentration region, as presented in Figure 7.21.

Of further importance is the vapour-liquid equilibrium uncertainty and this is presented in Figure 7.22 with an enlarged version provide in Figure 7.23. The VLE curve origin point is at a DIPE and water concentration of 78.3% and 21.7% respectively and the uncertainty is essentially zero. As the ethanol concentration is increased towards ca. 10% the uncertainty in the DIPE remains small at ca. 0.8%, but the water uncertainty increases to 3.7%. The trend continues and the uncertainty reaches a maximum at ca. 18% ethanol. It is estimated that at this point the VLE uncertainty for the respective component concentrations are ca. 2.1% (DIPE), 0.4% (ethanol) and 9.2% (water).

It is concluded that water is the component with the highest uncertainty in terms of the vapour-liquid equilibria concentrations, followed by DIPE and then ethanol with the lowest uncertainty.

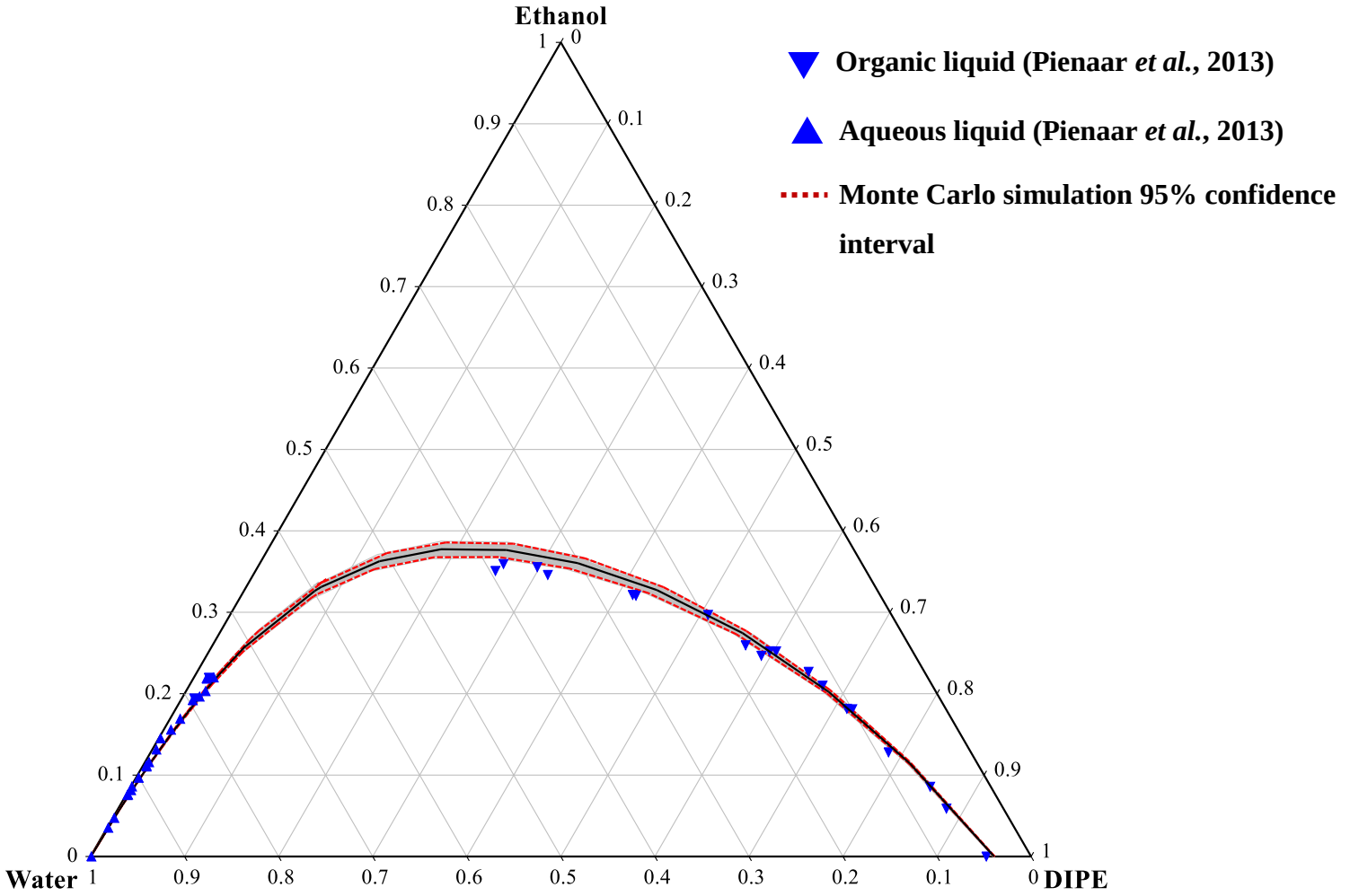

Figure 7.19. Propagated uncertainty in the NRTL model predictions for the ternary system Ethanol/DIPE/Water at 101.3 kPa. Grey lines represent the Monte Carlo simulations, red dashed lines are the 5th and 95th percentile of the simulations and black full lines are the mean of the simulation. Experimental data from Pienaar *et al.*, (2013).

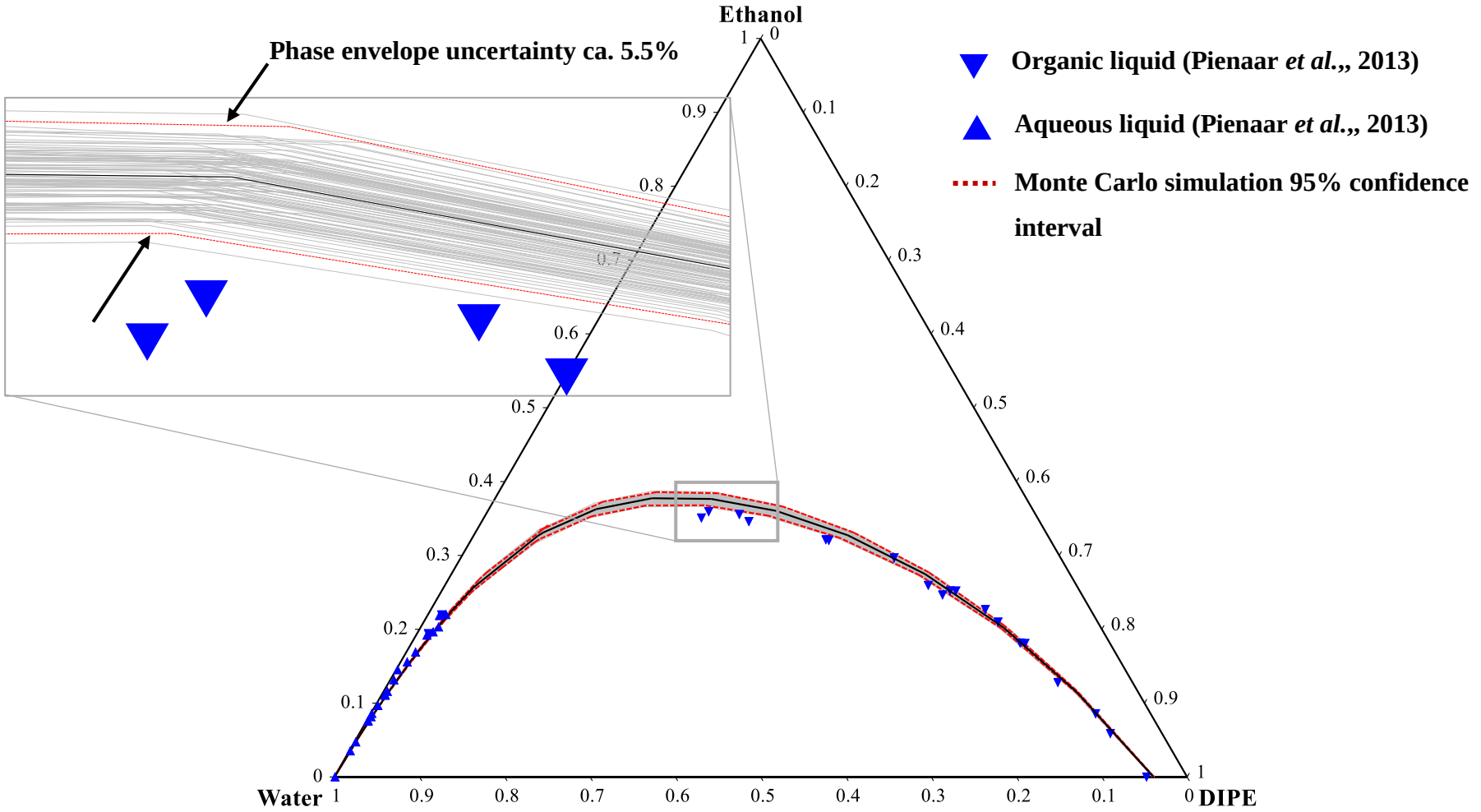

Figure 7.20. Propagated uncertainty in the NRTL model predictions for the ternary system Ethanol/DIPE/Water at 101.3 kPa. Grey lines represent the Monte Carlo simulations, red dashed lines are the 5th and 95th percentile of the simulations and black full lines are the mean of the simulation. Experimental data from Pienaar et al., (2013).

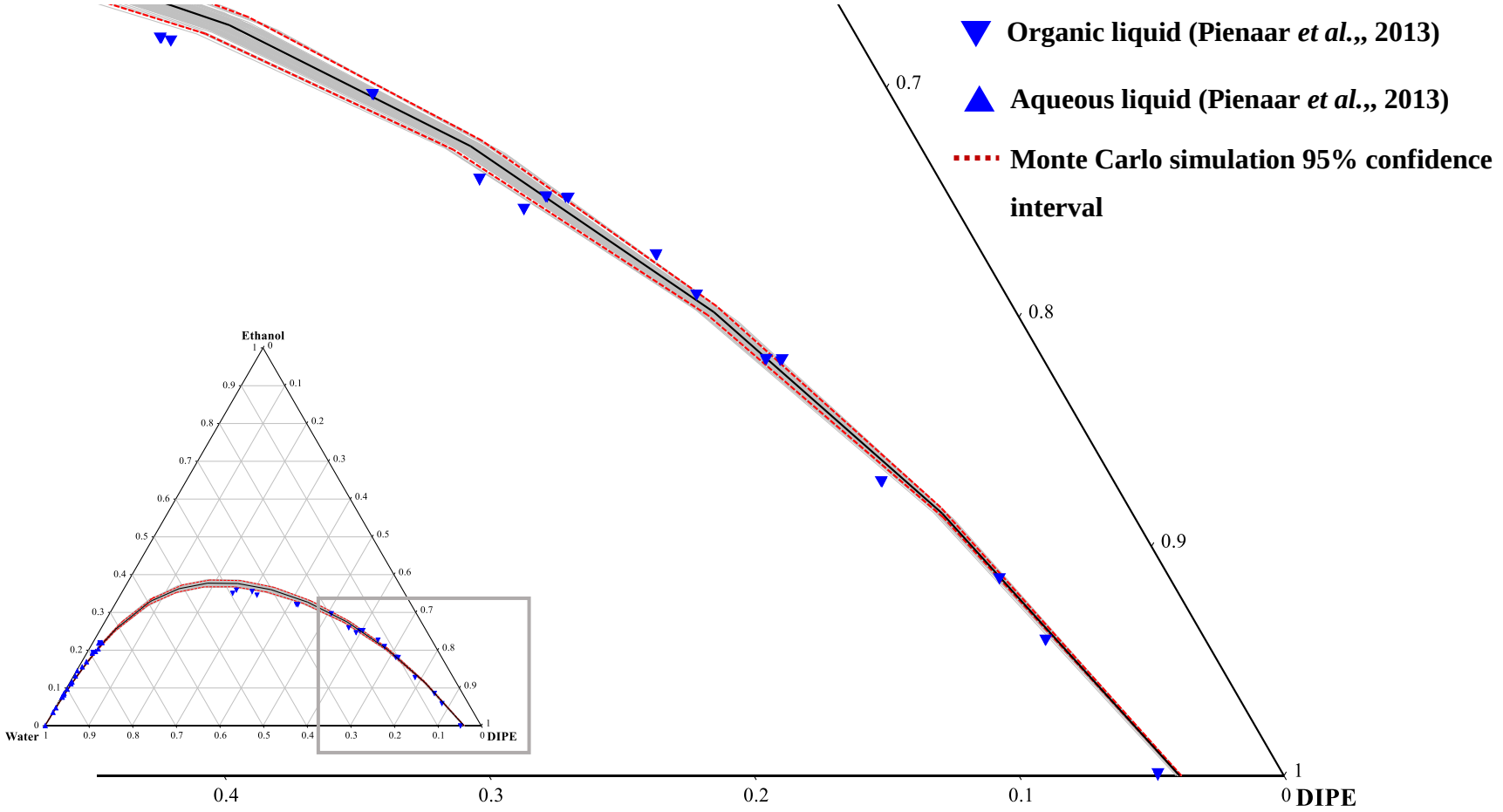

Figure 7.21. Propagated uncertainty in the NRTL model predictions for the ternary system Ethanol/DIPE/Water at 101.3 kPa. Grey lines represent the Monte Carlo simulations, red dashed lines are the 5th and 95th percentile of the simulations and black full lines are the mean of the simulation. Experimental data from Pienaar *et al.*, (2013).

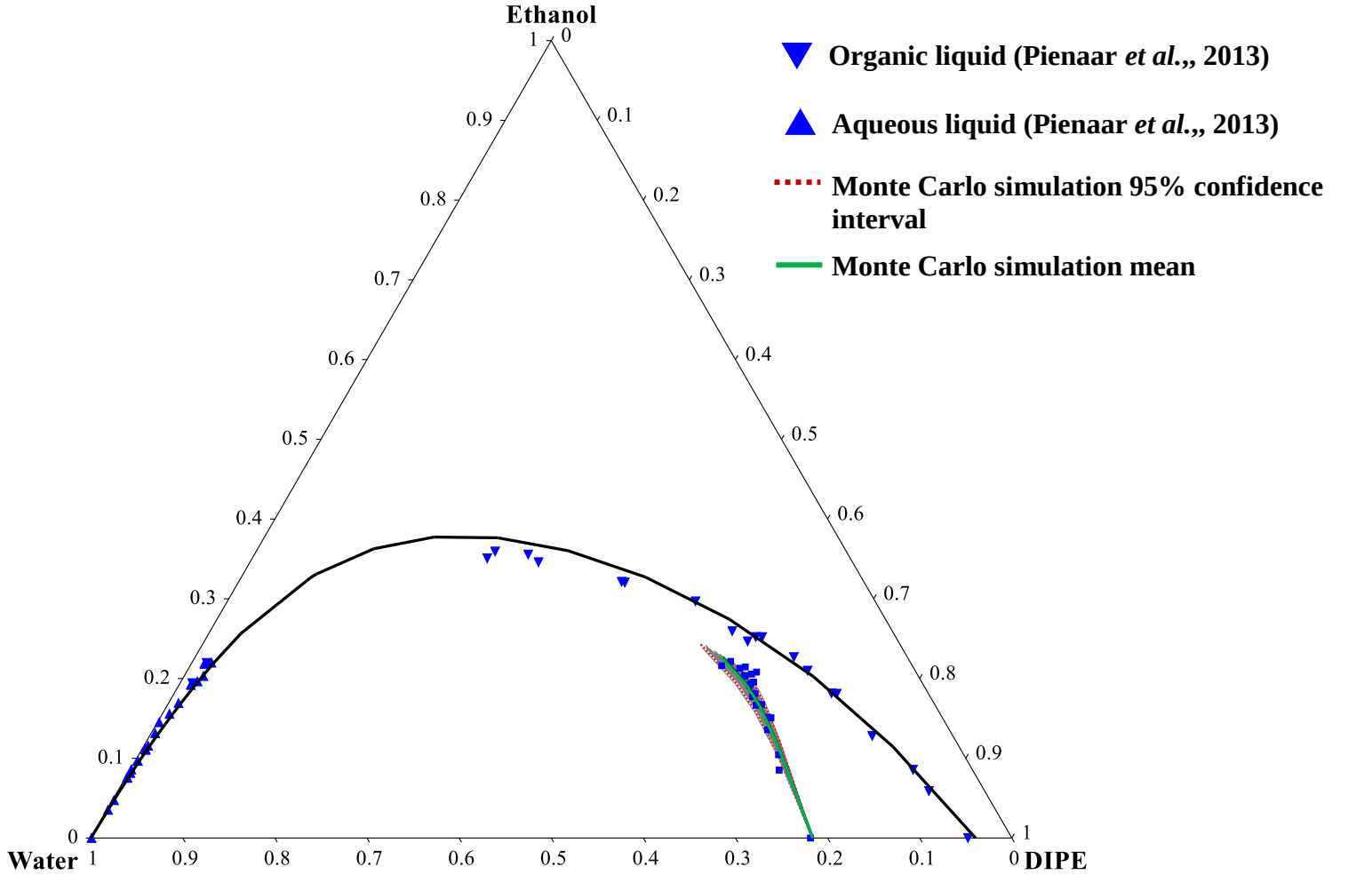

Figure 7.22. Propagated uncertainty in the NRTL model predictions for the ternary system Ethanol/DIPE/Water at 101.3 kPa. Grey lines represent the Monte Carlo simulations, red dashed lines are the 5th and 95th percentile of the simulations and black full lines are the mean of the simulation. Experimental data from Pienaar *et al.*, (2013).

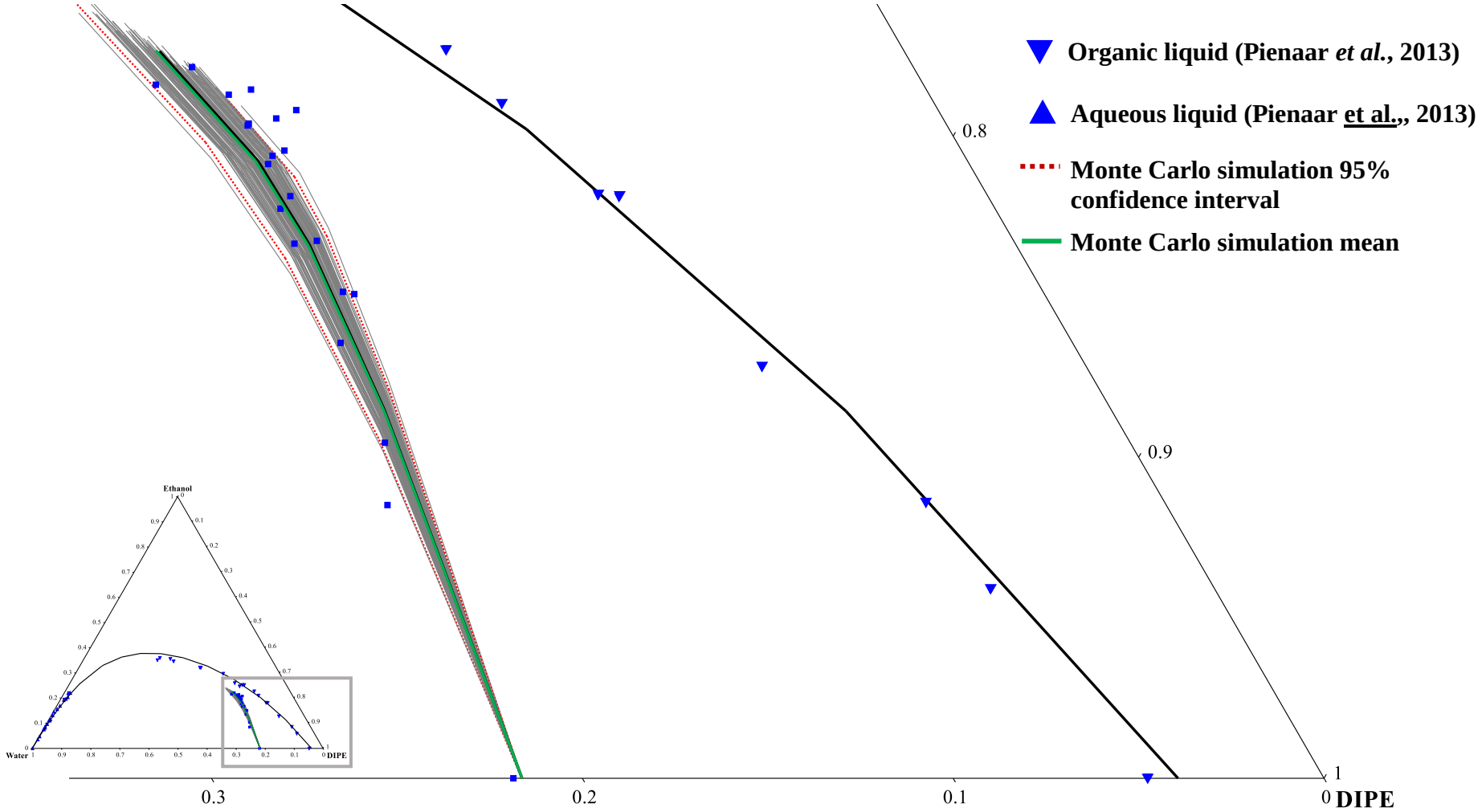

Figure 7.23. Propagated uncertainty in the NRTL model predictions for the ternary system Ethanol/DIPE/Water at 101.3 kPa. Grey lines represent the Monte Carlo simulations, red dashed lines are the 5th and 95th percentile of the simulations and black full lines are the mean of the simulation. Experimental data from Pienaar *et al.*, (2013).

Figure 7.24 summarises the results of the azeotrope uncertainty propagation. This system has a total of four azeotropes of which one is ternary and the rest are two-component. The DIPE + water azeotrope exhibits effectively no uncertainty and is in contrast with the three other azeotropes. The ethanol/water azeotrope is experimentally reported at 89.5 mole % ethanol and 10.5 mole % water (Gmehling *et al.*, 1994). The base case estimates the azeotrope at 90 mole % ethanol and 10 mole % water. The Monte Carlo simulation results indicate that the range of uncertainty for the ethanol concentration is between 88.7 and 91.4 mole percent and for water is between 8.6 and 11.2 mole %. It is therefore concluded that for the ethanol + water azeotrope the uncertainty associated with the ethanol concentration is ca. 3.0% and for the water concentration is ca. 23.2%. The DIPE/ethanol azeotrope is experimentally reported at 68.2 mole % DIPE and 31.8 mole % ethanol (Pienaar *et al.*, 2013). The base case estimates the azeotrope at 69 mole % DIPE and 31 mole % ethanol. The Monte Carlo simulation results indicate that the range of uncertainty for the DIPE concentration is between 67.8 and 71.3 mole percent and for ethanol is between 28.7 and 32.2 mole %. It is therefore concluded that for the DIPE/ethanol azeotrope the uncertainty associated with the DIPE concentration is ca. 5.2% and for the ethanol concentration is ca. 12.2%.

In the case of the ternary azeotrope, the experimentally reported composition is 66.6 mole % DIPE, 13.8 mole % ethanol and 19.6 mole % water. The base case estimates the azeotrope at 66.6 mole % DIPE and 14.2 mole % ethanol and 19.3 mole % water. The Monte Carlo simulation results indicate that the range of uncertainty for DIPE concentration is between 65.1 and 68.6 mole percent, and for ethanol is between 11.3 and 16.5 mole % and water is between 18.4 and 20.1 mole %. It is therefore concluded that for the ternary azeotrope the uncertainty associated with DIPE concentration is ca. 5.4%, for the ethanol concentration is ca. 31.5% and for water concentration is ca. 9.2%.

Therefore, in the context of the azeotropes, the DIPE concentration in general appears to have the lowest uncertainty at ca. 5% and the ethanol and water uncertainty are notably larger ranging from ca. 10% to as high as ca. 30%. Although the range of uncertainty is high for the latter two components, the MCS average is close to the base case for all the azeotropes. As such, the impact of the azeotrope uncertainty on the process design is to be determined in the next chapter.

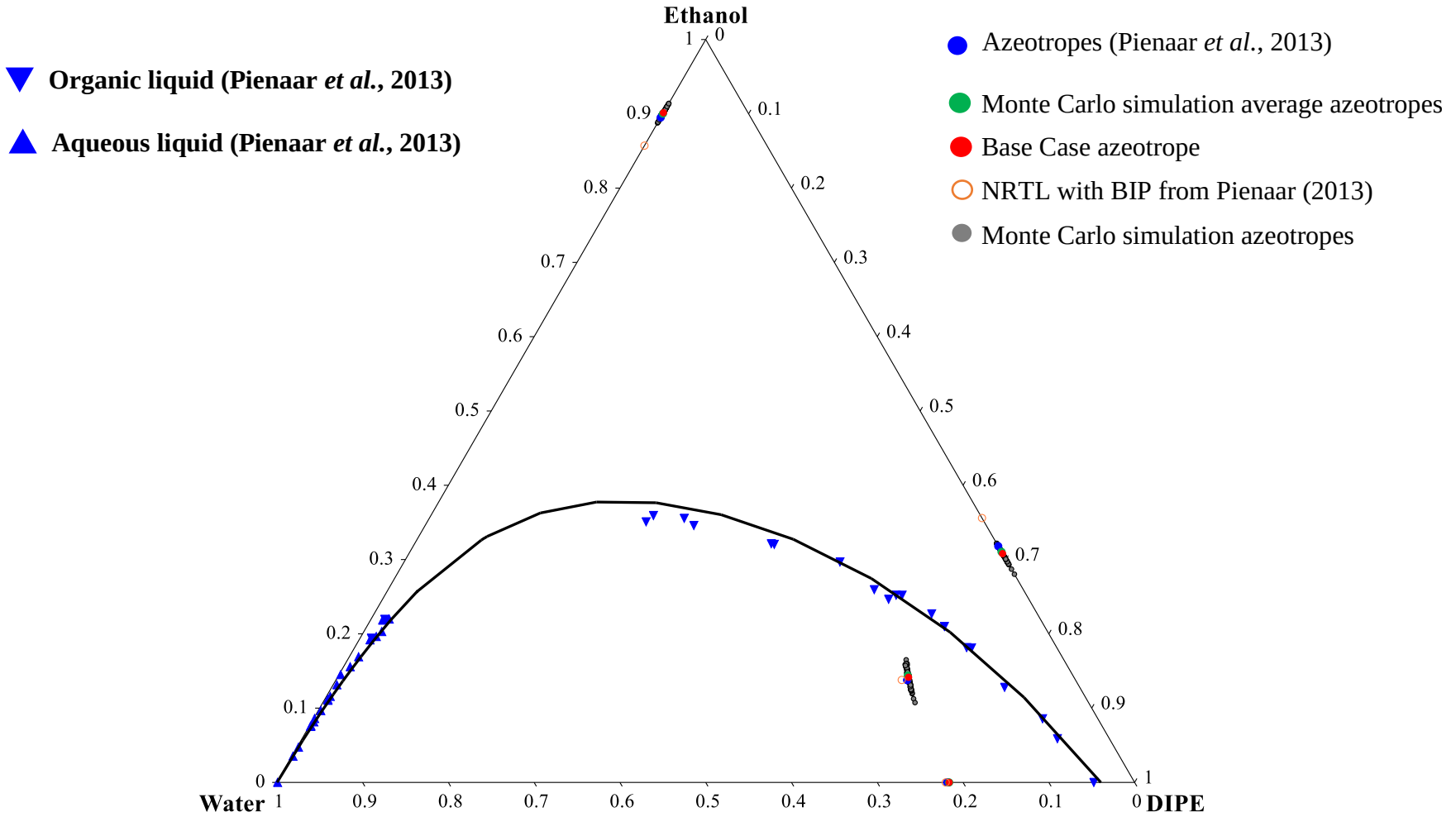

Figure 7.24. Propagated uncertainty in the NRTL model predictions for the ternary system Ethanol/DIPE/Water at 101.3 kPa. Experimental data from Pienaar *et al.*, (2013).

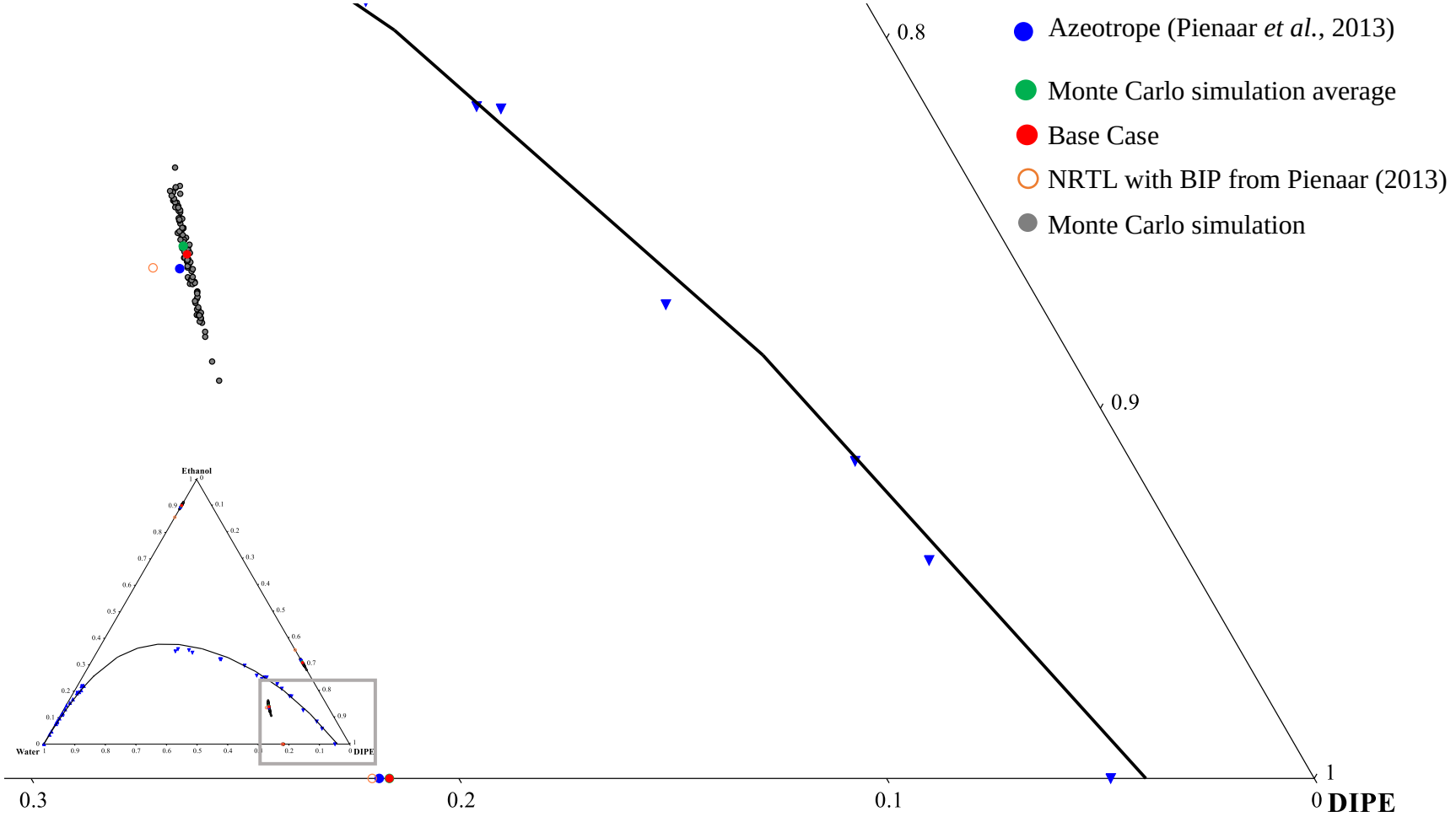

Figure 7.25. Propagated uncertainty in the NRTL model predictions for the ternary system Ethanol/DIPE/Water at 101.3 kPa. Grey lines represent the Monte Carlo simulations, red dashed lines are the 5th and 95th percentile of the simulations and black full lines are the mean of the simulation. Experimental data from Pienaar *et al.*, (2013).

7.5.5 Section Highlights

The performances of several thermodynamic models were evaluated to identify a model that offered accurate predictions of experimental data when considering the phase equilibria of the *DIPE/ethanol/water* system. The NRTL activity coefficient model was identified through a screening process and provides results with a high degree of accuracy. Subsequently, the parametric uncertainty of the experimental data was propagated through the NRTL model to the phase equilibria using a MCS approach. This revealed that the azeotrope composition was the phase equilibria element with the highest range of uncertainty. Despite this, it is may not contribute significantly to the process design uncertainty as the MCS averages were comparable to the azeotropes calculated through the base case parameter set.

7.6 Chapter summary

In this chapter, thermodynamic model screening and selection was performed for the DIPE/IPA/2-methoxyethanol and the DIPE/ethanol/water systems. The NRTL model provided good results for both systems and was selected to perform the process design calculations. The phase-equilibrium uncertainty was assessed and laid the foundation for the next chapter in which the effect of the phase-equilibrium uncertainty on the process design will be determined.

Chapter 8
Process Design Uncertainty Results

In Chapter 7, the parametric uncertainties of thermodynamically consistent experimental data were separately propagated to the phase equilibria of C_2 and C_3 low molecular weight alcohol systems. A comprehensive uncertainty analysis was performed on important phase equilibria elements, including azeotropes, vapour-liquid and liquid-liquid equilibrium. With the availability of uncertainty information for model parameters and phase equilibria, it is now possible to perform a rigorous uncertainty quantification of the process design for the systems of interest.

In this chapter, the aim is to evaluate the effect of the phase equilibrium uncertainties on the process simulation results, thereby addressing project *Objective (iii)* (***How reliable is the best model?***). The effects of these uncertainties are investigated through a probabilistic case study approach using the thermodynamic model parameter sets obtained through the Monte Carlo simulations. These model parameters are coupled with the Aspen Plus® process simulation software through Aspen Simulation Workbook (ASW). The key design output variables of unit operations in the process models are then assessed to determine the effect of the uncertainties and also, importantly, the confidence level of the designs. The results of the extractive distillation system are presented first, followed by the results of the azeotropic distillation system.

It is understood that the column design specifications may have a major impact on the way the errors propagate into the final design. In order to sustain an acceptable level of comparison with the reported optimum designs of Luo *et al.*, (2014) for System 1 and Pienaar *et al.*, (2013) for System 2, the simulation specifications of the original authors are retained as the basis of this work.

8.1 System 1: Extractive distillation

8.1.1 Process simulation setup (DIPE, IPA and 2-methoxyethanol)

The process simulation setup was based on the configuration parameters proposed by Luo *et al.*, (2014). The process simulations were performed in Aspen Plus® and both the extractive distillation column and the recovery column were modelled with the *RadFrac* option. *RadFrac* is a rigorous model for simulating all types of multistage vapour-liquid fractionation operations.

The columns were setup with the equilibrium calculation type and the strongly non-ideal liquid convergence option. The kettle reboiler option was chosen to maximise the heat exchanger surface area utilisation. The Aspen Plus® process model flowsheet is presented in Figure 8.1.

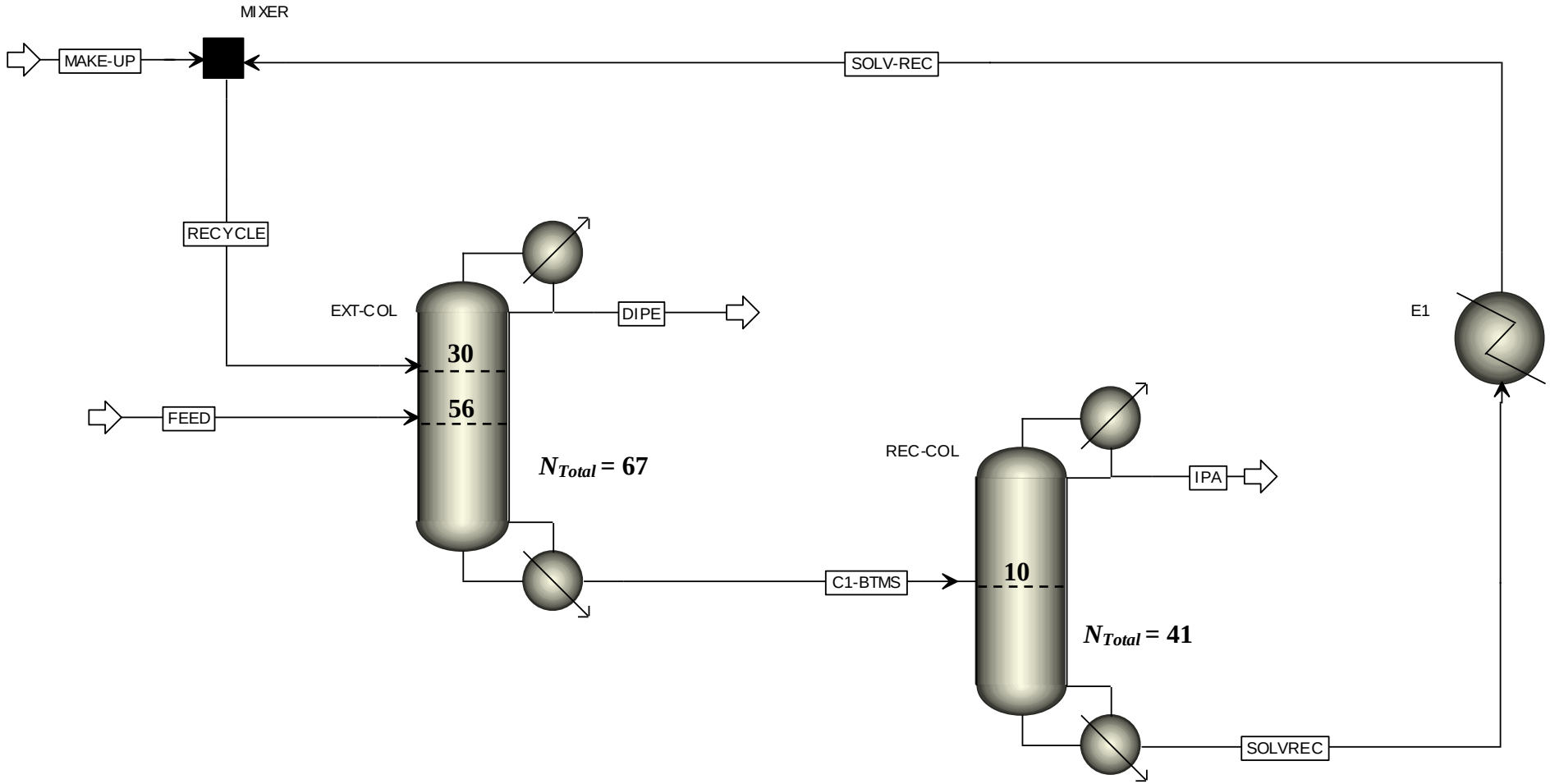

Figure 8.1. Aspen Plus® simulation flowsheet for the system DIPE + isopropanol +2-methoxyethanol.

For the extractive distillation column a reflux ratio of 1.54 (mole basis) was specified, as the optimal value according to Luo *et al.*, (2014). Furthermore, the distillate stream DIPE purity specification was set at 0.99 mass fraction and the bottoms stream 2-methoxyethanol purity was specified as 0.8 mass fraction. The adjustable variable was the extraction column distillate molar flow rate; the lower bound was 50 kmol/h and the upper bound was 200 kmol/h. For the recovery column a distillate stream IPA product purity of 0.993 mass fraction was specified and a reflux ratio of 1.95. The adjustable variable was the recovery column distillate molar flow rate; the lower bound was set at 10 kmol/h and the upper bound at 50 kmol/h. The solvent recycle heat exchanger outlet temperature was specified at 55 °C.

8.1.2 Process description

In this system, the objective is the separation of the DIPE/IPA minimum boiling azeotrope with heavy entrainer 2-methoxyethanol. The processing objective is achieved through extractive distillation.

The feed to the unit consists of a mixture of 75 mole percent DIPE and 25 mole percent IPA. The feed enters the extractive distillation column on theoretical stage no.56 at 55 °C and 142 kPa at a rate of 100 kmol/h. The column consists of 67 theoretical stages, a reboiler and condenser and operates at 101.3 kPa. The reboiler operates at ca. 122°C with a reboil ratio of ca. 1.91 and the top product is DIPE with a target purity of 99.3 weight percent. The bottoms product is routed as feed to tray 10 of the recovery column and is mostly 2-methoxyethanol with IPA. The recovery column consists of 41 theoretical stages, a reboiler and condenser and operates at 101.3 kPa. The reboiler operates at ca. 133 °C and the bottoms product is high purity 2-methoxyethanol of 99.9 mole percent and is recycled back to the extraction column. The overheads of the recovery column is condensed and is high purity IPA of 99.2 mole percent.

8.1.3 Extraction column results

The extraction column uncertainty quantification results are presented in Table 8.1. A total of ten key design output variables were considered for the extraction column. These output variables were selected based on its likely impact on equipment sizing. The base case values are presented first; these are the results obtained by the optimum regressed binary interaction parameters and represent the design values without considering input parametric uncertainty. The remainder of the table i.e. 95th percentile, standard deviation, absolute uncertainty and design uncertainty are the results of the Monte Carlo simulations. Here the 95th percentile values represent the design values that considered input parametric uncertainty and provides a design

with a 95% confidence level. Parameters marked with a "VARY" superscript indicates a specified adjustable variable and parameters marked with a "SPEC" superscript indicates a specified parameter in the Aspen Plus® column setup.

In general, it is observed that the overall design uncertainty associated with the extraction column is low. In particular, for the top section of the column there is no apparent difference between the base case and the 95th percentile case. In terms of the bottoms section of the extraction column, it is noted that reboiler is effected the most by the input parameter uncertainty, albeit to an acceptable extent.

Table 8.1. Extraction column uncertainty quantification results.

Key Output Variables	UOM	Base Case	95th %	Standard Deviation	Absolute Uncertainty	Design Uncertainty
Top Temperature	K	341	342	0.0514	0.10	0.03%
Condenser Duty	kW	-1587	-1592	3.6440	7.29	0.46%
Distillate Flow Rate^{VARY}	kmol/h	76.2	76.2	0.1269	0.25	0.33%
Reflux Flow Rate	kmol/h	117	117	0.1954	0.39	0.33%
Reflux Ratio^{SPEC}		1.54	1.54	0.0000	0.00	0.00%
Bottoms Temperature	K	392	395	1.0632	2.13	0.54%
Reboiler Duty	kW	1958	1999	36.33	72.66	3.71%
Bottoms Flow Rate	kmol/h	100	102	0.9244	1.85	1.85%
Reboiler Flow Rate	kmol/h	179	196	6.96	13.92	7.77%
Reboil Ratio		1.79	1.91	0.0619	0.12	6.91%

The results from Table 8.1 are ranked in a pareto chart and presented in Figure 8.2. The reboiler flow rate design uncertainty is the highest at ca. 7.8% with an absolute uncertainty of ca. 14 kmol/h at a base case value of 179 kmol/h. The reboiler duty design uncertainty is ca. 3.7% with an absolute uncertainty of ca. 73 kW at a base case duty of 1587 kW.

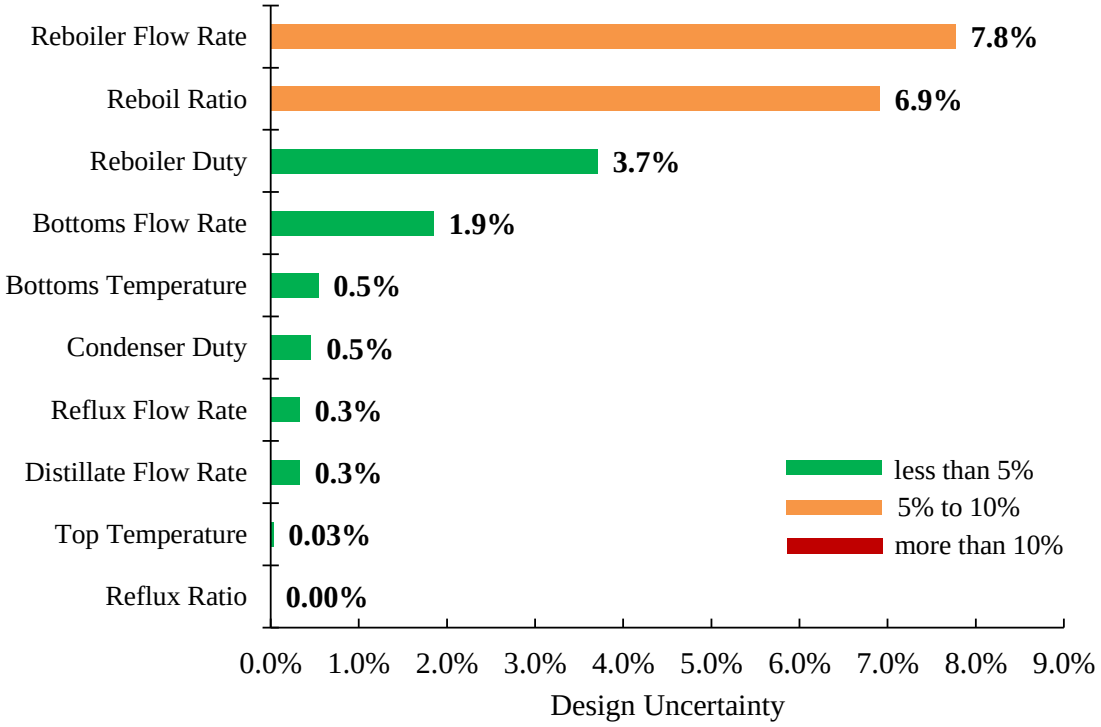

Figure 8.2. Pareto chart of extraction column uncertainty quantification results.

Figure 8.3 details the Monte Carlo simulation results for the extraction column reboiler duty and show that ca. 39% of the results are above the base case value. Consequently, as is evident from Figure 8.4 the base case reboiler duty is associated with only a ca. 61% confidence level. In order to improve the design confidence to the 95th percentile a reboiler duty of ca. 2000 kW is required.

Figure 8.5 shows that for the extraction column reboiler flow rate a large portion of the Monte Carlo simulation results are located above the base case value of 179 kmol/h and Figure 8.6 reveals that the base case confidence level is only ca. 25%. The design confidence can be improved by increasing the reboiler flow rate to at least 196 kmol/h along with the reboiler duty. The remainder of the key design output variables for the extraction column are all well below 5% design uncertainty and therefore represents a low design risk.

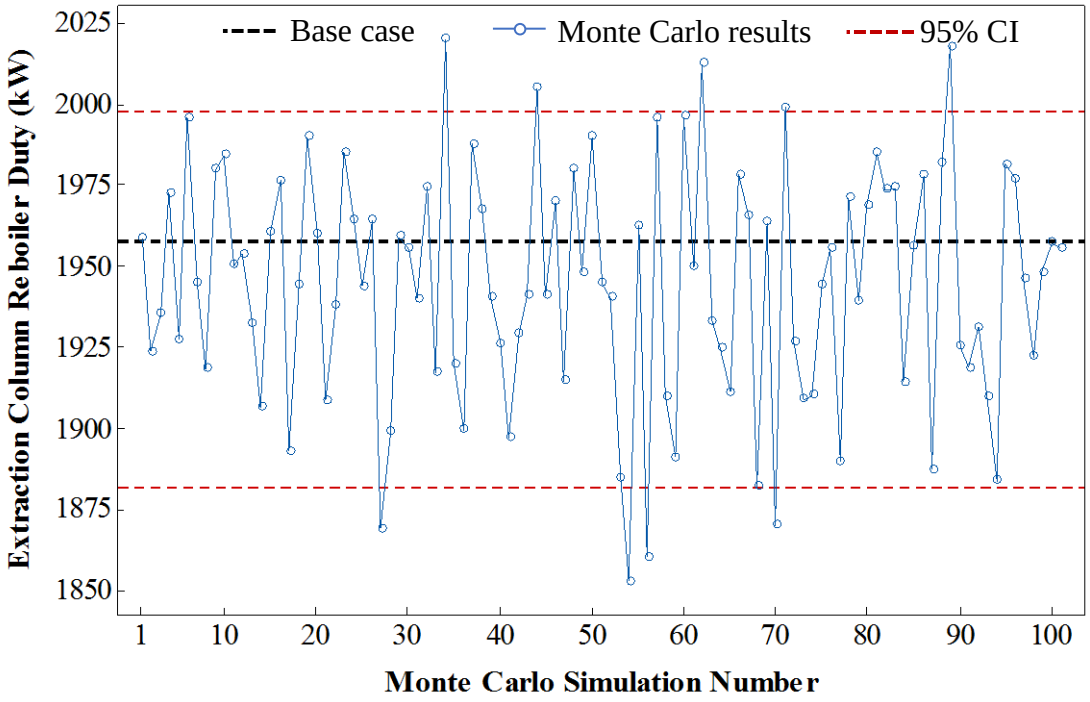

Figure 8.3. Monte Carlo simulation results for the extraction column reboiler duty (kW).

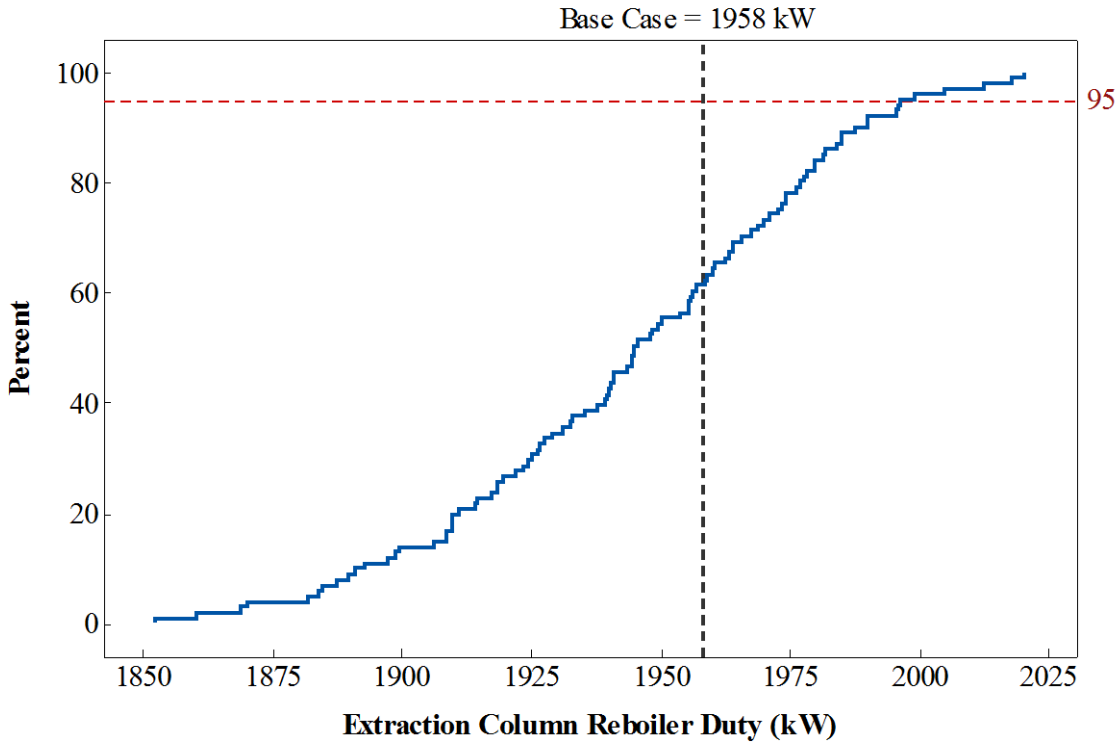

Figure 8.4. Uncertainty of extraction column reboiler duty (kW).

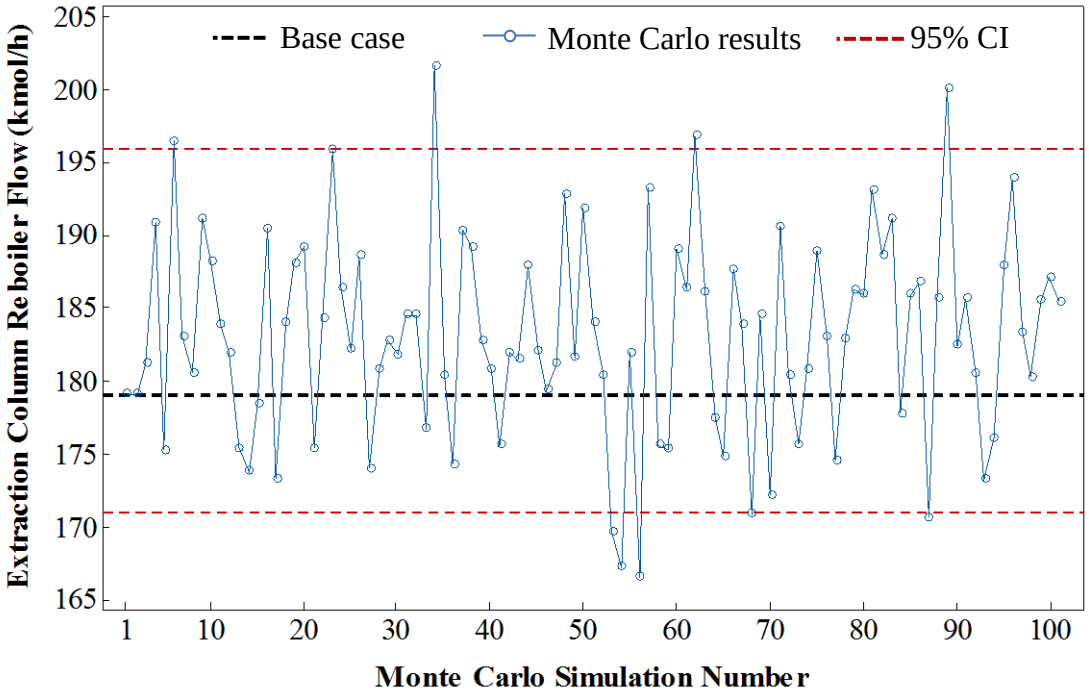

Figure 8.5. Monte Carlo simulation results for the extraction column reboiler flow rate (kmol/h).

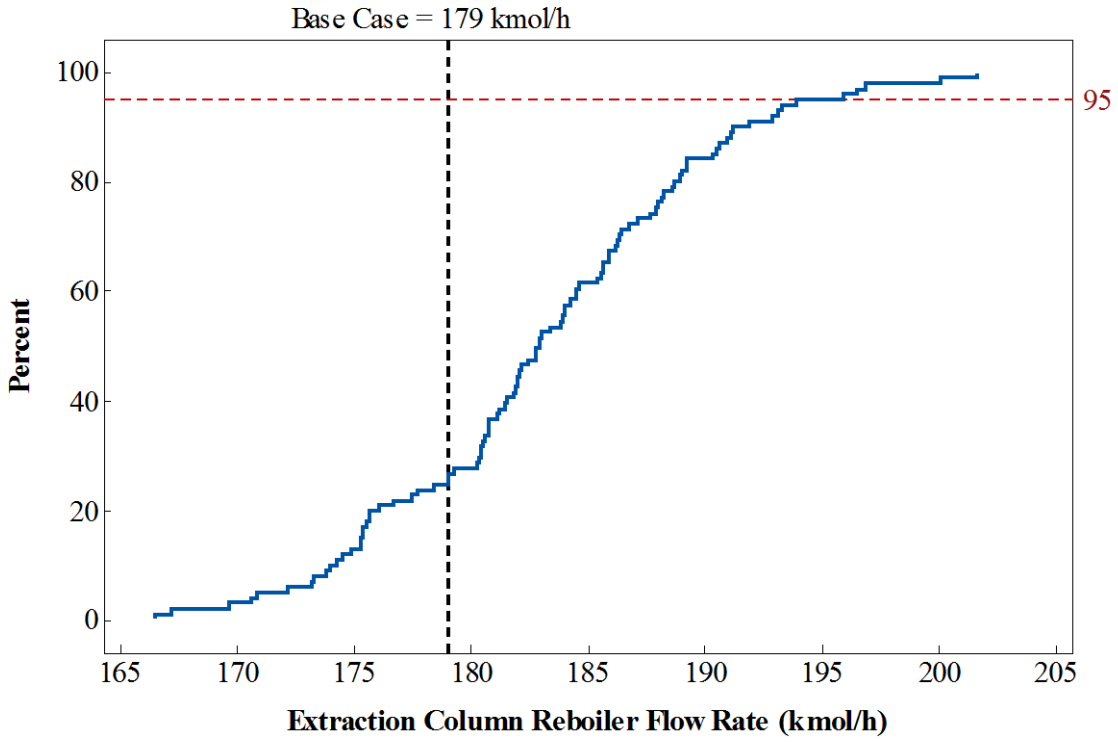

Figure 8.6. Uncertainty of extraction column reboiler flow rate (kmol/h).

8.1.4 Recovery column results

The recovery column uncertainty quantification results are shown in Table 8.2. A total of ten key design output variables were considered for the recovery column and are presented in the same format as previously in Table 8.1.

Table 8.2. Recovery column uncertainty quantification results.

Key Output Variables	UOM	Base Case	95th %	Standard Deviation	Absolute Uncertainty	Design Uncertainty
Top Temperature	K	355	355	0.1694	0.34	0.10%
Condenser Duty	kW	-812	-821	5.86	11.72	1.46%
Distillate Rate^{VARY}	kmol/h	24	25	0.1928	0.39	1.59%
Reflux Flow Rate	kmol/h	47	48	0.3760	0.75	1.59%
Reflux Ratio^{SPEC}		1.95	1.95	0.0000	0.00	0.00%
Bottoms Temperature	K	406	406	0.0258	0.05	0.01%
Reboiler Duty	kW	775	786	18.33	36.66	4.73%
Bottoms Flow Rate	kmol/h	76	78	0.7412	1.48	1.96%
Reboiler Flow Rate	kmol/h	72	73	1.71	3.42	4.72%
Reboil Ratio		0.96	0.97	0.0261	0.05	5.46%

In the case of the recovery column, a similar trend is observed as was for the extraction column. The top section of the column demonstrates no apparent difference between the base case and the 95th percentile case, whereas the uncertainty is also the highest in the bottom of the column. The results from Table 8.2 is ranked in a pareto chart and presented in Figure 8.7.

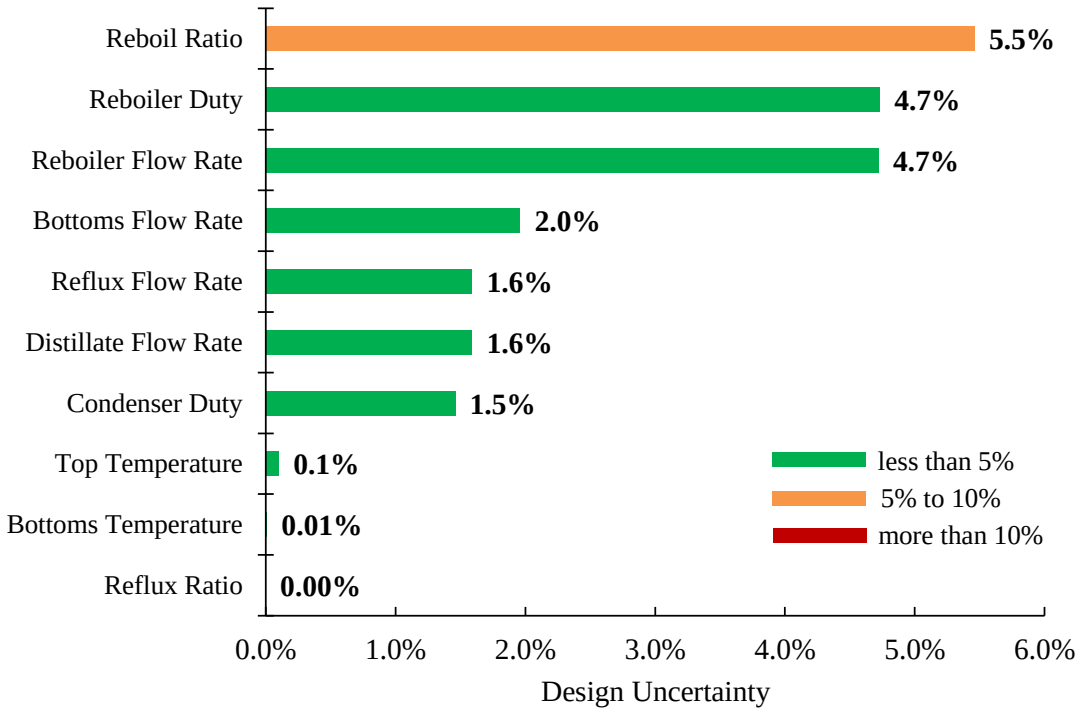

Figure 8.7. Pareto chart of recovery column uncertainty quantification results.

The reboiler duty design uncertainty is ca. 4.7% with an absolute uncertainty of ca. 37 kW at a base case duty of 775 kW. The reboiler flow rate design uncertainty is similar at ca. 4.7% with an absolute uncertainty of ca. 3.4 kmol/h at a base case value of 72 kmol/h.

Figure 8.8 details the Monte Carlo simulation results for the recovery column condenser duty and shows that ca. 55% of the results are above the base case value. Consequently, as is evident from Figure 8.9 the base case condenser duty is associated with only a ca. 45% confidence level. In order to improve the design confidence to the 95th percentile a condenser duty of ca. 821 kW is required. Even so, the standard deviation is small and consequently so is the uncertainty.

The Monte Carlo simulation results for the recovery column reboiler duty are presented in Figure 8.10 and the associated cumulative distribution function in Figure 8.11. The base case confidence level is ca. 82% and is acceptable assuming a typical safety margin of 10%. The remainder of the key design output variables for the recovery column are all well below 5% design uncertainty and therefore represents a low design risk.

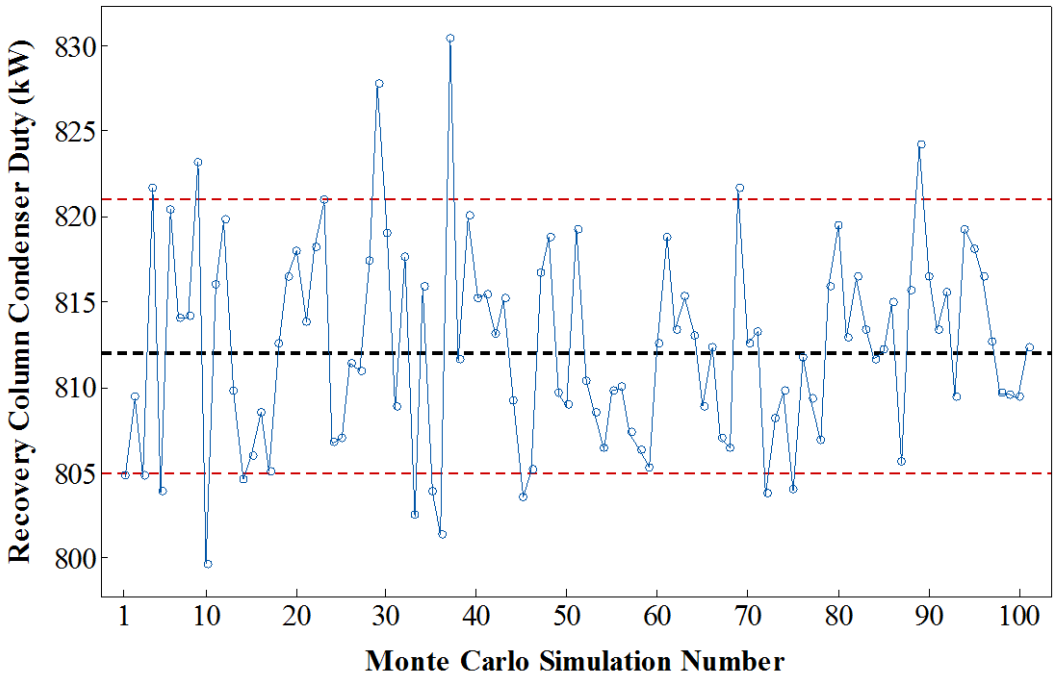

Figure 8.8. Monte Carlo simulation results for the recovery column condenser duty (kW).

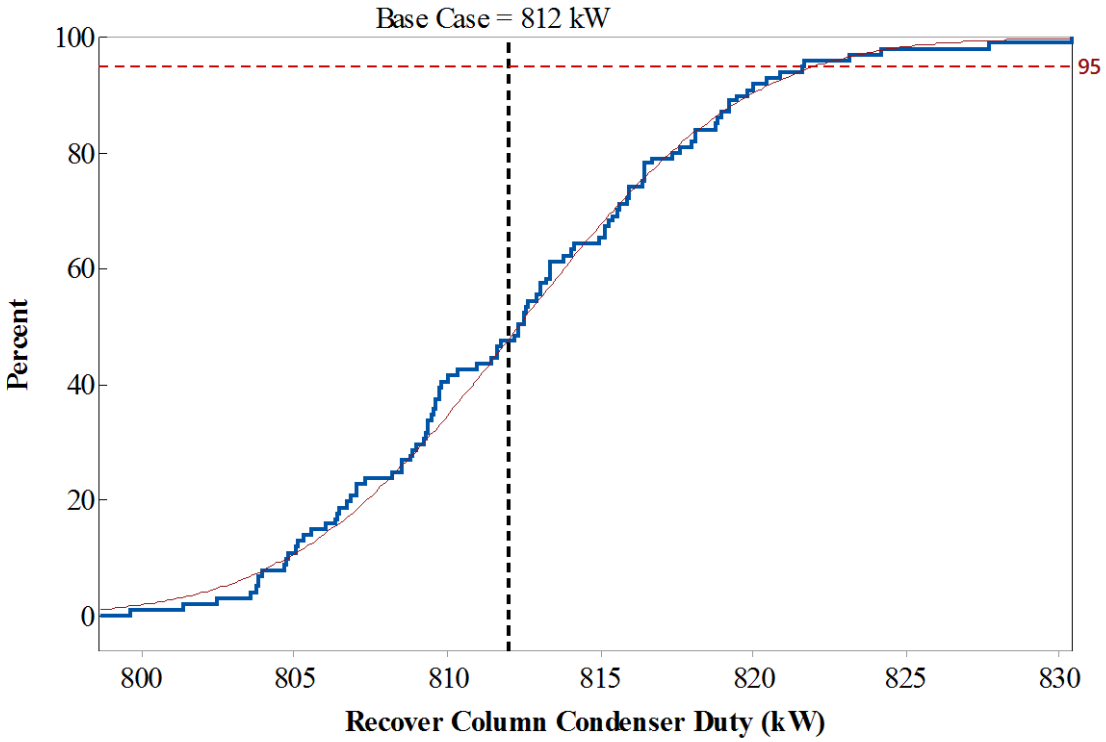

Figure 8.9. Uncertainty of recovery column condenser duty (kW).

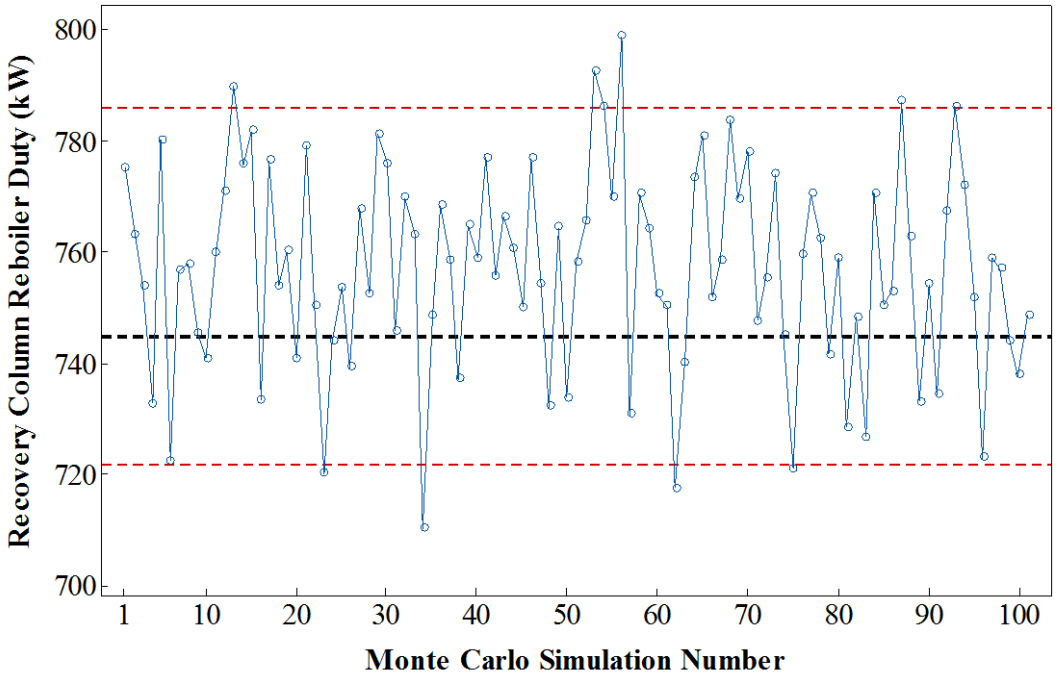

Figure 8.10. Monte Carlo simulation results for the recovery column reboiler duty (kW).

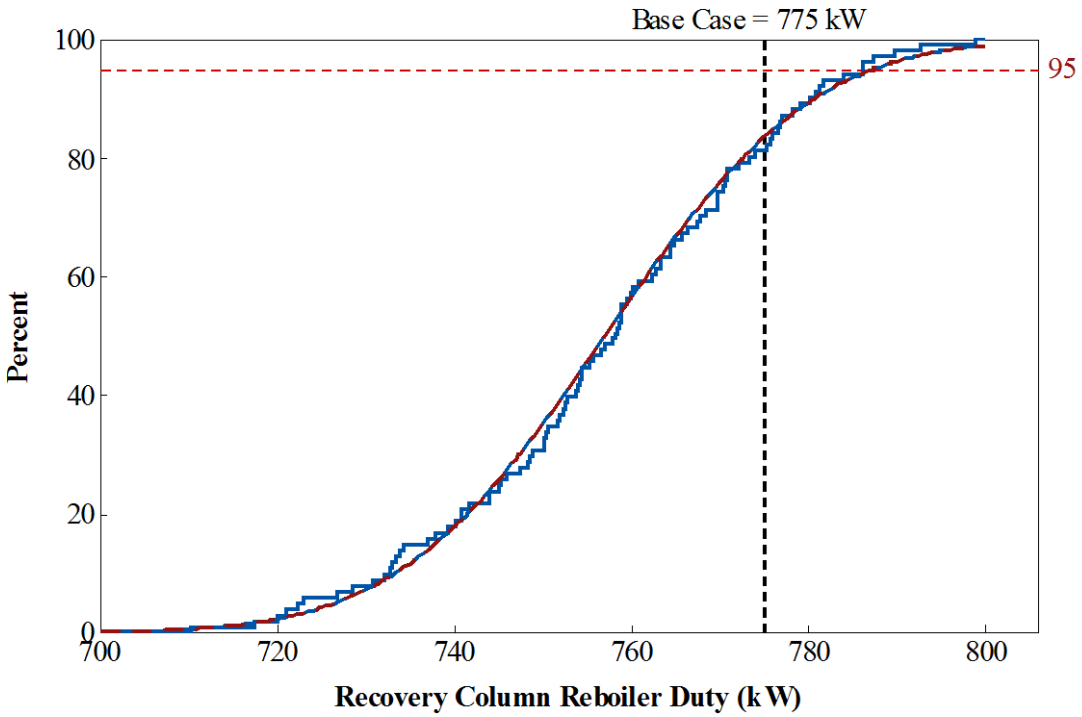

Figure 8.11. Uncertainty of recovery column reboiler duty (kW).

8.1.5 Section highlights

The results of the extractive distillation system uncertainty quantification process were presented in this section and are summarised on the process flow sheets for the base case parameters in Figure 8.12 and the 95th percentile confidence level case in Figure 8.13. A design case reported by Luo *et al.*, (2014) is presented in Figure 8.14 as a reference. It was observed that the extraction column uncertainty is predominantly in the bottom section of the column and is mainly related to the reboiler flow rate. The design confidence could be improved to an acceptable level through a marginal increase of the reboiler flow rate. Thus, the reboiler needs to be overdesigned to account for the increased flow rate, but maintain an adequate turndown ability.

The investigation further determined that the recovery column uncertainty is also limited to the bottom section of the column and only reboil ratio is of interest. The recovery column condenser and reboiler design confidence range from 45% to 82%, but a small increase in duty restored the design confidence to the required levels. It is therefore concluded that the design of the extractive distillation process for the separation of the diisopropyl ether + isopropanol azeotrope with 2-methoxyethanol is acceptable and the identified risk areas may be easily resolved.

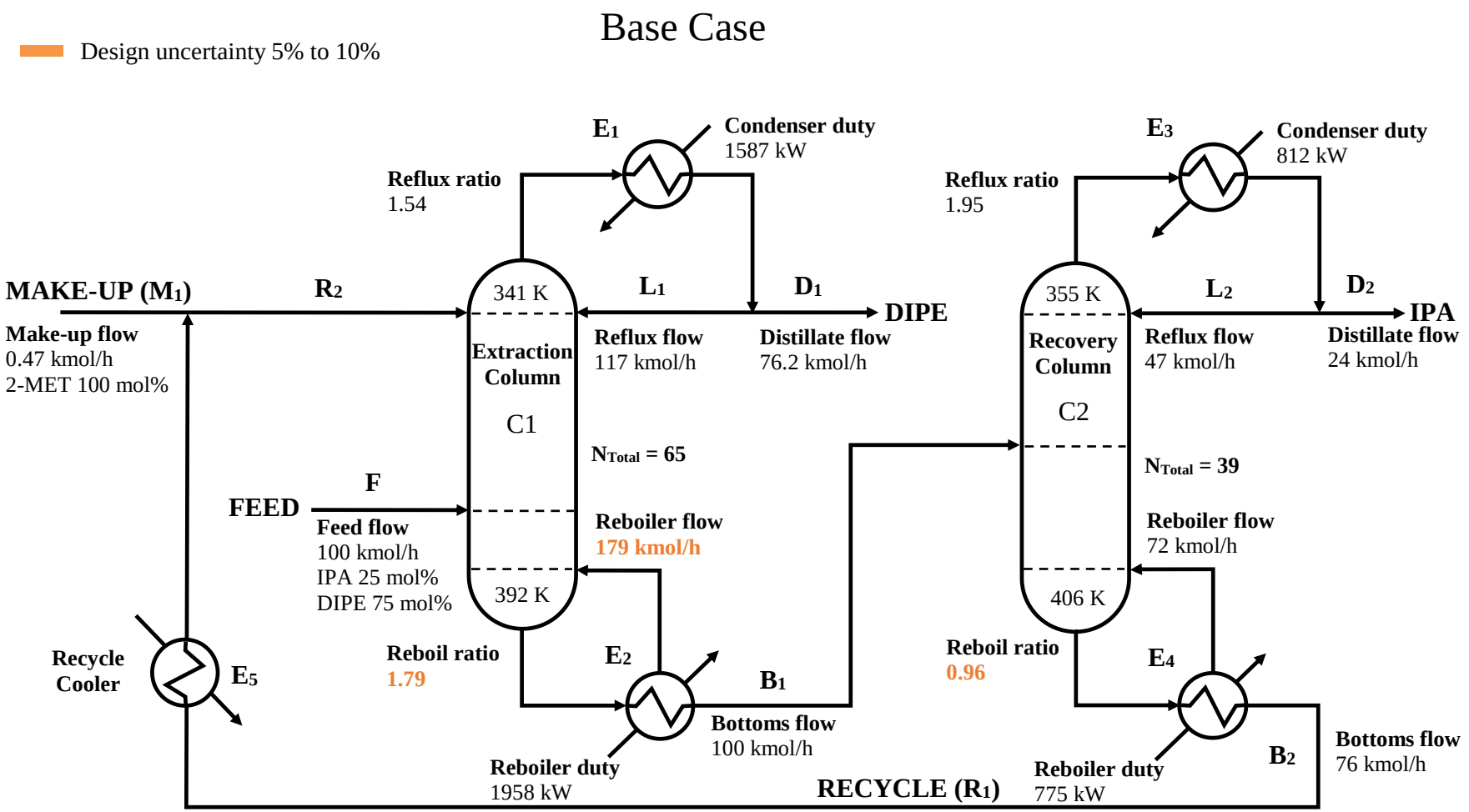

Figure 8.12. Flow sheet of the extractive distillation system with 2-methoxyethanol as the solvent. The simulation was performed with Aspen Plus using the NRTL model with the base case binary interaction parameter set.

95th Percentile Case

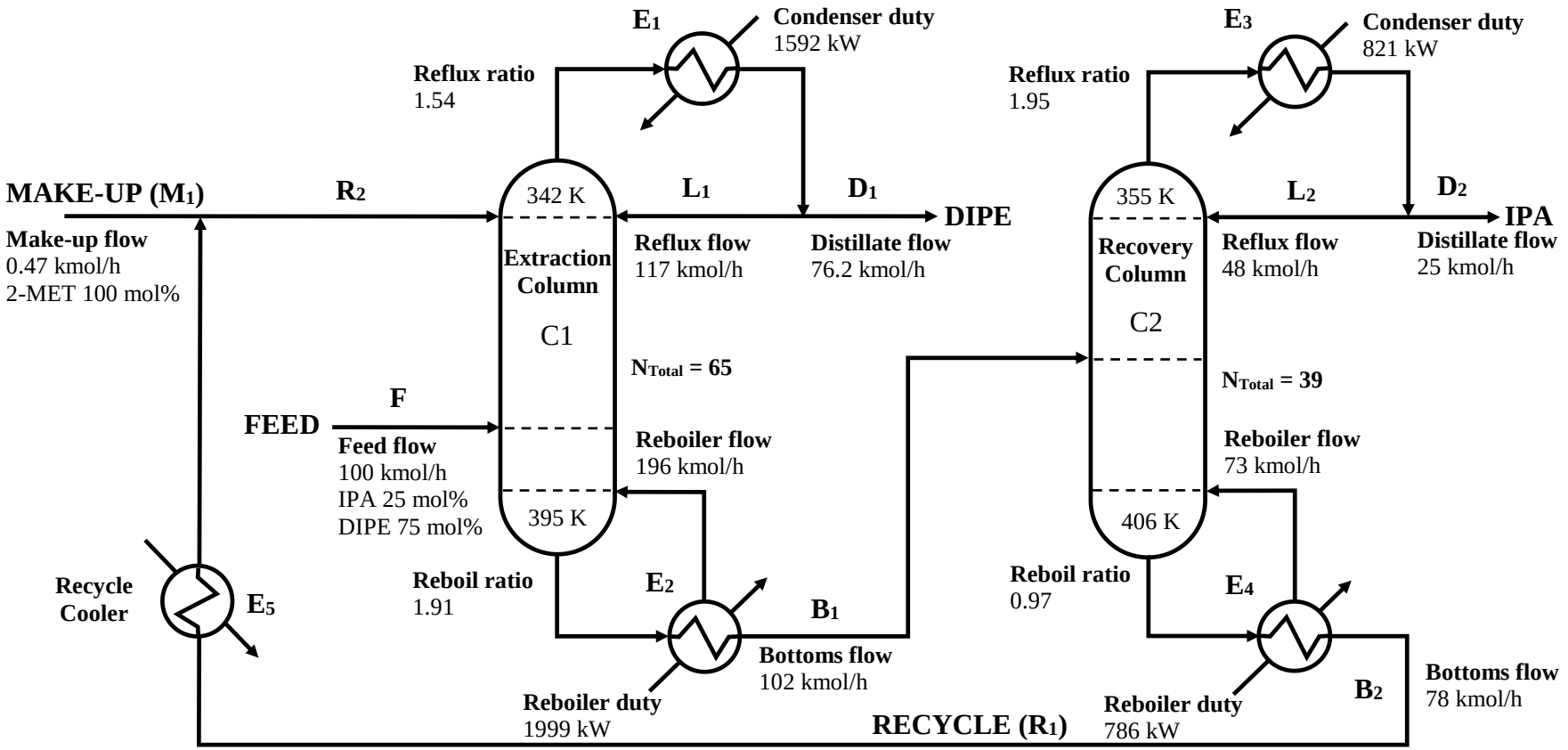

Figure 8.13. Flow sheet of the extractive distillation system with the simulation results of the 95th percentile confidence case.

Literature Reference Case

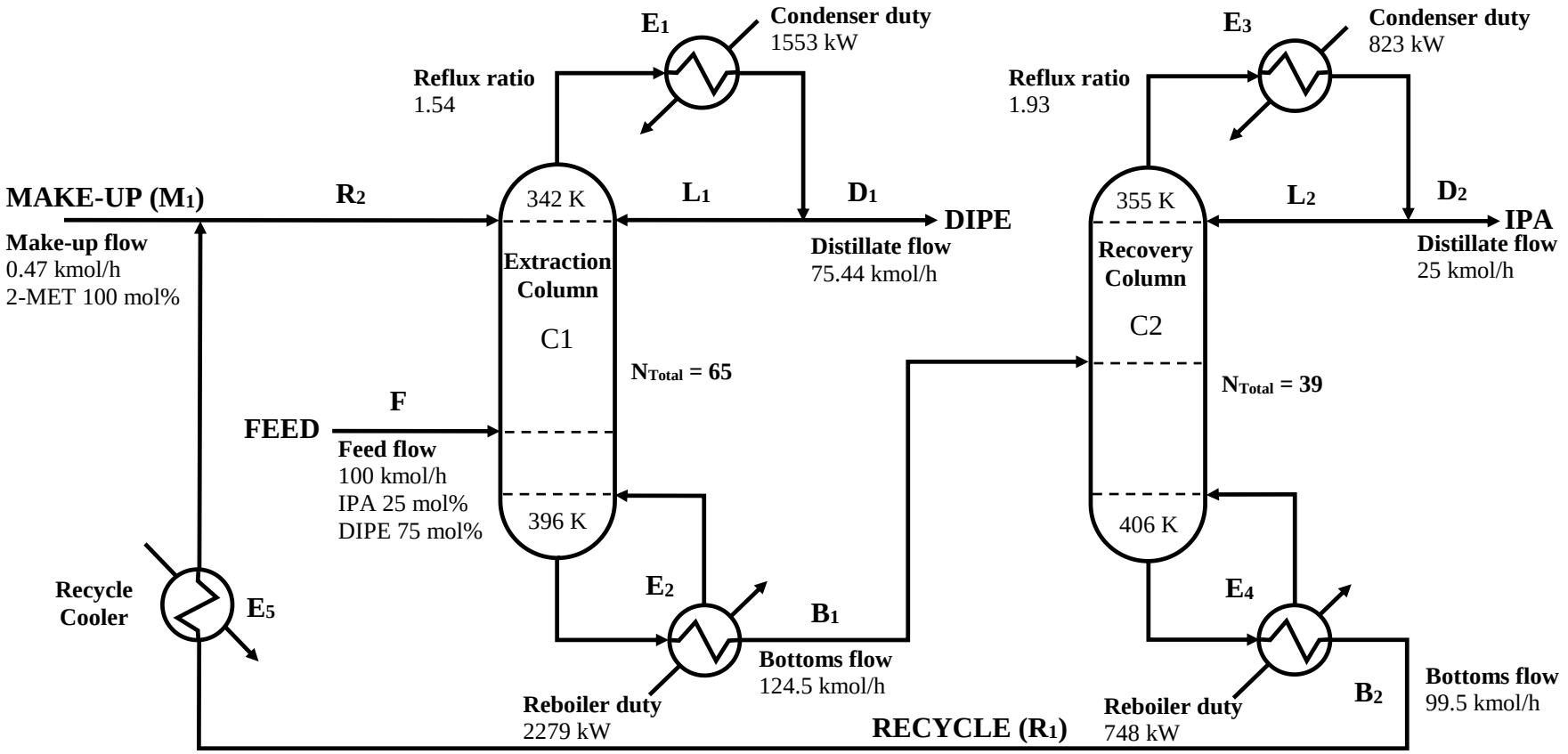

Figure 8.14. Flow sheet of the extractive distillation system with 2-methoxyethanol as the solvent reported by Luo *et al.*, (2014).

8.2 System 2: Heterogeneous azeotropic distillation

8.2.1 Process simulation setup (DIPE, ethanol and water)

The process simulation setup was based on the configuration parameters proposed by Pienaar (2012). In this work, the process simulations were performed in Aspen Plus® and both the azeotropic distillation column and the recovery column were modelled with the *RadFrac* option. The columns were setup with the equilibrium calculation type and the azeotropic convergence option. Furthermore, vapour-liquid-liquid were selected as the valid phase. The kettle reboiler option was chosen to maximise the heat exchanger surface area utilisation as ordinary shell and tube exchangers are generally limited to a reboiler outlet vapour fraction of ca. 35%. Selecting the kettle reboiler option further reduces the required reboiler flow rate and associated equipment sizing. In the case of the decanter, the *Flash3* model was used.

For the azeotropic column (C_1) two specifications were set on the bottoms stream, an ethanol mole fraction of 0.993 and a DIPE mole fraction of 0.005 to ensure minimum product specifications are satisfied. The adjustable variables were the bottoms molar flow rate and the reflux molar flow rate; no upper or lower bounds were placed on these variables. The decanter temperature and pressure was specified at 40 °C and 100 kPa to ensure that the net decanter duty is close to zero; this was determined iteratively. The recovery column (C_2) reflux ratio was specified on a mole basis at 45 and the boil-up ratio at 2.5 and no adjustable variables were specified for this column. The recovery column specifications were originally based on the values proposed by Pienaar (2012), i.e. reflux ratio 44.55 and boil-up ratio 3.63, and subsequently further optimised to the lowest feasible condenser and reboiler duties for the column.

The process flow scheme is presented in Figure 8.15 and the simplified Aspen Plus® process model flowsheet is presented in Figure 8.16. In Chapter 7, it was concluded that the *DIPE/ethanol/water* phase equilibria presented higher uncertainty than the extractive distillation system. Therefore a decision was made to perform a more in-depth assessment through the use of rigorous equipment sizing, specifically for the heat exchangers and distillation columns. The rigorous process model is presented in Figure 8.17, but is still based on the same process flow scheme as per Figure 8.15. The rigorous column sizing was based on the Koch Flexitray type and the minimum tray geometries were specified as a tray spacing of 0.6096 m and a column diameter of at least 0.3048 m.

8.2.2 Process description

The feed to the unit consists of an equal-molar mixture of ethanol and water. The feed enters the azeotropic column (C_1) on theoretical stage no.3 at 40 °C and 101.3 kPa at a rate of 100 kmol/h. The column consists of 40 theoretical stages, a reboiler and condenser. The reboiler (E_2) operates at ca. 77 °C with a reboil ratio of ca. 15 and the bottom product (B_1) is pure anhydrous ethanol with a target purity of 99.3 mole percent. The overheads product is condensed (E_1) and routed to a decanter to enable the separation of the two immiscible liquid phases. The organic phase forms ca. 90% of the total liquid phase in the decanter and the remainder is the aqueous phase. The organic liquid phase (L_1) of the decanter is returned to the azeotropic column as reflux on tray no.1 and is mostly DIPE. The separated aqueous liquid phase (D_1) from the decanter is routed as feed to tray 9 of the recovery column (C_2) and is mostly water. The recovery column consists of 12 theoretical stages, a reboiler and condenser and operates at 101.3 kPa. The reboiler (E_4) operates at ca. 100 °C and the bottoms product (B_2) is high purity water of 99.6 mole percent. The overheads of the recovery column is condensed (E_3) and is recycled back to tray no.2 of the azeotropic column (C_1).

8.2.3 Azeotropic column results

The azeotropic distillation column uncertainty quantification results are presented in Table 8.3. A total of 17 key design output variables were considered for the azeotropic column. These output variables were selected based on its likely impact on equipment sizing. The base case values are presented first; these are the results obtained by the optimum regressed binary interaction parameters and represent the design values without considering input parametric uncertainty. The remainder of the table i.e. 95^{th} percentile, standard deviation, absolute uncertainty and design uncertainty are the results of the Monte Carlo simulations. Here the 95^{th} percentile values represent the design values that considered input parametric uncertainty and provides a design with a 95% confidence level.

Table 8.3. Azeotropic column uncertainty quantification results.

Key Output Variables	UOM	Base Case	95th %	Standard Deviation	Absolute Uncertainty	Design Uncertainty
Top Temperature	C	60.39	61	0.27	0.55	0.90%
Condenser Duty	kW	6824	7184	246.9	493.7	7.24%
Condenser Area	m^2	336	365	15.9	31.8	11.11%
Distillate Rate	kmol/hr	541	566	16.14	32.30	5.97%
Reflux Rate^{VARY}	kmol/hr	681	702	13.70	27.40	4.02%
Reflux ratio		1.26	1.30	0.013	0.0263	2.09%
Bottom Temperature	C	77.57	77.67	0.056	0.113	0.15%
Reboiler Duty	kW	6709	6964	183	366	5.45%
Reboiler Area	m^2	126	129	2.2	4.4	3.50%
Bottoms Rate^{VARY}	kmol/hr	42.1	49	4.35	8.69	20.65%
Reboiler Rate	kmol/hr	625.15	647.3	15.87	31.74	5.08%
Boil-up Ratio		14.9	18.2	1.90	3.80	25.57%
Column Diameter	meter	2.56	2.6	0.0269	0.0537	2.09%
Downcomer Velocity	m/sec	0.05	0.05	0.0002	0.0004	0.85%
Flow Path Length	meter	1.76	1.8	0.0184	0.0369	2.09%
Downcomer Width	meter	0.40	0.41	0.0042	0.0084	2.09%
Side Weir Length	meter	1.86	1.9	0.0195	0.0390	2.09%

In contrast to the extractive distillation column, it is observed that the azeotropic distillation column design uncertainty is generally higher with results exceeding the typical 10% design margin. This is expected given the integration between the azeotropic column and decanter, coupled with variability in recycle from the recovery column. The results were ranked from high to low uncertainty and are presented in a Pareto graph in Figure 8.18.

The azeotropic column boil-up ratio, bottoms flow rate and condenser surface area have significant design uncertainty and this variability is unlikely to be absorbed by operational changes. In the top of the column, the condenser duty and distillate respective uncertainties are 7% and 6%, whereas the top temperature, reflux ratio and reflux rate uncertainties are relatively low. In the bottom of the column, the reboiler duty and the reboiler rate uncertainties are 5% and the effect of the phase equilibria uncertainty on the reboiler surface area seems to be minimal. In terms of the azeotropic column geometry, it is noted that the column diameter, downcomer width and flow path length uncertainties are low. It is concluded that the optimal column geometry is not significantly affected by the phase equilibria uncertainty.

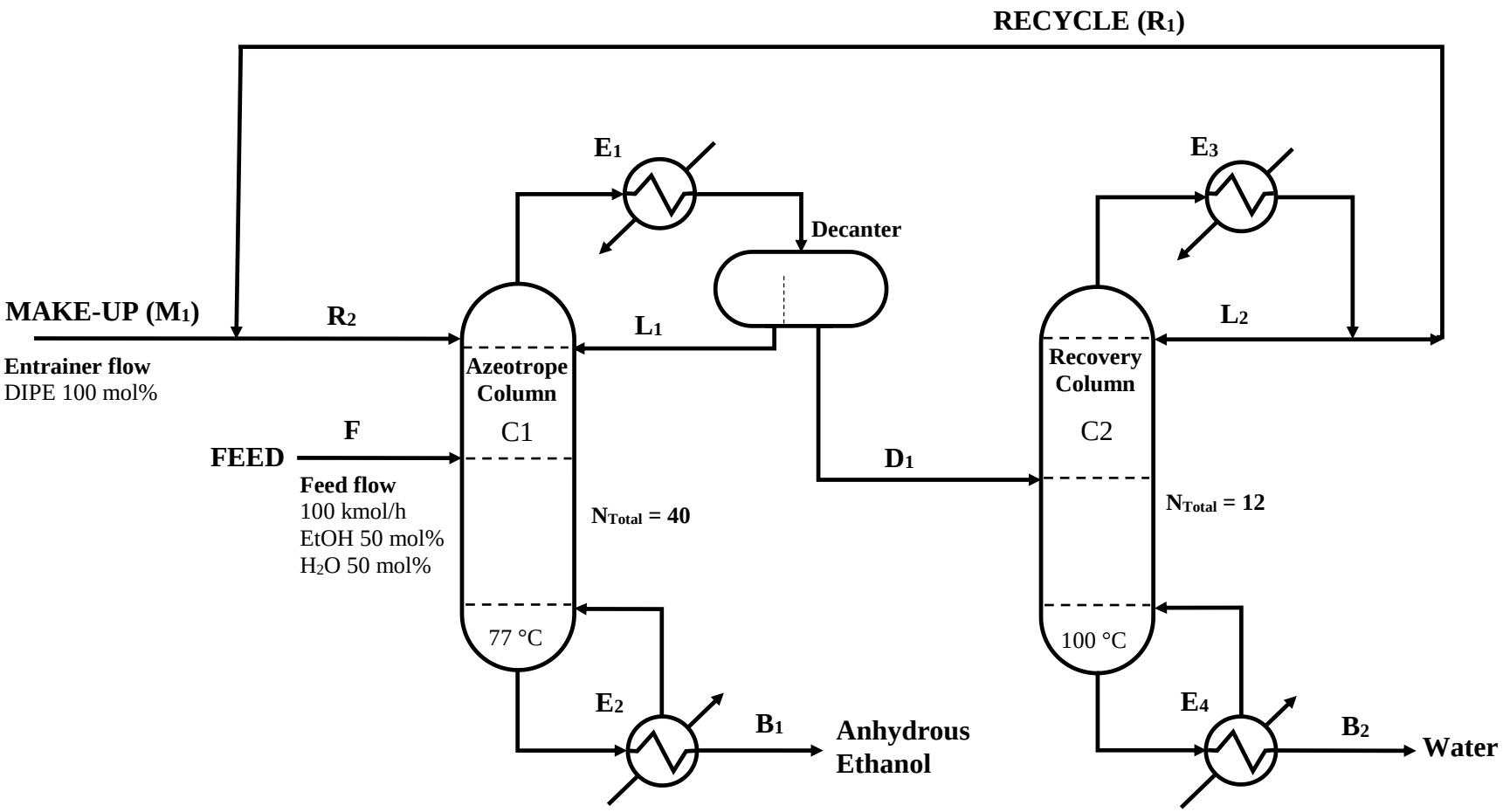

Figure 8.15. Flow sheet of the heterogeneous azeotropic distillation with the simulation results of the 95th percentile confidence case.

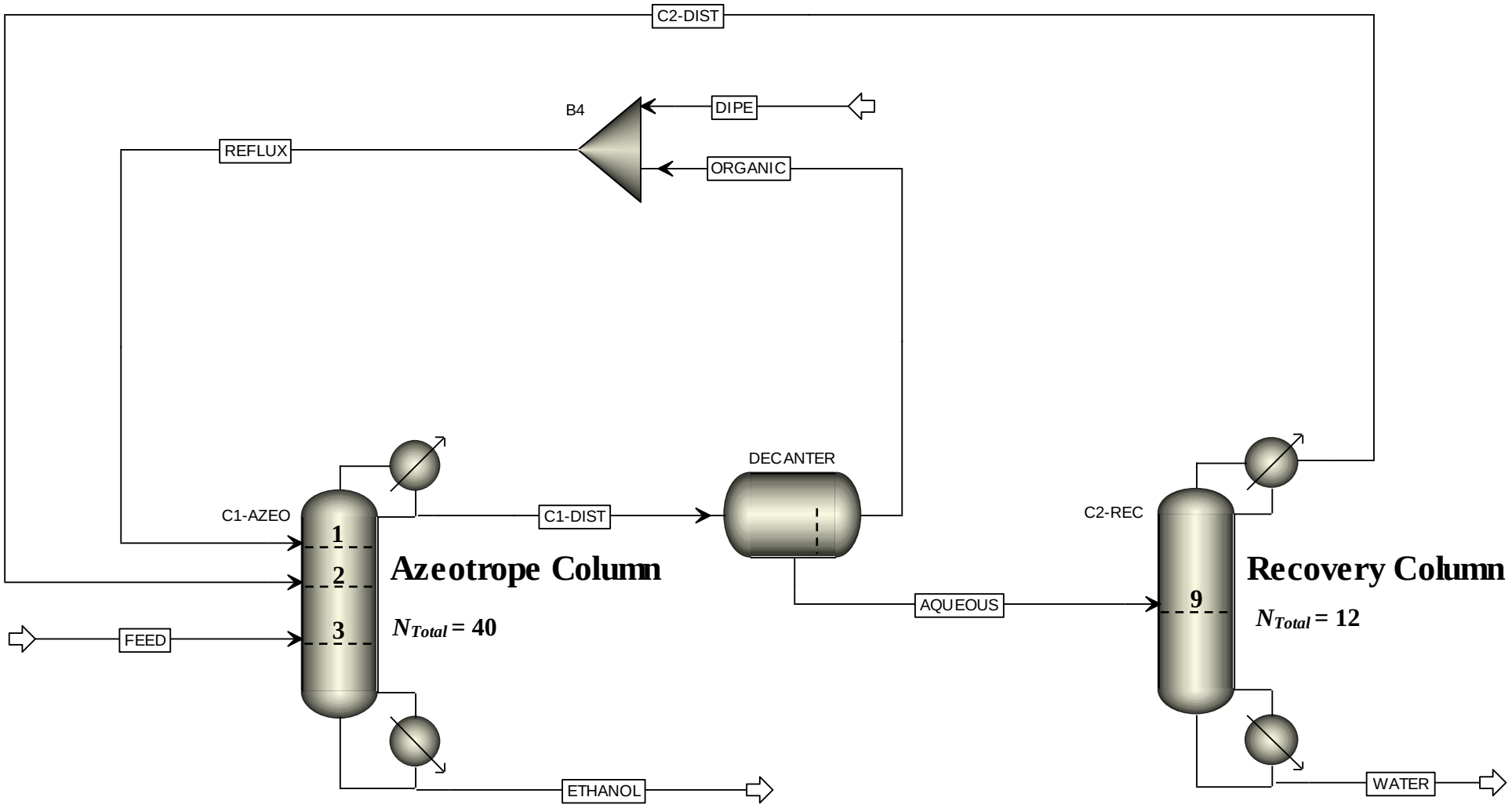

Figure 8.16. Aspen Plus® simulation flowsheet for the system DIPE + Ethanol + Water (simplified and not to scale).

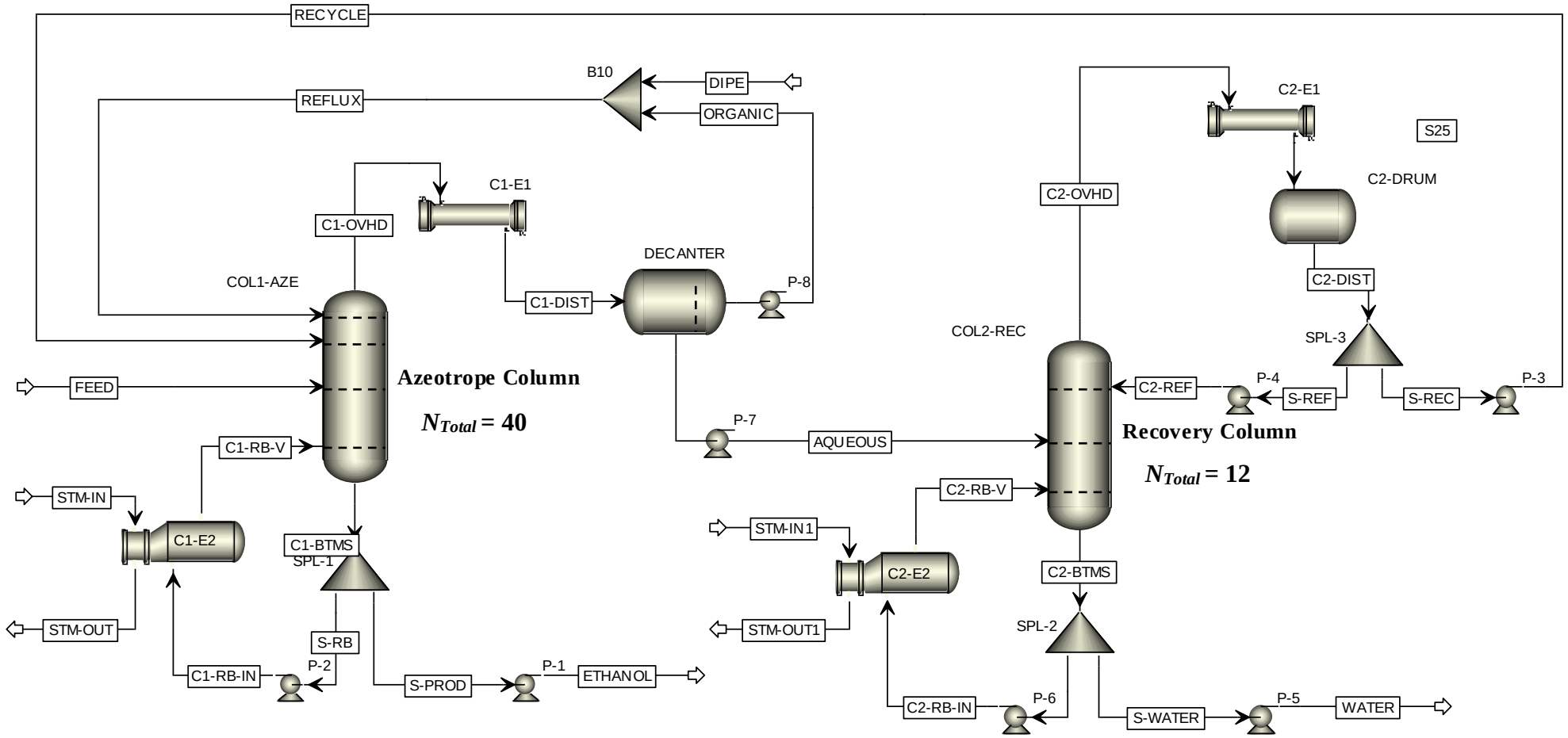

Figure 8.17. Aspen Plus® simulation flowsheet for the system DIPE + Ethanol + Water (rigorous).

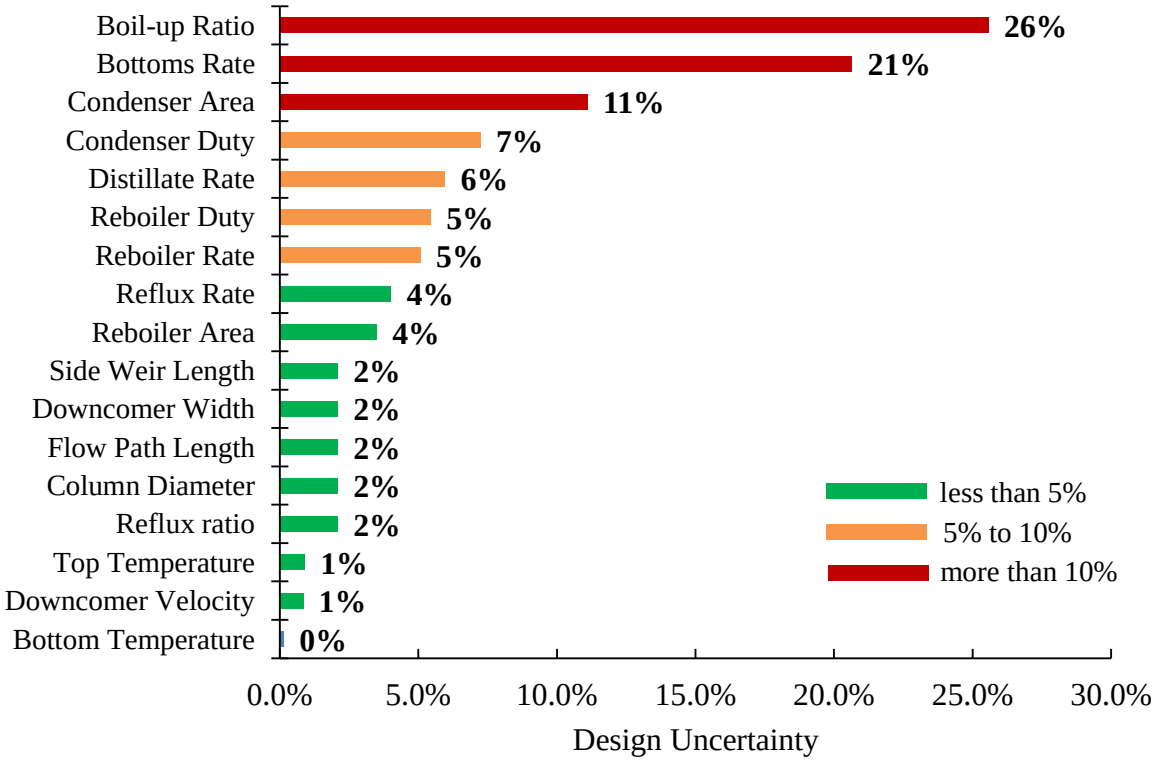

Figure 8.18. Pareto chart of azeotropic distillation column uncertainty quantification results.

The cumulative distribution function curves indicating the confidence levels for selected design parameters in the top and bottom sections of the azeotropic column are presented in Figures 8.19 to 8.23. For the base case, the condenser duty confidence level is 52.4% at 6824 kW, requiring a further increase to 7184 kW to meet the required design confidence level. The condenser surface area calculated from the base case is only 66.3% likely to achieve the required product specifications and a surface area increase from 336 m^2 to 365 m^2 is recommended.

The base case confidence levels for the reboiler duty and surface area are ca. 50% and 68.3 percent. Thus, the reboiler duty needs to increase from 6709 kW to 6964 kW and the surface area from 126 m^2 to 129 m^2. Finally, the bottoms flow rate base case confidence level is ca. 45% at 42 kmol/h and is specified as an adjustable variable to meet the product specifications. Therefore, to ensure the required design confidence is achieved a flow rate of 49 kmol/h is required.

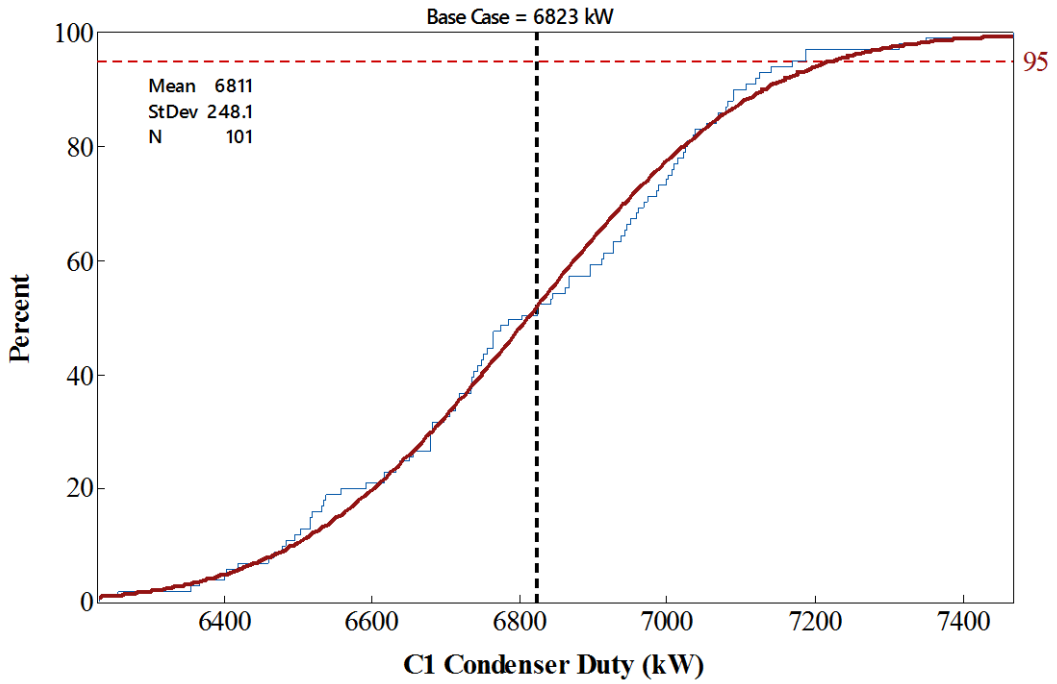

Figure 8.19a. Uncertainty of azeotropic distillation column reboiler (E_1) duty (kW) with NRTL model.

The effect of vapour phase association on the azeotropic column condenser duty was evaluated by repeating the MCS with different vapour phase EoS, but keeping all other conditions the same. The models were NRTL-RK, NRTL-HOC and NRTL-NTH. The CDF curves are presented in Figure 8.19b and the NRTL model serves as a reference. In order to determine if the underlying distributions are different a two sample Kolmogorov-Smirnov (K-S) normality test was performed and the result are presented in Table 8.4.

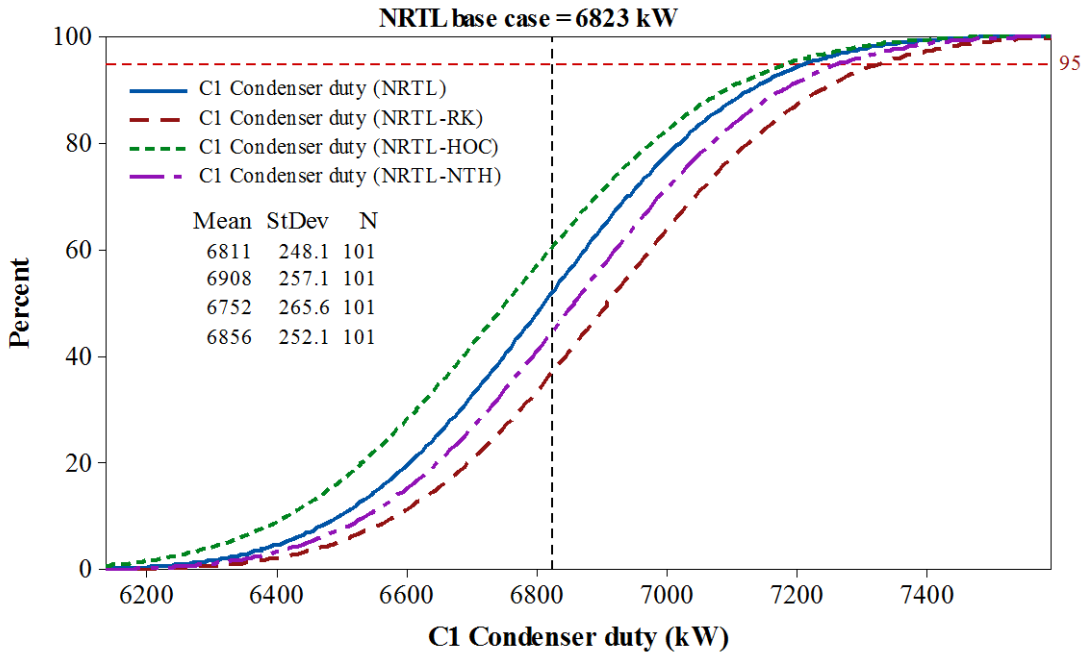

Figure 8.19b. Uncertainty of azeotropic distillation column reboiler (E_1) duty (kW) with NRTL, NRTL-RK, NRTL-HOC and NRTL-NTH.

Table 8.4. Two sample Kolmogorov-Smirnov normality test for C_1 condenser duty distributions with different NRTL vapour phase equations.

Parameter	NRTL-RK	NRTL-HOC	NRTL-NTH
K-S Test Statistic	0.207	0.138	0.118
K-S Critical Value	0.191	0.191	0.191
Alpha Level	0.05	0.05	0.05
Test Result	Different	Not different	Not different

The K-S two-sample test is a nonparametric test of the equality of continuous, one-dimensional probability distributions and shows that the underlying distributions for the NRTL-HOC and NRTL-NTH are not different compared to the NRTL model assuming an ideal gas. However. The test indicates that the NRTL-RK distribution is sufficiently different from the NRTL model. Analysis of the effect of vapour-phase association was not extended to all the design parameters, but serves to indicate that the process design may be sensitive in this regard. The RK EoS is only applicable to systems in which vapour-phase non-ideality is small and the Hayden-O'Connell model is recommended for a more non-ideal vapour phase. Considering the NRTL-HOC test equal to the NRTL model, vapour-phase association is likely not a concern for the condenser duty.

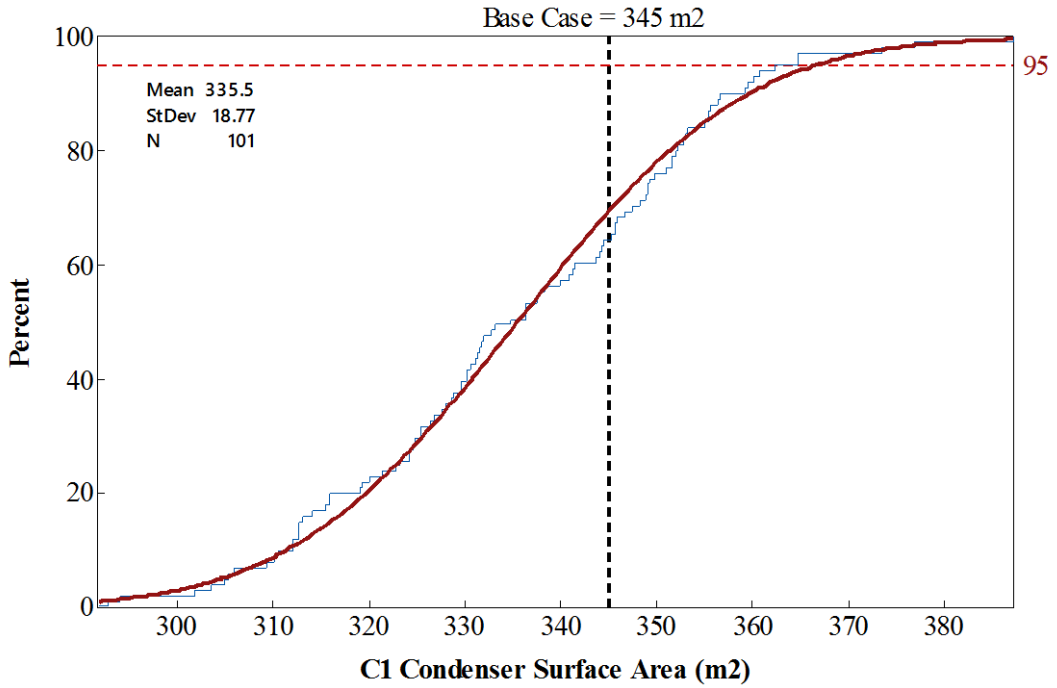

Figure 8.20. Uncertainty of azeotropic distillation column condenser (E_1) surface area (m^2).

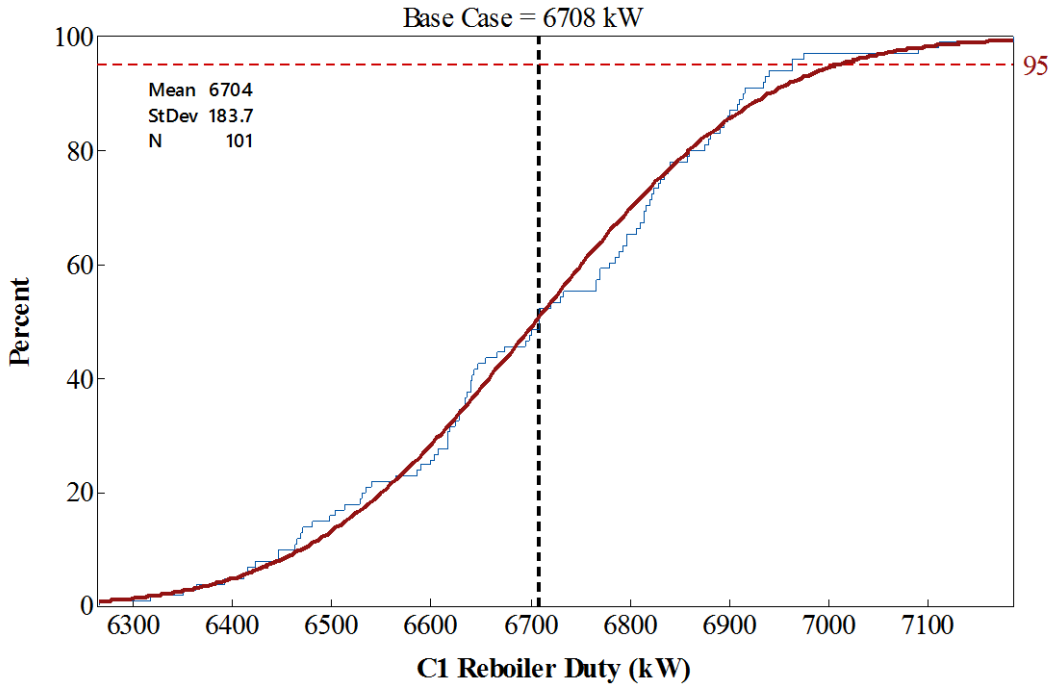

Figure 8.21a. Uncertainty of azeotropic distillation column reboiler (E_2) duty (kW).

The effect of vapour phase association on the azeotropic column reboiler duty was also evaluated and the CDF curves are presented in Figure 8.21b. A two sample Kolmogorov-Smirnov (K-S) normality test was performed and the result are presented in Table 8.5.

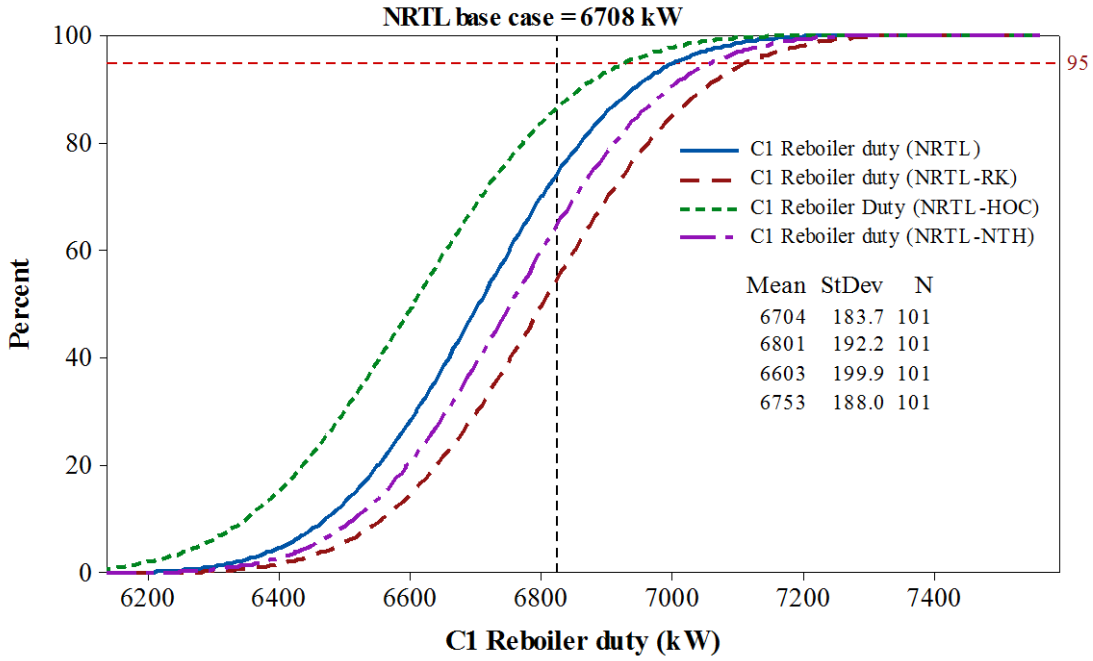

Figure 8.21b. Uncertainty of azeotropic distillation column reboiler (E_2) duty (kW) with NRTL, NRTL-RK, NRTL-HOC and NRTL-NTH.

Table 8.5. Two sample Kolmogorov-Smirnov normality test for C_1 reboiler duty distributions with different NRTL vapour phase equations.

Parameter	NRTL-RK	NRTL-HOC	NRTL-NTH
K-S Test Statistic	0.247	0.257	0.168
K-S Critical Value	0.191	0.191	0.191
Alpha Level	0.05	0.05	0.05
Test Result	Different	Different	Not different

For the azeotropic column reboiler duty, the two sample K-S determined that the distributions for the NRTL and NRTL-NTH models are the same, but is different for both NRTL-RK and NRTL-HOC. However, it does not pose a design concern as the confidence level for the NRTL-HOC model is higher than for the NRTL model at the base case conditions. This however, assumes the NRTL-HOC model is fundamentally better at predicting vapour-phase association compared to the NRTL-RK model.

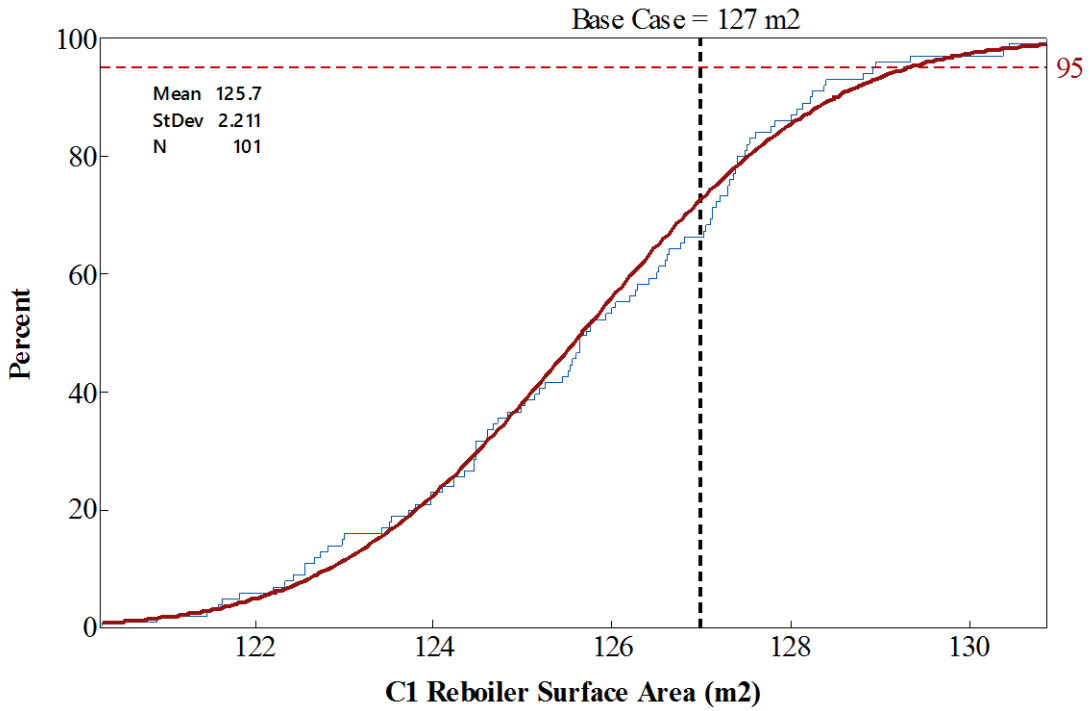

Figure 8.22. Uncertainty of azeotropic distillation column reboiler (E_2) surface area (m^2)

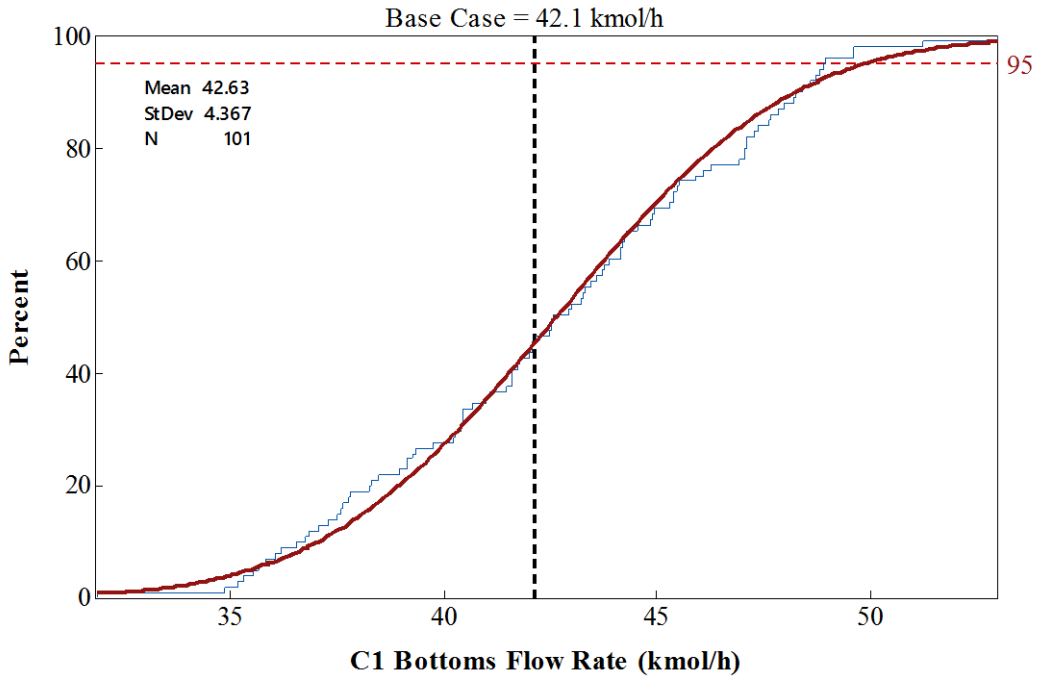

Figure 8.23. Uncertainty of azeotropic distillation column bottoms flow rate (kmol/h).

8.2.4 Decanter results

The decanter uncertainty quantification results are shown in Table 8.6. A total of five key design output variables were considered for the decanter.

Table 8.6. Decanter liquid composition uncertainty quantification results in mole fraction.

Key Output Variables	Base Case	95th %	Standard Deviation	Absolute Uncertainty	Design Uncertainty
Organic Liquid / Total	0.8976	0.9105	0.0085	0.0169	1.89%
Feed					
DIPE	0.6650	0.6570	0.0036	0.0072	1.08%
Ethanol	0.1434	0.1501	0.0068	0.0135	9.44%
Water	0.1916	0.1929	0.0033	0.0065	3.40%
Organic Liquid					
DIPE	0.7406	0.7335	0.0107	0.0215	2.90%
Ethanol	0.1567	0.1599	0.0061	0.0122	7.82%
Water	0.1027	0.1066	0.0049	0.0098	9.56%
Aqueous Liquid					
DIPE	0.0023	0.0027	0.0002	0.0004	18.33%
Ethanol	0.0270	0.0312	0.0028	0.0055	20.53%
Water	0.9707	0.9661	0.0030	0.0060	0.61%
Vapour					
DIPE	0.7641	0.7579	0.0034	0.0069	0.90%
Ethanol	0.0668	0.0729	0.0051	0.0102	15.20%
Water	0.1691	0.1691	0.0017	0.0034	2.00%

In the terms of the decanter feed composition, it is noted that the ethanol concentration uncertainty is the highest compared to DIPE and water. Nonetheless, it does not appear to impact the volumetric ratio split between the organic phase and aqueous phase to an appreciable extent as the organic liquid fraction uncertainty is only ca. 1.9 percent. The cumulative distribution function curve presented in Figure 8.24 supports the observation considering the rather narrow x-axis range.

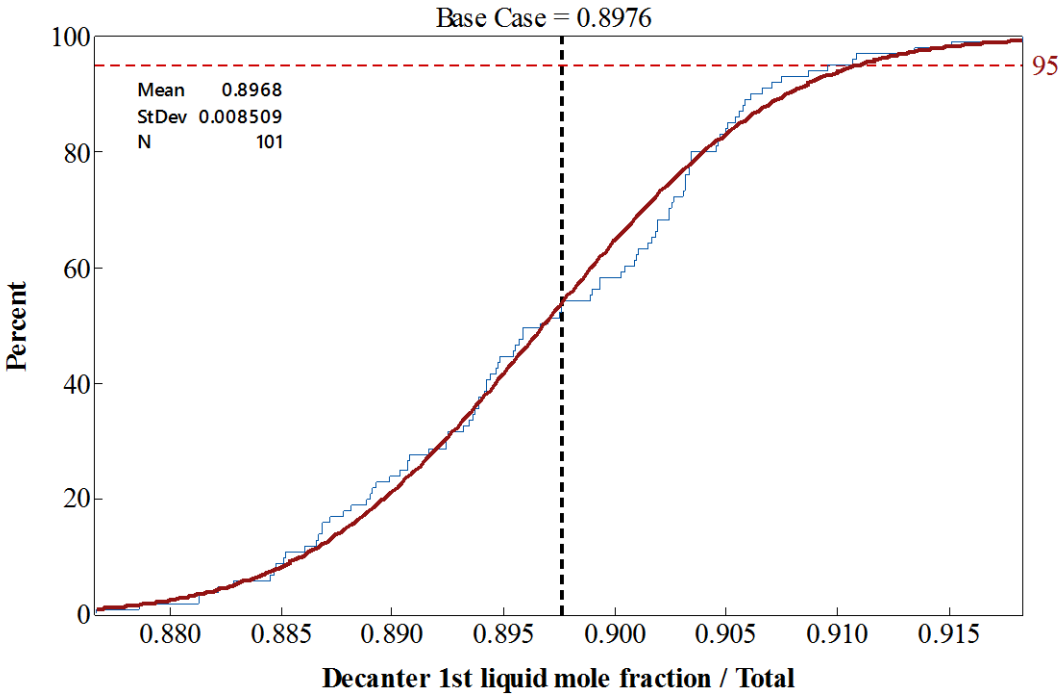

Figure 8.24. Uncertainty of decanter organic liquid phase fraction.

The DIPE concentration in the organic phase is ca. 74% and concentration uncertainty is low at 2.9 percent. It is observed that as the concentration of a component decreased in a particular liquid phase the uncertainty increases, as is the case for ethanol and water in the organic phase. It is equally true for the DIPE and ethanol in the aqueous phase, although the uncertainty range is higher at 18 to 20 percent. For ethanol, this translates to an increase from 2.7 mole percent to 3.12 mole percent in the feed to the recovery column. It is concluded that, although the dilute component uncertainties are high in the decanter, it does not appear to affect the overall performance of the decanter as the ratio of organic to aqueous liquid phase is high.

8.2.5 Recovery column results

The recovery column uncertainty quantification results are shown in Table 8.7. A total of sixteen key design output variables were considered for the recovery column and these output variables were selected based on its likely impact on equipment sizing.

Table 8.7. Recovery column uncertainty quantification results.

Key Output Variables	UOM	Base Case	95th %	Standard Deviation	Absolute Uncertainty	Design Uncertainty
Top Temperature	C	70.3	70.9	0.4	0.7	1.02%
Condenser Duty	kW	1415	1548	75	150	10.60%
Condenser Area	m^2	38.5	41.9	2.1	4.2	10.75%
Distillate Rate	kmol/hr	2.8	3.1	0.15	0.30	10.34%
Reflux Rate	kmol/hr	126.9	138.5	6.56	13.12	10.34%
Reflux Ratio^{SPEC}		45.00	45.00	0.0000	0.0000	0.00%
Bottom Temperature	C	99.7	99.7	0.0001	0.0001	0.00%
Reboiler Duty	kW	1487	1627	79	158	10.60%
Reboiler Area	m^2	43.3	47.7	2.5	5.0	11.50%
Bottoms Rate	kmol/hr	52.6	57.5	2.8	5.6	10.60%
Reboiler Rate	kmol/hr	131.5	143.8	7.0	14.0	10.60%
Boil-up Ratio^{SPEC}		2.50	2.50	0.0000	0.0000	0.00%
Downcomer Velocity	m/sec	0.03	0.04	0.0026	0.0052	16.75%
Flow Path Length	meter	0.45	0.48	0.0165	0.0331	7.40%
Downcomer Width	meter	0.10	0.11	0.0038	0.0075	7.40%
Side Weir Length	meter	0.47	0.51	0.0175	0.0350	7.40%

The results were ranked from high to low uncertainty and are presented in a Pareto graph in Figure 8.25.

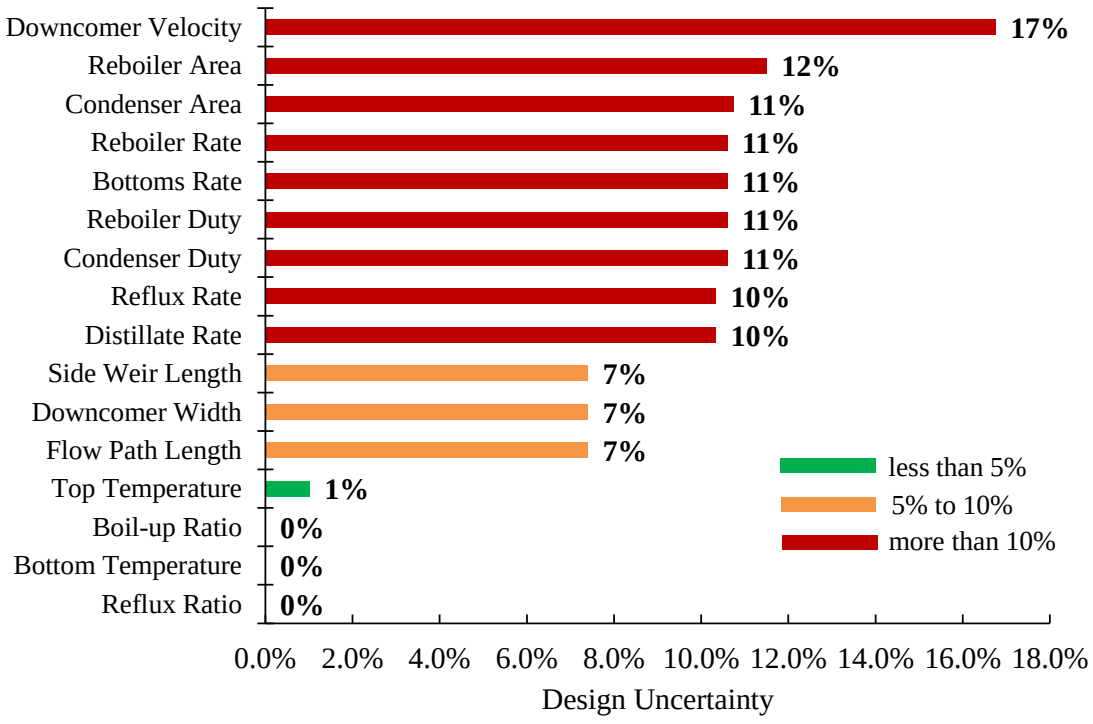

Figure 8.25. Pareto chart of recovery column uncertainty quantification results.

A total of 12 of the 16 key design output variables considered for the recovery column is associated with an uncertainty greater than 5%, of which 9 are greater than 10% and therefore significant. It is observed that both the top column and the bottom column sections are equally affected by the phase equilibria uncertainty. In the top of the column the base case confidence levels for the condenser duty and surface area are ca. 48.5% and 54.5%, as presented in Figures 8.27 to 8.28. Thus, the condenser duty needs to increase from 1415 kW to 1548 kW and the surface area from 38 m^2 to 42 m^2.

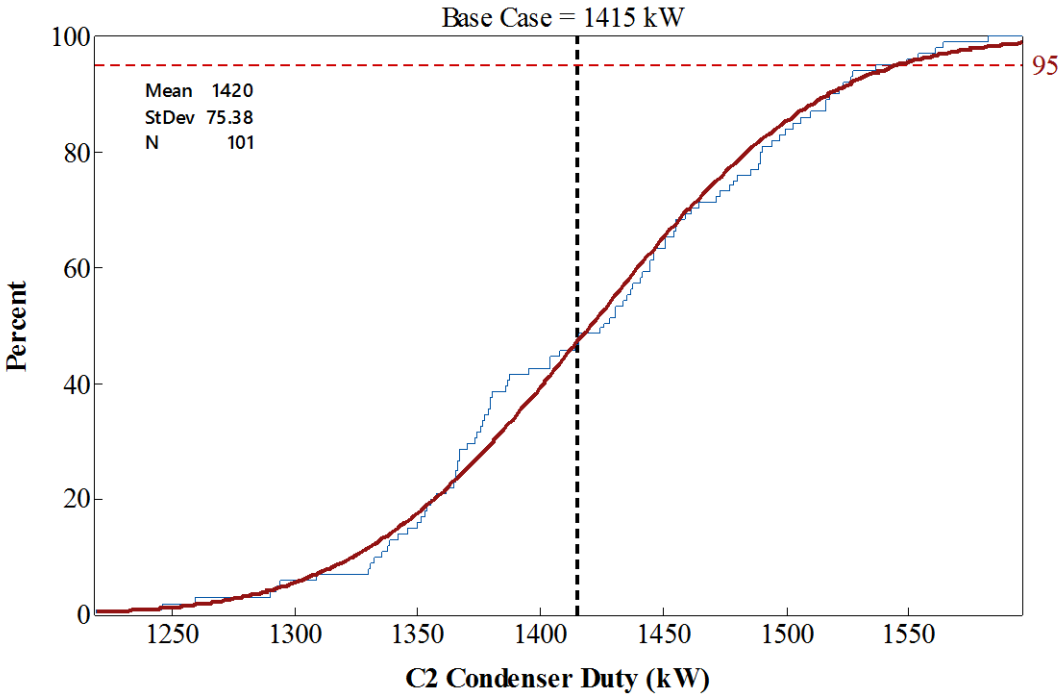

Figure 8.26. Uncertainty of recovery column condenser (E_3) duty (kW).

The recovery column reflux and distillate flow rate uncertainties are ca. 10% and may be considered higher than typical safety margins applied during design. However, in absolute terms, the distillate flow rate only needs to increase from 2.8 to 3.1 kmol/h and the reflux flow rate from 127 to 139 kmol/h. Thus, given the condenser duty and surface area uncertainty, it is concluded that in the top section of the recovery column, the key design output variables sensitive to phase equilibrium uncertainty are those related to condenser thermal requirements.

In the bottom of the column the base case confidence levels for the reboiler duty and surface area are ca. 46.5% and 49.5% as presented in Figures 8.28 to 8.29. Thus, the reboiler duty needs to increase from 1487 kW to 1627 kW and the surface area from 43 m^2 to 48 m^2. The column geometry design output variables are also affected to an extent by the phase equilibria uncertainty. The downcomer velocity, flow path length, downcomer width and side weir length all have an uncertainty ranging from ca. 7 to 17 percent. In absolute terms the effect may not

be of practical concern as, for example, a flow path length increase from 450 mm to 480 mm represents only a 4% increase in a column diameter of 750 mm. Therefore, it is concluded that the effect on the recovery column is worth noting, but does not have a significant impact in terms of the final equipment size.

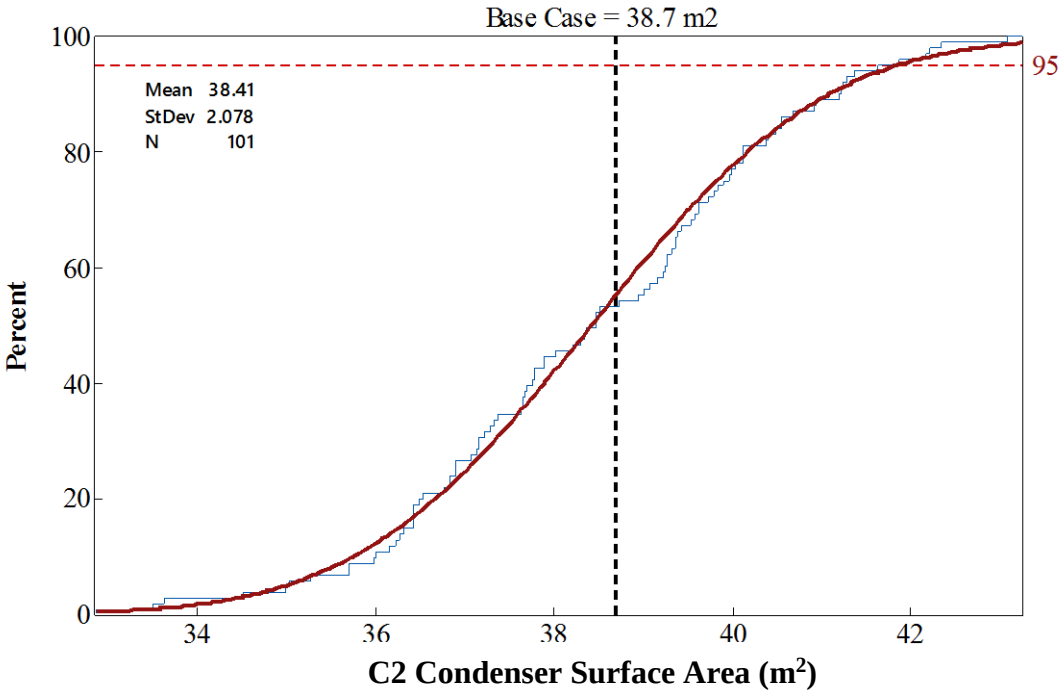

Figure 8.27. Uncertainty of recovery column condenser surface area (m^2).

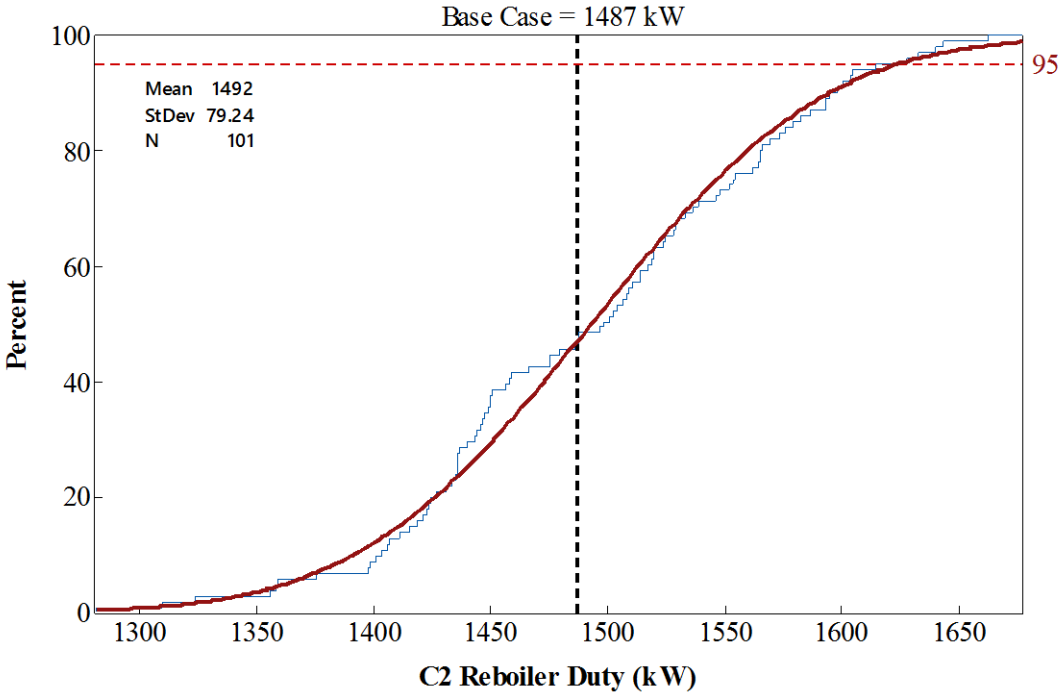

Figure 8.28. Uncertainty of recovery column reboiler (E_4) duty (kW).

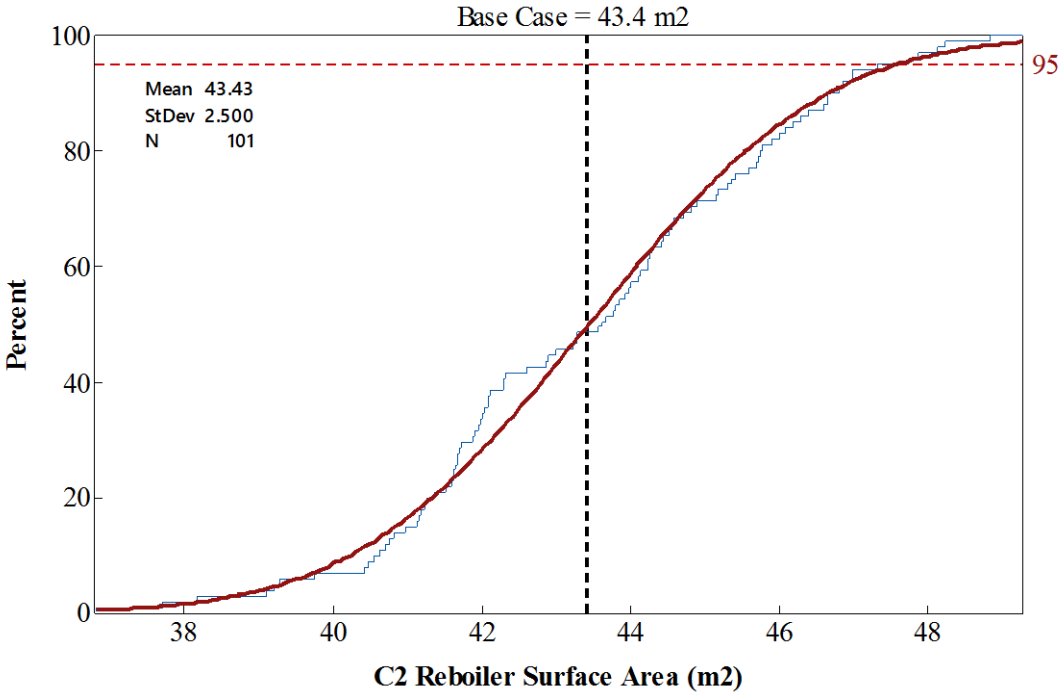

Figure 8.29. Uncertainty of recovery column reboiler surface area (m^2).

8.2.6 Section highlights

The results of the heterogeneous azeotropic distillation system uncertainty quantification process were presented in this section and are summarised on the process flow sheets for the base case parameters in Figure 8.30 and the 95th percentile confidence level case in Figure 8.31. A design case reported by Pienaar *et al.*, (2012) is presented in Figure 8.32 as a reference.

The investigation revealed that the azeotropic column boil-up ratio, bottoms flow rate and condenser surface area have the highest design uncertainty and appear to be the most influenced by the phase equilibria uncertainty. In terms of the azeotropic column geometry, it was noted that the column diameter, downcomer width and flow path length uncertainties were low and it was concluded that the column geometry was not significantly impacted by the phase equilibria uncertainty.

A limited sensitivity analysis was performed on the effect of vapour-phase association on the azeotropic column condenser and reboiler duties. Although the analysis was not extended to all the design variables, it was observed that an EoS accounting for vapour-phase association obtains slightly different results compared to when ideal gas behaviour is assumed. The effect was more pronounced on the reboiler duty as opposed to the condenser duty. Further investigation may be justified to validate these observations as the NRTL-RK model provided consistently lower confidence levels in the duty calculations compare to the other NRTL models.

In the terms of the decanter feed composition, it was noted that the ethanol concentration uncertainty was the highest compared to DIPE and water. Nonetheless, it did not appear to impact the volumetric ratio split between the organic phase and aqueous phase to an appreciable extent. Lastly, it was concluded that in the top section of the recovery column, the key design output variables sensitive to phase equilibrium uncertainty were those related to condenser thermal requirements.

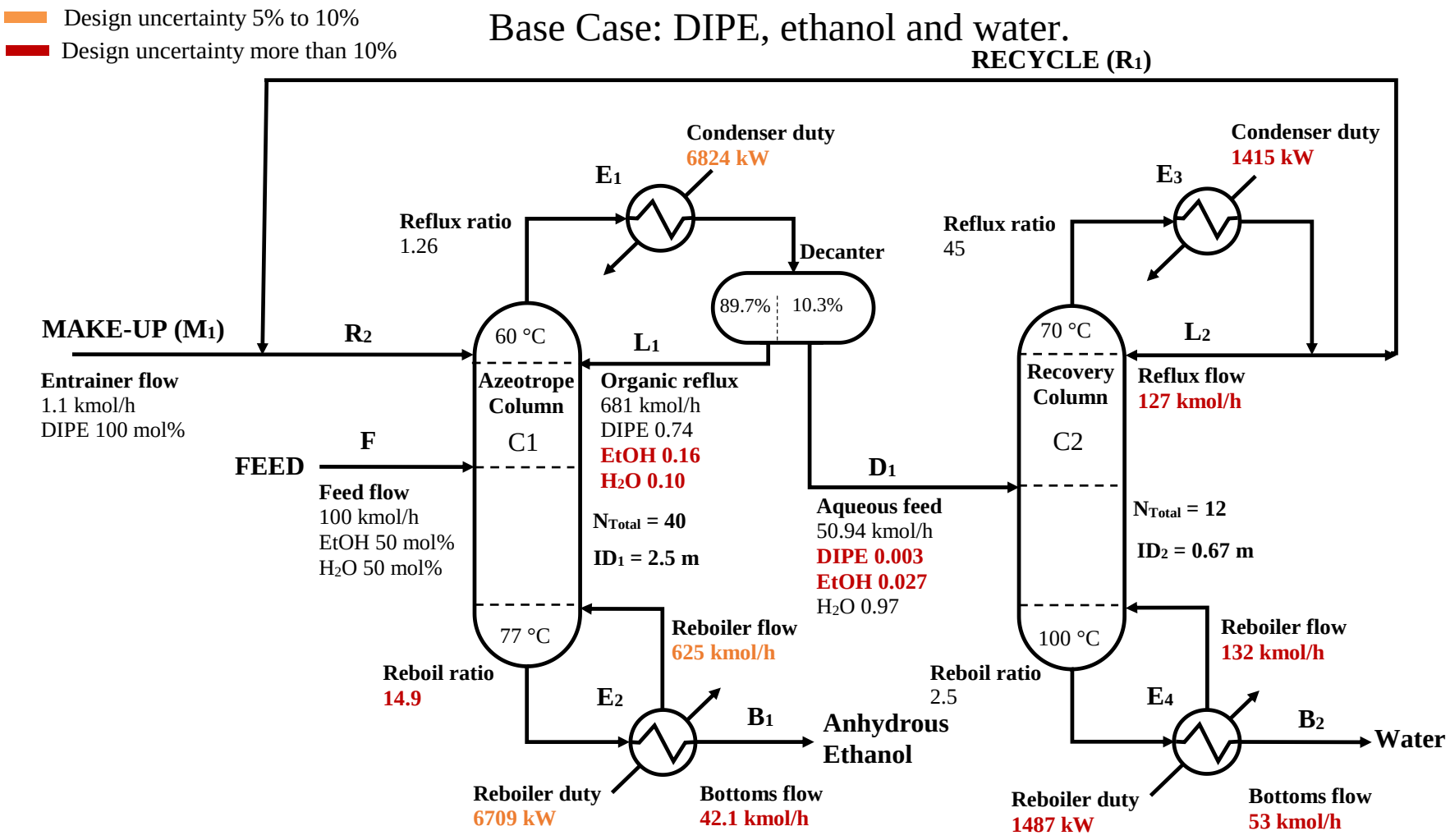

Figure 8.30. Flow sheet of the heterogeneuous azeotropic distillation system with DIPE as entrainer. The simulation was performed with Aspen Plus® using the NRTL model with the base case binary interaction parameter set.

95th Percentile Case

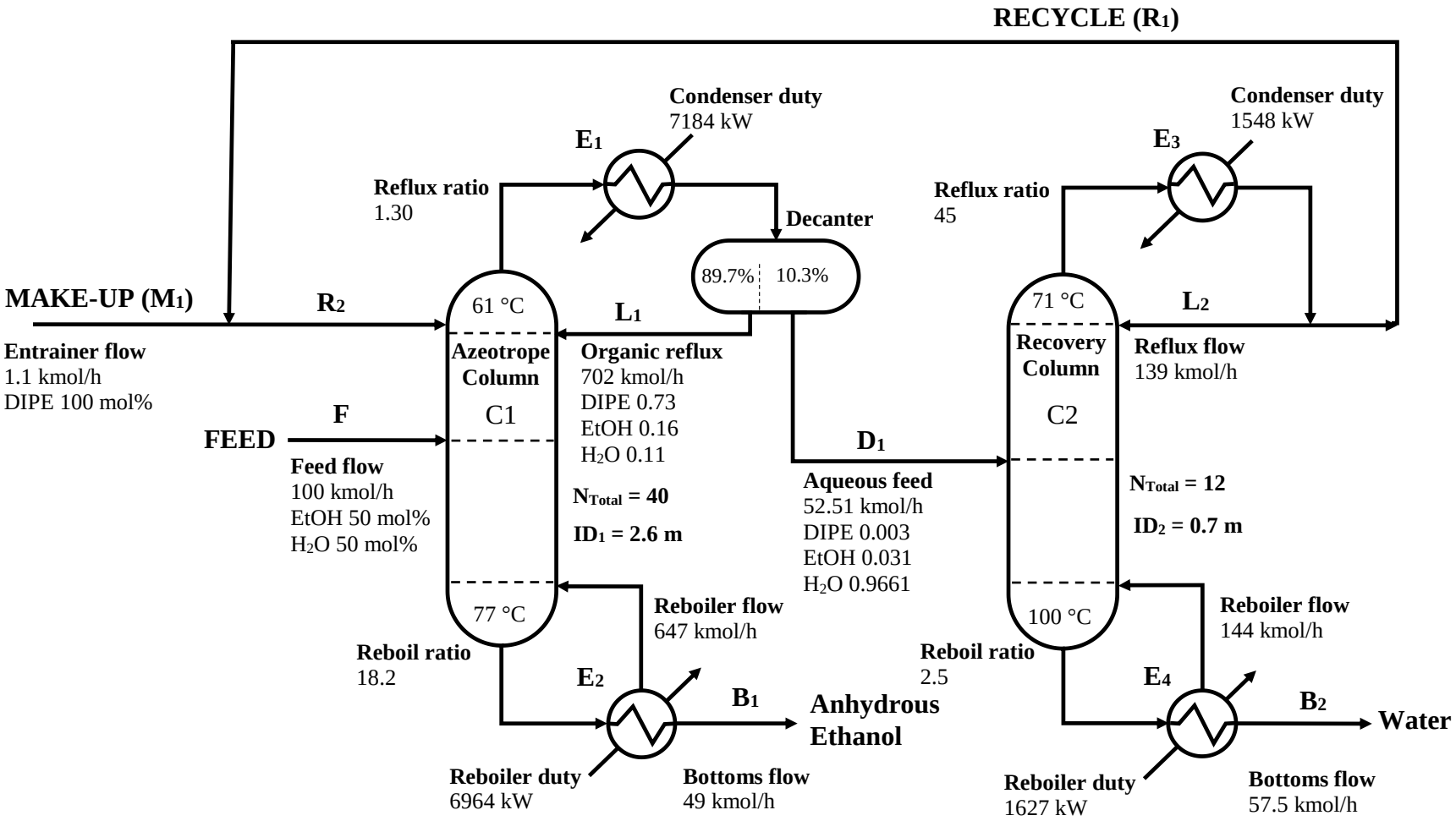

Figure 8.31. Flow sheet of the heterogeneous azeotropic distillation with the simulation results of the 95th percentile confidence case.

Literature Reference Case

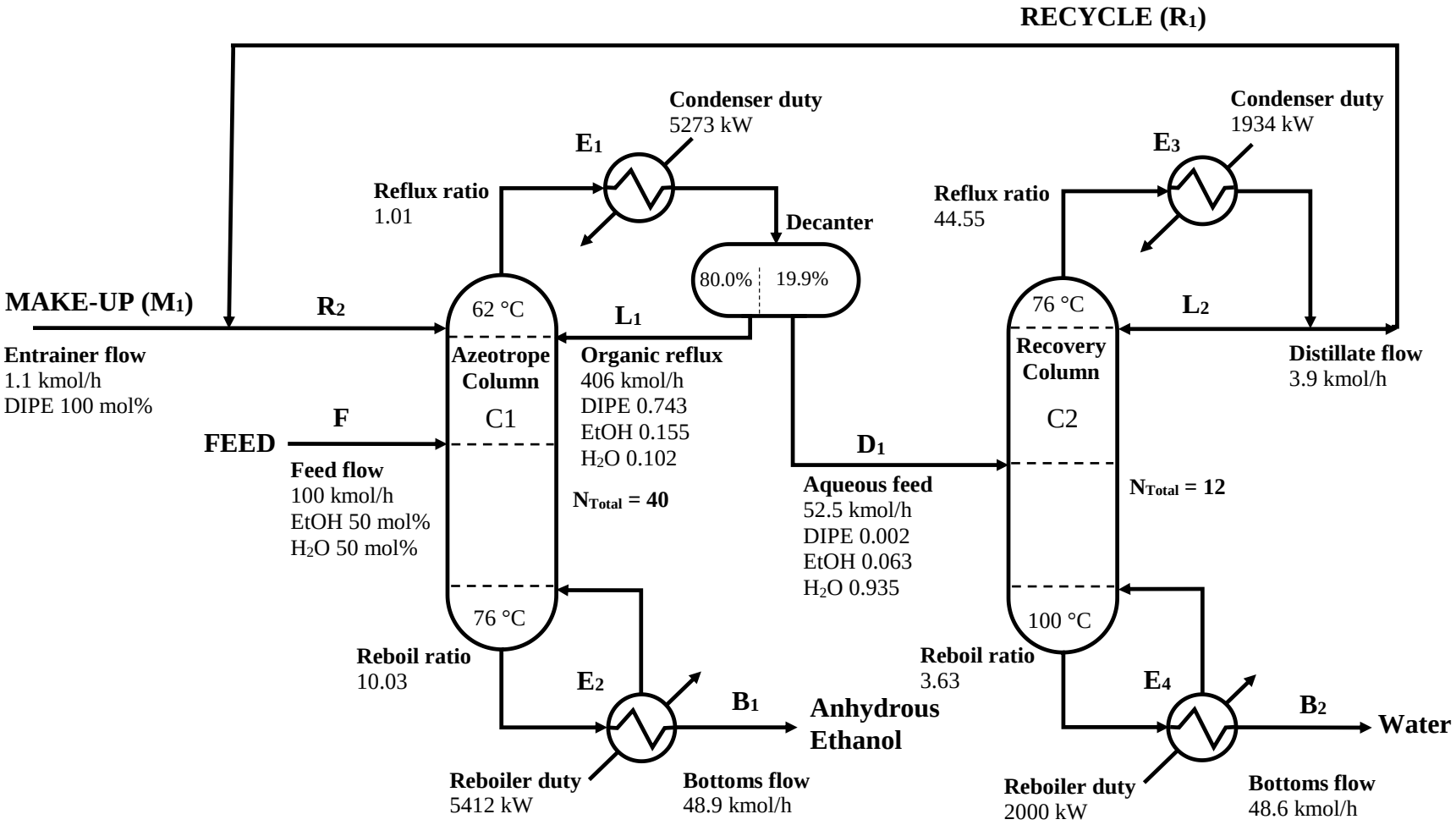

Figure 8.32. Flow sheet of the heterogeneous azeotropic distillation system with parameters reported by Pienaar (2012).

Chapter 9
Conclusions and Recommendations

The aim of this thesis was to determine the effect of phase equilibrium uncertainty on the process design of selected C_2 and C_3 low molecular weight alcohol separation systems. To this end, thermodynamic model screening was performed to identify the best model for the design process. Phase equilibrium uncertainty was assessed and the related effect on the process design was evaluated. Thus, with reference to the specific project objectives outlined in Section 1.4:

Objective (i): Evaluate the performance of selected thermodynamic models

A systematic evaluation of thermodynamic models was performed. The objective was to identify a model that offered the closest prediction of experimental data when considering the phase equilibria of the low molecular weight alcohol systems of interest to this work (*What is the best model?*).

The performance of the NRTL activity coefficient model in predicting the phase equilibria of the **DIPE/IPA/2-methoxyethanol** system (System 1) was of a high degree of accuracy. The prediction of the azeotrope temperature and composition was improved, although marginally, with the Hayden O'Connell and Nothnagel equations of state. However, this benefit was not extended to the binary VLE correlation ability of the model.

In terms of the **DIPE/ethanol/water** system (System 2), the evaluation process revealed that the NRTL activity coefficient model offered largely excellent results, with a high degree of accuracy apparent in the azeotrope and phase envelope predictions. The inclusion of LLE data provided a meaningful improvement of the model's ability to predict experimentally measure equilibrium data. The results reconfirmed the usefulness of the NRTL model for low molecular alcohol azeotrope modelling.

The **NRTL model** was thus identified as the best model for the *DIPE/IPA/2-methoxyethanol* system and the *DIPE/ethanol/water* system.

Objective (ii): Estimate the phase equilibrium uncertainty

The phase equilibrium uncertainty was estimated using a Monte Carlo simulation approach. The parametric uncertainties of the experimental data were propagated through the NRTL model calculations to the phase equilibria of the respective systems.

With respect to ***System 1***, it was observed that the model could predict the experimental data within its 95% percentile for all three binary pairs, given the input parametric uncertainty. In general, the vapour phase composition uncertainty was at a maximum at the equal-concentration region of the dew point curves. A similar pattern was observed for the bubble point curve of the *DIPE/IPA* binary pair. However, for the *DIPE/2-methoxyethanol* and the *IPA/2-methoxyethanol* binary pairs the maximum liquid phase uncertainty was observed in the low concentration region of the bubble point curves.

In the case of ***System 2***, the ternary VLLE phase envelope uncertainty was at a maximum close to the plait point in the higher alcohol concentration region and a component concentration uncertainty of 5 to 8 percent was observed. The investigation further revealed the vapour-liquid equilibrium uncertainty is at a maximum when the ethanol concentration reaches 18 mole percent; at this point, the component with the highest concentration uncertainty was water at ca. 9.2%. In terms of the binary and ternary azeotropes, the DIPE concentration, in general, was found to have the lowest uncertainty at ca. 5% and the ethanol and water uncertainties were notably larger, ranging from ca. 10% to as high as ca. 30%. Although the range of uncertainty is high for the latter two components, the Monte Carlo simulation average is close to the base case for all the azeotropes.

Objective (iii): Quantify the effect of the phase equilibrium uncertainty on the process design

A systematic uncertainty quantification process was performed using a Monte Carlo simulation approach.

In terms of ***System 1***, it was observed that the extraction column uncertainty was predominantly in the bottom section of the column and was mainly related to the reboiler flow rate. The design confidence could be improved to an acceptable level through a marginal increase of the reboiler flow rate. The investigation further determined that the recovery column uncertainty was also largest in the bottom section of the column and only the reboil ratio was of concern. The recovery column condenser and reboiler design confidence is 45% and 82%, but a small increase in duty restored the design confidence to the required levels. It was therefore concluded that the design of the extractive distillation process for the separation of the DIPE/IPA azeotrope with 2-methoxyethanol is acceptable and the identified risk areas may be easily resolved.

With respect to ***System 2***, it was observed that the azeotropic distillation column geometry was not significantly impacted by the phase equilibria uncertainty, but that boil-up ratio, bottoms flow rate and condenser surface area were. It was further noted that the dilute component uncertainties were high in the decanter, but did not appear to effect the overall performance of the decanter as the ratio of organic to aqueous liquid phase was high. Lastly, in the top section of the recovery column the key design output variables sensitive to phase equilibrium uncertainty were those related to condenser thermal requirements and that the effect of the phase equilibria uncertainty on the column geometry was negligible. It was therefore concluded that the design of the heterogeneous azeotropic distillation process for the separation of the ethanol/water azeotrope with DIPE may likely consist of under-designed process equipment if a typical 10% empirical safety factor is applied.

Summary

An approach based on Monte Carlo simulation coupled with a commercial process simulation software program was presented to estimate the confidence of process design variables under the effect of phase equilibrium parametric uncertainty. From the results, it is observed that the cumulative probability distribution characteristics can be affected significantly by the parametric uncertainty. An important conclusion is that only calculating the median or most likely result is not sufficient to provide the design engineer with a sense of either the precision or accuracy of the design.

The optimal design is more conservative, as expected, when phase equilibrium uncertainties are considered. However, the Monte Carlo simulation approach offers a more rigorous assessment of uncertainty than applying traditional overdesign factors. It was thus shown that a systematic uncertainty quantification process reveals the effect of phase equilibrium uncertainty on the process design of C_2 and C_3 low molecular weight alcohol separation systems. The approach presented can be used to facilitate decision making in fields related to safety factor selection. An acceptable safety factor for the DIPE, IPA and 2-methoxyethanol system is 10% for the key design output variables. For the DIPE, ethanol and water system a safety factor of 25% may be required for the azeotropic distillation column and 15% for the recovery column.

The findings from this thesis was presented:

L. Burger, C.E. Schwarz, *Sensitivity of Process Design to Phase Equilibrium Uncertainty: Study of the Isopropanol + DIPE + 2-methoxyethanol system*, Poster presentation at the 24th

IUPAC International Conference on Chemical Thermodynamics, Guilin, China, 21 – 26 August 2016.

The following recommendations are made in light of the results of this work:

- Explore different column design constraints to determine if the uncertainty maps changes.
- The focus of this study was to perform the uncertainty analysis from a design approach. However, it may be of interest to extend the investigation to consider a process revamp. Thus, with fixed equipment sizes the effect of thermodynamic modelling uncertainty on process performance and product purity may be investigated.
- The transfer of probabilistic information generated by the Monte Carlo simulation to the process simulation software needs to be improved. As part of this work, the thermodynamic model binary interactions parameters were entered manually into Aspen Plus® for all the cases, which is an enormously time consuming process. An attempt was made with the assistance of Aspen technical support to develop an Excel macro that could automatically write the data to an input file. Although partially successful it requires further development. Resolving the data transfer challenge will significantly increase the ease of using the probabilistic approach of this study.
- The approach of Whiting *et al.*, (1993) was found to be sensitive to the sum of errors of the regression parameters during the verification process in Chapter 6. The result was the generation of several infeasible parameter sets. Further research is required, but the problem may likely be resolved if an alternative sampling technique is utilised or if the input parameter correlation control can be improved.
- Finally, it is recommended to perform a comparative study with other uncertainty quantification methods on similar separation systems to further improve the overall quality of the process design.

Chapter 10
References

Abbas, R. and Gmehling, J. (2008) 'Vapour–liquid equilibria, azeotropic data, excess enthalpies, activity coefficients at infinite dilution and solid–liquid equilibria for binary alcohol–ketone systems', *Fluid Phase Equilibria*, 267(2), pp. 119–126. doi: 10.1016/j.fluid.2008.02.021.

Abrams, D.S. and Prausnitz, J.M. (1975) 'Statistical thermodynamics of liquid mixtures: A new expression for the excess Gibbs energy of partly or completely miscible systems', *AIChE Journal*, 21(1), pp. 116–128. doi: 10.1002/aic.690210115.

Adair, C. and Wilson, J.T. (2009) 'Prospects for anaerobic biodegradation of biofuels (ethanol and biodiesel) and proposed biofuels (n-propanol, iso-propanol, n-butanol, and 2, 5-dimethylfuran) in aquifer sediments', *In Situ and On-Site Bioremediation-2009: Proceedings of the 10th International In Situ and On-Site Bioremediation Symposium*.

Aien, M., Hajebrahimi, A. and Fotuhi-Firuzabad, M. (2016) 'A comprehensive review on uncertainty modelling techniques in power system studies', *Renewable and Sustainable Energy Reviews*, 57, pp. 1077–1089. doi: 10.1016/j.rser.2015.12.070.

Alonso, C., Montero, E.A., Chamorro, C.R., Segovia, J.J., Martín, M.C. and Villamañán, M.A. (2004) 'Vapor–liquid equilibrium of octane-enhancing additives in gasolines', *Fluid Phase Equilibria*, 217(2), pp. 157–164. doi: 10.1016/j.fluid.2003.01.001.

An, W., Lin, Z., Chen, J. and Zhu, J. (2014) 'Simulation and analysis of a Reactive distillation column for removal of water from Ethanol–Water mixtures', *Industrial & Engineering Chemistry Research*, 53(14), pp. 6056–6064. doi: 10.1021/ie403906z.

Arlt, W., Macedo, M.E.A., Rasmussen, P. and Sorensen, J.M. (1979) 'Dechema chemistry data series', *Chemical Engineering Science*, 5.

Ascough, J.C., Maier, H.R., Ravalico, J.K. and Strudley, M.W. (2008) 'Future research challenges for incorporation of uncertainty in environmental and ecological decision-making', *Ecological Modelling*, 219(3-4), pp. 383–399. doi: 10.1016/j.ecolmodel.2008.07.015.

ASPEN, Aspen Simulation Workbook User Guide. 2006.

Bankar, S.B., Survase, S.A., Ojamo, H. and Granström, T. (2013) 'Biobutanol: The outlook of an academic and industrialist', *RSC Advances*, 3(47), p. 24734. doi: 10.1039/c3ra43011a.

Batista, F.R.M. and Meirelles, A.J.A. (2011) 'Computer simulation applied to studying continuous spirit distillation and product quality control', *Food Control*, 22(10), pp. 1592–1603. doi: 10.1016/j.foodcont.2011.03.015.

Batista, F.R.M., Follegatti-Romero, L.A., Bessa, L.C.B.A. and Meirelles, A.J.A. (2012) 'Computational simulation applied to the investigation of industrial plants for bioethanol distillation', *Computers & Chemical Engineering*, 46, pp. 1–16. doi: 10.1016/j.compchemeng.2012.06.004.

Bayarri, M.J., Berger, J.O., Paulo, R., Sacks, J., Cafeo, J.A., Cavendish, J., Lin, C.-H. and Tu, J. (2007) 'A framework for validation of computer models', *Technometrics*, 49(2), pp. 138–154. doi: 10.1198/004017007000000092.

Brits, L. (2015) *Vapour-liquid-liquid equilibria measurements for the dehydration of low molecular weight alcohols via heterogeneous azeotropic distillation*. MEng. thesis. Stellenbosch University.

Bastidas, P. A. and Gil, I. D. (2010) 'Comparison of the main ethanol dehydration technologies through process simulation', *20th European Symposium on Computer Aided Process Engineering*.

Bhownathi, R. (2008) *The Use of n-Dodecane as a Solvent in the Extraction of Light Alcohols from Water*. MSc. thesis. Department of Chemical Engineering. University of Kwa-Zulu Natal.

Bjørner, M. G., Sin, G. and Kontogeorgis, G. M. (2016) 'Uncertainty analysis of the CPA and a quadrupolar CPA equation of state – With emphasis on CO2', *Fluid Phase Equilibria*. Elsevier Ltd, 414, pp. 29–47. doi: 10.1016/j.fluid.2015.12.037.

van der Byl, A. and Inggs, M. R. (2016) 'Constraining error—A sliding discrete Fourier transform investigation', *Digital Signal Processing*. Elsevier Inc., 51, pp. 54–61. doi: 10.1016/j.dsp.2016.01.008.

Carlson, E. C. (1996). 'Do not gamble with physical properties for simulations, *Chemical Engineering Progress* 92', 35-46 (October).

Chen, C.-C. (1993) 'A segment-based local composition model for the gibbs energy of polymer solutions', *Fluid Phase Equilibria*, 83, pp. 301–312. doi: 10.1016/0378-3812(93)87033-w.

Chen, C.-C. and Mathias, P. M. (2002) 'Applied thermodynamics for process modeling', *AIChE Journal*, 48(2), pp. 194–200. doi: 10.1002/aic.690480202.

Chen, C.-C. and Song, Y. (2004) 'Solubility modeling with a Nonrandom Two-Liquid segment activity coefficient model', *Industrial & Engineering Chemistry Research*, 43(26), pp. 8354–8362. doi: 10.1021/ie049463u.

Choi, H.C., Shin, J.S., Qasim, F. and Park, S.J. (2016) 'Liquid–Liquid equilibrium data for the Ternary systems of water, Isopropyl alcohol, and selected Entrainers', *Journal of Chemical & Engineering Data*, 61(4), pp. 1403–1411. doi: 10.1021/acs.jced.5b00542.

Clarke, D. D., Vasquez, V. R., Whiting, W. B. and Greiner, M. (2001) 'Sensitivity and uncertainty analysis of heat-exchanger designs to physical properties estimation', *Applied Thermal Engineering*, 21(10), pp. 993–1017. doi: 10.1016/S1359-4311(00)00101-0.

Davenport, B., Gubler, R. and Yoneyama, M. (2002) *Ethyl Alcohol. Chemical Economics Handbook*. California: SRI International.

Deiters, U. K., De Reuck, K. M. (1999) 'Remarks on publications dealing with Equations of State', *Fluid Phase Equilibria*, Vol. 161, pp. 205-219.

Derwent, D., Fraser, A., Abbott, J., Jenkin, J., Willis, P. and Murrells, T. (2010) *Evaluating the Performance of Air Quality Models. DEFRA Report. Issue 3*.

Diky, V., Chirico, R.D., Kazakov, A.F., Muzny, C.D. and Frenkel, M. (2009) 'ThermoData engine (TDE): Software implementation of the dynamic data evaluation concept. 3. Binary mixtures', *Journal of Chemical Information and Modeling*, 49(2), pp. 503–517. doi: 10.1021/ci800345e.

Diky, V., Chirico, R. D., Muzny, C. D., Kazakov, A. F., Kroenlein, K., Magee, J. W., Abdulagatov, I., Kang, J. W. and Frenkel, M. (2012) 'ThermoData Engine (TDE) software implementation of the dynamic data evaluation concept. 7. Ternary mixtures.', *Journal of chemical information and modeling*, 52(version 3), pp. 260–76. doi: 10.1021/ci200456w.

Dirk-Faitakis, C.B. and Chuang, K.T. (2004) 'Simulation studies of catalytic distillation for removal of water from ethanol using a rate-based kinetic model', *Industrial & Engineering Chemistry Research*, 43(3), pp. 762–768. doi: 10.1021/ie034123e.

Diwekar, U. M. and Kalagnanam, J. R. (1997) 'Efficient sampling technique for optimization under uncertainty', *AIChE Journal*, 43(2), pp. 440–447. doi: 10.1002/aic.690430217.

Doherty, M.F. and Knapp, J.P. (2000) *Distillation, Azeotropic and Extractive. Kirk-Othmer Encyclopedia of Chemical*. John Wiley & Sons, Inc.

Duong, P. L. T., Ali, W., Kwok, E. and Lee, M. (2016) 'Uncertainty quantification and global sensitivity analysis of complex chemical process using a generalized polynomial chaos approach', *Computers and Chemical Engineering*. Elsevier Ltd, 90, pp. 23–30. doi: 10.1016/j.compchemeng.2016.03.020.

Fair, J.R. Advance Process Engineering. *AIChE Monograph Series*, 1980, 76, 5-41.

Faramarzi, L., Kontogeorgis, G.M., Thomsen, K. and Stenby, E.H. (2009) 'Extended UNIQUAC model for thermodynamic modeling of CO2 absorption in aqueous alkanolamine solutions', *Fluid Phase Equilibria*, 282(2), pp. 121–132. doi: 10.1016/j.fluid.2009.05.002.

Ferrari, A., Gutiérrez, S. and Sin, G. (2016) 'Modeling a production scale milk drying process: Parameter estimation, uncertainty and sensitivity analysis', *Chemical Engineering Science*. Elsevier, 152, pp. 301–310. doi: 10.1016/j.ces.2016.06.019.

Fischer, K. and Gmehling, J. (1996) 'Further development, status and results of the PSRK method for the prediction of vapor-liquid equilibria and gas solubilities', *Fluid Phase Equilibria*, 121(1-2), pp. 185–206. doi: 10.1016/0378-3812(95)02792-0.

Font, A., Asensi, J.C., Ruiz, F. and Gomis, V. (2003) 'Application of Isooctane to the dehydration of ethanol. Design of a column sequence to obtain absolute ethanol by heterogeneous Azeotropic distillation', *Industrial & Engineering Chemistry Research*, 42(1), pp. 140–144. doi: 10.1021/ie0204078.

Fredenslund, A., Jones, R.L. and Prausnitz, J.M. (1975) 'Group-contribution estimation of activity coefficients in nonideal liquid mixtures', *AIChE Journal*, 21(6), pp. 1086–1099. doi: 10.1002/aic.690210607.

Frey, H.C. (1992) 'Quantitative Analysis of Uncertainty and Variability in Environmental Policy Making', *Environmental Science and Engineering*, (191).

Frey, H.C., Rubin, E.S. and Diwekar, U.M. (1994) 'Modelling uncertainties in advanced technologies: Application to a coal gasification system with hot-gas clean-up', *Energy*, 19(4), pp. 449–463. doi: 10.1016/0360-5442(94)90123-6.

Frolkova, A.K. and Raeva, V.M. (2010) 'Bioethanol dehydration: State of the art', *Theoretical Foundations of Chemical Engineering*, 44(4), pp. 545–556. doi: 10.1134/s0040579510040342.

Frurip, D.J., Curtiss, L.A. and Blander, M. (1981) 'Thermal conductivity measurements and molecular association in a series of alcohol vapors: Methanol, ethanol, isopropanol, and t-butanol', *International Journal of Thermophysics*, 2(2), pp. 115–132. doi:

10.1007/bf00503936.

Gao, X., Chen, J., Tan, J., Wang, Y., Ma, Z. and Yang, L. (2015) 'Application of mechanical vapor Recompression heat pump to double-effect distillation for Separating N, N-Dimethylacetamide/water mixture', *Industrial & Engineering Chemistry Research*, 54(12), pp. 3200–3204. doi: 10.1021/ie504664h.

Gau, C.-Y. and Stadtherr, M.A. (2002) 'New interval methodologies for reliable chemical process modelling', *Computers & Chemical Engineering*, 26(6), pp. 827–840. doi: 10.1016/s0098-1354(02)00005-4.

Gil, I.D., García, L.C. and Rodríguez, G. (2014) 'Simulation of ethanol extractive distillation with mixed glycols as separating agent', *Brazilian Journal of Chemical Engineering*, 31(1), pp. 259–270. doi: 10.1590/s0104-66322014000100024.

Gmehling, J. and Bölts, R. (1996) 'Azeotropic data for binary and Ternary systems at moderate pressures', *Journal of Chemical & Engineering Data*, 41(2), pp. 202–209. doi: 10.1021/je950228f.

Gmehling, J.; Menke, J.; Krafczyk, K.; Fischer, K. Azeotropic Data, Part I and Part II, VCH Publishers, Weiheim, New York, 1994.

Gmehling, J.; Menke, J.; Krafczyk, K.; Fischer, K. Azeotropic Data, 2nd Edition, 3 Volumes Wiley VCH Publishers, 2004.

Gmehling, J. and Weidlich, U. (1986) 'Results of a modified unifac method for alkane-alcohol systems', *Fluid Phase Equilibria*, 27, pp. 171–180. doi: 10.1016/0378-3812(86)87048-0.

Gomis, V., Font, A., Pedraza, R. and Saquete, M.D. (2005) 'Isobaric vapor–liquid and vapor–liquid–liquid equilibrium data for the system water+ethanol+cyclohexane', *Fluid Phase Equilibria*, 235(1), pp. 7–10. doi: 10.1016/j.fluid.2005.07.015.

Gomis, V., Font, A. and Saquete, M.D. (2006) 'Vapour–liquid–liquid and vapour–liquid equilibrium of the system water+ethanol+heptane at 101.3kPa', *Fluid Phase Equilibria*, 248(2), pp. 206–210. doi: 10.1016/j.fluid.2006.08.012.

Gomis, V., Font, A., Pedraza, R. and Saquete, M.D. (2007) 'Isobaric vapor–liquid and vapor–liquid–liquid equilibrium data for the water–ethanol–hexane system', *Fluid Phase Equilibria*, 259(1), pp. 66–70. doi: 10.1016/j.fluid.2007.04.011.

Gruhn, G. and Colditz, S. (1996) 'Interval approach to process system engineering problems', *Computers & Chemical Engineering*, 20, pp. S533–S538. doi: 10.1016/0098-1354(96)00098-1.

Hajipour, S. (2013) 'Error Estimation and Reliability in Process Calculations', *Journal of Chemical Information and Modeling*, 53(9), pp. 1689–1699. doi: 10.1017/CBO9781107415324.004.

Hajipour, S. and Satyro, M. (2011) 'Uncertainty analysis applied to thermodynamic models and process design – 1. Pure components', *Fluid Phase Equilibria*. Elsevier B.V., 307(1), pp. 78–94. doi: 10.1016/j.fluid.2011.05.014.

Hajipour, S., Satyro, M. and Foley, M. W. (2014) 'Uncertainty analysis applied to thermodynamic models and process design—2. Binary mixtures', *Fluid Phase Equilibria*. Elsevier B.V., 364, pp. 15–30. doi: 10.1016/j.fluid.2013.12.004.

Hansen, H.K., Rasmussen, P., Fredenslund, A., Schiller, M. and Gmehling, J. (1991) 'Vapor-liquid equilibria by UNIFAC group contribution. 5. Revision and extension', *Industrial & Engineering Chemistry Research*, 30(10), pp. 2352–2355. doi: 10.1021/ie00058a017.

Hayden, J.G. and O'Connell, J.P. (1975) 'A generalized method for predicting Second Virial coefficients', *Industrial & Engineering Chemistry Process Design and Development*, 14(3), pp. 209–216. doi: 10.1021/i260055a003.

Helton, J.C. and Burmaster, D.E. (1996) 'Guest editorial: Treatment of aleatory and epistemic uncertainty in performance assessments for complex systems', *Reliability Engineering & System Safety*, 54(2-3), pp. 91–94. doi: 10.1016/s0951-8320(96)00066-x.

Helton, J.C. and Oberkampf, W.L. (2004) 'Alternative representations of epistemic uncertainty', *Reliability Engineering & System Safety*, 85(1-3), pp. 1–10. doi: 10.1016/j.ress.2004.03.001.

de Hemptinne, J.-C. (2012) *Select thermodynamic models for process simulation a practical guide using a three steps methodology*. Paris: Editions Technip.

Henley, M., Letinski, D.J., Carr, J., Caro, M.L., Daughtrey, W. and White, R. (2014) 'Health assessment of gasoline and fuel oxygenate vapours: Generation and characterization of test materials', *Regulatory Toxicology and Pharmacology*, 70(2), pp. S13–S17. doi: 10.1016/j.yrtph.2014.05.012.

Hildebrand, J.H. and Scott, R.L. (1964) 'The Solubility of Nonelectrolytes', *Journal of Chemical Education*, 42(4), p. A318. doi: 10.1021/ed042pa318.1.

Hilmen, E. (2000) *Separation of Azeotropic Mixtures: Tools for Analysis and Studies on Batch Distillation Operation*. Dr. Ing thesis. Norwegian University of Science and Technology.

Holderbaum, T. and Gmehling, J. (1991) 'PSRK: A group contribution equation of state based on UNIFAC', *Fluid Phase Equilibria*, 70(2-3), pp. 251–265. doi: 10.1016/0378-3812(91)85038-v.

Horsley, L.H. (1973) 'Azeotropic Data - III', *Analytical Chemistry*, 45(8), pp. 752A–752A. doi: 10.1021/ac60330a755.

Horstmann, S., Jabłoniec, A., Krafczyk, J., Fischer, K. and Gmehling, J. (2005) 'PSRK group contribution equation of state: Comprehensive revision and extension IV, including critical constants and α-function parameters for 1000 components', *Fluid Phase Equilibria*, 227(2), pp. 157–164. doi: 10.1016/j.fluid.2004.11.002.

Hou, S.-X., Maitland, G.C. and Trusler, J.P.M. (2013) 'Measurement and modelling of the phase behaviour of the (carbon dioxide+water) mixture at temperatures from 298.15K to 448.15K', *The Journal of Supercritical Fluids*, 73, pp. 87–96. doi: 10.1016/j.supflu.2012.11.011.

Hwang, I.-C., Park, S.-J. and Choi, J.-S. (2008) 'Liquid–liquid equilibria for the binary system of di-isopropyl ether (DIPE)+water in between 288.15 and 323.15K and the ternary systems of DIPE+water+C1–C4 alcohols at 298.15K', *Fluid Phase Equilibria*, 269(1-2), pp. 1–5. doi: 10.1016/j.fluid.2008.04.010.

Içten, E., Nagy, Z.K. and Reklaitis, G.V. (2015) 'Process control of a dropwise additive manufacturing system for pharmaceuticals using polynomial chaos expansion based surrogate model', *Computers & Chemical Engineering*, 83, pp. 221–231. doi: 10.1016/j.compchemeng.2015.07.014.

Iman, R. L. and Conover, W. J. (1982) 'A distribution-free approach to rank correlation', *Communications in Statistics - Simulation and Computation*, pp. 311–334.

Kallrath, J. (2005) 'Solving planning and design problems in the process industry using mixed integer and global optimization', *Annals of Operations Research*, 140(1), pp. 339–373. doi: 10.1007/s10479-005-3976-2.

Kennedy, M.C. and O'Hagan, A. (2001) 'Bayesian calibration of computer models', *Journal of the Royal Statistical Society: Series B (Statistical Methodology)*, 63(3), pp. 425–464. doi: 10.1111/1467-9868.00294.

Kiss, A. a., Flores Landaeta, S. J. and Infante Ferreira, C. a. (2012) 'Towards energy efficient distillation technologies – Making the right choice', *Energy*. Elsevier Ltd, 47(1), pp. 531–542. doi: 10.1016/j.energy.2012.09.038.

Kiss, A. a. and Ignat, R. M. (2012) 'Innovative single step bioethanol dehydration in an extractive dividing-wall column', *Separation and Purification Technology*. Elsevier B.V., 98, pp. 290–297. doi: 10.1016/j.seppur.2012.06.029.

Kiss, A.A. (2013) *Advanced distillation technologies: Design, control, and applications*. Chichester, West Sussex, United Kingdom: John Wiley & Sons.

Kister, H. (2002) 'Can we believe the simulation results?', *Chemical Engineering Progress* (October), pp. 52–58.

Knauf, R., Meyer-Blumenroth, U. & Semel, J. 1998, "Membrane Processes in the Chemical Industry", *Chemie Ingenieur Technik*, vol. 70, no. 10, pp. 1265-1270.

Knol, A.B., Petersen, A.C., van der Sluijs, J.P. and Lebret, E. (2009) 'Dealing with uncertainties in environmental burden of disease assessment', *Environmental Health*, 8(1). doi: 10.1186/1476-069x-8-21.

Knuth, D.E. (1974) 'Computer programming as an art', *Communications of the ACM*, 17(12), pp. 667–673. doi: 10.1145/361604.361612.

Kontogeorgis, G.M. and Folas, G.K. (2010) *Thermodynamic models for industrial applications: From classical and advanced mixing rules to association theories*. United States: Wiley, John & Sons.

Koretsky, M.D. (2010) *Engineering and chemical thermodynamics*. New York, NY, United States: Wiley, John & Sons.

Ku, H.-C. and Tu, C.-H. (2006) 'Vapour–liquid equilibria for binary and ternary mixtures of diisopropyl ether, ethanol, and 2,2,4-trimethylpentane at 101.3kPa', *Fluid Phase Equilibria*, 248(2), pp. 197–205. doi: 10.1016/j.fluid.2006.08.004.

Lai, H.-S., Lin, Y.-F. and Tu, C.-H. (2014) 'Isobaric (vapor+liquid) equilibria for the ternary system of (ethanol+water+1, 3-propanediol) and three constituent binary systems at P=101.3kPa', *The Journal of Chemical Thermodynamics*, 68, pp. 13–19. doi: 10.1016/j.jct.2013.08.020.

Lee, L. and Shen, H. (2003) 'Azeotropic behavior of a water + n -Propanol + Cyclohexane mixture using Cyclohexane as an Entrainer for separating the water + n -Proponal mixture at 760 mmHg', *Industrial & Engineering Chemistry Research*, 42(23), pp. 5905–5914. doi: 10.1021/ie0208220.

Liang, K., Li, W., Luo, H., Xia, M. and Xu, C. (2014) 'Energy-efficient Extractive distillation process by combining Preconcentration column and Entrainer recovery column', *Industrial & Engineering Chemistry Research*, 53(17), pp. 7121–7131. doi: 10.1021/ie5002372.

Lilwanth, H. (2014) *Vapour-Liquid Equilibrium Measurements at Moderate Pressures using a Semi-Automatic Glass Recirculating Still*. MSc. thesis. University of Kwa-Zulu Natal.

Lin, S.H. and Wang, C.S. (2004) 'Recovery of isopropyl alcohol from waste solvent of a semiconductor plant', *Journal of Hazardous Materials*, 106(2-3), pp. 161–168. doi: 10.1016/j.jhazmat.2003.11.012.

Lladosa, E., Montón, J. B., Burguet, Mc. and Muñoz, R. (2007) 'Effect of pressure and the capability of 2-methoxyethanol as a solvent in the behaviour of a diisopropyl ether-isopropyl alcohol azeotropic mixture', *Fluid Phase Equilibria*, 262(1–2), pp. 271–279. doi: 10.1016/j.fluid.2007.09.014.

Lladosa, E., Montón, J. B., Burguet, M. and de la Torre, J. (2008) 'Isobaric (vapour + liquid + liquid) equilibrium data for (di-n-propyl ether + n-propyl alcohol + water) and (diisopropyl ether + isopropyl alcohol + water) systems at 100 kPa', *Journal of Chemical Thermodynamics*, 40(5), pp. 867–873. doi: 10.1016/j.jct.2008.01.002.

Ludwig, E.E. (1997) *Applied process design for chemical and petrochemical plants: V. 2: Distillation and packed towers*. 3rd edn. Houston: Gulf Professional Publishing.

Luo, H., Liang, K., Li, W., Li, Y., Xia, M. and Xu, C. (2014) 'Comparison of Pressure-Swing Distillation and Extractive Distillation Methods for Isopropyl Alcohol/Diisopropyl Ether Separation', *Industrial & Engineering Chemistry Research*, 53(39), pp. 15167–15182. doi: 10.1021/ie502735g.

Luyben, W.L. (2010) *Design and control of distillation systems for separating azeotropes*. Hoboken, N.J.: Wiley.

Luyben, W.L. and Chien, I.-L. (2010) *Design and control of distillation systems for separating azeotropes*. United States: John Wiley & Sons.

Macchietto, S., Maduabeuke, G. and Szczepanski, R. (1986) 'Exact determination of process sensitivity to physical properties', *Fluid Phase Equilibria*, 29, pp. 59–67. doi: 10.1016/0378-3812(86)85011-7.

Mahdi, T., Ahmad, A., Nasef, M.M. and Ripin, A. (2014) 'State-of-the-art technologies for separation of Azeotropic mixtures', *Separation & Purification Reviews*, 44(4), pp. 308–330. doi: 10.1080/15422119.2014.963607.

Mandur, J. and Budman, H. (2014) 'Robust optimization of chemical processes using Bayesian description of parametric uncertainty', *Journal of Process Control*, 24(2), pp. 422–430. doi: 10.1016/j.jprocont.2013.10.004.

Mara, T. A., Delay, F., Lehmann, F. and Younes, A. (2016) 'A comparison of two Bayesian approaches for uncertainty quantification', *Environmental Modelling & Software*, 82, pp. 21–30. doi: 10.1016/j.envsoft.2016.04.010.

Matott, L.S., Babendreier, J.E. and Purucker, S.T. (2009) 'Evaluating uncertainty in integrated environmental models: A review of concepts and tools', *Water Resources Research*, 45(6), p. n/a–n/a. doi: 10.1029/2008wr007301.

Mathias, P. M. (2014) 'Sensitivity of Process Design to Phase Equilibrium—A New Perturbation Method Based Upon the Margules Equation', *Journal of Chemical & Engineering Data*, 59(4), pp. 1006–1015. doi: 10.1021/je400748p.

Mathias, P. M. (2016) 'Effect of VLE uncertainties on the design of separation sequences by distillation - Study of the benzene-chloroform-acetone system', *Fluid Phase Equilibria*. Elsevier Ltd, 408, pp. 265–272. doi: 10.1016/j.fluid.2015.09.004.

Mathias, P.M. and Copeman, T.W. (1983) 'Extension of the Peng-Robinson equation of state to complex mixtures: Evaluation of the various forms of the local composition concept', *Fluid Phase Equilibria*, 13, pp. 91–108. doi: 10.1016/0378-3812(83)80084-3.

Matschke, D. E. and Thodos, G. (1962) 'Vapor-Liquid Equilibria for the Ethane-Propane System', *The Technological Institute, Northwestern UNiversity*, 7(2), pp. 232–234. doi: 10.1021/je60013a022.

McKay, M.D., Beckman, R.J. and Conover, W.J. (1979) 'A comparison of Three methods for selecting values of input variables in the analysis of output from a computer code', *Technometrics*, 21(2), p. 239. doi: 10.2307/1268522.

Moore, R.E., Kearfott, B.R., Cloud, M.J., R, C. and J, M. (2009) *Introduction to interval analysis. Ramon E. Moore, R. Baker Kearfott, Michael J. Cloud*. Philadelphia, PA: Society for Industrial & Applied Mathematics,U.S.

Nagy, Z.K. and Braatz, R.D. (2007) 'Distributional uncertainty analysis using power series and polynomial chaos expansions', *Journal of Process Control*, 17(3), pp. 229–240. doi: 10.1016/j.jprocont.2006.10.008.

Nannapaneni, S., Mahadevan, S. and Rachuri, S. (2016) 'Performance evaluation of a manufacturing process under uncertainty using Bayesian networks', *Journal of Cleaner Production*, 113, pp. 947–959. doi: 10.1016/j.jclepro.2015.12.003.

Nel, R.J.J. and de Klerk, A. (2007) 'Fischer−Tropsch aqueous phase refining by catalytic alcohol dehydration', *Industrial & Engineering Chemistry Research*, 46(11), pp. 3558–3565. doi: 10.1021/ie061555r.

Nelson, A. R., Olson, J. H. and Sandler, S. I. (1983) 'Sensitivity of distillation process design and operation to VLE data', *Industrial and Engineering Chemistry Process Design and Development*, 22(3), pp. 547–552.

Nguyen-Tuan, L., Lahmer, T., Datcheva, M. and Schanz, T. (2016) 'Global and local sensitivity analyses for coupled thermo-hydro-mechanical problems', *International Journal for Numerical and Analytical Methods in Geomechanics*, . doi: 10.1002/nag.2573.

Péneloux, A., Rauzy, E. and Fréze, R. (1982) 'A consistent correction for Redlich-Kwong-Soave volumes', *Fluid Phase Equilibria*, 8(1), pp. 7–23. doi: 10.1016/0378-3812(82)80002-2.

Perry, R.H., Green, D.W., Chilton, C.H. and Maloney, J.O. (1997) *Perry's chemical engineers' handbook*. 6th edn. New York, NY: McGraw-Hill Publishing Co.

Pham, H.N. and Doherty, M.F. (1990) 'Design and synthesis of heterogeneous azeotropic distillations—III. Column sequences', *Chemical Engineering Science*, 45(7), pp. 1845–1854. doi: 10.1016/0009-2509(90)87060-6.

Pienaar, C. (2012) *Evaluation of entrainers for the dehydration of C_2 and C_3 alcohols via azeotropic distillation*. MEng. thesis. Stellenbosch University.

Pienaar, C., Schwarz, C. E., Knoetze, J. H. and Burger, A. J. (2013) 'Vapor–Liquid–Liquid Equilibria Measurements for the Dehydration of Ethanol, Isopropanol, and n -Propanol via Azeotropic Distillation Using DIPE and Isooctane as Entrainers', *Journal of Chemical & Engineering Data*, 58(3), pp. 537–550. doi: 10.1021/je300847v.

Pineda Rojas, A. L., Venegas, L. E. and Mazzeo, N. A. (2016) 'Uncertainty of modelled urban peak O3 concentrations and its sensitivity to input data perturbations based on the Monte Carlo analysis', *Atmospheric Environment*. Elsevier Ltd, 141(x), pp. 422–429. doi: 10.1016/j.atmosenv.2016.07.020.

Pla-Franco, J., Lladosa, E., Loras, S. and Montón, J. B. (2014) 'Thermodynamic Analysis and Process Simulation of Ethanol Dehydration via Heterogeneous Azeotropic Distillation', *Industrial & Engineering Chemistry Research*, 53(14), pp. 6084–6093. doi: 10.1021/ie403988c.

Pla-franco, J., Lladosa, E., Monto, J. B. and Loras, S. (2013) 'Evaluation of the 2 - Methoxyethanol as Entrainer in Ethanol − Water and 1 - Propanol − Water Mixtures'.

Prausnitz, J.M., Anderson, T.F., Grens, E.A., Eckert, C.A. and Hseih, R. (1980) *Computer calculations for multicomponent vapour-liquid and liquid-liquid equilibria*. 2nd edn. United States: Prentice-Hall.

Prausnitz, J.M., Lichtenthaler, R.N. and de Azevedo, E.G. (1999) *Molecular thermodynamics of fluid-phase equilibria*. 3rd edn. London, United Kingdom: Prentice-Hall PTR.

Ramos, W. B., Figueiredo, M. F., Brito, R. P., Kiss, A. A., Ignat, R. M. and Bildea, S. (2014) *24th European Symposium on Computer Aided Process Engineering, 24 European Symposium on Computer Aided Process Engineering*. Elsevier (Computer Aided Chemical Engineering). doi: 10.1016/B978-0-444-63455-9.50057-X.

Rangaiah, G.P. (ed.) (2016) *Chemical process retrofitting and revamping: Techniques and applications*. 1st edn. John Wiley & Sons.

Reagan, M.T., Najm, H.N., Pébay, P.P., Knio, O.M. and Ghanem, R.G. (2005) 'Quantifying uncertainty in chemical systems modeling', *International Journal of Chemical Kinetics*, 37(6), pp. 368–382. doi: 10.1002/kin.20081.

Reddy, P., Benecke, T.P. and Ramjugernath, D. (2013) 'Isothermal (vapour+liquid) equilibria for binary mixtures of diisopropyl ether with (methanol, or ethanol, or 1-butanol): Experimental data, correlations, and predictions', *The Journal of Chemical Thermodynamics*, 58, pp. 330–

339. doi: 10.1016/j.jct.2012.11.005.

Red-Horse, J.R. and Benjamin, A.S. (2004) 'A probabilistic approach to uncertainty quantification with limited information', *Reliability Engineering & System Safety*, 85(1-3), pp. 183–190. doi: 10.1016/j.ress.2004.03.011.

Reed, M. E. and Whiting, W. B. (1993) 'Sensitivity and Uncertainty of Process Designs To Thermodynamic Model Parameters: a Monte Carlo Approach', *Chemical Engineering Communications*, 124(1), pp. 39–48. doi: 10.1080/00986449308936176.

Regan, H. M., Colyvan, M., Burgman, M. a, Applications, E. and Apr, N. (2008) 'A Taxonomy and Treatment of Uncertainty for Ecology and Conservation Biology A TAXONOMY AND TREATMENT OF UNCERTAINTY FOR ECOLOGY', 12(2), pp. 618–628.

Renon, H. and Prausnitz, J.M. (1968) 'Local compositions in thermodynamic excess functions for liquid mixtures', *AIChE Journal*, 14(1), pp. 135–144. doi: 10.1002/aic.690140124.

Riemenschneider, W. and Bolt, H. M. (2005) 'Esters , Organic', *Ullmann's Encyclopedia of Industrial Chemistry*, pp. 8676–8694. doi: 10.1002/14356007.a09.

Ripin, A., Abdul Mudalip, S.K., Sukaimi, Z., Yunus, R.M. and Manan, Z.A. (2009) 'Effects of ultrasonic waves on vapor-liquid equilibrium of an Azeotropic mixture', *Separation Science and Technology*, 44(11), pp. 2707–2719. doi: 10.1080/01496390903014474.

Rousseau, R.W. (1987) *Handbook of separation process technology*. New York: Wiley, John & Sons.

Rubinstein, R.Y. and Kroese, D.P. (2016) *Simulation and the Monte Carlo method*. 2nd edn. United States: Wiley-Blackwell.

Ryan, P.J. and Doherty, M.F. (1989) 'Design/optimization of ternary heterogeneous azeotropic distillation sequences', *AIChE Journal*, 35(10), pp. 1592–1601. doi: 10.1002/aic.690351003.

Sadeq, J., Duarte, H. A. and Serth, R. W. (1997) 'Anomalous results from process simulators', *Chemical Engineering Education*, pp. 46–51.

Sandler, S.I. (2006) *Chemical, biochemical, and engineering thermodynamics*. 4th edn. New York: John Wiley & Sons.

Sandler, S.I. (2015) *Using aspen plus in thermodynamics instruction: A step-by-step guide*. Hoboken, NJ, United States: Wiley-AIChE.

Scheibel, E.G. and Montross, C.F. (1948) 'Optimum feed tray in Multicomponent distillation calculations', *Industrial & Engineering Chemistry*, 40(8), pp. 1398–1401. doi: 10.1021/ie50464a013.

Schmid, B. and Gmehling, J. (2010) 'From van der Waals to VTPR: The systematic improvement of the van der Waals equation of state', *The Journal of Supercritical Fluids*, 55(2), pp. 438–447. doi: 10.1016/j.supflu.2010.10.018.

Schwartzentruber, J. and Renon, H. (1991) 'Equations of state: How to reconcile flexible mixing rules, the virial coefficient constraint and the "Michelsen-Kistenmacher syndrome" for multicomponent systems', *Fluid Phase Equilibria*, 67, pp. 99–110. doi: 10.1016/0378-3812(91)90050-h.

Seader, J.D. and Henley, E.J. (2006) *Separation Process Principles*. 2nd edn. New York, NY, United States: John Wiley & Sons.

Seferlis, P. and Hrymak, A.N. (1996) 'Sensitivity analysis for chemical process optimization', *Computers & Chemical Engineering*, 20(10), pp. 1177–1200. doi: 10.1016/0098-1354(96)82074-6.

Shapiro, A. (2003) 'Stochastic Programming', *Handbooks in Operations Research and Management Science*, 10, pp. 353–425. doi: 10.1016/S0927-0507(03)10006-0.

Shulgin, I., Fischer, K., Noll, O. and Gmehling, J. (2001) 'Classification of homogeneous binary Azeotropes', *Industrial & Engineering Chemistry Research*, 40(12), pp. 2742–2747. doi: 10.1021/ie990897c.

Sigel, K., Klauer, B. and Pahl-Wostl, C. (2010) 'Conceptualising uncertainty in environmental decision-making: The example of the EU water framework directive', *Ecological Economics*, 69(3), pp. 502–510. doi: 10.1016/j.ecolecon.2009.11.012.

Smith, B.D. (1963) *Design of equilibrium stage processes*. New York: McGraw-Hill Inc.,US.

Smith, J.M., Van Ness, H.C. and Abbott, M.M. (2005) *Introduction to chemical engineering thermodynamics*. 7th edn. Boston: McGraw Hill Higher Education.

Soave, G. (1972) 'Equilibrium constants from a modified Redlich-Kwong equation of state', *Chemical Engineering Science*, 27(6), pp. 1197–1203. doi: 10.1016/0009-2509(72)80096-4.

van der Spek, M., Ramirez, A. and Faaij, A. (2015) 'Improving uncertainty evaluation of process models by using pedigree analysis. A case study on CO_2 capture with

Monoethanolamine', *Computers & Chemical Engineering*. Elsevier Ltd, 85(October), pp. 1–15. doi: 10.1016/j.compchemeng.2015.10.006.

Stephenson, R.M. (1992) 'Mutual solubilities: Water-ketones, water-ethers, and water-gasoline-alcohols', *Journal of Chemical & Engineering Data*, 37(1), pp. 80–95. doi: 10.1021/je00005a024.

Sullivan, T.J. (2015) *Introduction to uncertainty quantification. Texts in Applied Mathematics. Volume 63.* Springer.

Szitkai, Z., Lelkes, Z., Rev, E. and Fonyo, Z. (2002) 'Optimization of hybrid ethanol dehydration systems', *Chemical Engineering and Processing: Process Intensification*, 41(7), pp. 631–646. doi: 10.1016/s0255-2701(01)00192-1.

Tavan, Y. and Hosseini, S.H. (2013) 'A novel integrated process to break the ethanol/water azeotrope using reactive distillation – part I: Parametric study', *Separation and Purification Technology*, 118, pp. 455–462. doi: 10.1016/j.seppur.2013.07.036.

Towler, G. and Sinnott, R.K. (2014) *Chemical engineering design: Principles, practice and economics of plant and process design*. 2nd edn. Oxford, United Kingdom: Butterworth-Heinemann.

Vane, L. M., Alvarez, F. R., Huang, Y. and Baker, R. W. (2009) 'Experimental validation of hybrid distillation-vapor permeation process for energy efficient ethanol water separation', *Journal of Chemical Technology & Biotechnology*, (November 2009), p. n/a-n/a. doi: 10.1002/jctb.2318.

Vasquez, V. R. and Whiting, W. B. (1998) 'Uncertainty of predicted process performance due to variations in thermodynamics model parameter estimation from different experimental data sets', *Fluid Phase Equilibria*, 142(1–2), pp. 115–130. doi: 10.1016/S0378-3812(97)00232-X.

Vasquez, V.R. and Whiting, W.B. (1999) 'Effect of systematic and random errors in thermodynamic models on chemical process design and simulation: A Monte Carlo Approach', *Industrial & Engineering Chemistry Research*, 38(8), pp. 3036–3045. doi: 10.1021/ie980748e.

Vasquez, V. R. and Whiting, W. B. (2000) 'Uncertainty and sensitivity analysis of thermodynamic models using equal probability sampling (EPS)', *Computers & Chemical Engineering*, 23(11–12), pp. 1825–1838. doi: 10.1016/S0098-1354(00)00297-0.

Vasquez, V.R. and Whiting, W.B. (2004) 'Analysis of random and systematic error effects on uncertainty propagation in process design and simulation using distribution tail

characterization', *Chemical Engineering Communications*, 191(2), pp. 278–301. doi: 10.1080/00986440490261890.

Vasquez, V. R. and Whiting, W. B. (2005) 'Accounting for both random errors and systematic errors in uncertainty propagation analysis of computer models involving experimental measurements with Monte Carlo methods', *Risk Analysis*, 25(6), pp. 1669–1681. doi: 10.1111/j.1539-6924.2005.00704.x.

Vásquez, V. R., Whiting, W. B. and Meerschaert, M. M. (2010) 'Confidence interval estimation under the presence of non-Gaussian random errors: Applications to uncertainty analysis of chemical processes and simulation', *Computers & Chemical Engineering*, 34(3), pp. 298–305. doi: 10.1016/j.compchemeng.2009.11.004.

Verhoeye, L.A.J. (1970) 'System 2-isopropoxypropane-2-propanol-water', *Journal of Chemical & Engineering Data*, 15(2), pp. 222–226. doi: 10.1021/je60045a028.

Villegas, M., Augustin, F., Gilg, A., Hmaidi, A. and Wever, U. (2012) 'Application of the Polynomial Chaos Expansion to the simulation of chemical reactors with uncertainties', *Mathematics and Computers in Simulation*. International Association for Mathematics and Computers in Simulation (IMACS), 82(5), pp. 805–817. doi: 10.1016/j.matcom.2011.12.001.

Vořechovský, M. and Novák, D. (2009) 'Correlation control in small-sample Monte Carlo type simulations I: A simulated annealing approach', *Probabilistic Engineering Mechanics*. Elsevier Ltd, 24(3), pp. 452–462. doi: 10.1016/j.probengmech.2009.01.004.

Vorenberg, D.G., Raal, J.D. and Ramjugernath, D. (2005) 'Vapor−Liquid equilibrium measurements for MTBE and TAME with Toluene', *Journal of Chemical & Engineering Data*, 50(4), pp. 1499–1500. doi: 10.1021/je050155s.

Walas, S.M. (1985) *Phase equilibria in chemical engineering*. Boston: Butterworth.

Walker, W.E., Harremoës, P., Rotmans, J., van der Sluijs, J.P., van Asselt, M.B.A., Janssen, P. and Krayer von Krauss, M.P. (2003) 'Defining uncertainty: A conceptual basis for uncertainty management in model-based decision support', *Integrated Assessment*, 4(1), pp. 5–17. doi: 10.1076/iaij.4.1.5.16466.

Wang, C., Qiu, Z. and Yang, Y. (2016) 'Uncertainty propagation of heat conduction problem with multiple random inputs', *International Journal of Heat and Mass Transfer*. Elsevier Ltd, 99, pp. 95–101. doi: 10.1016/j.ijheatmasstransfer.2016.03.094.

Wechsung, A., Oldenburg, J., Yu, J. and Polt, A. (2009) 'Supporting Chemical Process Design Under Uncertainty', *Computer Aided Chemical ...*, 27(3), pp. 451–460. Available at: http://www.sciencedirect.com/science/article/pii/S1570794609703773.

Whiting, W.B. (1996) 'Effects of uncertainties in thermodynamic data and models on process calculations', *Journal of Chemical & Engineering Data*, 41(5), pp. 935–941. doi: 10.1021/je9600764.

Whiting, W.B., Tong, T.M. and Reed, M.E. (1993) 'Effect of uncertainties in thermodynamic data and model parameters on calculated process performance', *Industrial & Engineering Chemistry Research*, 32(7), pp. 1367–1371. doi: 10.1021/ie00019a011.

Whiting, W. B., Vasquez, V. R. and Meerschaert, M. M. (1999) 'Techniques for assessing the effects of uncertainties in thermodynamic models and data', *Fluid Phase Equilibria*, 158–160, pp. 627–641. doi: 10.1016/S0378-3812(99)00054-0.

Wyss, G.D. and Jorgensen, K.H. (1998) *A user's guide to LHS: SANDIA Latin hypercube sampling software*.

Yorizane, M., Yoshimura, S. and Yamamoto, T. (1967) 'Measurement of the Ternary vapor-liquid equilibrium', *Chemical engineering*, 31(5), pp. 451–457, a1. doi: 10.1252/kakoronbunshu1953.31.451.

You, M.X. (2015) *Thermodynamic Insight for the Design and Optimization of Extractive Distillation of 1.0-1a Class Separation*. PHD thesis. University of Toulouse.

You, X., Rodriguez-Donis, I. and Gerbaud, V. (2016) 'Low pressure design for reducing energy cost of extractive distillation for separating Diisopropyl ether and Isopropyl alcohol', *Chemical Engineering Research and Design*. Institution of Chemical Engineers, 109, pp. 540–552. doi: 10.1016/j.cherd.2016.01.026.

Yuan, S., Zou, C., Yin, H., Chen, Z. and Yang, W. (2014) 'Study on the separation of binary azeotropic mixtures by continuous extractive distillation', *Chemical Engineering Research and Design*. Institution of Chemical Engineers, (April), pp. 2–8. doi: 10.1016/j.cherd.2014.05.005.

Zhu, Y., Legg, S. and Laird, C.D. (2010) 'Optimal design of cryogenic air separation columns under uncertainty', *Computers & Chemical Engineering*, 34(9), pp. 1377–1384. doi: 10.1016/j.compchemeng.2010.02.007.

Appendix A: Thermodynamic Consistency

A.1 Thermodynamic Consistency Testing

Distillation process design generally involves the use of some experimental vapour-liquid equilibrium data. In experimental data measurement, a potential for uncertainty arises from systematic and random errors. Consistency tests are methods that, in principle, allow for the evaluation of experimental vapour-liquid equilibrium data to detect systematic errors (Wisniak, Apelblat & Segura, 1997). In order to consider the phase equilibria data of any system as appropriate for design and modelling purposes, the data needs to satisfy the criteria of well-formulated thermodynamic consistency tests (Sandler, 2006).

A range of consistency tests are reported in the literature (Wisniak *et al*., 1997) and those generally used to evaluate phase equilibrium data of short chain alcohols-water-entrainer systems similar to this study are further expanded upon in this section. The validity of experimental vapour-liquid equilibrium data are tested for conformance to thermodynamic principles, particularly, the Gibbs-Duhem equation (Wisniak *et al.*, 1997):

$$\left(\frac{\partial \widetilde{M}}{\partial T}\right)_{P,\underline{z}} dT + \left(\frac{\partial \widetilde{M}}{\partial P}\right)_{T,\underline{z}} dP - \sum z_i d\widetilde{M}_i = 0 \qquad \text{(A.1)}$$

where in Equation A.1 $\widetilde{M}$ is a generic molar property, "z_i" the molar fraction of component *i* in the phase under consideration, $\underline{z}$ the relevant set of compositions and $\widetilde{M}_i$ the partial contribution of component *i* to $\widetilde{M}$.

According to the Gibbs-Duhem equation, the partial properties of the species forming a solution have an interdependency on each other owing to molecular interactions (Smith et al., 2005). Data that conforms to the Gibbs-Duhem equation are considered thermodynamically consistent, with acceptable systematic experimental error and thus suitable for modelling purposes. Cripwell (2014), referring to Sandler (2006), reported that this relation can be transformed applying the excess Gibbs energy and other appropriate thermodynamic relations to yield the well-known relation:

$$-\left(\frac{\Delta \widetilde{H}}{RT^2}\right) dT + \left(\frac{\Delta \widetilde{V}}{RT}\right) dP - \sum x_i d\ln \gamma_i = 0 \qquad \text{(A.2)}$$

where $\Delta\tilde{H}$ and $\Delta\tilde{V}$ represents the *molar enthalpy of mixing* and *volume of mixing* of the liquid phase respectively and

$$\frac{\tilde{G}^E}{RT} = \sum x_i ln\, \gamma_i \tag{A.3}$$

Combining Equations A.2 and A.3 yields

$$d\left[\frac{\tilde{G}^E}{RT}\right] - \sum ln\, \gamma_i dx_i = \sum x_i d\ \ln \gamma_i = -\frac{\Delta\tilde{H}}{RT^2}dT + \frac{\Delta\tilde{V}}{RT}dP \tag{A.4}$$

Applied to a binary system gives

$$d\left[\frac{\tilde{G}^E}{RT}\right] - ln\frac{\gamma_1}{\gamma_1}dx_1 = -\frac{\Delta\tilde{H}}{RT^2}dT + \frac{\Delta\tilde{V}}{RT}dP \tag{A.5}$$

Solving Equations A.3 and A.5 simultaneously yields

$$\ln \gamma_1 = \frac{\tilde{G}^E}{RT} + x_2\left[\frac{\Delta\tilde{H}}{RT^2}\frac{dT}{dx_1} - \frac{\Delta\tilde{V}}{RT}\frac{dP}{dx_1} + \frac{d}{dx_1}\left(\frac{\tilde{G}^E}{RT}\right)\right] \tag{A.6}$$

$$\ln \gamma_2 = \frac{\tilde{G}^E}{RT} + x_1\left[\frac{\Delta\tilde{H}}{RT^2}\frac{dT}{dx_1} - \frac{\Delta\tilde{V}}{RT}\frac{dP}{dx_1} + \frac{d}{dx_1}\left(\frac{\tilde{G}^E}{RT}\right)\right] \tag{A.7}$$

Wisniak et al. (1997) report that Equations A.4, A.5, A.6 and A.7 establish the origin of all currently used thermodynamic consistency tests. Moreover, for the simple case of binary mixtures for constant temperature and pressure conditions, equation A.2 reduces to:

$$x_1\frac{dln\gamma_1}{dx_1} + x_2\frac{dln\gamma_2}{dx_1} = 0 \tag{A.8}$$

The activity coefficient values and subsequently $ln\gamma_i$ can be determined from experimental data. Furthermore, as the Gibbs-Duhem equation needs to be satisfied for data to be considered thermodynamically consistent and as the activity coefficient values are determined independently of the Gibbs-Duhem equation, thermodynamic consistency tests can be derived from Equation A.8. The method developed by McDermott and Ellis (1965) is one such test.

A.1.1 McDermott-Ellis Thermodynamic Consistency Test

The McDermott-Ellis consistency test is derived from the isothermal-isobaric form of the Gibbs-Duhem equation by integrating using the trapezoidal rule, and reducing to any pair of points (say, for example, point *c* and *d*), yielding (McDermott & Ellis, 1965):

$$0 = \sum_{i=1}^{N} (x_{ic} + x_{id})(\ln \gamma_{id} - \ln \gamma_{ic}) \qquad (A.9)$$

To determine whether or not data is consistent, McDermott and Ellis (1965) originally recommend a maximum deviation in Equation A.9 of 0.01 if the accuracy of the reported vapour and liquid fractions is within ±0.001. Later, Wisniak and Tamir (1977) proposed a refined criterion in that the local maximum deviation should not be regarded as constant, but as a function of Equation A.10:

$$0 = \sum_{i=1}^{N} (x_{ic} + x_{id}) \left(\frac{1}{x_{ic}} + \frac{1}{x_{id}} + \frac{1}{y_{ic}} + \frac{1}{y_{id}} \right) \Delta x + 2 \sum_{i=1}^{N} |\ln \gamma_{id} - \ln \gamma_{ic}| \Delta x + \sum_{i=1}^{N} (x_{ic} + x_{id}) \frac{\Delta P}{P} + \sum_{i=1}^{N} (x_{ic} + x_{id}) \beta_i \left(\frac{1}{|T_c + \delta_i|^2} + \frac{1}{|T_d + \delta_i|^2} \right) \Delta T \qquad (A.10)$$

where Δx, ΔP and ΔT are measurement errors in concentration, pressure and temperature and β_i and δ_i are the Antoine constants (B_i and C_i respectively) of the specific component.

The McDermott-Ellis thermodynamic consistency test is classed as a point-to-point (slope) type consistency test. Another class of consistency tests are the Area Test and of particular interest is the L-W test of consistency.

A.1.2 L-W Thermodynamic Consistency Test

Wisniak (1993) proposed the L-W consistency test as an alternative approach by considering the excess Gibbs free energy of a mixture at constant pressure and its related boiling point at equilibrium, instead of relating it to the Gibbs-Duhem equation. Calculating activity coefficients from Equation A.11:

$$\gamma_k = \frac{y_k P \Phi_k}{x_k P_k^{sat}} \qquad (A.11)$$

and subsequently considering the Clapeyron relation gives:

$$\ln \gamma_k = \ln \frac{\gamma_k}{\gamma_k} + \ln \Phi_k + \frac{\Delta \tilde{H}_k^V}{R}\left(\frac{1}{T_k^0} - \frac{1}{T}\right) \tag{A.12}$$

where T_k^0 and $\Delta \tilde{H}_k^V$ are the boiling point and enthalpy of vaporisation of the pure component at the operating pressure. Wisniak (1993) rearranged Equation A.12 to yield:

$$L_i = \sum_k^C \frac{x_k T_k^0 \Delta \tilde{S}_k^0}{\Delta \tilde{S}} - T = \frac{\tilde{G}^E}{\Delta \tilde{S}} - \frac{RT\omega}{\Delta \tilde{S}} - RT \sum_k^C \frac{x_k \ln \Phi_k}{\Delta \tilde{S}} = W_i \tag{A.13}$$

here C is the number of components, $\Delta \tilde{S}^0$ is the entropy of vapourization ($\Delta \tilde{S}^0 = \Delta \tilde{H}^0 / T^0$) and

$$\Delta \tilde{S} = \sum_k^C x_k \Delta \tilde{S}_k^0 \tag{A.14}$$

$$\omega = \sum_i^C x_i \ln \frac{y_i}{x_i} \tag{A.15}$$

Integrating both side of Equation A.13 over the whole composition range gives:

$$L = \int_0^1 L_i dx_i = \int_0^1 W_i dx_i = W \tag{A.16}$$

So, equality of L and W serves as a thermodynamic consistency test if parameter D, as defined in Equation A.17, is less than 3 when measured heats of vaporisation are available, or less than 5 when heats of vaporisation are unknown and must be estimated (Wisniak *et al*., 1997):

$$D = 100 \times \frac{|L - W|}{|L + W|} \tag{A.17}$$

The benefit of the L-W consistency test is that no heat and/or volume of mixing data for the liquid phase is required. Furthermore, Wisniak (1993) states that it may be used for systems containing any number of components, but advises that a second test derived from the Gibbs-Duhem equation must always be used in conjunction with the L-W test for reliable data qualification.

A.1.3 Summary of Thermodynamic Consistency

The use of multiple consistency tests is always recommended as there is no single test that can provide a conclusive answer whether to accept or reject the experimental data. Where possible, a comparison should also be performed to other measurements available for the specific system under similar conditions in order to ascertain the extent of uncertainty in the experimental data.

Appendix B: System 1 Model Screening Results

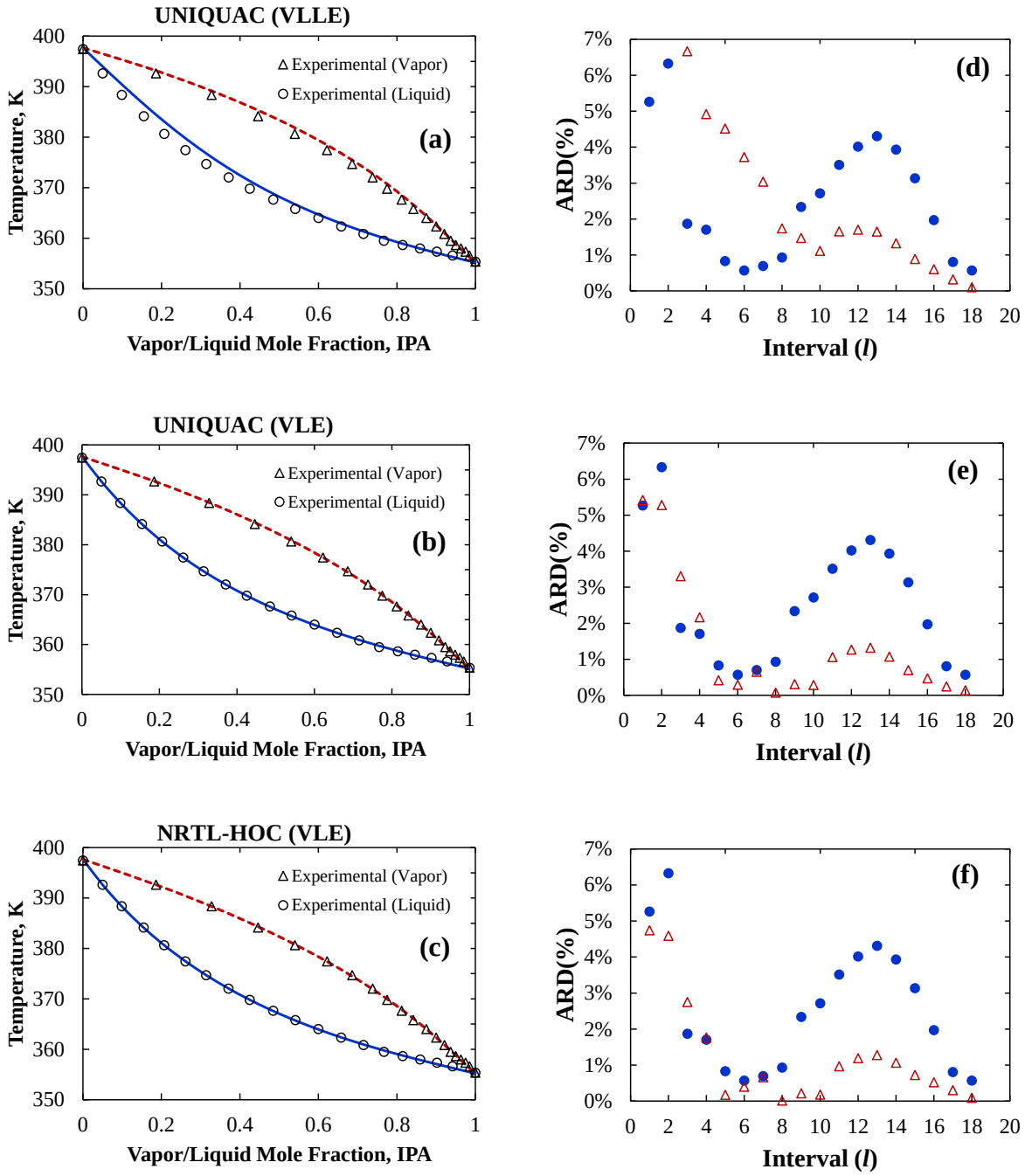

Figure B.1. Binary system IPA/2-Methoxy-ethanol, (a-c) Temperature-composition diagrams for UNIQUAC model with binary interaction parameters regressed by this work (VLLE), this work (VLE) and NRTL-HOC regressed by this work (VLE, (d-f) Deviations in the individual Txy diagram points (ARD%) for liquid phase and vapour phase.

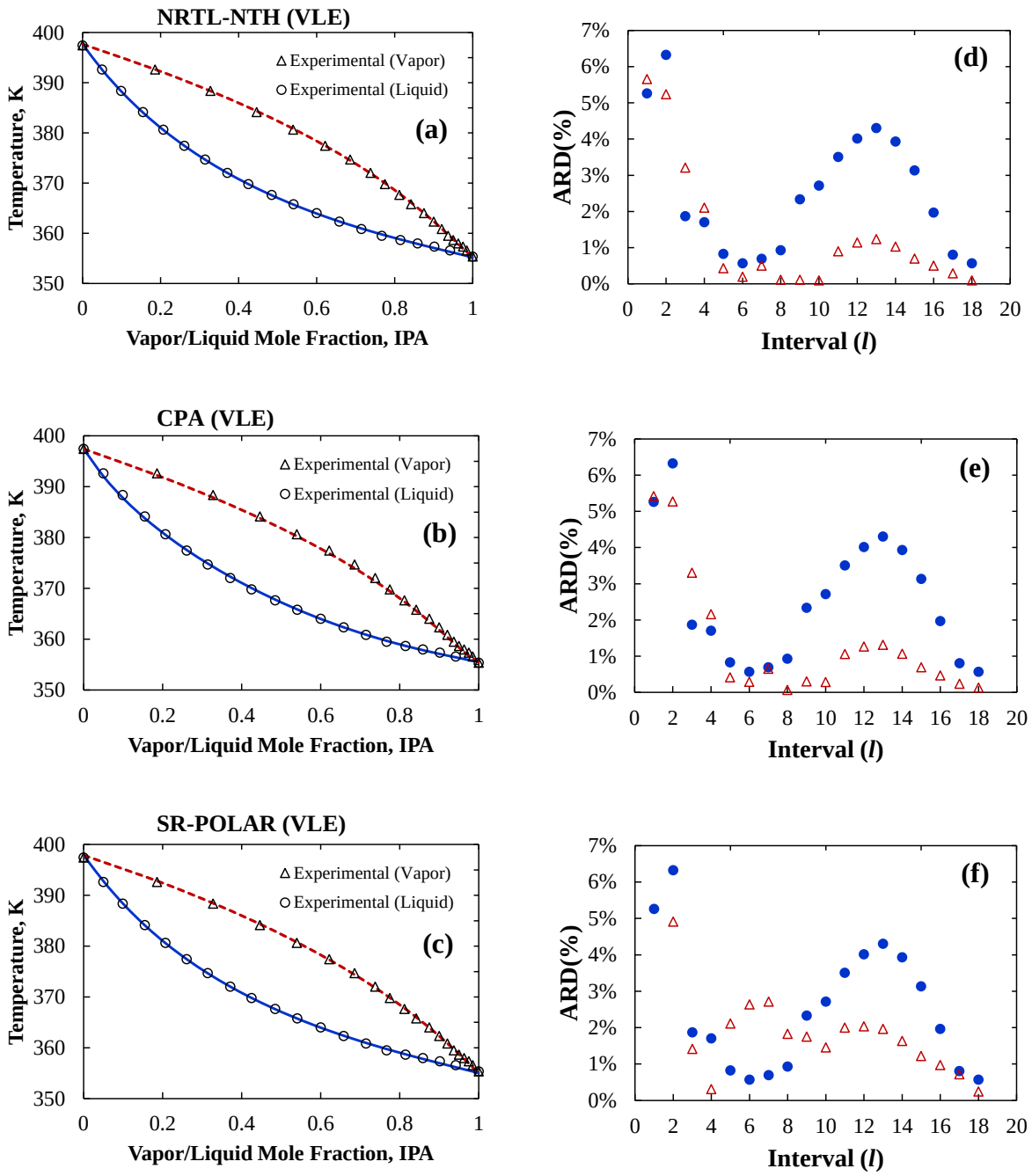

Figure B.2. Binary system IPA/2-Methoxy-ethanol, (a-c) Temperature-composition diagrams with binary interaction parameters regressed by this work for NRTL-NTH (VLE), CPA (VLE) and SR-POLAR (VLE), (d-f) Deviations in the individual Txy diagram points (ARD%) for liquid phase and vapour phase.

Appendix C: System 1 Model Parameters CDF

The probability distribution for the NRTL parameters for the extractive distillation system.

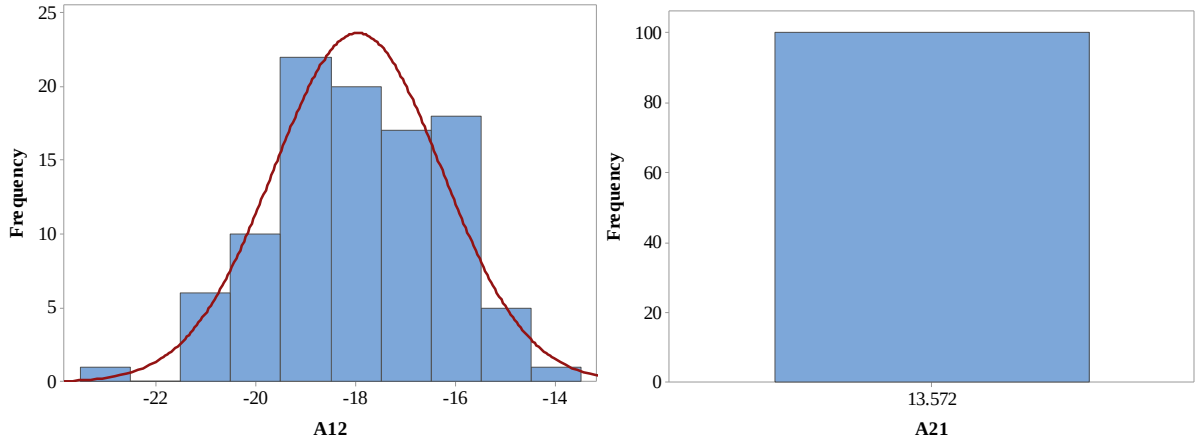

Figure C.1. Histogram approximating the distribution of each binary interaction parameter obtained from 100 Monte Carlo simulations. Parameter A for DIPE/IPA.

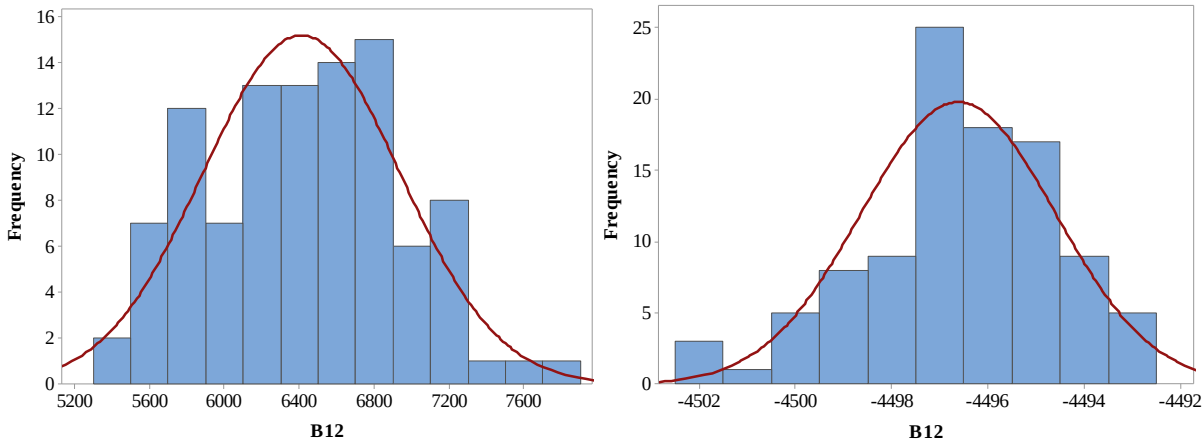

Figure C.2. Histogram approximating the distribution of each binary interaction parameter obtained from 100 Monte Carlo simulations. Parameter B for DIPE/IPA

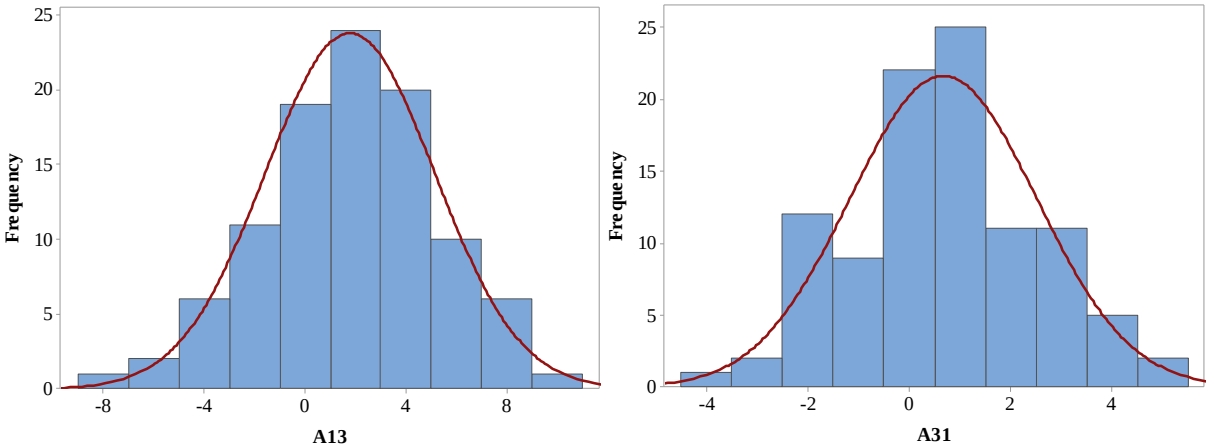

Figure C.3. Histogram approximating the distribution of each binary interaction parameter obtained from 100 Monte Carlo simulations. Parameter A for DIPE/2-methoxyethanol.

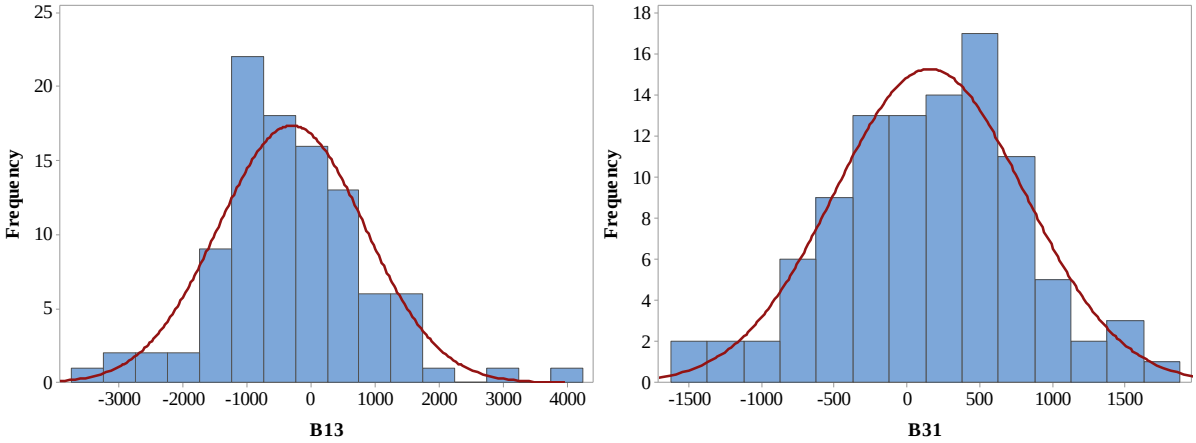

Figure C.4. Histogram approximating the distribution of each binary interaction parameter obtained from 100 Monte Carlo simulations. Parameter B for DIPE/2-methoxyethanol.

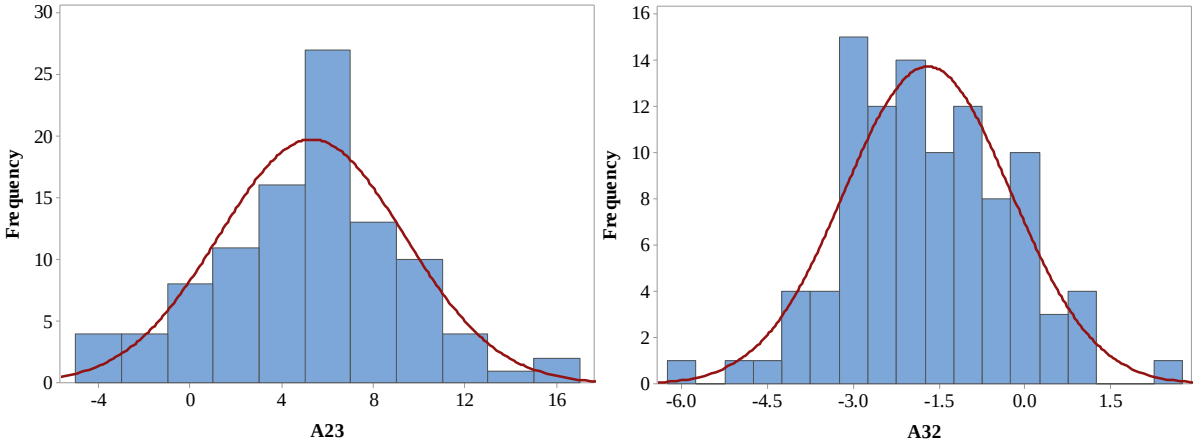

Figure C.5. Histogram approximating the distribution of each binary interaction parameter obtained from 100 Monte Carlo simulations. Parameter A for IPA/2-methoxyethanol.

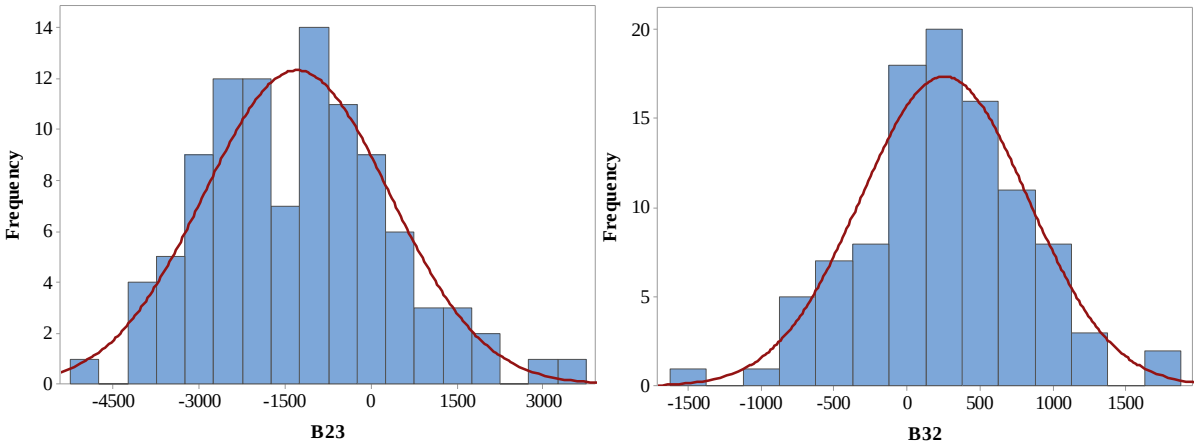

Figure C.6. Histogram approximating the distribution of each binary interaction parameter obtained from 100 Monte Carlo simulations. Parameter B for IPA/2-methoxyethanol.

Appendix D: Experimental VLE System 1

Literature sources for isobaric phase equilibrium data at 101.3 kPa used for parameter regression in this work.

Table D-1: Experimental vapour–liquid equilibrium data for the binary system diisopropyl ether (1)/isopropyl alcohol (2) at 101.3 kPa by Lladosa *et al.*, (2007). Activity coefficient (γ) and K-value calculated with Aspen Plus® using NRTL model using parameters regressed in this work.

***T* (K)**	x_1	y_1	γ_1	γ_2	***x2***	***y2***	***K1***	***K2***	***RV12***
355.35	0	0		1	1	1		1	
352.6	0.029	0.104	2.549	1.024	0.971	0.896	3.59	0.92	3.89
350.39	0.066	0.21	2.427	1.028	0.934	0.79	3.18	0.85	3.76
348.69	0.102	0.29	2.291	1.032	0.898	0.71	2.84	0.79	3.60
347.12	0.142	0.361	2.141	1.04	0.858	0.639	2.54	0.74	3.41
345.58	0.189	0.427	1.996	1.053	0.811	0.573	2.26	0.71	3.20
344.46	0.232	0.475	1.871	1.07	0.768	0.525	2.05	0.68	3.00
343.38	0.281	0.517	1.739	1.103	0.719	0.483	1.84	0.67	2.74
342.5	0.331	0.557	1.634	1.13	0.669	0.443	1.68	0.66	2.54
341.75	0.382	0.586	1.528	1.18	0.618	0.414	1.53	0.67	2.29
341.07	0.439	0.619	1.435	1.234	0.561	0.381	1.41	0.68	2.08
340.46	0.499	0.649	1.347	1.311	0.501	0.351	1.30	0.70	1.86
340.05	0.555	0.675	1.277	1.393	0.445	0.325	1.22	0.73	1.67
339.73	0.613	0.7	1.214	1.494	0.387	0.3	1.14	0.78	1.47
339.47	0.672	0.727	1.16	1.621	0.328	0.273	1.08	0.83	1.30
339.31	0.728	0.755	1.117	1.77	0.272	0.245	1.04	0.90	1.15
339.28	0.785	0.784	1.075	1.987	0.215	0.216	1.00	1.00	0.99
339.4	0.842	0.82	1.045	2.233	0.158	0.18	0.97	1.14	0.85
339.71	0.894	0.861	1.024	2.532	0.106	0.139	0.96	1.31	0.73
340.37	0.947	0.92	1.011	2.844	0.053	0.08	0.97	1.51	0.64
341.49	1	1	1		0	0	1		

Table D-2: Experimental vapour–liquid equilibrium data for the binary system diisopropyl ether (1)/2-methoxyethanol (3) at 101.3 kPa by Lladosa *et al.*, (2007). Activity coefficient (γ) and K-value calculated with Aspen Plus® using NRTL model using parameters regressed in this work.

T (K)	x1	y1	γ1	γ3	x3	y3	K1	K3	RV13
397.44	0	0		1	1	1			
393.2	0.009	0.124	3.47	1.011	0.991	0.876	13.78	0.88	15.59
387.75	0.022	0.279	3.452	1.01	0.978	0.721	12.68	0.74	17.20
382.46	0.038	0.41	3.413	1.003	0.962	0.59	10.79	0.61	17.59
377.01	0.057	0.527	3.343	0.994	0.943	0.473	9.25	0.50	18.43
371.72	0.079	0.62	3.231	0.993	0.921	0.38	7.85	0.41	19.02
365.79	0.115	0.711	3.008	0.981	0.885	0.289	6.18	0.33	18.93
359.47	0.168	0.788	2.726	0.983	0.832	0.212	4.69	0.25	18.41
356.41	0.211	0.822	2.47	0.982	0.789	0.178	3.90	0.23	17.27
354.28	0.258	0.844	2.207	1.002	0.742	0.156	3.27	0.21	15.56
352.3	0.313	0.86	1.968	1.056	0.687	0.14	2.75	0.20	13.48
350.78	0.369	0.871	1.77	1.124	0.631	0.129	2.36	0.20	11.55
349.41	0.427	0.88	1.612	1.224	0.573	0.12	2.06	0.21	9.84
348.43	0.48	0.887	1.489	1.33	0.52	0.113	1.85	0.22	8.50
347.58	0.534	0.895	1.386	1.429	0.466	0.105	1.68	0.23	7.44
346.74	0.593	0.899	1.289	1.621	0.407	0.101	1.52	0.25	6.11
346.01	0.65	0.905	1.212	1.829	0.35	0.095	1.39	0.27	5.13
345.21	0.71	0.914	1.148	2.079	0.29	0.086	1.29	0.30	4.34
344.45	0.779	0.925	1.084	2.474	0.221	0.075	1.19	0.34	3.50
343.75	0.834	0.935	1.047	2.918	0.166	0.065	1.12	0.39	2.86
343.03	0.887	0.949	1.022	3.524	0.113	0.051	1.07	0.45	2.37
342.24	0.941	0.971	1.011	3.962	0.059	0.029	1.03	0.49	2.10
341.49	1	1	1		0	0	1		

Table D-3 Experimental vapour–liquid equilibrium data for the binary system isopropyl alcohol (2)/2-methoxyethanol (3) at 101.3 kPa by Lladosa *et al.*, (2007). Activity coefficients (γ) and K-values calculated with Aspen Plus® using NRTL model using parameters regressed in this work.

T (K)	x2	y2	γ2	γ3	x3	y3	K2	K3	RV23
397.44	0	0		1	1	1			
392.64	0.05	0.186	1.029	0.997	0.95	0.814	3.72	0.86	4.34
388.36	0.099	0.328	1.046	0.997	0.901	0.672	3.31	0.75	4.44
384.14	0.155	0.446	1.04	1.009	0.845	0.554	2.88	0.66	4.39
380.64	0.207	0.54	1.057	1.006	0.793	0.46	2.61	0.58	4.50
377.42	0.261	0.622	1.076	0.992	0.739	0.378	2.38	0.51	4.66
374.67	0.314	0.686	1.083	0.979	0.686	0.314	2.18	0.46	4.77
372.03	0.371	0.738	1.081	0.98	0.629	0.262	1.99	0.42	4.78
369.77	0.425	0.775	1.074	1	0.575	0.225	1.82	0.39	4.66
367.62	0.485	0.812	1.065	1.011	0.515	0.188	1.67	0.37	4.59
365.79	0.541	0.842	1.058	1.021	0.459	0.158	1.56	0.34	4.52
363.99	0.6	0.875	1.059	0.993	0.4	0.125	1.46	0.31	4.67
362.33	0.658	0.9	1.057	0.991	0.342	0.1	1.37	0.29	4.68
360.84	0.715	0.921	1.053	0.996	0.285	0.079	1.29	0.28	4.65
359.48	0.767	0.937	1.052	1.025	0.233	0.063	1.22	0.27	4.52
358.64	0.815	0.95	1.036	1.059	0.185	0.05	1.17	0.27	4.31
357.96	0.859	0.963	1.023	1.056	0.141	0.037	1.12	0.26	4.27
357.33	0.902	0.975	1.011	1.053	0.098	0.025	1.08	0.26	4.24
356.59	0.942	0.985	1.007	1.1	0.058	0.015	1.05	0.26	4.04
355.35	1	1	1		0	0	1		

Appendix E: Uncertainty Evaluation Methods

Table E.1. Qualitative Uncertainty Evaluation methods. Redrawn from supplementary data in (van der Spek, Ramirez and Faaij, 2015)

Method/tool	Short description	Source
Actor Analysis		(Van der Sluijs et al., 2004)
Critical Review of Assumptions	To systematically identify, prioritise, and analyse importance and strength of assumptions in models	(Van der Sluijs *et al.*, 2004)
Peer Review	To review the model by people considered experts in the field, thus enhancing credibility and acceptance of model outputs	(Van der Sluijs *et al.*, 2004)
Extended Peer Review (by stakeholders)	To complement peer review with review by stakeholders, thus enhancing credibility and acceptance of model outputs	(Van der Sluijs *et al.*, 2004)
Model Quality Checklist	To assist in the quality control process for modelling; to provide diagnostic help as to where problems with regard to quality and uncertainty may occur and why; to raise awareness of pitfalls in the modelling process	(Van der Sluijs *et al.*, 2004)
Quality Assurance	To conduct the process of assessment and modelling in such a way, as to assure the quality of the output	(Pohjola *et al.*, 2013)
Stakeholder Involvement	To involve users and stakeholders of the model, as to increase quality of outcomes, reduce uncertainty, and increase acceptance	(Van der Sluijs *et al.*, 2004)
Pedigree Analysis	To systematically review the knowledge base of data used as model inputs	(Van der Sluijs *et al.*, 2004)

Appendix F: System 2 – Ternary Diagrams

This appendix contains results of the SR-POLAR model for the DIPE/ethanol/water system. As the model did not offer accurate results, with the parameters regressed in this work, it is not shown in the main text.

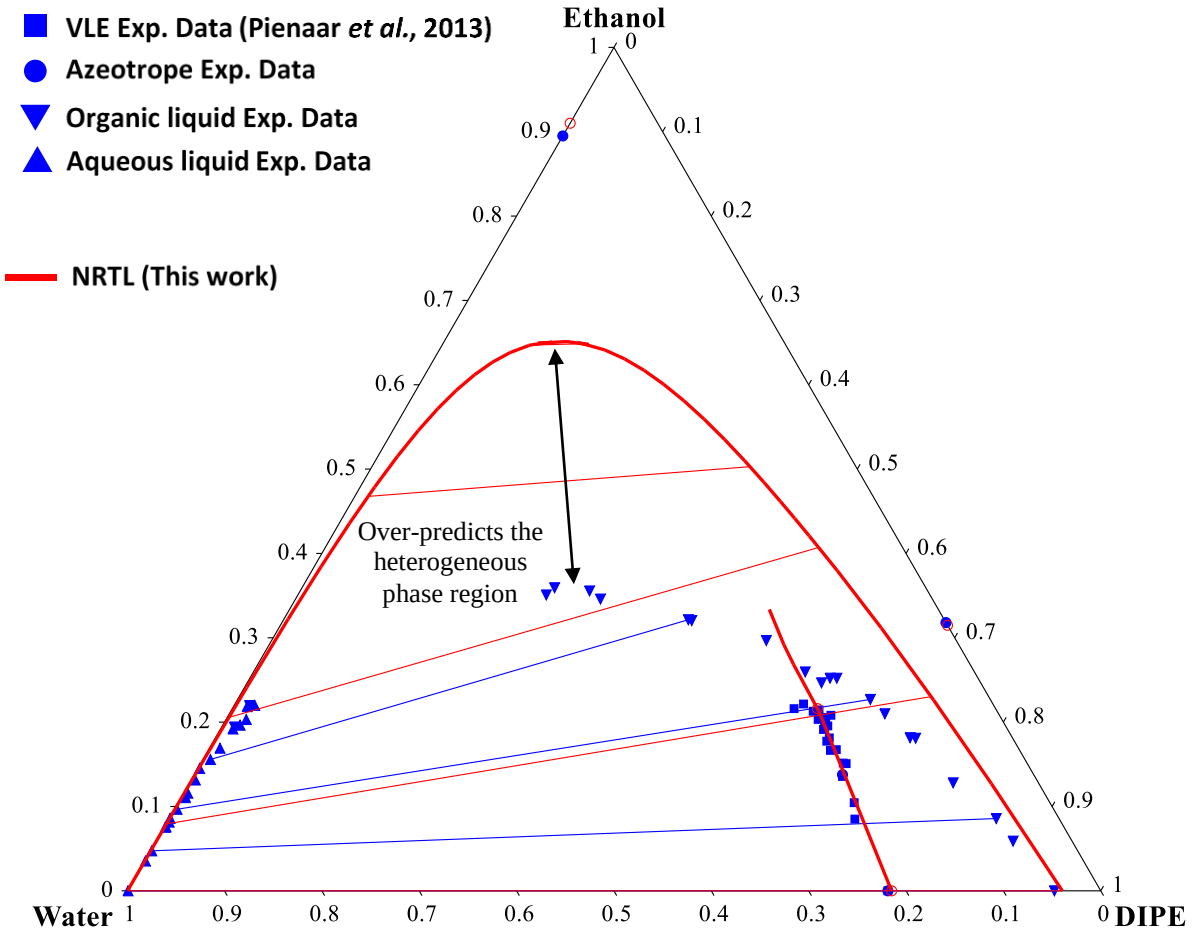

Figure F.1. Ternary phase diagram for SR-POLAR model with parameters regressed in this work for System 2. Experimental data from Pienaar *et al.*, (2013).